PNL-2080 12

COMPILATION OF CRITICALITY DATA INVOLVING THORIUM OR ^{233}U AND LIGHT WATER MODERATION

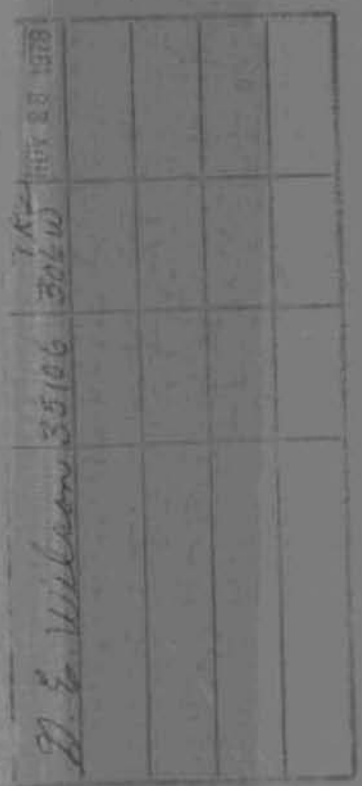

B. F. Gore

July 1978

Prepared for the U.S. Department of Energy
Fuel Cycle Program Office
Under Contract EY-76-C-06-1830

BASE TECHNOLOGY

Pacific Northwest Laboratory
Operated for the U.S. Department of Energy
By

Battelle
Memorial Institute

NOTICE

PACIFIC NORTHWEST LABORATORY
operated by
BATTELLE
for the
UNITED STATES DEPARTMENT OF ENERGY
Under Contract EY-76-C-06-1830

Printed in the United States of America
Available from
National Technical Information Service
United States Department of Commerce
5285 Port Royal Road
Springfield, Virginia 22151

Price: Printed Copy $9.25, Microfiche $3.00

PNL-2080-12
UC-83

COMPILATION OF CRITICALITY DATA INVOLVING THORIUM OR ^{233}U AND LIGHT WATER MODERATION

B. F. GORE

BASE TECHNOLOGY

PACIFIC NORTHWEST LABORATORIES

RICHLAND, WASHINGTON 99352

PREPARED FOR THE
DEPARTMENT OF ENERGY
FUEL CYCLE PROGRAM OFFICE
UNDER CONTRACT EY-76-C-06-1830

Form 189 Number 840.3

ABSTRACT

The literature has been searched for criticality data for light water moderated systems which contain thorium or ^{233}U, and data found are compiled herein. They are from critical experiments, extrapolations, and exponential experiments performed with homogeneous solutions and metal spheres of ^{233}U; with lattices of fuel rods containing highly enriched $^{235}UO_2$ - ThO_2 and $^{233}UO_2$ - ThO_2; and with arrays of cylinders of ^{233}U solutions.

The extent of existing criticality data has been compared with that necessary to implement a thorium-based fuel cycle. No experiments have been performed with any solutions containing thorium. Neither do data exist for homogeneous ^{233}U systems with H/U < 34, except for solid metal systems. Arrays of solution cylinders up to 3 x 3 x 3 have been studied. Data for solutions containing fixed or soluble poisons are very limited.

All critical lattices using $^{233}UO_2$ - ThO_2 fuels (LWBR program) were zoned radially, and in most cases axially also. Only lattice experiments using $^{235}UO_2$ - ThO_2 fuels have been performed using a single fuel rod type. Critical lattices of $^{235}UO_2$ - ThO_2 rods poisoned with boron have been measured, but only exponential experiments have been performed using boron-poisoned lattices of $^{233}UO_2$ - ThO_2 rods.

No criticality data exist for denatured fuels (containing significant amounts of ^{238}U) in either solution or lattice configurations.

CONTENTS

FIGURES

No figures were prepared specifically for this document. Figures reproduced from other documents are located with the descriptive material from the same document.

TABLES

Tables reproduced from other documents are located with the descriptive material from the same document.

INTRODUCTION

The Thorium Fuel Cycle Technology Program (TFCT Program) was initiated in 1977 at Savannah River Laboratory. Its purpose is to develop the technical information required to support future decisions on establishing fuel recycle facilities. In support of the TFCT program, PNL will perform critical experiments involving thorium-based fuels, to serve as benchmarks for the validation of nuclear analysis techniques used in system design and safety analysis studies. As a first step in planning such experiments the literature has been searched for reports of critical experiments using either the fertile element thorium or the fissile isotope ^{233}U. This document is a compilation of the criticality data which have been found in that search.

As perusal of this compilation will show, a significant amount of criticality data exists for lattices of fuel rods containing thorium and uranium, and for ^{233}U solutions and metal systems without thorium. This compilation brings the existing data together from diverse, hard-to-acquire sources by reprinting appropriate portions of the source doucments. (Data are not compiled for either ^{235}U or ^{239}Pu without thorium, because of the large amount of such data and its ready availability in the literature). Effort has been expended to ensure that sufficient description of experimental details is included so that this compilation can serve as the basis for calculations validating criticality analysis codes and cross sections. To a great extent, the descriptions of the experiments have been photocopied directly from the source documents. Where relevant information was scattered, it was collected and rewritten. However, an attempt was made to retain the original authors' prose. The intent was to provide a maximum of criticality information, with a minimum of "filtering," retyping, and rewording.

Thanks are extended to the original authors for permission to reproduce their work, and also to the American Nuclear Society for permission to reproduce copyrighted material taken from Nuclear Science and Engineering.

Although the completeness of this compilation cannot be guaranteed, it is not likely that any major data sources were missed in the reviews of abstracts, bibliographies, and journal references performed to identify data sources. Therefore, by comparing the extent of the information contained herein with that needed to implement a thorium fuel cycle, needs for additional experimentation can be identified. This was, of course, the primary reason for searching the literature. This comparison is shown in Tables 1 and 2, for geometrically simple systems and for lattices. Upon inspection of these tables one is struck by the total absence of thorium from all experiments with geometrically simple systems. Critical experiments with solutions containing thorium will clearly be very important to meeting the needs of the TFCT program, as will experiments with both solutions and lattices in which ^{233}U is denatured with ^{238}U.

TABLE 1. Existing Data - Geometrically Simple Systems

Fissile Material/Form	Fully Enriched	Contains Thorium	Denatured With ^{238}U	Poisoned		Arrays of Units
				Soluble	Fixed	
^{235}U						
Aqueous Solutions	✓	No	✓	✓	✓	✓
Low Moderated	✓	No	✓	--	✓	✓
Metal	✓	No	✓	--	--	✓
^{233}U						
Aqueous Solutions	✓	No	No	Little	Sub-critical	Limited
Low Moderated	No	No	No	--	No	No
Metal	✓	No	No	--	--	No

TABLE 2. Existing Data - Lattices

Fuel (Oxides)	Moderators				Lattice Not Zoned	^{238}U in Fuel Rods
	Water	Fresh Acid	Dissolver Solution	Poisons		
^{235}U-Th	✓	No	No	Boron	✓	No
^{233}U-Th	✓	No	No	Boron*	✓*	No
^{233}U-Zr	✓	No	No	No	one exp.	No

* Exponential experiments only. No un-zoned or poisoned critical lattices.

The criticality data compiled in this document are presented in two sections, one on geometrically simple systems and one on lattices. The geometrically simple systems include homogeneous solutions and metal spheres (and would include hydrogenous compacts if they had been investigated). Each of these sections has a brief introduction summarizing the extent of the information contained and further identifying information of criticality significance which is not present in the literature. Descriptions of the individual experiments follow these discussions.

CRITICAL EXPERIMENTS WITH GEOMETRICALLY SIMPLE SYSTEMS

This section contains data from experiments using aqueous solutions of uranium highly enriched in ^{233}U.[1, 2, 3, 4, 5, 6, 7, 8] This is followed by data from spheres of highly enriched ^{233}U metal.[9, 10, 11, 12]

Data are not compiled for either ^{235}U or ^{239}Pu in any form, because of the large amount of such data, and its ready availability in the literature. The reader desiring such information is referred to the extensive annotated bibliography by Paxton.[13]

No criticality data exist for simple systems containing thorium. Consequently they are not found in this section. The total absence of such data indicates the need for benchmark experiments, to allow verification of calculations assessing the nuclear safety of equipment designed to reprocess thorium-based fuels.

The characteristics of the experiments compiled in this section are summarized in Table 3. Examination of this table shows that no solution experiments have been performed with $H/^{233}U < 34$. In fact, the lowest value of $H/^{233}U$ for which criticality was actually achieved was 45 (excluding the metal systems). The importance of filling this gap in the existing data lies in the fact that calculations indicate that the minimum critical radii of spheres and cylinders of UO_2F_2 occur for an $H/^{233}U$ ratio near 40.[14] Benchmark experiments in this low moderation range are needed to validate calculations of minimum critical radii.

As is seen in Table 3, four experiments have been performed with the soluble poison boric acid present. However, the $H/^{233}U$ range covered is only from 1300 to 1500, and the boron concentration in no case exceeds 0.1 g/ℓ.

Validation of analyses predicting the minimum safe size of poisoned systems will require data at much lower $H/^{233}U$ ratios, and over a range of values. No criticality data exist for ^{233}U solutions poisoned with gadolinium (which may be more effective than boron at low fissile concentrations), or on mixtures of B and Gd (which may be more effective than either when both high and low fissile concentrations are considered).

Table 3. Summary of Critical Experiments with ^{1}H-Moderated ^{233}U in Geometrically Simple Systems

Reference	Form[a]	Geometry[b]	Reflector[c]	Number of Experiments	$H/^{233}U$ Ratio
1	N	S	W	1	405
1	N	C	W	1	514
1	N	C	P	28	42 - 757
1	F	S	-, W	5	381 - 663
1	F	C	-, W	2	158
1	F	C	P	18	34 - 775
2	N	S	-	2	1533 - 1986
2	N	C	-	4	1820 - 2106
2	N + B	S	-	4	1324 - 1470
4	N	S	-, W	7	73 - 581
4	N	C	-	12	73 - 581
4	N	C	W	7	194 - 548
5	F	S	W	8	378 - 663
5	F	S	-	1	381
7	F	C	-,W	10	254 - 854
8	N	C	-	22	∿150 - 1000
8	N	C	W	15	∿120 - 700
9-12	M	S	-, ^{235}U, U(N), Be, W	11	0

a. N = $UO_2(NO_3)_2$; F = UO_2F_2; N + B = $UO_2(NO_3)_2 + HBO_3$; M = Metal

b. S = Sphere; C = Cylinder

c. U(N) = Natural U; W = Alloy, 91.3 w/o tungsten; P = Paraffin; Unreflected experiments are indicated by -

ORNL-2143: $^{233}UO_2(NO_3)_2$ & $^{233}UO_2F_2$, 34 < H/U < 780 (Reference 1)

The largest number of experiments is reported in this document: 31 criticals and 24 extrapolations to critical. Experiments were performed with uranyl nitrate and with uranyl oxyfluoride solutions, in cylindrical and spherical geometry. Most of the cylinder experiments were reflected by paraffin. The sphere experiments, plus a few of the cylinder experiments, were either water reflected or bare. These experiments covered the range of $H/^{233}U$ from 34 to 775, although the lowest $H/^{233}U$ for which criticality was achieved was 45.

The critical parameters of the nitrate and fluoride solutions are given in "Tables B-1 and B-2" respectively. Values in parenthesis indicate that criticality was not achieved. They were derived by extrapolation of curves of neutron multiplication values for subcritical assemblies. The reader's attention is called to footnote c of "Table B-2" which indicates limits of accuracy associated with these results. Additional discussion of accuracy is reproduced after the tables.

The compositions of solutions for which critical parameters are reported are listed in Table A-1. Note that the nitrate solutions contained some excess acid, so that $N/^{233}U = 2.66$. Isotopic composition and impurties are listed in "Tables A-2 and A-3."

The solutions were contained in vessels made of 3S aluminum. The wall thickness of the vessels was not specified. Cylinder height for cylinders having diameters less than 6.7 in. was 36 in. Cylinders having diameters from 6.7 to 12 in. were approximately equilateral. The cylinders of larger diameter and the spheres were mounted in an outer cylinder of sufficient capacity to provide an effectively infinite water or paraffin neutron reflector

completely surrounding the vessel under study. (Neoprene gaskets were used to seal the cylinder tops.) The smaller diameter cylinders had reflectors on the sides and bottom but not on the top.

A discussion from the source document of the accuracy of the measurements is also reproduced. It is followed by a graphical presentation of the results in "Figures 4, 5 and 6."

Appendix B

TABULATIONS OF CRITICAL DATA

Table B-1. Critical Parameters of Uranyl Nitrate Solutions (Ref. 1)

(Numbers in parentheses represent extrapolated values derived from source neutron multiplication curves of subcritical assemblies.)

H:U^{233} Atomic Ratio[a]	Reflector	Critical Parameters: Height (cm)	Volume (liters)	Mass (kg of U^{233})	Maximum Values of Subcritical Assemblies: Height (cm)	Volume (liters)	Mass (kg of U^{233})
Cylinder 12.7 cm (5.0 in.) in Diameter[b]							
57.5	Paraffin	c			51	6.40	2.11
67.0	"	c			59	7.40	2.49
84.4	"	c			61	7.65	2.10
145	"	c			55	6.90	1.15
Cylinder 15.1 cm (6.0 in.) in Diameter[b]							
57.5	Paraffin	27.9	5.00	1.91			
67.0	"	29.0	5.20	1.75			
84.4	"	30.7	5.50	1.51			
120	"	(38.5 ± 0.5)	(6.9 ± 0.1)	(1.37 ± 0.02)	36.8	6.60	1.30
151	"	(46.8 ± 0.5)	(8.4 ± 0.1)	(1.34 ± 0.02)	45.4	8.15	1.31
193	"	(73 ± 2)	(13.0 ± 0.4)	(1.65 ± 0.08)	55.4	9.80	1.24
Cylinder 19.1 cm (7.5 in.) in Diameter							
57.5	Paraffin	16.3	4.65	1.77			
67.0	"	16.2	4.60	1.55			
145	"	18.6	5.30	0.89			
Cylinder 20.5 cm (8.0 in.) in Diameter							
42.2	Paraffin	(16.1 ± 0.2)	(5.30 ± 0.06)	(2.6 ± 0.03)	14.0	4.60	2.25
57.5	"	14.4	4.75	1.81			
84.4	"	14.7	4.85	1.33			
120	"	16.4	5.40	1.07			
145	"	16.7	5.51	0.92			
151	"	16.7	5.51	0.88			
193	"	18.8	6.20	0.79			
213	"	19.3	6.37	0.75			
247	"	(21.2 ± 0.3)	(7.0 ± 0.1)	(0.70 ± 0.01)	19.9	6.56	0.66
Cylinder 21.5 cm (8.5 in.) in Diameter							
247	Paraffin	19.4	7.00	0.70			
297	"	21.5	7.78	0.65			
Cylinder 22.9 cm (9.0 in.) in Diameter							
356	Paraffin	21.3	8.75	0.62			
379	"	22.9	9.39	0.62			
Cylinder 25.5 cm (10.0 in.) in Diameter							
394	Paraffin	19.3	9.82	0.63			
461	"	22.5	11.45	0.63			
514	"	(25.2 ± 0.1)	(12.9 ± 0.05)	(0.63 ± 0.03)	25.1	12.77	0.63
514	Water	(25.5 ± 0.1)	(13.0 ± 0.05)	(0.64 ± 0.03)	25.1	12.77	0.63
Cylinder 30.5 cm (12.0 in.) in Diameter							
582	Paraffin	21.1	15.40	0.68			
630	"	23.8	17.40	0.70			
757	"	30.4	22.20	0.75			
Sphere 26.6 cm (10.4 in.) in Diameter							
405	Water	Full	9.66	0.60			

a. The compositions of the solutions are given in Appendix A.

b. No reflector on the top surface.

c. Apparently this assembly cannot be made critical at any height.

Table B-2. Critical Parameters of Uranyl Fluoride Solutions (Ref. 1)

(Numbers in parentheses represent extrapolated values derived from source neutron multiplication curves for subcritical assemblies.)

$H:U^{233}$ Atomic Ratio[a]	Reflector	Critical Parameters			Maximum Values of Subcritical Assemblies		
		Height (cm)	Volume (liters)	Mass (kg of U^{233})	Height (cm)	Volume (liters)	Mass (kg of U^{233})
			Cylinder 11.2 cm (4.5 in.) in Diameter[b,c]				
34.2	Paraffin	d			29.9	2.95	2.02
39.4	"	d			34.9	3.43	2.07
45.9	"	d			42.6	4.19	2.18
53.7	"	d			49.9	4.82	2.18
74.1	"	d			68.5	6.76	2.24
			Cylinder 12.7 cm (5.0 in.) in Diameter[b]				
34.2	Paraffin	(38 ± 2)	(4.8 ± 0.25)	(3.3 ± 0.2)	23.8	2.99	2.05
39.4	"	(41 ± 2)	(5.1 ± 0.25)	(3.1 ± 0.2)	27.6	3.46	2.08
45.9	"	(41 ± 1)	(5.2 ± 0.1)	(2.7 ± 0.1)	32.4	4.07	2.11
74.1	"	(56.5 ± 0.5)	(7.1 ± 0.06)	(2.36 ± 0.02)	53.3	6.70	2.22
			Cylinder 13.7 cm (5.4 in.) in Diameter[b,c]				
74.1	Paraffin	(48.7 ± 0.5)	(7.13 ± 0.06)	(2.37 ± 0.02)	46.3	6.77	2.25
			Cylinder 15.1 cm (6.0 in.) in Diameter[b,c]				
74.1	Paraffin	24.0	4.31	1.43			
			Cylinder 16.7 cm (6.6 in.) in Diameter[c]				
34.2	Paraffin	(20 ± 1)	(4.4 ± 0.2)	(3.0 ± 0.15)	13.5	2.94	2.01
39.4	"	(16.7 ± 0.2)	(3.66 ± 0.04)	(2.20 ± 0.03)	16.3	3.55	2.13
45.2	"	(17.4 ± 0.2)	(3.79 ± 0.04)	(2.01 ± 0.03)	16.9	3.69	1.96
45.9	"	16.9	3.67	1.91			
47.9	"	(17.7 ± 0.2)	(3.85 ± 0.04)	(1.94 ± 0.03)	16.9	3.69	1.86
53.7	"	(18.0 ± 0.3)	(3.93 ± 0.06)	(1.77 ± 0.03)	16.9	3.69	1.66
74.1	"	(19.1 ± 0.4)	(4.15 ± 0.09)	(1.38 ± 0.04)	16.9	3.69	1.23
			Cylinder 19.1 cm (7.5 in.) in Diameter				
154	Paraffin	18.4	5.25	0.87			
			Cylinder 20.5 cm (8.0 in.) in Diameter				
250	Paraffin	(20.2 ± 0.05)	(6.66 ± 0.02)	(0.68 ± 0.02)	20.1	6.63	0.68
			Cylinder 21.5 cm (8.5 in.) in Diameter				
329	Paraffin	(22.2 ± 0.1)	(8.04 ± 0.04)	(0.63 ± 0.05)	21.6	7.80	0.61
			Cylinder 22.9 cm (9.0 in.) in Diameter				
396	Paraffin	(23.1 ± 0.1)	(9.47 ± 0.04)	(0.61 ± 0.05)	22.6	9.26	0.60
			Cylinder 25.5 cm (10.0 in.) in Diameter				
522	Water	(25.9 ± 0.1)	(13.18 ± 0.05)	(0.65 ± 0.05)	25.6	13.05	0.64
154	None	(24.0 ± 0.05)	(12.22 ± 0.03)	(2.02 ± 0.05)	23.8	12.15	2.01
			Cylinder 30.5 cm (12.0 in.) in Diameter				
775	Paraffin	30.5	22.28	0.74			
			Sphere 26.6 cm (10.4 in.) in Diameter				
426	Water		(9.80 ± 0.10)	(0.59 ± 0.06)	Full	9.66	0.58
419	"	e	9.62	0.59			
390	"	f	9.28	0.61			
			Sphere 31.9 cm (12.6 in.) in Diameter				
663	Water	Full	17.02	0.66			
381	None	e	16.98	1.14			

a. The compositions of the solutions are given in Appendix A.
b. No reflector on the top surface.
c. Vessels coated with Unichrome; masses about 2% high because of impurities.
d. Apparently this assembly cannot be made critical at any height with the absence of a top reflector and the presence of Unichrome.
e. There was a 40-cm^3 void above the critical solution.
f. There was a 380-cm^3 void above the critical solution.

Appendix A

COMPOSITION OF URANIUM SOLUTIONS

Table A-1. U^{233} Concentrations in Solutions (Ref. 1)

$H:U^{233}$ Atomic Ratio	Solution Density (g/cc)	U^{233} Concentration	
		g per g of Solution	g per cc of Solution
In $UO_2(NO_3)_2$ Solution with $N:U^{233}$ = 2.66			
42.2	1.697	0.289	0.490
57.5	1.543	0.247	0.381
67.0	1.480	0.227	0.336
84.4	1.394	0.197	0.275
120	1.287	0.154	0.198
145	1.238	0.135	0.167
151	1.232	0.130	0.160
193	1.185	0.107	0.127
213	1.165	0.100	0.117
247	1.145	0.088	0.101
297	1.121	0.075	0.084
356	1.101	0.064	0.070
379	1.093	0.061	0.067
394	1.090	0.058	0.063
405	1.087	0.057	0.062
461	1.077	0.051	0.055
514	1.069	0.046	0.049
582	1.061	0.041	0.044
630	1.056	0.038	0.040
757	1.046	0.032	0.033
In UO_2F_2 Solution			
34.2	1.801	0.380	0.684
39.4	1.707	0.352	0.600
45.2	1.625	0.327	0.531
45.9	1.604	0.324	0.519
47.9	1.592	0.316	0.503
53.7	1.530	0.295	0.451
74.1	1.388	0.239	0.332
153	1.199	0.138	0.165
154	1.198	0.138	0.165
250	1.121	0.091	0.102
329	1.090	0.071	0.078
381	1.079	0.062	0.067
390	1.076	0.061	0.066
396	1.075	0.060	0.065
419	1.071	0.057	0.061
426	1.070	0.056	0.060
522	1.059	0.047	0.049
663	1.043	0.037	0.039
775	1.035	0.032	0.033

Table A-2. Isotopic Composition of Uranium in Solutions (Ref. 1)

Isotope	wt% In $UO_2(NO_3)_2$ Solution	wt% In UO_2F_2 Solution
U^{233}	98.7	98.7
U^{234}	0.50	0.54
U^{235}	0.01	0.04
U^{238}	0.79	0.72

Table A-3. Principal Impurities* in Solutions

Element	ppm In $UO_2(NO_3)_2$ Solution		ppm In UO_2F_2 Solution	
	Before Use	After Use	Before Use	After Use
Al	15	50	400	8000
Ca	300	1500		
Cr	10	15	8	250
Fe	20	300	40	2500
Mg	10	125	0	55
Mo			0	200
Na			650	100
Ni	20	70	0	250
Sn			0	225
Th	150			

* Determined by spectrographic analysis.

III. ACCURACY OF THE MEASUREMENTS (Ref. 1)

The results of these experiments are subject to the usual errors in uranium analyses and solution densities and in the calibration of the vessel capacities, all estimated to be ±0.5%. There are, however, two additional sources of error which broaden the uncertainty. In the experiments in which uranyl nitrate solutions were used the indirect method of measuring the height, and hence the volume, of the solution in the vessels makes the results less certain than those from later experiments with uranyl fluoride in which the position of the liquid surface was measured directly.

An error in the experiments with the uranyl fluoride solutions is a bias resulting from the properties of a corrosion-inhibiting coating material with which one spherical and three cylindrical vessels were lined. This coating was a polyvinyl chloride plastic, Unichrome, which is about 30 wt% chlorine. It is difficult to evaluate the increase in critical mass due to the absorption of neutrons by the chlorine because the effect is a function of geometry. It is noted in Table B-1, however, that the critical volume at a particular concentration ($H:U^{233} = 74.1$) in a 14-cm-dia cylinder lined with Unichrome is about the same as that in a 12.7-cm-dia cylinder lined with a phenol base plastic, Heresite, whereas it would be expected to be somewhat less. After the discovery of the chlorine impurity, one definitive experiment was performed to determine the effect of a Unichrome liner on the critical concentration of a U^{235} uranyl fluoride solution in a sphere 32 cm in diameter. A 2% decrease in the concentration was observed upon removal of the Unichrome.

In summarizing the question of accuracy, it is believed that the results from critical experiments with uranyl fluoride in Heresite-lined vessels are good to ±1%; data from the same vessels with uranyl nitrate have an uncertainty of no more than ±3%. The critical mass measured in the 32-cm-dia sphere is high by about 2% because of a bias. The masses in the 14- and 17-cm-dia cylinders are too high by an amount not well known but probably less than 10%.

Extrapolations have been made of the source neutron multiplication curves obtained in those tests which could not be made critical because of inventory or geometric limitations. The critical parameters obtained in this manner are given in the tabulated results with the maxima from which the extrapolations were made. The accuracy of these values is strongly dependent upon the length of the extrapolation.

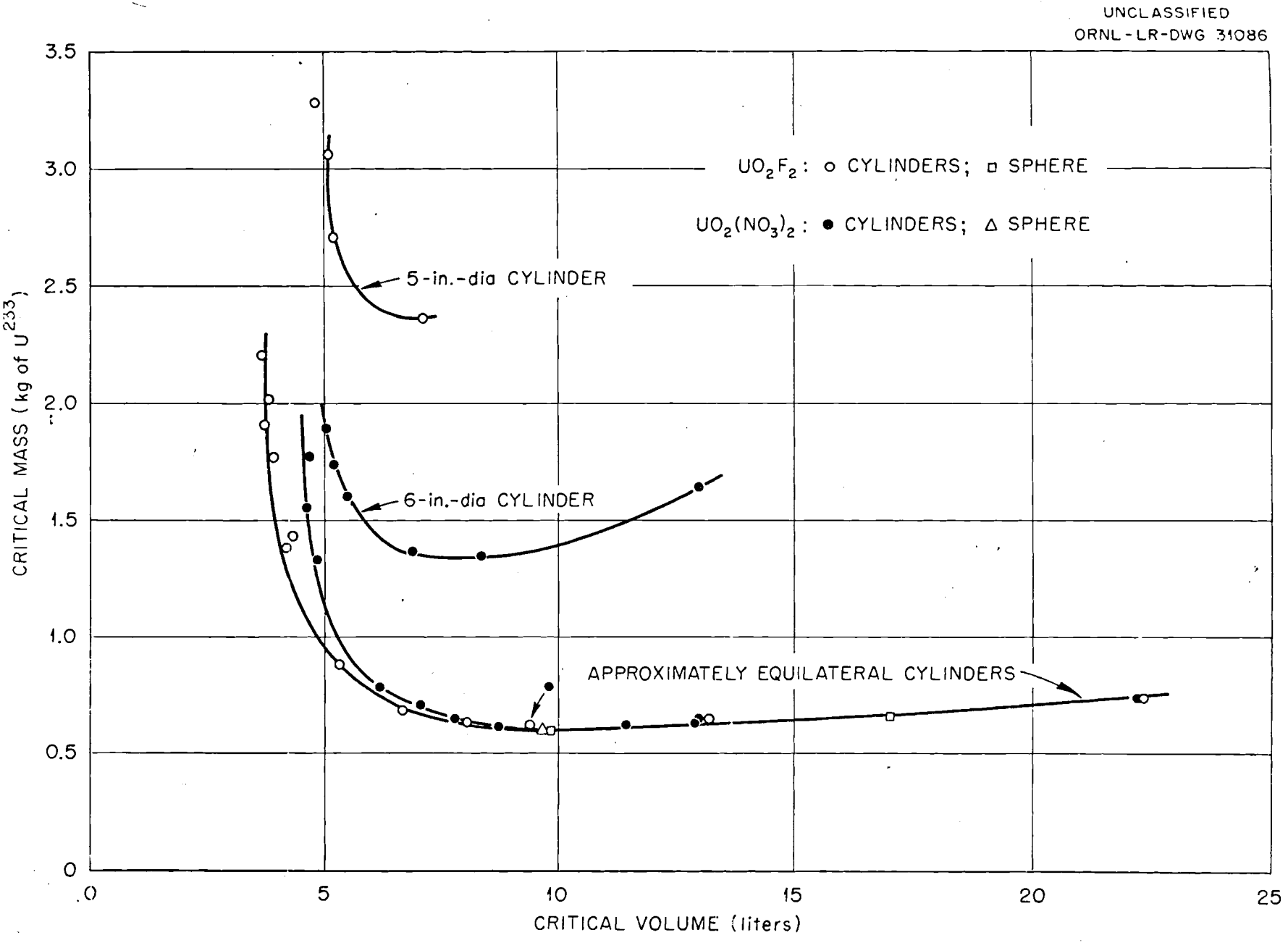

Fig. 4. Critical Mass as a Function of Critical Volume of Reflected Vessels Containing Aqueous Solutions of U^{233}. (Ref. 1)

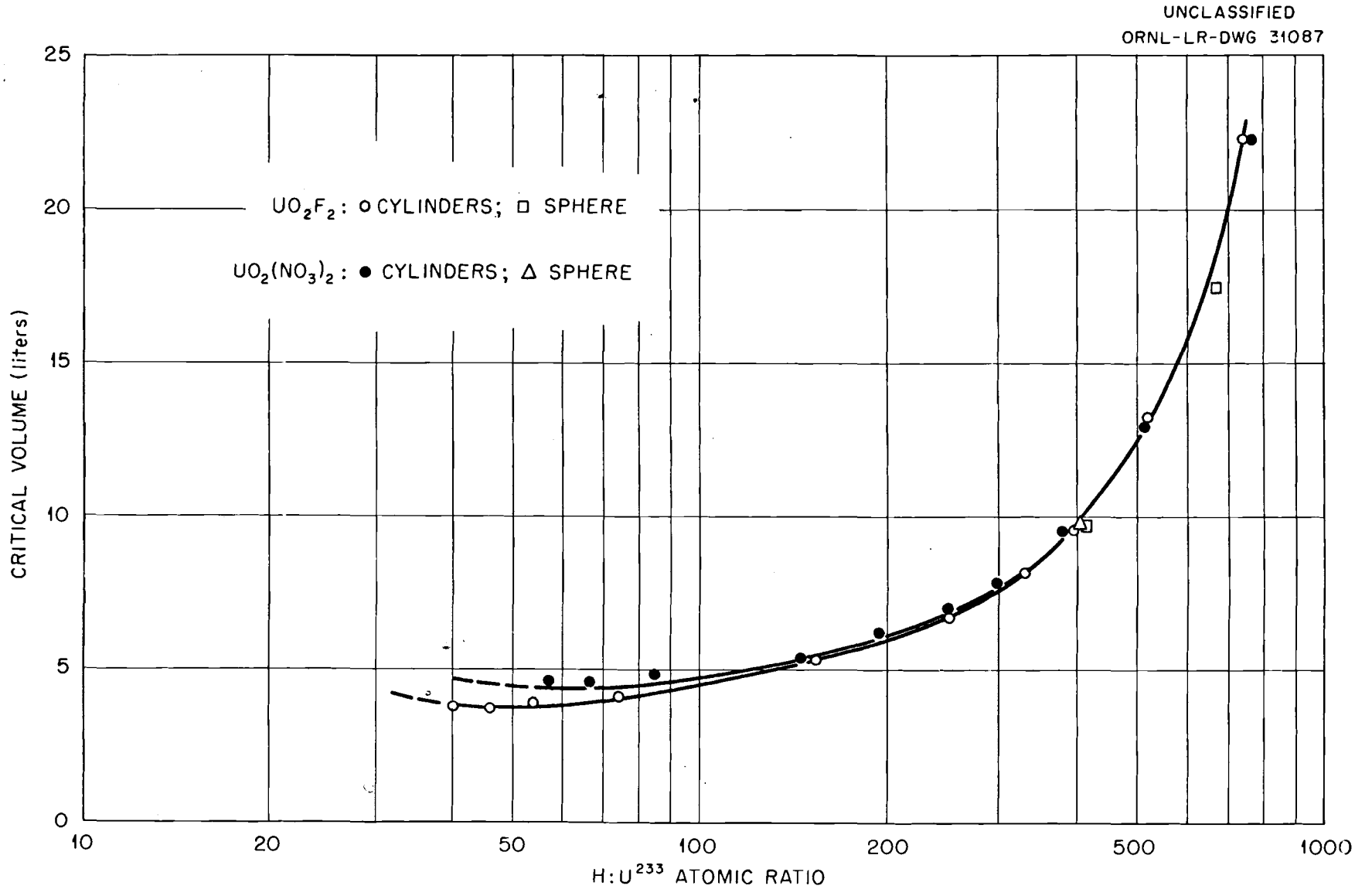

Fig. 5. Critical Volume as a Function of the H:U^{233} Atomic Ratios of Solutions Contained in Reflected Equilateral Cylinders and Spheres (Ref. 1)

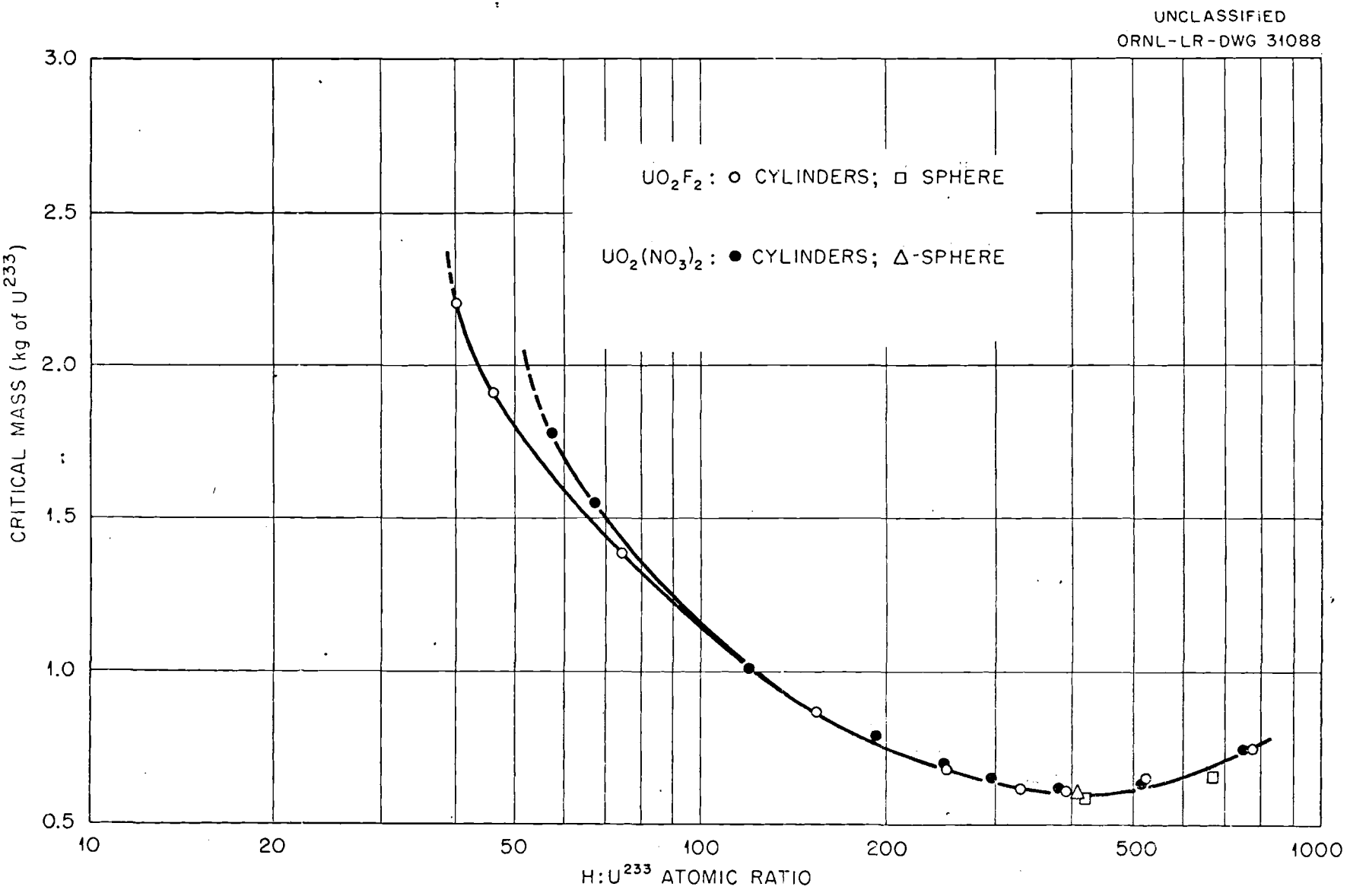

Fig. 6. Critical Mass as a Function of the H:U^{233} Atomic Ratios of Solutions Contained in Reflected Equilateral Cylinders and Spheres (Ref. 1)

Gwin and Magnuson: $^{233}UO_2(NO_3)_2$ 1320 < H/U < 2100 (Reference 2, 3)

The critical systems from which data were obtained in these experiments consisted of aqueous solutions of uranyl nitrate enriched in either the U^{233} or the U^{235} isotope. A 27.24-in.-diam aluminum sphere was made critical with both unpoisoned and several boric acid poisoned solutions of both isotopes. A 48.04-in.-diam aluminum sphere was used only with unpoisoned solutions of U^{233} and U^{235}. A 5-ft-diam stainless steel cylinder, the diameter having been chosen to minimize the buckling for the available amount of U^{233}, was made critical at several heights with both U^{233} and U^{235}. The concluding experiments were performed with U^{235} solutions in a 9-ft-diam steel cylinder. At the maximum critical height in this container the neutron leakage was less than 2% .

The experimental data for the critical spheres and cylinders are summarized in "Tables IX and X." In "Table IX," experiments 1 - 9 were performed in the 27.24 in. diameter Al sphere. Atom densities are listed in "Table XI."

TABLE IX (Ref. 2)

EXPERIMENTAL DATA FOR CRITICAL CONDITIONS OF SPHERES

Experiment number	Isotopic composition (wt.%)					Solution density (gm/ml)	Total uranium (mg/gm)	Total boron (mg/gm)	Total nitrate (mg/gm)	Total thorium (mg/gm)	$(k-1) \times 10^4$ at 20°C
	U^{233}	U^{234}	U^{235}	U^{236}	U^{238}						
1	0.00	1.04	93.18	0.27	5.51	1.0288	19.56	0.00	18.7	0.00	11.8
2	0.00	1.04	93.18	0.27	5.51	1.0333	22.77	0.0905	21.2	0.00	7.3
3	0.00	1.04	93.18	0.27	5.51	1.0387	25.77	0.18	23.7	0.00	9.0
4	0.00	1.04	93.18	0.27	5.51	1.0445	27.24	0.22	25.1	0.00	2.8
5	97.70	1.62	0.04	0.00	0.64	1.0226	16.76	0.00	11.9	0.074	5.0
6	97.70	1.62	0.04	0.00	0.64	1.0253	17.42	0.0233	12.3	0.077	10.3
7	97.70	1.62	0.04	0.00	0.64	1.0274	18.03	0.0453	12.8	0.080	10.9
8	97.70	1.62	0.04	0.00	0.64	1.0275	18.67	0.0670	13.2	0.083	3.3
9	97.70	1.62	0.04	0.00	0.64	1.0286	19.27	0.0887	13.6	0.085	4.4
48.04-in.-diam aluminum sphere											
10	0.01	1.05	93.21	0.54	5.19	1.0216	14.82	0.00	11.3	0.00	12.9
11	97.67	1.54	0.03	0.00	0.76	1.0153	13.05	0.00	7.6	0.056	4.6

TABLE X (Ref. 2)

EXPERIMENTAL DATA FOR CRITICAL CONDITIONS OF CYLINDERS

Experiment number	Critical[a] solution height (in.)	Isotopic composition (wt. %) U^{233}	U^{234}	U^{235}	U^{236}	U^{238}	Solution density (gm/ml)	Total uranium (mg/gm)	Total nitrate (mg/gm)	Total thorium (mg/gm)
60.92-in.-diam cylinder										
12	18.31	0.00	1.05	93.22	0.55	5.18	1.0229	16.92	12.8	0.00
13	19.20	0.00	1.03	93.03	0.51	5.43	1.0247	16.61	14.2	0.00
14	29.23	0.00	1.04	93.12	0.54	5.30	1.0209	14.96	12.0	0.00
15	42.06	0.00	1.06	93.11	0.52	5.31	1.0204	14.31	12.2	0.00
16	80.68	0.00	1.06	93.01	0.52	5.41	1.0197	13.79	12.6	0.00
17	20.02	97.37	1.50	0.04	0.00	1.09	1.0203	14.21	8.3	0.014
18	23.85	97.35	1.52	0.05	0.00	1.08	1.0198	13.62	8.6	0.012
19	31.12	97.30	1.49	0.05	0.00	1.16	1.0169	13.00	8.1	0.014
20	55.18	97.25	1.55	0.05	0.00	1.16	1.0166	12.33	8.1	0.098
107.7-in.-diam cylinder										
21	35.8	0.00	1.08	92.79	0.66	5.47	1.0194	14.00	14.2	0.00
22	47.0	0.00	1.06	92.78	0.65	5.51	1.0218	13.66	13.8	0.00
23	94.9	0.00	1.05	92.82	0.63	5.50	1.0210	13.33	13.5	0.00

[a] In the 60.92-in.-diam cylinder critical height values include a correction of 0.53 in. for the bottom structure. In the 107.7-in.-diam cylinder no correction has been included for the effects of structure.

TABLE XI (Ref. 2)

ATOM DENSITIES $\times 10^{-20}$ FOR THE CRITICAL EXPERIMENTS (CM^{-3})

Experiment number	Uranium Isotope U^{233}	U^{234}	U^{235}	U^{236}	U^{238}	N	H	B	H/X
27.24-in.-diam sphere									
1		0.00538	0.48066	0.00138	0.02807	1.869	662.28		1378
2		0.00631	0.56206	0.00163	0.03281	2.129	661.48	0.052	1177
3		0.00716	0.63944	0.00184	0.03734	2.392	660.70	0.104	1033
4		0.00762	0.67959	0.00197	0.03967	2.548	660.28	0.128	972
5	0.43284	0.00716	0.00018		0.00281	1.178	663.60		1533
6	0.45120	0.00744	0.00018		0.00291	1.224	663.45	0.0133	1470
7	0.46798	0.00772	0.00018		0.00301	1.274	663.29	0.0259	1417
8	0.48455	0.00801	0.00021		0.00311	1.319	663.15	0.0383	1368
9	0.50066	0.00827	0.00021		0.00327	1.363	663.00	0.0508	1324
48.04-in.-diam sphere									
10		0.00409	0.36185	0.00220	0.01985	1.116	663.94		1835
11	0.33460	0.00525	0.00010		0.00256	0.753	664.67		1986
60.92-in.-diam cylinder									
12		0.00469	0.41364	0.00243	0.02271	1.272	663.45		1604
13		0.00451	0.40595	0.00222	0.02339	1.409	663.43		1634
14		0.00409	0.36452	0.00209	0.02048	1.185	663.83		1821
15		0.00397	0.34845	0.00194	0.01962	1.208	663.89		1905
16		0.00384	0.33519	0.00186	0.01924	1.244	663.91		1981
17	0.36498	0.00556	0.00019		0.00410	0.826	664.39		1819
18	0.34960	0.00525	0.00018		0.00395	0.849	664.44		1900
19	0.33275	0.00507	0.00017		0.00375	0.802	664.59		1996
20	0.31556	0.00481	0.00016		0.00354	0.795	664.70		2106
107.7-in.-diam cylinder									
21		0.00397	0.33940	0.00240	0.01975	1.407	663.67		1955
22		0.00381	0.33124	0.00232	0.01942	1.367	663.74		2004
23		0.00368	0.32347	0.00220	0.01894	1.338	663.85		2052

Additional information useful for calculations of these experiments is published in Ref. 3, which is an analysis of the data. It is noted that the spherical containers were made from Type 1100 aluminum, with thicknesses of 0.13 and 0.30 inches for the 27.24 and 48.04 in. diameter vessels respectively.

Atom densities for oxygen, thorium and ^{10}B are calculated and listed in "Tables I and II." It is assumed that the ^{10}B content in natural boron is 19.78%, and that the solutions are made up of

1) H_2O
2) $UO_2(NO_3)_2 \cdot 6H_2O$,
3) HNO_3,
4) H_3BO_4, and
5) $Th(NO_3)_4 .4H_2O$ so that $n(O)$ is given by

so that

$$n(O) = \tfrac{1}{2}\, n(H) + \tfrac{5}{2}\, n(B) + 3n(U) + \tfrac{5}{2}\, n(N) + 2n(Th) \ .$$

TABLE I (Ref. 3)

Nuclear Number Densities (in units of $10^{24}/cm^3$) for ^{235}U Fueled Spheres

	Experiment Number				
	1	2	3	4	10
	Sphere Diameter (in.)				
	27.24	27.24	27.24	27.24	48.04
^{10}B	0.0	1.0286×10^{-6}	2.0571×10^{-6}	2.5318×10^{-6}	0.0
H	0.066228	0.066148	0.066070	0.066028	0.066394
O	0.033736	0.033800	0.033865	0.033902	0.033592
N	1.869×10^{-4}	2.129×10^{-4}	2.392×10^{-4}	2.548×10^{-4}	1.116×10^{-4}
^{234}U	5.38×10^{-7}	6.31×10^{-7}	7.16×10^{-7}	7.62×10^{-7}	4.09×10^{-7}
^{235}U	4.8066×10^{-5}	5.6206×10^{-5}	6.3944×10^{-5}	6.7959×10^{-5}	3.6185×10^{-5}
^{236}U	1.38×10^{-7}	1.63×10^{-7}	1.84×10^{-7}	1.97×10^{-7}	2.20×10^{-7}
^{238}U	2.807×10^{-6}	3.281×10^{-6}	3.734×10^{-6}	3.967×10^{-6}	1.985×10^{-6}

TABLE II (Ref. 3)

Nuclear Number Densities (in units of $10^{24}/cm^3$) for ^{233}U Fueled Spheres

	Experiment Number					
	5	6	7	8	9	11
	Sphere Diameter (in.)					
	27.24	27.24	27.24	27.24	27.24	48.04
^{10}B	0.0	2.6307×10^{-7}	5.1230×10^{-7}	7.5757×10^{-7}	1.0048×10^{-6}	0.0
H	0.066360	0.066345	0.066329	0.066315	0.066300	0.066467
O	0.033607	0.033620	0.033633	0.033646	0.033657	0.033525
N	1.178×10^{-4}	1.224×10^{-4}	1.274×10^{-4}	1.319×10^{-4}	1.363×10^{-4}	7.530×10^{-5}
^{233}U	4.328×10^{-5}	4.5120×10^{-5}	4.6798×10^{-5}	4.8455×10^{-5}	5.0066×10^{-5}	3.3460×10^{-5}
^{234}U	7.16×10^{-7}	7.44×10^{-7}	7.72×10^{-7}	8.01×10^{-7}	8.27×10^{-7}	5.25×10^{-7}
^{235}U	1.8×10^{-8}	1.8×10^{-8}	1.8×10^{-8}	2.1×10^{-8}	2.1×10^{-8}	1.0×10^{-8}
^{238}U	2.81×10^{-7}	2.91×10^{-7}	3.01×10^{-7}	3.11×10^{-7}	3.27×10^{-7}	2.56×10^{-7}
^{232}Th	1.9641×10^{-7}	2.0491×10^{-7}	2.1333×10^{-7}	2.2135×10^{-7}	2.2693×10^{-7}	1.4757×10^{-7}

The analysis includes an assessment of corrections to the neutron multiplication eigenvalue reported in Ref. I due to improved values for delayed neutron yields; reflection by the Al container; fill and drain tubes connected to the spheres; asphericity; and the reflection of escaping neutrons by walls, ceiling and floor of the experimental cell. These corrections are listed in "Table III" along with a "corrected measured" eigenvalue for the solution sphere alone.

TABLE III (Ref. 3)

Measured and Corrected Multiplication Factors λ

Exp No.	Fuel	Diam of Sphere (in.)	Reported Measured λ	Delayed-Neutron Importance, I	Eigenvalue Corrections (In Units of 10^{-4})				Corrected Measured λ
					$(\delta\lambda)_{\beta I}$	$(\delta\lambda)_{Al}$	$(\delta\lambda)_{tubes}$	$(\delta\lambda)_{room\ return}$	
1	^{235}U	27.24	1.00118	1.1059	1.5	-7.2	-0.7	-2.8	1.00026
2	^{235}U	27.24	1.00073	1.1060	0.9	-7.2	-0.7	-2.8	0.99975
3	^{235}U	27.24	1.00090	1.1059	1.1	-7.2	-0.7	-2.8	0.99994
4	^{235}U	27.24	1.00028	1.1044	0.3	-7.2	-0.7	-2.8	0.99924
10	^{235}U	48.04	1.00129	1.0402	0.7	-6.9	-0.2	-3.4	1.00031
5	^{233}U	27.24	1.00050	1.1062	0.6	-7.2	-0.7	-2.8	0.99949
6	^{233}U	27.24	1.00103	1.1056	1.3	-7.2	-0.7	-2.8	1.00009
7	^{233}U	27.24	1.00109	1.1050	1.3	-7.2	-0.7	-2.8	1.00015
8	^{233}U	27.24	1.00033	1.1063	0.4	-7.2	-0.7	-2.8	0.99930
9	^{233}U	27.24	1.00044	1.1055	0.5	-7.2	-0.7	-2.8	0.99942
11	^{233}U	48.04	1.00046	1.0400	0.3	-6.9	-0.2	-3.4	0.99944

ORNL-4280: $^{233}UO_2(NO_3)_2$, 70 < H/U < 580 (Reference 4)

The discussion of these experiments presented in the source document is extremely terse. In one page it covers the homogeneous experiments of interest here, plus raschig ring poisoned and array experiments as well. Portions of interest are reproduced below:

> Presented in Table 2.16.3 are the critical conditions for water-reflected and unreflected spherical and cylindrical volumes of the solution which had a value of k_{eff} of 1.0000 ± 0.0005. A concentration at which a sphere was critical was first established, and then several critical cylindrical volumes were measured. The results for unreflected cylinders have been corrected for the 1.27-cm-thick aluminum base of the container, so the results describe cylindrical volumes having aluminum on the lateral surface only.

Table 2.16.3. Critical Conditions of $^{233}UO_2(NO_3)_2$ Aqueous Solution in Water-Reflected and Unreflected Simple Geometries (Ref. 4)

$UO_2(NO_3)_2$ Solution[a]			Critical Dimensions									
			Spheres		Cylinders[b]							
					50.8-cm diam		38.1-cm diam		25.3-cm diam		20.3-cm diam	
Uranium Concentration (g/liter)	Specific Gravity	H:^{233}U	Radius (cm)	Mass (kg of U)	Height (cm)	Mass (kg of U)	Height (cm)	Mass (kg of U)	Height (cm)	Mass (kg of U)	Height (cm)	Mass (kg of U)
Unreflected Assemblies												
333	1.468	73			13.36	9.02						
204	1.280	122			13.51	5.59	15.14	3.52	24.69	2.53		
131	1.183	195	14.579	1.70	14.07	3.74	16.35	2.44	28.52	1.88		
102	1.144	253	15.078	1.46			17.60	2.05	33.40	1.71		
74.6	1.106	349	15.821	1.24			19.35	1.65	43.69	1.64		
44.6	1.050	581	18.378	1.16			26.37	1.34				
Water-Reflected Assemblies[c]												
132	1.186	194	11.170	0.769			13.42	1.77	17.22	1.14	22.86	0.976
95.0	1.135	273	11.847	0.662			*d*	*d*	19.67	0.939	20.02	0.824
47.9	1.068	548	14.579	0.621			19.6	1.07	31.53	0.757	*d*	*d*

[a] See Table 2.16.1 for isotopic content of the uranium.

[b] Aluminum cylinders had a 1.5-mm-thick wall and 1.27-cm-thick bottom. Spheres were of aluminum with 1.22-mm-thick wall.

[c] There was no reflector on the top of any cylinder. The surface of the reflector water was 24.3 cm above the solution, a distance equal to the bottom reflector thickness.

[d] There was insufficient solution inventory to achieve criticality; the maximum solution height was 12.5 cm in the 38.1-cm-diam cylinder and 68.2 cm in the 20.3-cm-diam cylinder.

The isotopic content of the uranium used is given in the following table:

Isotopic content of uranium (%)	
^{232}U (ppm)	6.47
^{233}U	97.54
^{234}U	1.05
^{235}U	0.03
^{236}U	<0.01
^{238}U	1.39

The document states that, "There were no impurities present in significant quantities." No comment is contained in the document about the presence or absence of excess acid. The article from which this description was extracted is reproduced in full in the last section of this document on "Arrays and Raschig Ring Poisoned Solutions."

Thomas, Fox & Callihan: $^{233}UO_2F_2$, 380 < H/U < 660 (Reference 5, 6)

Criticality was achieved in two water-reflected spherical vessels of diameters 26.4 and 32.0 cm over the temperature range from 20° to 100° C. A single unreflected criticality was also achieved at room temperature in the large vessel.

The remainder of this discussion is reproduced from Ref. 5. No other information is given in either Ref. 5 or 6 from which to calculate number densities of solution isotopes.

SOLUTIONS

Aqueous solutions of uranium oxyfluoride containing predominately the U^{233} and U^{235} isotopes were used in these experiments. The isotopic concentrations were 98.7% U^{233} and about 90% U^{235}. Spectrographic analysis of the solutions and reflector water were made during the experiments and no significant buildup of impurities was observed.

REACTORS

Two spherical reactors having diameters of 26.4 cm and 32.0 cm were fabricated of 3S aluminum 1.27 mm thick. (These diameters are nominal in the sense that they are determined from the calibrated volumes.) To provide 15 cm of water as an effectively infinite neutron reflector, the spheres were mounted in cylinders of appropriate dimensions. The inside surfaces of the spheres were coated with a plastic to prevent excessive corrosion.

Water was used to measure the capacity of the reactors as a function of liquid depth in the temperature range from 20° to 100°C. At 26°C, the volume of the 26.4-cm sphere was 9.660 ± 0.005 liters and that of the 32.0 cm sphere was 17.020 ± 0.005 liters.

METHOD AND RESULTS

The experiments consisted, essentially, of determining the chemical concentrations of the solutions of uranium which were required to make the spherical volumes critical. From these results a comparison can be made of the values of η for the two isotopes. The critical masses of U^{233} and U^{235} in the two spheres as a function of temperature can also be obtained from the concentrations. A brief description of the experimental method and a summary and analysis of the data are presented.

Reflected Reactor Experiments

Experimental Procedure and Data

In a typical experiment the concentration of the solution was adjusted to have the sphere critical when filled and at a particular temperature. The concentration was then increased and the temperature raised to make the sphere again critical when filled. Immediately after the reactor had been critical, duplicate samples of the oxyfluoride solutions were taken. In most cases the analyses of these samples differed by no more than 0.5%.

Table I summarizes the data of the reflected sphere experiments. The atomic ratios, H/U^{233} and H/U^{235}, as functions of temperature for both spheres are presented in Figs. 3 and 4. Figures 5 and 6 illustrate the variation of critical mass with temperature for the two isotopes.

Unreflected Reactor Experiments

Experimental Data

The following are the critical conditions observed for U^{233} and U^{235} uranyl oxyfluoride solutions in the 32.0-cm sphere (17.020 liters volume) at 27.0°C[2] without a water reflector:

U^{233}	gm U^{233}/L (at 25°C):	67.37
	H/U^{233} atomic ratio:	381.0
	Critical mass U^{233}:	1146.0 gm
U^{235}	gm U^{235}/L (at 25°C):	125.18
	H/U^{235} atomic ratio:	203.5
	Critical mass U^{235}:	2128.8 gm

TABLE I (Ref. 5)

CRITICAL CONDITIONS FOR WATER REFLECTED SPHERICAL ALUMINUM VESSELS

Fuel concentration		Temperature (°C)	Volume (L)	Mass of X (gm)
gm X[a]/L (at 25°C)	H/X			
		U^{233} Oxyfluoride Solutions		
26.4-cm diameter sphere				
61.34	418.3	32.0[b]	9.666	591.0
61.89	414.6	39.5	9.675	596.3
64.05	400.5	65.5	9.704	611.0
65.84	389.6	83.2	9.723	623.0
67.80	378.1	96.5	9.737	638.0
32.0-cm diameter sphere[c]				
38.75	663.1	26.3	17.020	659.0
39.97	643.1	56.0	17.042	673.0
42.65	602.8	99.5	17.074	703.0
		U^{235} Oxyfluoride Solutions		
26.4-cm diameter sphere				
95.14	268.8	27.5	9.661	918.3
97.10	263.3	39.5	9.675	935.3
104.09	245.4	74.0	9.713	989.8
106.75	239.3	85.5	9.726	1010.1
32.0-cm diameter sphere[c]				
50.29	515.1	27.0[b]	17.020	855.8
51.50[d]	502.6	43.0	17.032	872.0
51.44[d]	503.4	43.0	17.032	870.8
52.13	496.5	54.0	17.042	879.2
53.07	487.6	64.5	17.049	890.3
54.27[d]	476.8	87.5	17.065	899.6
56.28[d]	459.6	87.5	17.065	932.0

[a] X = U^{233} or U^{235}

[b] In these experiments the vessel was critical with the order of 0.1% of its capacity unfilled and at a temperature 5°C lower than this value. Figure 1 and the capacity of the sphere calibrated over the temperature range were used to obtain this temperature at which the sphere would have been full and critical.

[c] The values of the concentrations and masses measured with this sphere are believed to be about 2% high because of a systematic error.

[d] Duplicate samples.

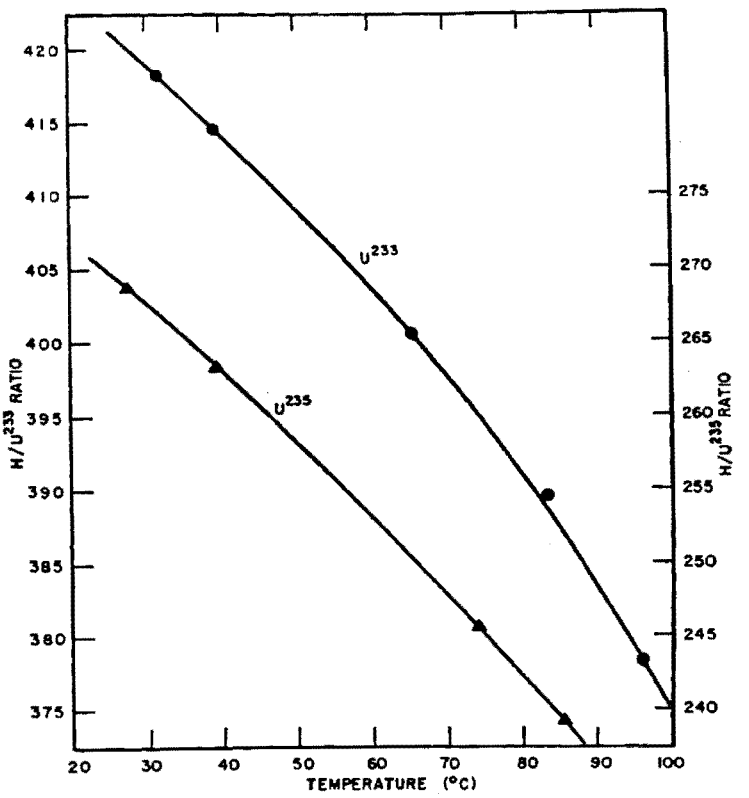

FIG. 3. Ratio of H:U^{233} and H:U^{235} in 26.4 cm diameter water-reflected spherical reactor vs temperature. (Ref. 5)

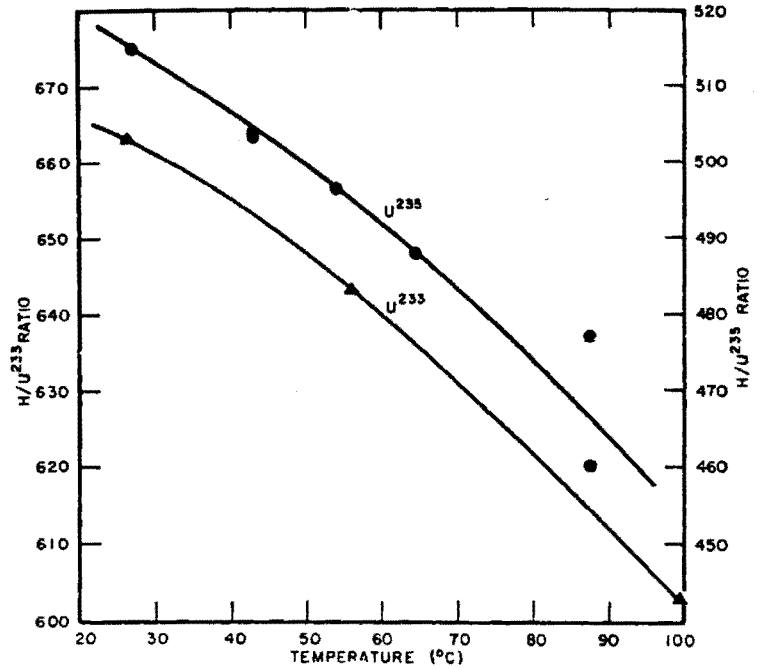

FIG. 4. Ratio of H:U^{233} and H:U^{235} in 32.0 cm diameter water-reflected spherical reactor vs temperature. (Ref. 5)

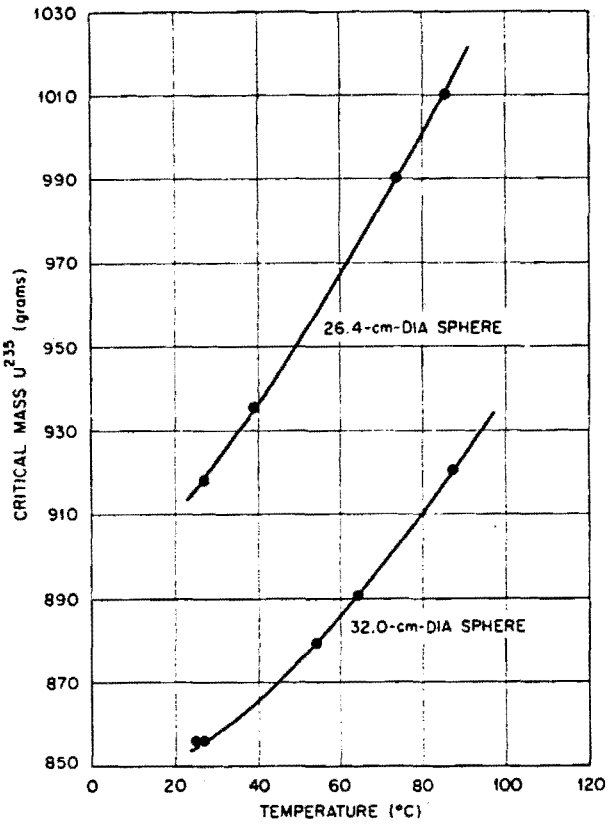

FIG. 5. Critical mass of U^{235} in water-reflected spherical reactors as a function of temperature. (Ref. 5)

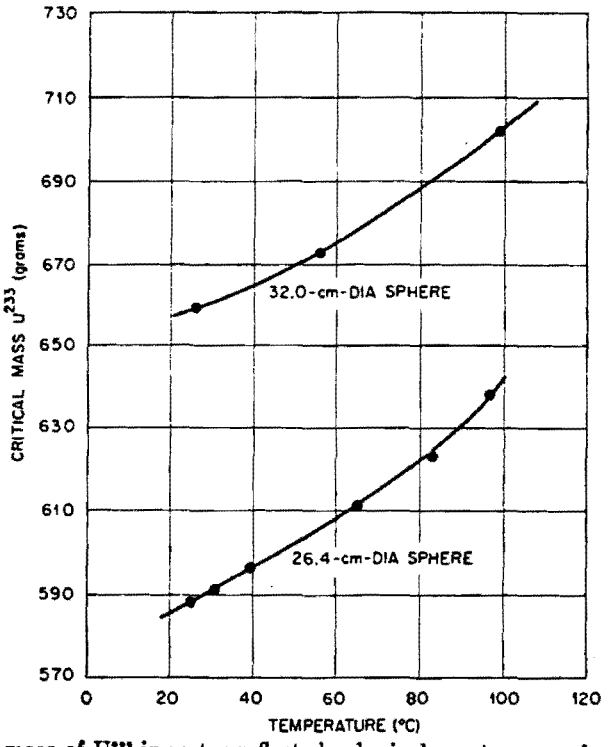

FIG. 6. Critical mass of U^{233} in water-reflected spherical reactors as a function of temperature. (Ref. 5)

AERE R/R 2051: $^{233}UO_2F_2$, 250 < H/U < 850 (Reference 7)

Experiments were performed at room temperature in cylindrical geometry with uranyl oxyfluoride (UO_2F_2) solutions. Both ^{233}U and ^{235}U were used as fissile isotopes, at enrichments of 99.6 wt% and 44.6 wt% respectively. Criticality was not achieved in the measurements reported here, and critical solution heights were obtained from extrapolations of inverse count rate curves.

Fissile solution was contained in a stainless steel cylindrical tank of internal radius 15.24 cm having walls 1/8 in. thick. This tank sat on the bottom of an aluminum tank of diameter 2 ft. 6 in. Experiments were performed with the outer tank empty and with water reflector having the same depth as the fissile solution. "Fast reflection" was also investigated, using a cadmium tube of about 13 in. diameter (thickness unspecified) encircling the core tank, to cut off "all" reflection of thermal neutrons from the water.

A brass walled BF_3 counter (natural boron) of diameter 1/2 in. was positioned within a reentrant tube of radius 0.79 cm located on the axis of the tanks. Four other counters were also located in the reflector water.

The critical parameters derived for the solutions investigated are listed in "Table I."

3.3 Results (Ref. 7)

Measurements made at 15°C - 18°C on aqueous uranyl fluoride (UO_2F_2) solutions in $\frac{1}{8}$in. thick stainless steel cylinders.

TABLE I

OBSERVED CRITICAL DATA

Fissile Isotope	$H/U_{fissile}$ (atomic ratio)	Critical Mass of the Fissile Isotope (grms.)			Critical Height of the Solution (cms.)			Concentration of the solution (mgrms. U per gm. of sol.)	Density of the solution(3)(4) (grms/cc)	Hydrogen Density (atoms/cc ÷ 10^{22})
		Reflected	Fast Reflected	Unreflected	Reflected	Fast Reflected	Unreflected			
Core tank internal radius of 15.24 cms.										
U^{235}	258	1647 ± 11	1759 ± 22	1879 ± 43	23.15±0.15	24.75±0.3	26.45 ± 0.6	175.2	1.247	6.45
U^{235}	493	1264 ± 4	1612 ±188	>2019	33.75±0.1	43 ± 5	> 55	102.9	1.130	6.55
U^{235}	678	1513 ± 6	-	-	55.15±0.2	-	-	77.64	1.096	6.59
U^{233}	253.5	1254 ± 5	1310 ± 16	1445 ± 39	17.10±0.07	17.85±0.2	19.7 ± 0.5	90.14	1.114	6.58
U^{233}	483	917 ± 2	994 ± 12	1217 ± 58	23.81±0.05	25.8 ±0.3	31.6 ± 1.5	50.11	1.060	6.63
U^{233}	769	984 ± 2	1165 ± 86	-	40.58±0.08	48 ± 3	-	32.27	1.037	6.65
U^{233}	854	1093 ± 4	1458 ± 88	-	50.22±0.15	67 ± 4	-	29.16	1.033	6.65
Core tank internal radius of 6.35 cms.										
U^{235}	60	Will not become critical						431.9	1.913	5.63
U^{233}	32.3	>1750	>1750	-	>20	>20	-	392.3	1.785	5.85

Saclay: $^{233}UO_2(NO_3)_2$, 120 < H/U < 1000 (Reference 8)

Experiments were carried out with nitrate solutions of ^{233}U in cylindrical geometry, with and without reflection. Results are presented for a H/U range from 120 to 1000. The results are presented only graphically, on a plot of critical mass vs critical volume. Uncertainty in values read from the graph, due to symbol size and lack of grid lines, makes the results hard to use, however.

Because the H/U range covered in these experiments is covered in other experiments summarized herein, no translation has been performed from the published version (in French). For completeness, the sections describing the experiments and presenting the results are reproduced here.

INTRODUCTION

Les assemblages critiques ALECTO sont destinés à l'étude des conditions critiques de récipients cylindriques contenant des solutions aqueuses de matériau fissile avec et sans réflecteur. Le dispositif critique comporte essentiellement la cuve à essayer dans laquelle on introduit la solution fissile, entourée éventuellement d'un réflecteur d'eau ou d'un réflecteur solide (béton, acier, etc.). Bien que ces expériences aient commencé sur une cuve à fond bombé, elles se sont poursuivies sur des cuves dites «académiques», à fond plat, réfléchies éventuellement sur leur surface latérale seulement.

Les expériences ont porté sur le plutonium-239, l'uranium-235 et l'uranium-233[1]. Les buts poursuivis étaient les suivants: Démarrer en

[1] Ces deux derniers corps ont été obtenus grâce à l'obligeance de l'USAEC.

France des expériences de criticité, qui ont commencé sur le plutonium, seul disponible à cette époque. Bien que portant sur des géométries simples, les premiers résultats expérimentaux devaient permettre, d'une part de familiariser les ingénieurs chargés de la criticité dans les usines avec les ordres de grandeur des masses critiques en solution, d'autre part d'apporter les premières vérifications expérimentales des calculs et de mieux asseoir les méthodes utilisées dans la sécurité nucléaire.

A part cet aspect pratique, les expériences ont revêtu un caractère plus général. En effet, en dehors des masses critiques proprement dites, qui ont donné lieu à diverses comparaisons avec le calcul ou d'autres expériences, on a étudié les constantes neutroniques de ces milieux, en particulier les sections efficaces «effectives», les constantes cinétiques etc.

Ce mémoire a pour but principal de donner un aperçu de quelques résultats expérimentaux, en insistant surtout sur les enseignements tirés de ces expériences, tant du point de vue fondamental que dans le domaine pratique.

Les expériences décrites ont porté sur des cuves cylindriques de diamètres variant entre 250 et 420 mm; on passe en revue les masses critiques obtenues. Des calculs simples permettent de retrouver, moyennant certains ajustements, les résultats expérimentaux. Les sections efficaces utilisées peuvent d'ailleurs être vérifiées par d'autres méthodes (neutrons pulsés par exemple). Enfin certaines transformations géométriques ont permis, d'une part une détermination expérimentale des gains de réflecteurs, d'autre part des comparaisons avec d'autres résultats.

I. MASSES CRITIQUES

Les expériences faites à Saclay sur les appareillages du type ALECTO ont porté successivement sur le plutonium-239, l'uranium-235 et l'uranium-233. Les géométries n'ont pratiquement pas été modifiées d'un matériau fissile à l'autre, ce qui permet des comparaisons sur les propriétés nucléaires des trois matériaux fissiles. Par ailleurs, on s'est efforcé de garder toutes les autres conditions inchangées, par exemple la composition chimique, l'entourage etc.

1. Description [1-3]

Les trois expériences ALECTO ont été effectuées un hall situé à Saclay, qui avait abrité précédemment la première expérience critique homogène PROSERPINE. Dans ces ensembles, on peut rendre critiques des solutions fissiles dans des cuves cylindriques à fond plat, de diamètres variant entre 200 et 500 mm, la hauteur pouvant aller jusqu'à 1000 mm dans diverses conditions de réflexion et d'interaction. Chaque expérience est effectuée dans une cabine étanche, entourée elle-même d'une protection. A l'intérieur de cette cabine se trouve le châssis supportant la cuve à l'essai, que l'on peut voir, démonté, sur la figure 1. Les solutions fissiles sont stockées dans des réservoirs circulaires ou plats, de géométrie sûre.

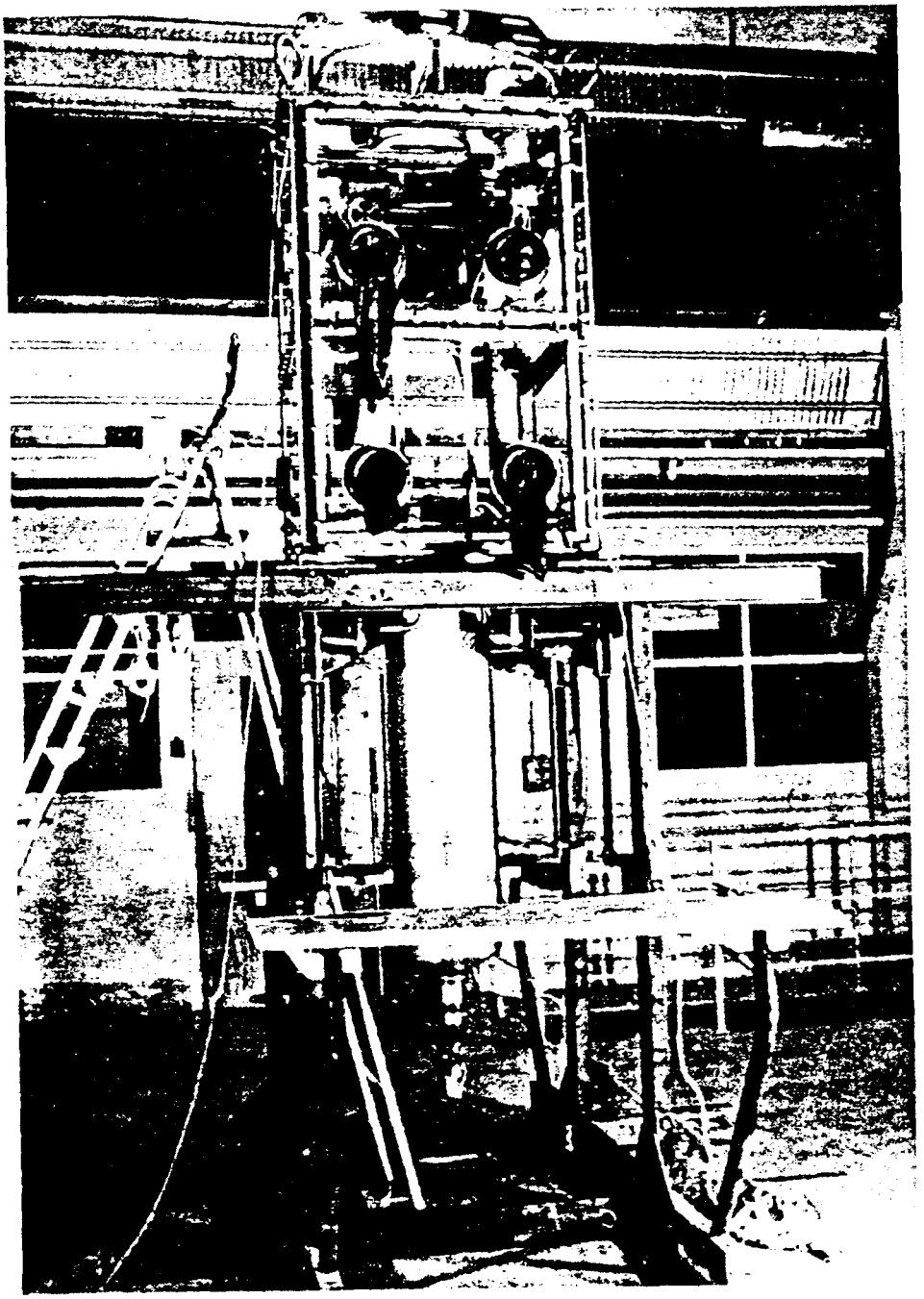

FIG. 1. ALECTO - Cœur démonté - Vue d'une des cuves (Ref. 8)

Les cuves elles-mêmes sont en acier inoxydable NS 22S, de 3 mm d'épaisseur, entourées d'un détecteur de fuite constitué par une couche isolante de buvard entouré d'un clinquant de cuivre.

2. Résultats expérimentaux

2.1. Les solutions

Les trois corps fissiles plutonium-235, uranium-235, uranium-233 sont utilisés sous forme de nitrate dissous dans l'eau, avec une acidité très voisine de 2N. Le contrôle des propriétés des solutions est effectué par analyse chimique qui porte sur les points suivants:

détermination de la concentration en corps fissile
détermination de la concentration en ions $(NO_3)^-$ et en H^+
détermination de la densité de la solution
détermination de la concentration en fer.

2.2. Caractéristiques des solutions

Plutonium – Composition isotopique en poids pour 100 g

^{239}Pu	98,48 ± 0,02 g
^{240}Pu	1,48 ± 0,015 g
^{241}Pu	0,032 ± 0,005 g

Uranium-235 – Composition isotopique en poids pour 100 g

^{235}U	89,95 ± 0,1 g
^{238}U	8,97 ± 0,9 g
^{234}U	0,78 ± 0,01 g
^{236}U	0,30 ± 0,01 g

Uranium-233 – Composition isotopique en poids pour 100 g

^{233}U	96,98 ± 0,04 g
^{234}U	2,34 ± 0,02 g
^{235}U	0,22 ± 0,01 g
^{236}U	0,024 ± 0,002 g
^{238}U	0,43 ± 0,01 g

Signalons pour ce dernier la présence de 3,2% de ^{232}Th et de 50 ppm de ^{232}U.

L'acidité des solutions est voisine de 2N.

2.3. Masses critiques (diamètres 420, 300, 250 mm)

Nous avons présenté les résultats expérimentaux sur les figures 2 (plutonium), 3 (uranium-235), et 4 (uranium-233). L'erreur expérimentale

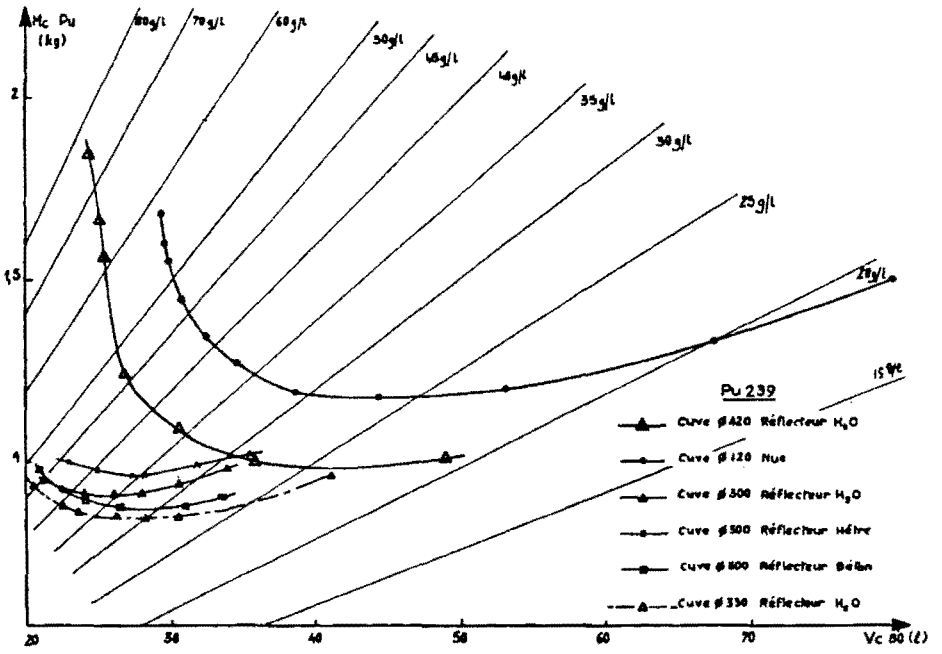

FIG. 2. Masses critiques (plutonium) (Ref. 8)

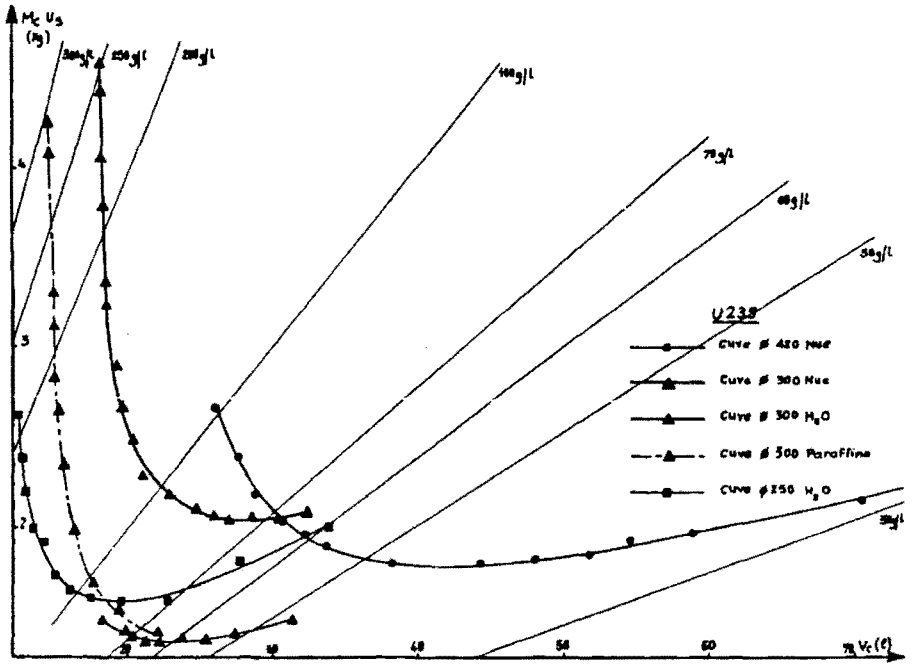

FIG. 3. Masses critiques (uranium-235) (Ref. 8)

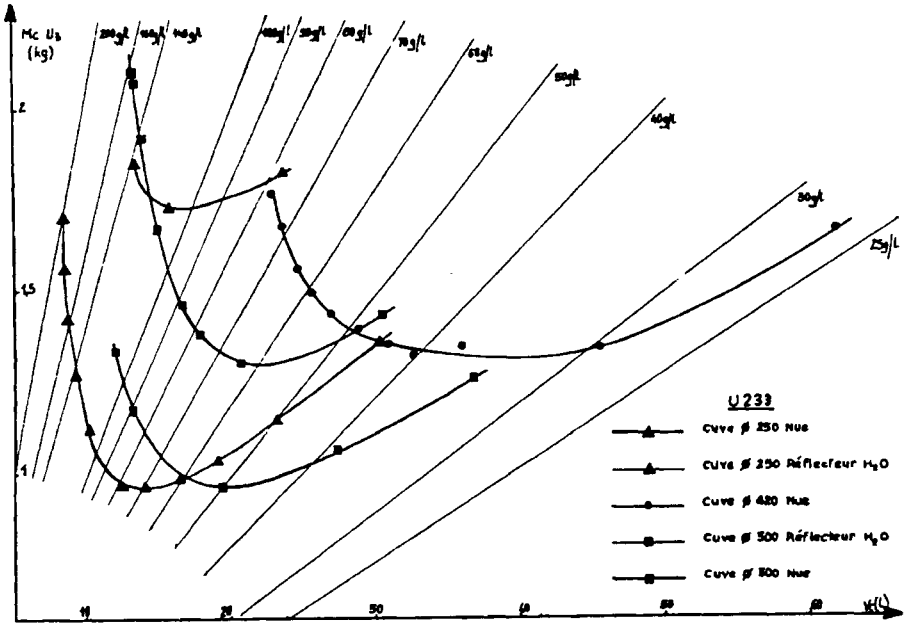

FIG. 4. Masses critiques (uranium-233) (Ref. 8)

provient très peu des erreurs de géométrie (hauteur et volume), mais beaucoup plus de l'incertitude dans la connaissance des concentrations (1%). C'est elle qui conditionne l'incertitude sur la masse. On peut remarquer, en examinant ces trois figures, les points suivants:

A géométrie identique, pour nos cylindres, les masses critiques les plus petites sont celles obtenues avec le plutonium, puis viennent dans l'ordre l'uranium-233, puis l'uranium-235. Pour une même cuve, les volumes correspondant aux masses critiques minimales sont, dans les cas étudiés, plus faibles pour l'uranium-233 que pour les autres corps.

On constate également que, grâce à un stock de matière fissile suffisant, on a pu approcher les volumes critiques minimaux pour les cuves de 300 mm de diamètre de 13 litres pour l'uranium-233 et de 18 litres pour l'uranium-235.

^{233}U Metal Sphere Criticals (References 9, 10, 11, 12)

In Reference 9, several of the experimental values reported in References 10, 11 and 12 have been reevaluated (taking into account asphericity of the experimental assembly, neutron reflection from room walls and support bands, nickel plate coatings, etc.). The experiments reanalyzed were selected by the authors as being of greatest precision and general interest. The results of that reanalysis are presented here, in Table 4. For the sake of completeness, this table is followed by tabulations taken from each of the other documents, labled "Table IV,"[10] "Table VA,"[10] "Table IV"[11] and "Table I."[12]

Table 4. Bare and Uranium-Reflected Spheres of ^{233}U (Ref. 9)

Assembly Name	Core						Reflector (Spherical Shell)		
	Mass (kg U)	Composition				ρ(U) g/cm^3	Thickness (inches)	^{235}U (wt%)	ρ(U) (g/cm^3)
		^{233}U	^{234}U	^{235}U	^{238}U				
Jezebell	16.53 ± 0.4%	98.13 a/o*	1.24 a/o	0.03 a/o	0.60 a/o	18.424	-----	-----	-----
--------	7.601	98.2 w/o+	1.1 w/o	----	0.7 w/o	18.644	0.783 ± 1%	93.2	18.80
--------	10.012	98.2 w/o	1.1 w/o	----	0.7 w/o	18.621	0.481 ± 1%	93.2	18.80
Flattop	5.74	98.13 w/o	1.24 w/o	0.03 w/o	0.60 w/o	18.42	7.84	N‡	19.0

* a/o = atom percent

\+ w/o = weight percent

‡ Natural uranium reflector

TABLE IV (Ref. 10)

U-233 METAL SPHERES

Reflected cores consist of hemispheres coated with 0.005" thick Ni

	core				spheric reflector				
	composition			$\bar{\rho}$ (U)		$\bar{\rho}$	thickness	m_c	
ref	w/o U^{233}	w/o U^{234}	w/o U^{238}	(g/cm^3)	material	(g/cm^3)	(in.)	(kg U^{233})	m_{max}
† (1)	98.2	1.2	0.6	18.45		none		16.09 ± 0.05[a]	critical
‡ (52)	98.7[b]	0.5	0.8	18.42	U(N)	19.0	7.86	5.63 ± 0.03[c]	critical
‡‡ (48)	98.2	1.1	0.7	18.64	U(N)	18.92	2.09 ± 1%	7.47[d] (3.622" dia)	>m_c[e]
(48)	98.2	1.1	0.7	18.62	U(N)	18.92	0.906 ± 1%	9.84[d] (3.972" dia)	>m_c[e]
(48)	98.2	1.1	0.7	18.64	W-alloy[f]	17.21	2.28 ± 1%	7.47[d] (3.622" dia)	>m_c[e]
(48)	98.2	1.1	0.7	18.62	W-alloy[f]	17.21	0.960 ± 1%	9.84[d] (3.972" dia)	>m_c[e]
(48)	98.2	1.1	0.7	18.64	Be (98%)	1.83	1.652 ± 1%	7.47[d] (3.622" dia)	>m_c[e]
(48)	98.2	1.1	0.7	18.62	Be (98%)	1.83	0.805 ± 1%	9.84[d] (3.972" dia)	>m_c[e]

[a] Corrected for effects of Ni coating, supports and small asphericity

[b] Analysis available for one hemisphere only

[c] Corrected for effects of Ni coating, oversize core and compensating gap between core and reflector

[d] Corrected for effects of Ni and clearances between assembly parts

[e] Effect of small compensating gap was adjusted to zero; reflector thickness modified

[f] Composition 91.3 w/o W, 5.5 w/o Ni, 2.5 w/o Cu, 0.7 w/o Zr

† (1) Ref. 11 This report

‡ (52) Private communication, G. E. Hansen (October, 1963).

‡‡ (48) Ref. 12 This report

TABLE VA (Ref. 10)

Pu OR U-233 METAL SPHERES WITHIN U(~93) METAL SPHERES

	central ball			U(~93) shell, $\bar{\rho}$ = 18.8 g/cm^3		U(N) reflector sphere,	m_c		M_{max}
ref	composition	$\bar{\rho}$ (Pu, U) (g/cm^3)	dia (in.)	enrichment w/o U^{235}	critical thickness (in.)	$\bar{\rho}$ = 19.0 g/cm^3 thickness (in.)	kg Pu or U^{233}	kg U^{235}	
(48)	Pu(1 w/o Ga), 4.9% Pu^{240}	15.62	3.970	93.17	0.652 ± 1%	none	8.39	12.64[a]	$m_{max} > m_c$[b]
(53)	Pu(1 w/o Ga), 1.5% Pu^{240}	15.56	3.510	93.18	1.006	none	5.72	18.8 ± 0.3[a]	65
(53)	Pu(1 w/o Ga), 4.7% Pu^{240}	15.60	2.486	93.17	1.948	none	2.02_2	36.7 ± 0.1[a]	130
(53)	Pu(1 w/o Ga), 1.5% Pu^{240}	15.62	2.484	93.17	1.938	none	2.02_4	36.3_5 ± 0.1[a]	118
(53)	Pu (100%), 4.7% Pu^{240}	19.22	2.484	93.17	1.651	none	2.52_7	26.8 ± 0.1[c]	233
(54)	Pu (100%), 2.34% Pu^{240}	19.48	2.130	93.2	0.974	7.45	1.615	8.87[d]	critical
(54)	Pu (100%), 4.73% Pu^{240}	19.42	2.130	93.2	0.988	7.43	1.610	9.09[d]	critical
(54)	Pu (100%), 16.1% Pu^{240}	19.43	2.130	93.2	1.039	7.38	1.611	9.90[d]	m_{max} = 9.75 kg U^{235}
†(48)	U^{233} (98.2 w/o)[e]	18.62	3.972	93.30	0.478 ± 1%	none	9.84	8.58[a]	$m_{max} > m_c$[b]
†(48)	U^{233} (98.2 w/o)[e]	18.64	3.622	93.16	0.780 ± 1%	none	7.47	13.77[a]	$m_{max} > m_c$[b]
‡(53)	U^{233} (98.9 w/o)[f]	18.35	2.478	93.17	1.896	none	2.37_1	34.8 ± 0.1[a]	138

[a] Corrected for effects of 0.005" thick Ni on Pu or U^{233} hemispheres and for clearances between assembly parts

[b] Effect of small compensating gap was adjusted to zero; reflector thickness modified

[c] Corrected for effects of 0.005" thick Cu about Pu sphere and for clearances between assembly parts

[d] No correction for 0.012" thick gap containing 0.010" thick Ni between Pu and U(93.2)

[e] 1.1 w/o U^{234}, 0.7 w/o U^{238}

[f] 0.9 w/o U^{234}, 0.2 w/o U^{238}

† (48) Ref. 12 This report

‡ (53) Private communication, H. C. Paxton, G. E. Hansen, D. P. Wood & E. A. Plassmann (May 1960).

TABLE IV (Ref. 11)

COMPUTATIONAL AND EXPERIMENTAL CORRELATIONS

Parameter	U^{235}	U-refl. U^{235}	U^{233}	U-refl. U^{233}	Pu^{239}	U-refl. Pu^{239}
$\sigma_f(U^{235})/\sigma_f(U^{238})$						
obs.	6.4	7.1_6	4.9_5	5.6_3	4.9_7	5.4
comp.	6.42	6.98	5.13	5.69	5.39	6.16
$\sigma_f(Np^{237})/\sigma_f(U^{235})$						
obs.	0.864	0.78	1.026	0.92_3	0.99_6	—
comp.	0.869	0.811	0.978	0.909	0.949	0.859
$\sigma_f(Pu^{239})/\sigma_f(U^{235})$						
obs.	—	—	—	—	—	—
comp.	1.403	1.384	1.441	1.418	1.437	1.398
$\sigma_f(U^{233})/\sigma_f(U^{235})$						
obs.	—	—	—	—	—	—
comp.	1.536	1.536	1.530	1.532	1.531	1.532
$\sigma_c(U^{238})/\sigma_f(U^{238})$						
obs.	—	—	—	—	—	—
comp.	0.543 (0.475)	0.612 (0.531)	0.391 (0.349)	0.458 (0.404)	0.423 (0.374)	0.517 (0.452)
Critical mass* (kg core) obs.	52.0_4	17.4_1	16.1	—	16.2_8	5.7_9
comp.	51.6	16.7	16.0	5.6	16.1	5.5
Effective delayed-neutron fraction obs.**	0.0065_9	—	0.0029_0	—	0.0019_3	—
comp.***	0.0069_1	—	0.0028_7	—	0.0019_9	—
Rossi-α at delayed critical (per μs) obs.	—1.10	—	—1.00	—	—0.65	—
comp.	—1.22	—	—	—	-0.63_7	—

* Specifically the computed and observed critical masses refer to the following idealized systems:
U^{235} ≡ a critical sphere of Oy (93.8% U^{235}) at ϱ (Oy) = 18.75 g/cm³.
U-refl. U^{235} ≡ a critical sphere of Oy (94.1% U^{235}) at ϱ (Oy) = 18.7 g/cm³ and close reflected with $8^1/_2$ in of normal uranium at ϱ (U) = 18.8 g/cm³.
U^{233} ≡ a critical sphere of "23" (98.1% U^{233}) at ϱ ("23") = 18.6 g/cm³.
U-refl. U^{233} ≡ a critical sphere of "23" (98.1% U^{233}) at ϱ ("23") = 18.6 g/cm³ and close reflected with $7^1/_2$ in of normal uranium at ϱ (U) = 18.9 g/cm³.
Pu^{239} ≡ a critical sphere of Pu (95 $^1/_2$% Pu^{239}) at ϱ (Pu) = 15.66 g/cm³ [2].
U-refl. Pu^{239} ≡ a critical sphere of Pu (98$^1/_2$% Pu^{239}) at ϱ (Pu) = 15.63 g/cm³ and close reflected with $9^1/_2$ in of normal uranium at ϱ (U) = 18.8 g/cm³ [2].

** The direct observation is the surface mass increment between delayed and prompt critical. The S_4 computed reproduction number change for this mass increment is then identified with the effective delayed neutron fraction. This is a customary step leading to a computation of the Rossi-α at delayed critical. The step may be deleted when interest in the Rossi-α measurements is confined to implications of flux spectra for then observed derivatives of α with respect to surface mass permit interpretation without mention of delayed neutrons. The last row of Table IV effectively treats the Rossi-α in this fashion.

*** From the Keepin and Wimett [10] delayed-neutron fractions $\beta(U^{235}) = 0.0064_8$, $\beta(U^{238}) = 0.015_7$, $(U^{233}) = 0.0026_6$, $(Pu^{239}) = 0.00209$ and $(Pu^{240}) = 0.0025_7$ and relative effectiveness computations.

CRITICAL U^{233} AND Pu^{239} SPHERES

TABLE I (Ref. 12)

CRITICAL CORE-REFLECTOR CONFIGURATIONS

Core					Critical reflector thickness[a]			
Material	Diameter (in.)	Weight (Kg)	Density	Enrichment	U(93) ρ = 18.80 (in.)	Be(98 w/o) ρ = 1.83 (in.)	Natural uranium ρ = 18.92 (in.)	W alloy (91.3 w/o) ρ = 17.21 (in.)
U^{233}	3.622	7.601	18.62	98.25 w/o	0.780	1.652	2.090	2.280
U^{233}	3.972	10.012	18.62	98.25 w/o	0.478	0.805	0.906	0.960
Pu^{239}	3.970	8.386 Pu	15.62 Pu[b]		0.652	1.452	1.625	1.850

[a] Probable error is 1% for these critical reflector thicknesses.

[b] The Pu^{239} used in this experiment contains 4.90 atomic % Pu^{240}, 0.31 atomic % Pu^{241}, and a minor amount of inert diluent.

CRITICAL LATTICE EXPERIMENTS

Lattice experiments are the only critical experiments which include thorium in significant amounts. Critical lattice experiments using ^{235}U and ^{232}Th as fissile and fertile isotopes were performed by Babcock and Wilcox to support the design of the Consolidated Edison Thorium Reactor[15] (CETR-the Indian Point PWR), and in a parallell BWR development effort called the Thorium Uranium Physics Experiments[16] (TUPE). The Elk River Reactor (a BWR built by Allis-Chalmers, which utilized thorium in its first core) was designed without benefit of critical experiments.[17] Consequently, the only critical experiments performed in support of thorium-loaded convertor reactor development are those of the CETR and TUPE programs.

An extensive series of critical lattice experiments utilizing ^{233}U and ^{232}Th as fissile and fertile isotopes has been performed in support of the Light Water Breeder Reactor program (LWBR).[18, 19, 20] However, all of the thorium-containing cores were zoned radially, and successive experiments used increasingly complex radial and axial zoning patterns.

The earliest (and geometrically simplest series) of these LWBR experiments[18] utilized alternately ^{235}U and ^{233}U as fissile fuel, to allow direct comparison of lattice characteristics of these two fissile materials. However, even these lattices were radially zoned into "seed" and "blanket" regions, and thorium was contained only in the blanket. (ZrO_2 was used to dilute the enriched fissile fuel in the seed rods.) Additional differences between seed and blanket regions included rod size and lattice pitch.

In the second and third series of LWBR experiments geometrical complexity was greatly increased, as the objectives of those measurements were to develop and refine design analysis methods,[19] and to determine power distributions in realistic core mockups.[20] Heterogeneities such as the presence of control rods, axial fuel zoning, and the use of multiple seed/blanket modules make these critical experiments of little usefulness for straightforward validation of criticality calculational techniques. However, descriptions of these lattices are included here for the sake of completeness.

A series of exponential experiments using ^{233}U and thorium was performed at Brookhaven National Laboratory.[21] However, although the lattices were clean (no zoning - radially or axially - and no control rods) criticality was not achieved - just measurements of material bucklings. These lattices are also described here for completeness.

The characteristics of the lattice experiments compiled in this section are summarized in Table 4. Examination of this table shows that the critical experiments performed with un-zoned lattices containing thorium (Ref's. 15 & 16) used only ^{235}U for the fissile material. Despite the fact that a fairly broad range of metal/water ratios was covered, only one rod size and two values of $Th/^{235}U$ were studied. Thus the total lack of homogeneous solution data for ^{235}U-Th systems is complimented by a limited amount of clean cylindrical critical lattice data. However, for validation of dissolver analyses for such fuel, data for additional fuel rod sizes and fissile enrichments is needed.

Table 4. Summary of Critical Lattice Experiments with ^{1}H-Moderated ^{233}U or Thorium

Ref.	Fissile Material†	Fertile or Diluent Material†	Thorium / Fissile Ratios ‡	Rod O. D. (in.)	Metal/Water Ratios	Lattice Type	Number of Experiments
15	^{235}U	^{232}Th	15.0 & 25.8	0.312	0.15 - 1.12	Sq.	10
16	^{235}U	^{232}Th	15.0 & 25.3	0.309	0.48 - 1.02	Sq.	5
18						Sq. & Hex.	10
Seed	^{233}U or ^{235}U	Zr	0	0.225	0.22 & 0.64		
Blanket	^{233}U or None	^{232}Th	99,-	0.570	0.95 & 9.3		
19						Hex.	8
Seed	^{233}U or None*	^{232}Th	7, 10, 19, 49,-	0.25	1.19 & 1.64		
Blanket	^{233}U or None	^{232}Th	49, -	0.63	2.89 & 1.09		
20						Hex.	7
Seed	^{233}U or None*	^{232}Th	15, 23, -	0.305	1.65		
Blanket	^{233}U or None	^{232}Th	34, 46, 57, -	0.528, 0.572, 0.626	1.7 - 2.9		
21**	^{233}U	^{232}Th	32	0.499	0.15 - 1.35	Hex.	21

† All materials are in oxide form

* Axial reflector region

‡ -Indicates no fissile content

** Exponential experiments

A single un-zoned critical lattice containing ^{233}U was reported in Ref. 18. However, zirconium oxide was used as diluent for the ^{233}U fuel in that experiment, and no thorium was present. In that series of experiments Th was contained only in blanket rods which were driven by a seed region of $^{233}UO_2$-ZrO_2. Thus data from these experiments are only indirectly useful for validation of calculations for ^{233}U-Th rod lattices.

The only critical lattice data for rods containing ^{233}U and thorium is found in References 19 and 20. As has been noted, all of these lattices were zoned radially and axially into seed and blanket regions. And all but one of these lattices had axial zoning of fissile enrichment in the seed and/or blanket regions. The complexity of these lattices makes them of extremely limited usefulness for validation of criticality analysis calculations.

For the validation of criticality analyses of dissolvers designed for ^{233}U-Th oxide fuel rods, data is needed from geometrically simple critical lattice assemblies of single-enrichment rods in water. Such critical lattices should include a minimum of perturbations due to control rods, fuel assembly cans, etc. Fuel rod sizes, fissile enrichments, and lattice pitches should be varied to confirm the accuracy of calculations over the ranges of these variables appropriate to the fuels under consideration.

No criticality data exist for lattices of thorium bearing rods having either ^{235}U or ^{233}U fissile content immersed in dissolver acid (HNO_3), or dissolver solution [$UO_2(NO_3)_2$]. Such data are needed to validate analyses of operating and off-normal conditions.

Many critical experiments have been performed using lattices of $^{235}UO_2$ - ThO_2 rods immersed in water poisoned with boron. However, no such critical experiments have been performed using lattices fueled by ^{233}U. Exponential experiments have been performed using boron-poisoned lattices of $^{233}UO_2$ - ThO_2, however.

No data, either critical, or exponential, exist for lattices poisoned with gadolinium or cadmium. Data are particularly needed for gadolinium because it is of special interest for use in dissolver vessels to increase the batch size allowed by criticality considerations. In addition to its excellent neutron capture properties, it is highly soluble in nitrate solutions and has no tendency to plate out, precipitate, or stratify. It is also highly compatible with the separations processes used in spent fuel reprocessing, and is thus a prime candidate for use in dissolvers.

Finally, no data exist for thorium-containing lattices which also contain significant quantities of ^{238}U. The present interest in "denatured" fuels (having sufficient ^{238}U present with either ^{235}U or ^{233}U fissile material so that its use for nuclear weapons is precluded) strongly suggests the need for criticality data on thorium fuels containing ^{238}U in significant quantities.

Consolidated Edison Thorium Reactor Criticals (Reference 15)

Critical experiments were performed on two types of lattices in this program. The first lattices investigated were geometrically clean, lacking heterogeneities due to fuel element cans or water channels between cans. The second type of lattices studied were three-zoned, canned element cores having the same cross sectional area as the first lattices. Both types of lattices had a cylindrical array of fuel pins on a square pitch. Sections from Reference 15 describing the cores and the results of the critical measurements are reproduced below.

One of the lattices used for the clean critical measurements was further investigated with the addition of boric acid neutron poison. The section describing the measurements and analysis are reproduced below, except that extensive tabulations of flux traverse measurements are omitted.

The reproductions follow.

SECTION 2
PHYSICAL DESCRIPTION OF CORES

The cores for the critical experiments were assembled from fuel pins containing pellets fired from mixtures of ThO_2 and fully enriched UO_2. The fuel pins were fabricated from AISI type 304 stainless steel with welded end plugs. Two concentrations were used with nominal thorium to U-235 atomic ratios of 15/1 and 25/1. The pins were arranged on square pitches. Seven clean lattice cores of this type were assembled. Each core consisted of a cylindrical array of a single type of fuel pin. There were no heterogeneities from can walls or water channels between cans. The cores differed in either thorium-to-uranium ratio or spacing between pins.

A three-zone core containing 120 offset cans was assembled with each can containing 206 of the fuel pins. The cans were fabricated from aluminum and the cans were assembled to allow space for control rods or followers. The type of pin used in each can was varied to suit the particular experiment. Other data were measured using square cans containing 196 pins.

2.1 FUEL PINS

A total of 24,741 fuel pins were fabricated for this experiment by the Davidson Chemical Company. These fuel pins (see Fig. 2.1) consisted of ThO_2-UO_2 pellets enclosed in type 304 stainless steel tubing. The tubing was 50 in. long, 0.312 in. OD, with a wall thickness of 0.019 in. The fuel pellets were 0.260 in. OD with an average density of 8.35 gm/cc. The tubing was filled with fuel pellets to give an active fuel length of 48 ± 1/8 in. Type 304 SS end plugs were welded in each end of the tube, occupying 3/4 in. of space each. The remaining 1/2-in. space was packed with Kaowool to keep the pellets stationary.

The Th to U-235 atomic ratio for 12,378 of the pins was 15.00 ± 0.05; the ratio for the remaining 12,363 pins was 25.76 ± 0.05. For all illus-

trations in this report, the 15/1 pins are represented by shaded circles, the 25.76/1 pins by open circles. (The 25.76/1 pins are referred to as 25/1 pins.)

To fabricate the pellets, ThO_2 and U_3O_8 powders were compressed into pellets, using an organic resin binder. In sintering ovens, the binder was driven off and the pellets were sintered to a higher density. The uranium content was determined from samples taken from each batch; pellet length varied from 1/4 to 1/2 in.

The uranium content in any pin was determined from the total weight of pellets in the pin and the sinter batch analysis. A statistical analysis of this information is summarized in Table 2.1. The average mass of U-235 per pin was calculated using the average U-235 content of the uranium as 93.17%.

Davidson's chemical analyses of ThO_2 were averaged. A fictitious element called thorium impurity (ThI) was invented and assigned the same atomic weight and thermal cross section as iron. Then weight percent of ThI having the same thermal absorption as all impurities in ThO_2 other than Gd and B was found. The Th in ThO_2 was considered to be composed as follows.

B	0.9 ppm
Gd	3.1 ppm
ThI	0.14%
Th	99.86%

Three lots of ThO_2 with high impurity content (Table 2.2) were accidentally used in fabricating the 25/1 pins. A total of 4,387 of the 25/1 pins contained the substandard ThO_2; these were kept separate and when used will be referred to as "bad" 25/1 pins.

The Type 304 SS cladding and end plugs were analyzed for B, Cd, Co, and rare earths at B&W's Research Center. The results are given in Table 2.3.

2.2 PIN-ELEMENT CORES

Two aluminum tube sheets, one above and one below the fuel region, held the fuel pins in a square lattice in the pin element cores. One pair of tube sheets defined a pin lattice with a 0.3805 in. pitch spacing and a 1.119 metal-to-water ratio. Another pair of tube sheets determined a

TABLE 2.1

SUMMARY OF FUEL PIN LOADING

Parameter	15/1 Pins	25/1 Pins
Sinter batches	1-119	120-187
Excluding sinter batches	7, 19, 33, 44 72, 84, 85, 87 90, 119, 2, 3 8, 9, 41, 42 46, 89	126, 134, 147 155, 162 182, 183, 184 185, 186, 187
Number of pins from each sinter batch	5	5
50% confidence interval for average weight of fuel per pin, gm	347.7 ± 0.1	347.9 ± 0.1
Sample variance of weight of fuel per pin, gm^2	4.73	4.57
* 50% confidence interval for average percent uranium in given ratio sinter batches, %	5.94 ± 0.00	3.55 ± 0.00
Sample variance of percent uranium in given ratio sinter batches, $(\%)^2$	1.81×10^{-3}	1.07×10^{-3}
50% confidence interval for average weight of uranium per fuel pin, gm	20.64 ± 0.01	12.36 ± 0.01
50% confidence interval for average weight of U-235 per fuel pin, gm	19.23 ± 0.01	11.51 ± 0.01
Sample variance of weight of uranium per fuel pin, gm^2	0.0385	0.0187
** Equivalent fuel density, gm/cm^3	8.35	8.35

* Davison analyses.

** Fuel volume = 41.65 cm^3 per rod.

0.4027 in. spacing and a 0.892 metal-to-water ratio. Using different combinations of the two pairs of grid plates and two sets of fuel pins, four different cores were obtained. Three more cores were assembled with larger pitch spacing by removing pins from the basic lattice. Nomenclature and description of the cores are given in Section 3.

Figure 2.2 is a photograph of one pin element core. The upper tube sheet, visible in this figure, is made of 5052 Al; it is 4 1/2 ft in diameter and 3/4 in. thick. The 0.321 ± 0.005 in. diameter pin holes are spaced 0.3805 ± 0.004 in. apart. Since the distance along an entire row of holes was held to a tolerance of 0.004 in., the average spacing is 0.3805 ± 0.0000 in. Safety rod guides, visible in Fig. 2.2, occupy 60 pin positions each. The cruciform, boron stainless steel, safety rods are 5 1/2 in. wide tip-to-tip and 3/16 in. thick. The rod guides are 1/8 in. thick 5052 Al. The top of a special 25-pin test bundle is visible at the center of the core in Fig. 2.2. The lower tube sheet (not visible) is similar to the upper tube sheet, except the holes are smaller to receive the tapered end plugs.

A second pair of grids defined a 0.4027 in. pitch lattice. These grids were of "egg crate" construction (interlacing flat metal strips) and were fabricated with a pin spacing tolerance approximately equal to that of the drilled type grid plates.

Table 2.4 shows the type of pin and the metal-to-water ratio (M/W) for the four basic pin-element cores. Three other cores were made by omitting some of the pins in Core 9B for special criticality studies. Every other row and column were omitted in Core (2.0) 9B giving a square pitch twice that of the 9B Core. Every other diagonal row was omitted in Core (1.4) 9B resulting in a square pitch $\sqrt{2}$ times the 9B pitch. One-fourth of the pins were omitted in Core (1.15) 9B giving a 0.439 in. average pitch.

2.3 CANNED ELEMENT CORES

One hundred and twenty cans (see Fig. 2.3) were fabricated from 3/16 in. thick 5052 Al, and filled with 206 of the 15/1 and 25/1 fuel pins described in Section 2.1. Three grid plates per can held the pins in a square lattice on a 0.3805 in. pitch. The bottom and top grids, made of 5052 Al, were outside the fuel region, and a plexiglas grid was placed

just below the center of the fuel region. Figure 2.4 is a photograph of a can and its three grids. Figure 2.5 is a diagram of the three-zone, canned element core made up of 120 of the cells shown in Fig. 2.3.

The cans were placed in the core on a flat aluminum plate. Aluminum strips, 0.080 in. thick, were fastened to the plate for proper can spacing. The bottom grid plate extends 1/8 in. below the can wall, and the spacer strips butt against the bottom grid plates rather than the can wall. This provides the correct water space between the pins in one can and the pins in the adjacent can, and also makes the core less sensitive to variations in can size. Clips, designed to slip over the top of the can walls, gave true spacing between cans at the top of the core. Figure 2.6 is a photograph of one of the canned element cores.

The canned cores were loaded with a mixture of "good" and "bad" 25/1 pins in Zone I, a mixture of 25/1 and 15/1 pins in Zone II, and 15/1 pins in Zone III.

In some cores only 25/1 pins were used around rod guides and the perimeter of the core. Since the exact distribution of pins was varied to suit the experiment, the distribution of pins in the core will be specified along with the description of each experiment.

For special experiments 16 square cans were fabricated from 0.160 in. thick 6061 Al, as shown in Fig. 2.7. Offset grid plates were milled square for use in these square cans. The square cans contained 196 pins in a 14 x 14 square array, spaced 0.3805 in. center-to-center.

TABLE 2.2

IMPURITIES IN SUBSTANDARD ThO_2

Thorium Lot Number	C, ppm	B, ppm	Dy, ppm	Eu, ppm	Gd, ppm	Sm, ppm
14	300	20	29	1	19	9
15	380	5	42	1-6	21	12
16	400	20	34	0-9	12	6.6

TABLE 2.3

STAINLESS STEEL IMPURITIES

Sample	Co, ppm	B, ppm	Cd, ppm	Eu, ppm	Sm, ppm	Gd, ppm
Type 304 SS from Sawhill Tubular Prod.						
HT-69570	1140	3-8	< 5	< 0.1	< 0.1	< 0.1
HT-69560	945	3-8	< 5	< 0.1	< 0.1	< 0.1
HT-69500	1330	5-10	< 5	< 0.1	< 0.1	< 0.1
HT-97227	1175	8-13	< 5	< 0.1	< 0.1	< 0.1
HT-52327	1300	3-8	< 5	< 0.1	< 0.1	< 0.1
End Plug, Type 304 SS	1150	5-10	< 5	< 0.1	< 0.1	< 0.1

Other Elements in Type 304 SS

Element	Typical Content, %	Element	Typical Content, %
Cr	19.0	Cu	0.29
Ni	9.5	Mo	0.165
Mn	1.5	W	0.205
Fe	67.7	Si	0.55
Sn	0.013	P	0.515

TABLE 2.4

PIN-ELEMENT CORE PARAMETERS

Core Number	Type of Fuel Pins	Center-to-Center Spacing of Pins, in.	M/W
9B	15/1	0.3805	1.119
7B	25/1	0.3805	1.119
9A	15/1	0.4027	0.892
7A	25/1	0.4027	0.892

FIG. 2.1: FUEL PIN

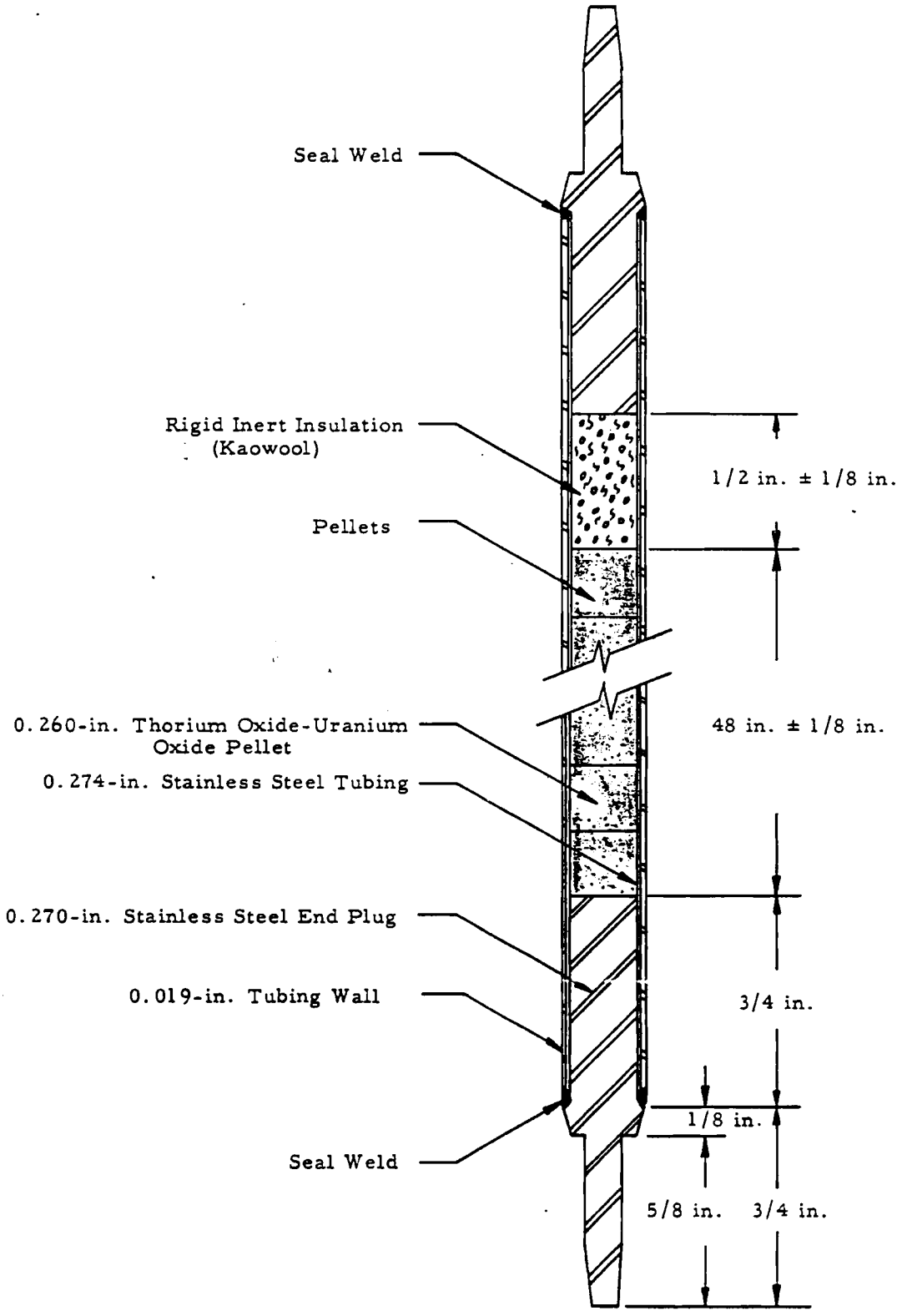

FIG. 2.2: CORE 9 B

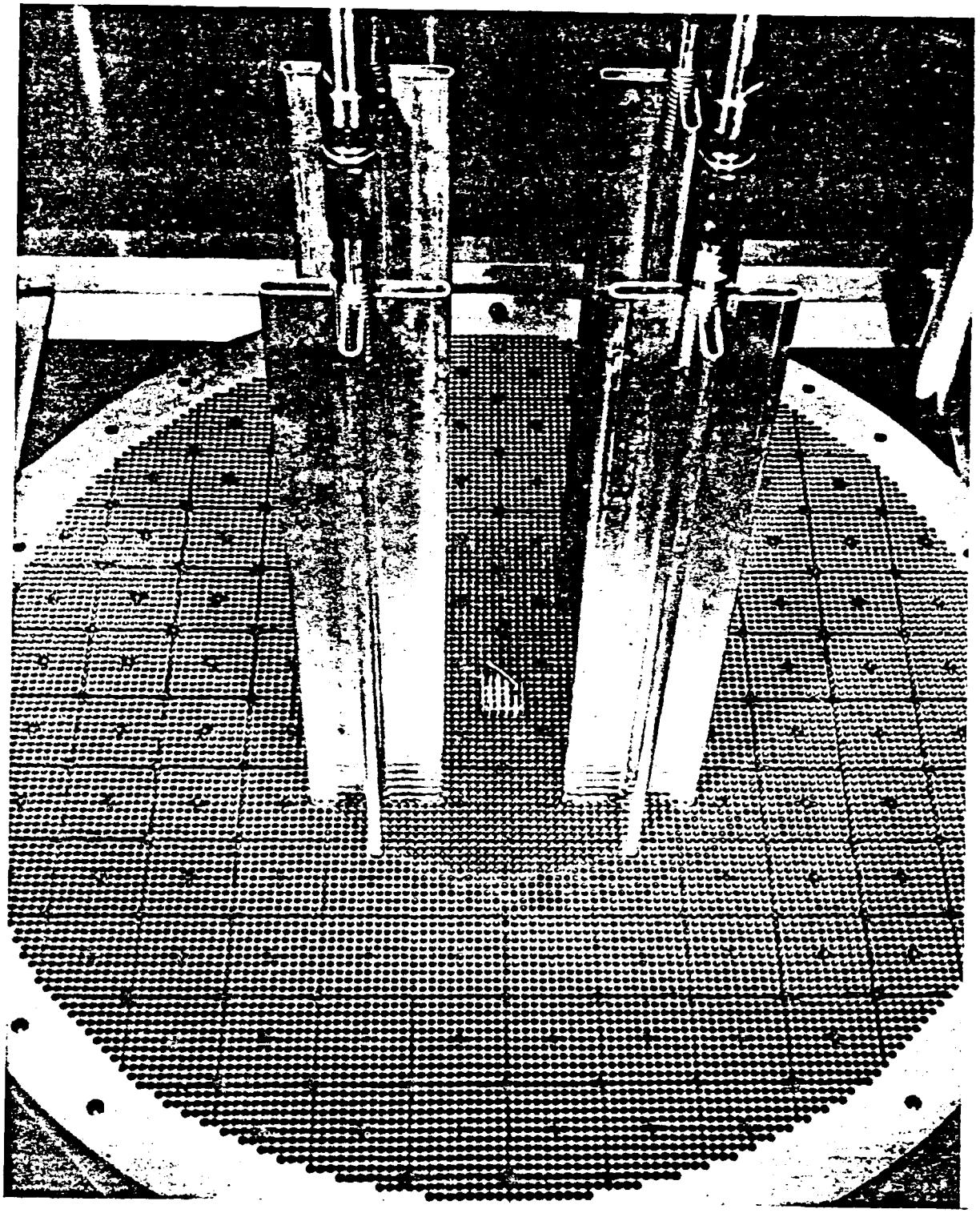

FIG. 2.3: OFFSET CAN

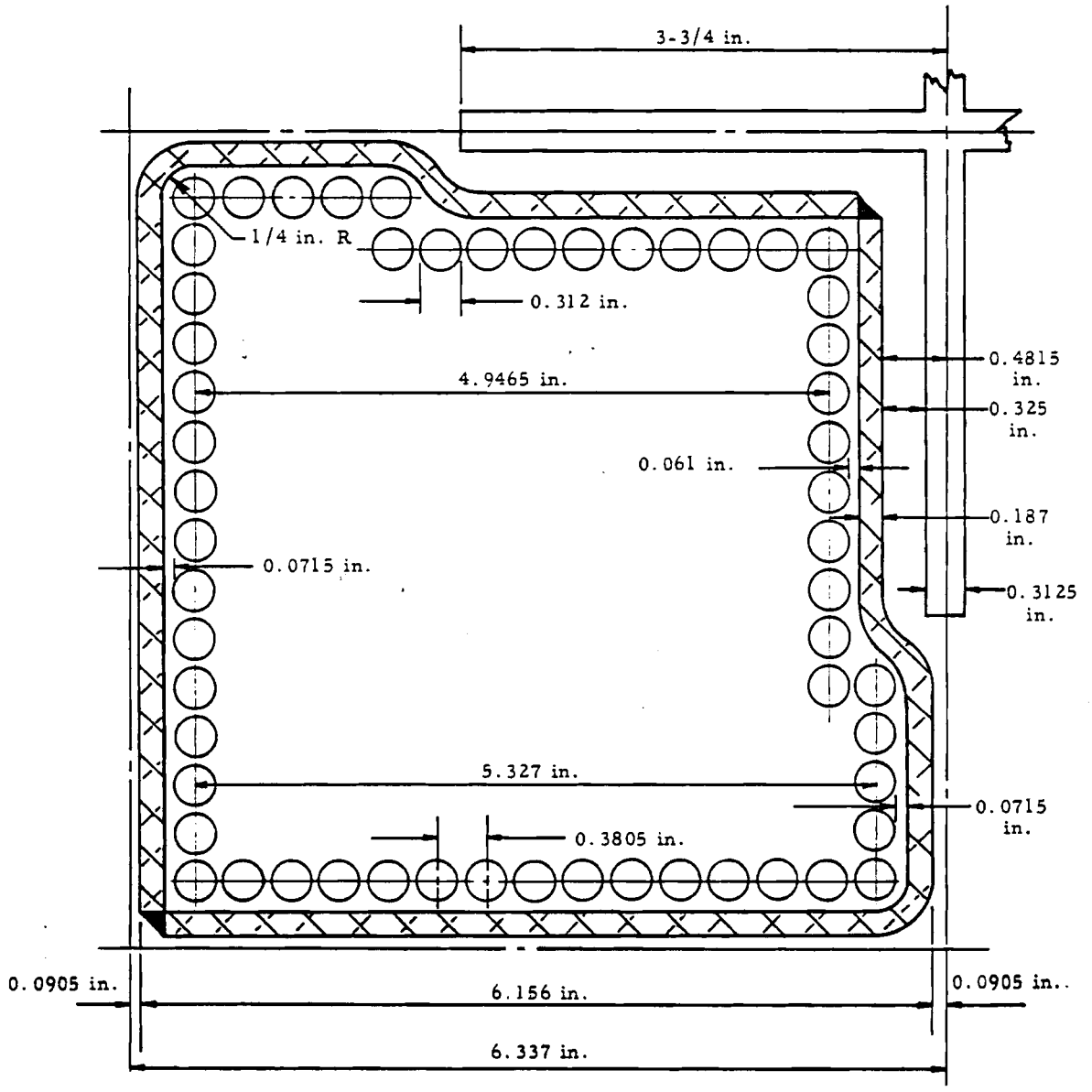

FIG. 2.4: CAN WALL AND GRIDS

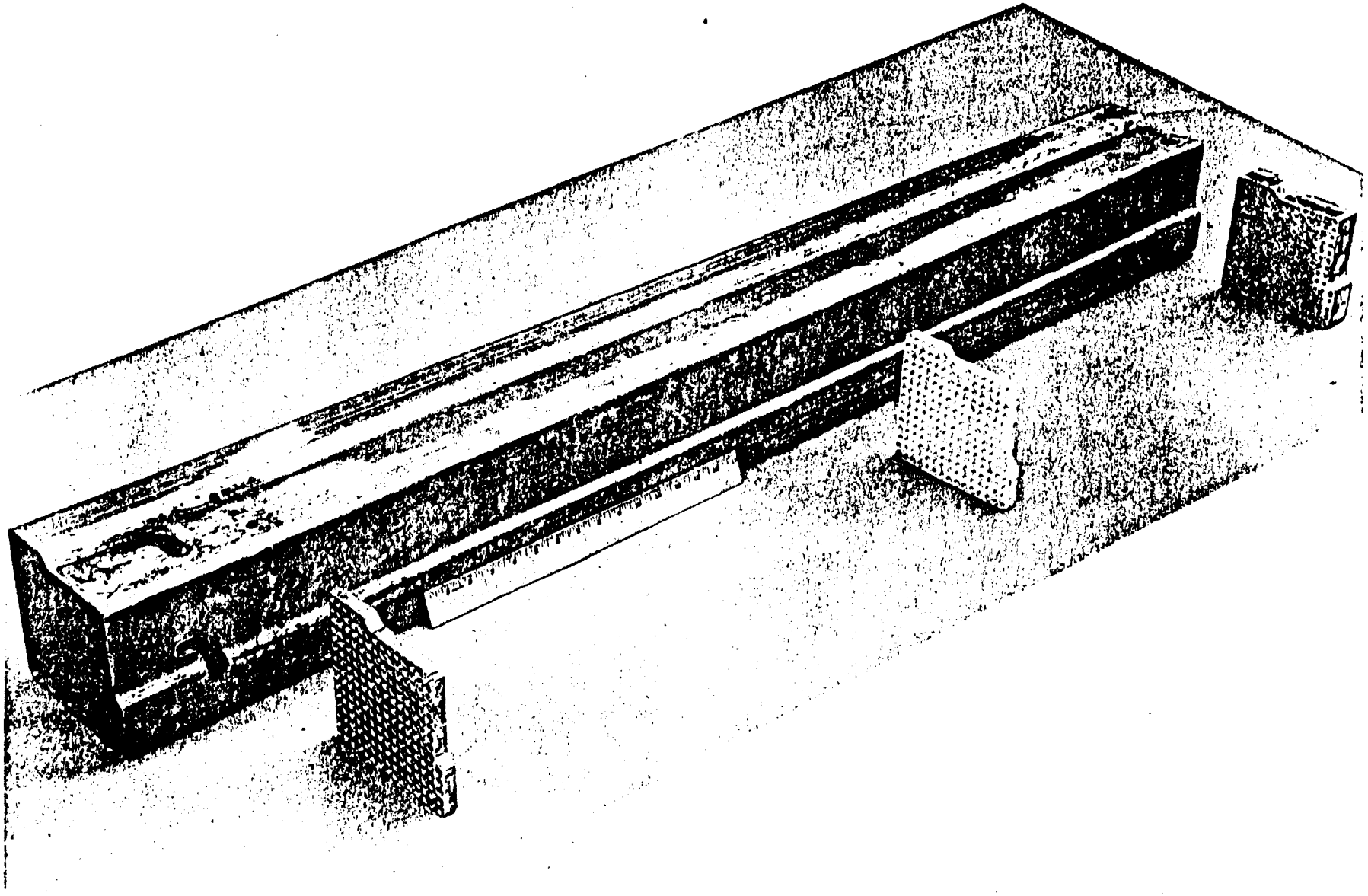

FIG. 2.5: DIAGRAM OF THREE-ZONE CORE

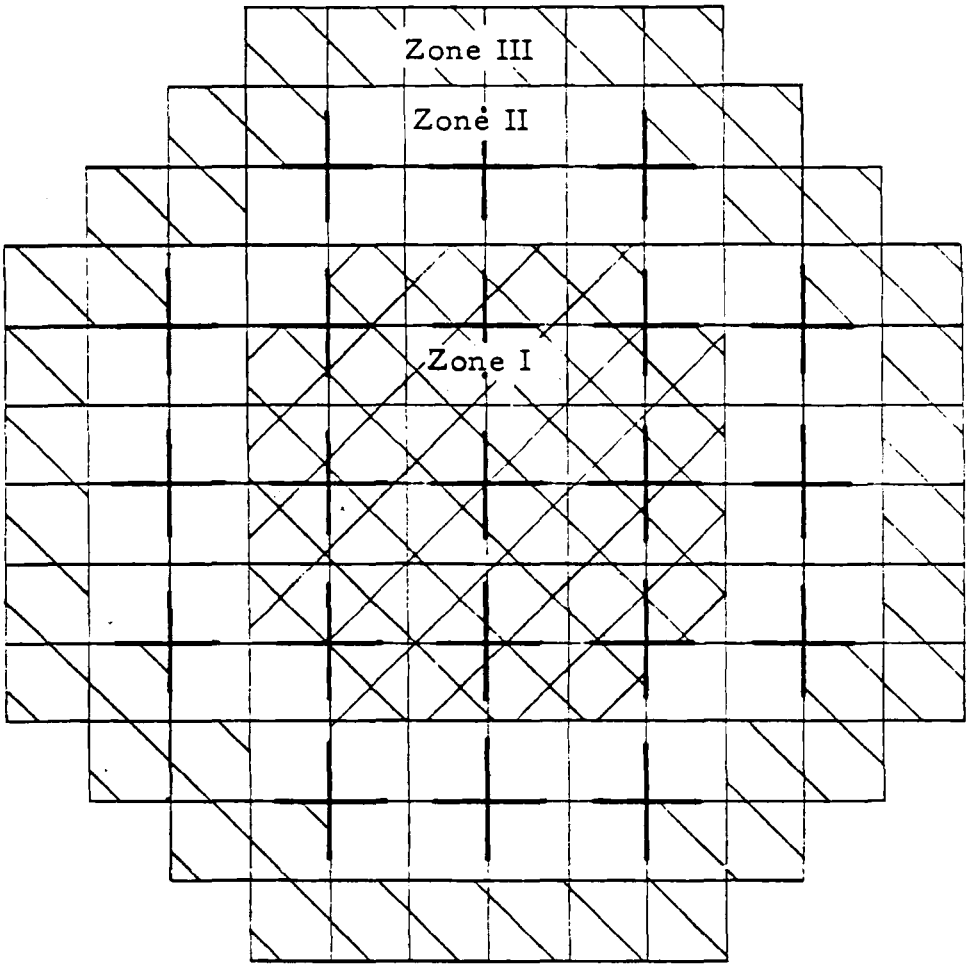

FIG. 2.6: THREE ZONE CAN CORE

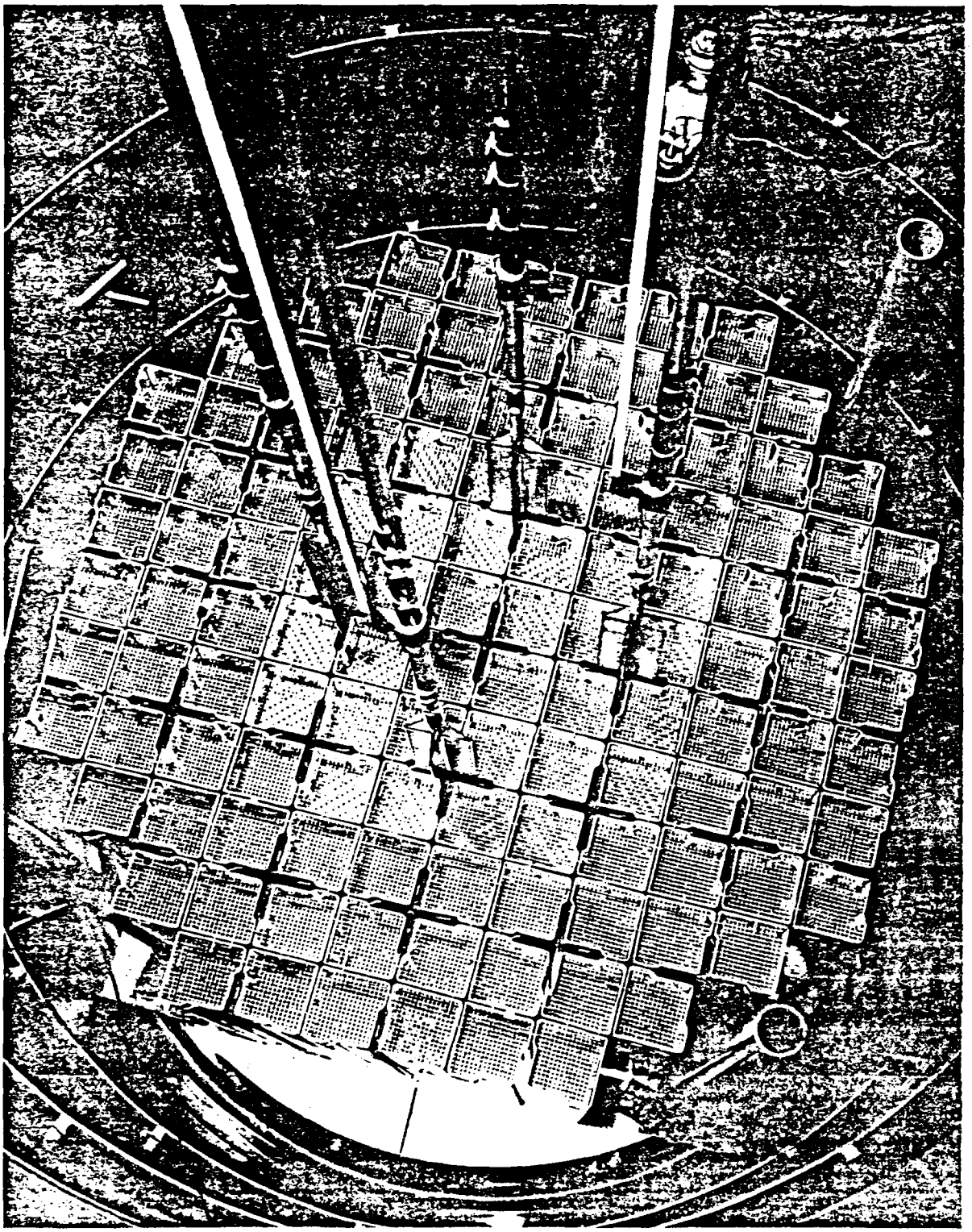

FIG. 2.7: SQUARE CAN

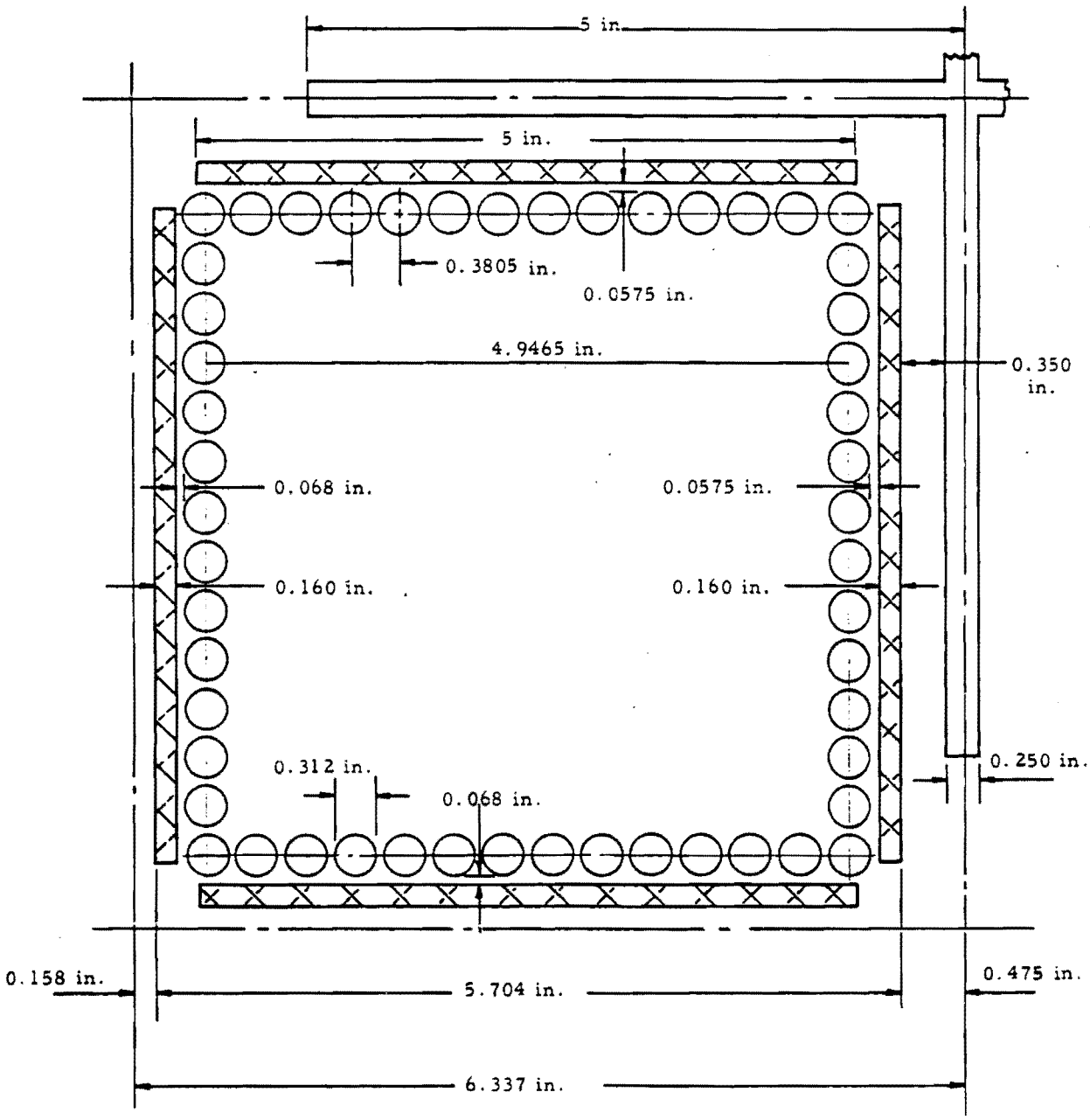

SECTION 3
CRITICAL MASS DETERMINATION

3.1 CLEAN LATTICE CORES

The critical mass was determined for clean lattice cores 7B, 7A, 9B, 9A, (1.15) 9B, (1.4) 9B and (2.0) 9B. Table 3.1 gives the pertinent data. There were four safety rod channels in these cores, with the exception that in cores 7A and 9A two of these channels were removed and a reactivity evaluation was done. In Core 9B one channel was removed and the reactivity was evaluated. By assuming constant material buckling and equal reactivity worth for each channel, the critical mass of these cores can be calculated for the case where all channels are removed.

In cores (1.15) 9B, (1.4) 9B, and (2.0) 9B perturbations caused by the safety rod channels were compensated by loading the displaced pins in vacant positions near the channels.

3.2 CAN ELEMENT CORES

3.2.1 Single Zone

A critical mass determination was done on a core of square can elements, arranged in CETR geometry, and containing only 15/1 pins. This determination was to establish the k_∞ of the Zone III of reference core. The critical configuration and core data are shown in Fig. 3.1.

3.2.2 Multiple Zone

The three zone core was built using offset cans of fuel pins. The center cans were placed in the core first, and additional cans and pins were added around the outside until criticality was reached with full water height. The buildup to the full core was continued in steps of reduced water height. The reactivity of the full water height core was estimated by using the integral water height curve (Fig. 8.2). The results of these determinations are shown in Table 3.2.

TABLE 3.1

CRITICAL MASSES OF CLEAN LATTICE CORES

Core	Lattice Pitch, in.	M/W	H/X*	Number of Rod Guides	Number of Pins	Core Radius, cm	U-235 Mass, kg	Core Reactivity, cents
7B	0.3805	1.12	123	4	6529	44.9	75.15	+ 9.8
7A	0.403	0.892	160	4	4465	40.5	53.69	+ 7.4
				2	4785	40.5	55.08	+38.9
				0	4771	39.9	54.91	0
9B	0.3805	1.12	73.7	4	1771	24.2	34.17	+ 3.0
				3	1825	24.2	35.09	+ 9.9
				0	1941	24.0	37.32	0
9A	0.403	0.892	95.8	4	1331	22.3	25.25	+ 6.3
				2	1401	22.3	26.94	+45.7
				0	1452	22.0	27.92	0
(1.15) 9B	0.439	0.647	125	1	1014	20.0	19.5	0
(1.4) 9B	0.538	0.359	229	1	619	19.2	11.9	0
(2.0) 9B	0.761	0.152	537	4	656	28.0	12.6	0

*Hydrogen to U-235 Atom Ratio.

TABLE 3.2

CRITICALITY OF CLEAN ZONED CORES

Zone	Number of Pins 25/1	15/1	U-235 Mass, kg	Critical Water Height, cm	Reactivity Worth at Full Water Height, $
I	2208* 4384**		75.87		
II	2442	2090	68.30		
Total	9034	2090	144.17	Full	0.05
I	2208* 4384**		75.87		
II	4884	4180	136.59		
Total	11476	4180	212.46	70.82	Not Measured
I	2208* 4384**		75.87		
II	4884	4180	136.59		
III	900	8164	167.35		
Total	12376	12344	379.81	43.92	10.20

* Reference Pins.
** "Bad" Pins.

FIG. 3.1: CRITICAL CONFIGURATION OF ZONE 3, SQUARE-CAN CORE

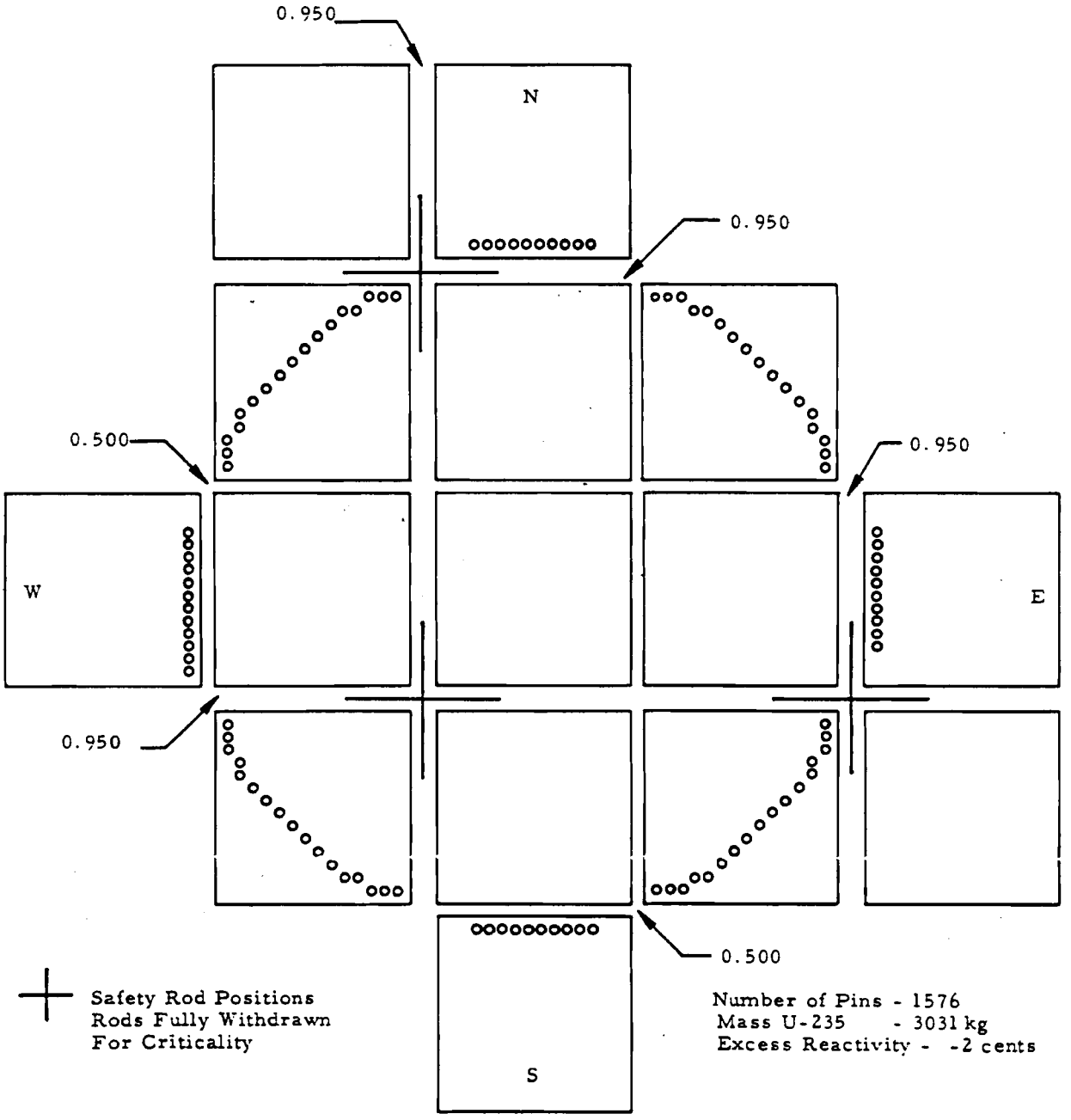

SECTION 7
LATTICE POISONING EXPERIMENTS

Boric acid was added to the moderator of Core 9B and the buckling was determined for different core sizes and boric acid concentrations. The objective of the experiment was to obtain relations between k_∞ and M^2. These measurements, in addition to the $d\rho/dh$ determinations of M^2 and k_∞ (Section 7), should allow the determination of these constants to a greater accuracy.

7.1 METHOD OF BORON ADDITION AND ANALYSIS

Boron was added to the water in batches, using a mixing tank, stirrer, and associated valving. A 5-lb charge was dissolved in the mixing tank with approximately 30 gal of dump tank water; the mixing tank was then emptied by pumping the solution through filters and back into the dump tank. After the desired amount of acid was dissolved, the dump tank water was thoroughly mixed by circulation from the bottom of the dump tank through the fill pump to the core tank, and then back into the dump tank through the dump valve. A 45-min circulation time proved satisfactory

The amount of boron in the water was determined quantitatively by titrating with a standard KOH solution after the boron was complexed with mannitol [$HOCH_2 (CHOH)_4 CH_2 OH$]. Helium was continuously bubbled through the sample under analysis to purge entrapped CO_2. The pH was read on a Beckman Zeromatic pH Meter; the amount of base solution added was read directly from the burette. The neutral point was the point of inflection in the plot of pH versus amount of base added.

At least two analyses were performed on each sample. In general, random error from instrument readings was about 1%; but there exists an additional 1% systematic error from standardizing the KOH solution.

7.2 MEASUREMENTS AND RESULTS

Core 9B was used for these measurements. Fuel pins were removed at safety rod positions. The aluminum rod guides, normally used in Core 9B, were also out for this experiment. Buckling and dρ/dh measurements were taken as functions of radius and boron concentration. The results are summarized in Table 7.1 and in Figure 7.1.

The rate of change of reactivity with water height was determined as described in Section 6.2. The critical water height as a function of boron concentration is shown in Figure 7.2; the critical water height with and without aluminum guides is shown as a function of radius in Figure 7.3.

Buckling measurements were done with Cd covered In foils in all determinations except Run 9, where Cd covered Au foils were used. The vertical traverses were fitted to a cosine curve and the radial traverses to a J_0 curve using the procedure described in Section 4.1. The results of the flux traverses are shown in Tables 7.4 through 7.16. The axial bucklings in Table 7.1 have been corrected for reactivity holddown caused by the Cd covered foils (less than 1% in B^2).

The effect of aluminum rod guides on B^2 was estimated by assuming that reflector savings does not change with the presence or absence of the guides. The reflector savings was then obtained from buckling measurements in Runs 9 and 13, and the critical water height with guides in from Figure 7.3. The results of this correction are given in Table 7.2 along with the results of Core 9B from Section 4.2.

These results were analyzed to obtain k_∞ and M^2. The basic relations used in the analysis are as follows:

$$W_i \, k_\infty(0) = 1 + M^2 \, B_i^2,$$

where

$$\frac{k_\infty (N_B)_i}{k_\infty (0)}.$$

$(N_B)_i$ is the ith boron concentration and B_i^2 is the total material buckling at the ith boron concentration. Then,

$$W_{i+1}/W_i = 1 - \int_{h_i}^{h_{i+1}} d\rho/dh \, (0) \, dh,$$

TABLE 7.1

SUMMARY OF LATTICE POISONING MEASUREMENTS -- CORE 9 B

Run	Number of Pins	Number of Pins Missing At Safety Rod Positions	R, cm	h_c, cm	N_B, gm Boron/ liter H_2O	$N_B \times 10^{-19}$, Atoms/ cm^3 of core	$d\rho/dh$, ¢/cm	B_r^2, $\times 10^{-3}$, cm^{-2}	σB_r^2, $\times 10^{-3}$, cm^{-2}	B_z^2 $\times 10^{-3}$, cm^{-2}	σB_z^2 $\times 10^{-3}$, cm^{-2}	B^2 $\times 10^{-3}$, cm^{-2}	σB^2 $\times 10^{-3}$, cm^{-2}
6	1905	224	25.15	77.0	0	0	6.5						
7	2089	240	26.30	64.9	0	0	10.9						
8	2337	240	27.67	56.45	0	0	30.5						
9	2337	240	27.67	57.25	0	0		4.531	0.060	1.970	0.015	6.501	0.062
10	2777	240	29.94	48.51	0	0	34.5						
11	3645	240	33.97	40.59	0	0	38.0						
12	3645 Plus One Rod Guide	240	33.97	40.94	0	0							
13	3645	240	33.97	40.92	0	0		3.434	0.030	3.271	0.046	6.705	0.055
14	3645	240	33.97	47.97	0.2439	0.6410	27.6						
15	3645	240	33.97	69.19	0.5537	1.455	16.97						
16	3645	240	33.97	78.90	0.7563	1.988				1.118	0.010	4.843	0.060
17	3645	240	33.97	78.99	0.7563	1.988		3.725	0.059				
18	3645	240	33.97	78.24	0.7563	1.988	10.5						
19	3645	240	33.97	109.6	0.9600	2.523		3.745	0.055			4.420	0.056
20	3645	240	33.97	109.51	0.9600	2.523				0.675	0.005		
21	3645	240	33.97	107.8	0.9600	2.523	4.6						
22	4921	240	39.15	66.06	0.9600	2.523	15.62						
23	6769	240	45.63	51.84	0.9600	2.523	18.51						
24	6769	240	45.63	60.82	1.211	3.183	18.5						
25	6769	240	45.63	72.85	1.425	3.745	12.81						
26	6769	240	45.63	108.1	1.748	4.594	5.26						
27	6769	240	45.63	110.0	1.748	4.594		1.994	0.020			2.672	0.021
28	6769	240	45.63	(112.8)*	1.748	4.594				0.678	0.004		
29	9905	240	54.89	66.56	1.748	4.594	18.4						
30	9905	240	54.89	(67.35)	1.748	4.594		1.329	0.022			2.724	0.024
31	9905	240	54.89	(67.38)	1.748	4.594				1.395	0.009		
32	9905	240	54.89	76.68	1.934	5.083	10.9						
34	9905	240	54.89	(119.3)*	2.316	5.083				0.613	0.003	1.866	0.025
35	9905	240	54.89	(120.2)*	2.316	5.083		1.253	0.025				

* Exposure Height, $\rho/B = \$0.15$

TABLE 7.2

BUCKLING CORRECTION FOR ROD GUIDES — CORE 9B

R cm	No Guides H_c, cm	With Guides H_c, cm	No Guides $B^2 \times 10^3$, cm^{-2}	With Guides $B^2 \times 10^3$, cm^{-2}	Detector
24.45		122 plus infinite reflector		6.15	Cd Covered Au
24.45		122 plus infinite reflector		6.07	Cd Covered In
27.67	56.45	62.7	6.50	6.19	Cd Covered Au
33.97	40.59	41.99	6.70	6.36	Cd Covered In

where h_i is the critical water height with $N_B = (N_B)_i$, and h_{i+1} is the critical water height with $N_B = (N_B)_{i+1}$. Both heights are for the same core radius. The case i = 0 is for zero boron concentration and $W_0 = 1$. Values of $d\rho/dh(0)$ for zero boron concentration were taken from Table 6.1. All other parameters were taken from Table 7.1; the parameters used are shown in Table 7.3. Values for W_i and B_i^2 were least squares fitted for $k_\infty(0)$ and M^2. The analysis yields

$$k_\infty(0) = 1.308 \pm 0.011, \text{ and}$$

$$M^2 = 45.7 \pm 1.8.$$

TABLE 7.3

PARAMETERS USED IN k_∞ AND M^2 ANALYSIS

R, cm	h, cm	N_B, g boron/liter H_2O	W_i	B_i^2 x 10^{-3}, cm^{-2}
27.67	56.45	0	1.000	6.501
33.97	40.59	0	1.000	6.705
33.97	78.24	0.7563	0.9274	4.843
33.97	107.8	0.9600	0.9105	4.420
45.63	51.84	0.9600		
45.63	108.1	1.748	0.8607	2.672
54.89	66.56	1.748	0.8607	2.724
54.89	114.6	2.316	0.8337	1.866

$d\rho/dh = 69.0\ \pi^2/(h + 14.5)^3$ for Boric Acid Concentration = 0

FIG. 7.1: CRITICAL WATER HEIGHT VERSUS RADIUS

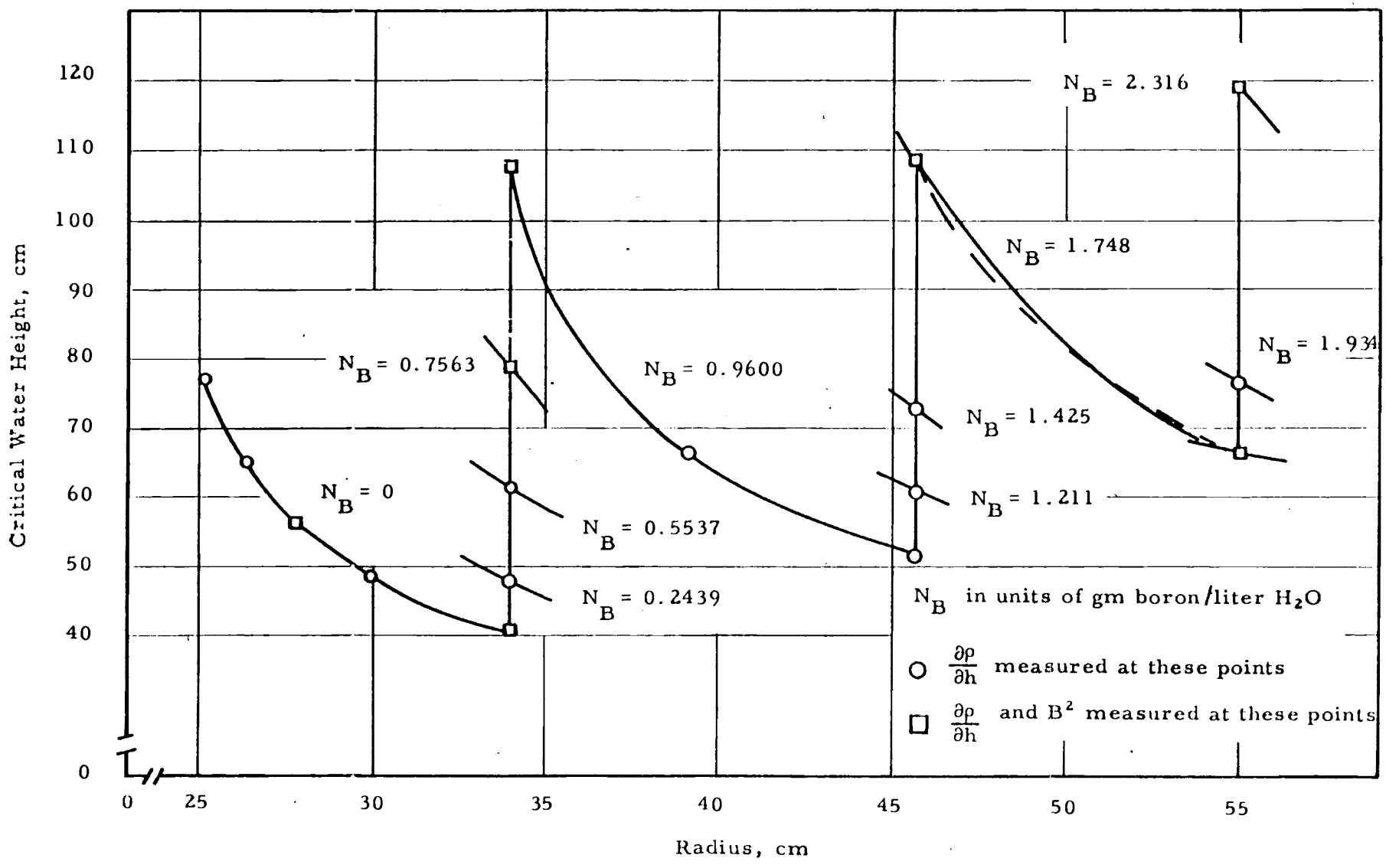

FIG. 7.2: CRITICAL WATER HEIGHT VERSUS BORON CONCENTRATION

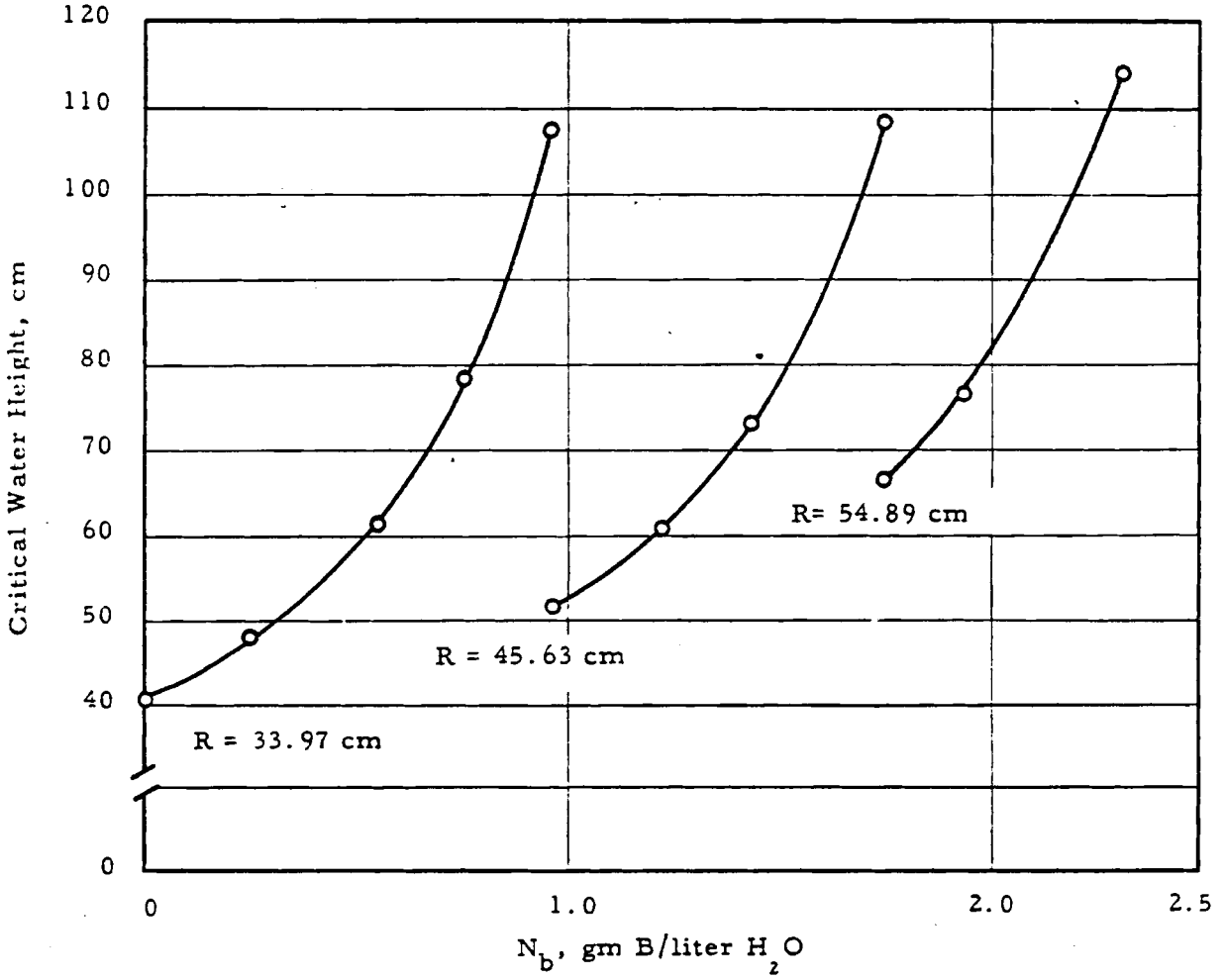

FIG. 7.3: CRITICAL WATER HEIGHT WITH AND WITHOUT Al GUIDES

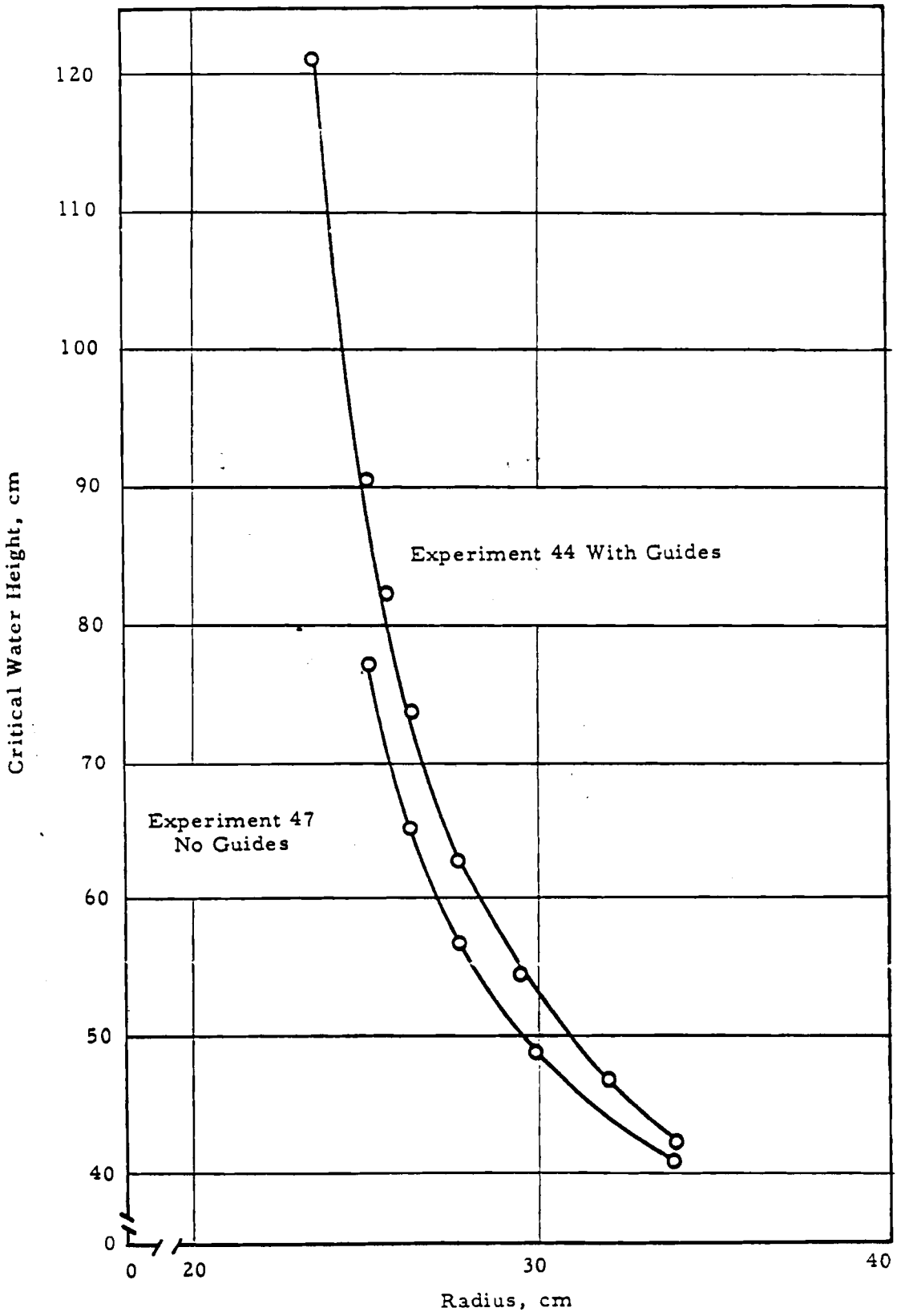

Thorium Uranium Physics Experiments (Reference 16)

Critical experiments were performed using five geometrically clean lattices. Each lattice used fuel pins of a single type located on a square pitch, in a cylindrical array. Sections from Reference 16 describing the cores and the results of the clean critical measurements are reproduced below.

In addition to the clean core measurements, an extensive series of leakage experiments was performed on four of the lattices. For two of the lattices, measurements were made with boric acid added to the water, at several different concentrations. Data include critical radius and height for the various boron concentrations, and hence are of interest here. The entire section, describing the measurements and analysis is included.

SUMMARY

The Thorium Uranium Physics Experiment (TUPE) is a study of uniform lattice cores moderated with light water. TUPE cores contain thorium oxide-uranium oxide pins clad with aluminum and have metal-to water volume ratios, M/W, ranging from 0.3 to 1.0.

Critical experiments for the Consolidated Edison Thorium Reactor (CETR) have provided data on thorium oxide-uranium oxide fuel, in stainless steel cladding, moderated with light water. These data are for cores with M/W near one — the region of interest in pressurized water reactor design. Experiments at Argonne National Laboratory (ANL) have provided data on similar fuel in aluminum cladding moderated with heavy water. These data are for the low metal-to-water volume ratios that accompany heavy water moderation.

TUPE is intended to complement these data by providing information on lattices with ratios between the CETR and ANL values — the region of interest for boiling water reactor design.

The basic aim of the TUPE project is to measure lattice parameters of cores with ratios ranging from 0.3 to 1.0, and to compare the results with different theoretical models.

A series of "clean core" measurements were done on five lattices (the contract required three), including (1) flux mappings, (2) critical mass determinations, M_c, (3) cadmium ratio measurements for U-235 - C_{25} and thorium, C_{02} and (4) flux depression measurements.

These data were then analyzed to obtain material buckling, B_m^2; the ratio of infinite medium thermal multiplication to infinite medium resonance multiplication, k_2/k_1; the thermal disadvantage factors for moderator $\bar{\phi}_w/\bar{\phi}_f$ and for cladding, $\bar{\phi}_{Al}/\bar{\phi}_f$; the thorium resonance escape probability, p_{02}; and the U-235 resonance escape probability. These results are summarized in Table 1.

Leakage experiments, including partial water height experiments and lattice poisoning experiments, were performed on two cores.

Leakage experiments were performed on two additional cores without lattice poisoning (the contract required leakage experiments on two cores). The leakage experiments consisted of determination of the water height coefficient of reactivity, $\partial\rho/\partial h$, as a function of water height and boric acid concentration in the moderator. These data were analyzed to determine migration area, M^2; and infinite medium multiplication constant, $k_\infty = k_1 + k_2$. These results are also summarized in Table 1.

TABLE I

SUMMARY OF RESULTS

Parameter	Core Number				
	$25\sqrt{2}B$	25 D	15 D	15 B	15 A
M/W	0.301	0.480	0.480	0.860	1.024
N_{02}/N_{25}	25.34	25.34	15.00	15.00	15.00
N_H/N_{25}	528	329	165	131	78.0
R_c, cm*	27.3 27.2▽	23.5 23.2▽	15.5 15.8▽	17.0 17.6▽	18.1 18.3▽
M_c, kg*	13.46	13.99	9.73	20.79	25.96
$B_m^2 \times 10^{-3}$, cm^{-2}	5.355	6.401	11.42	9.425	8.531
C_{25}	19.8 19.9▽	12.8 13.4▽	8.7 9.5▽	5.5 5.7▽	4.8 4.9▽
C_{02}	2.82 4.13▽	2.26 3.12▽	1.78 2.24▽	1.48 1.70▽	1.37 1.56▽
k_2/k_1	18.8 18.9▽	11.8 12.4▽	7.7 8.5▽	4.5 4.7▽	3.8 3.9▽
$\bar{\phi}_w/\bar{\phi}_f$	1.22 1.14▽	1.16 1.12▽	1.22 1.19▽	1.12 1.18▽	1.22 1.18▽
$\bar{\phi}_{Al}/\phi_f$	1.04▽	1.05▽	1.08▽	1.09▽	1.10▽
p_{02}	0.916 0.945▽	0.878 0.918▽	0.870 0.910▽	0.810 0.864▽	0.756 0.849▽
p_{25}	0.960 0.956▽	0.933 0.932▽	0.886 0.895▽	0.816 0.822▽	0.786 0.792▽
M^2, cm^2 **		41.7	36.6	54.4	57.4
M^2, cm^2 ★		32.9	28.5	37.7	38.4
M^2, cm^2 △	41.7▽	45.5▽	45.3▽	52.2▽	54.8▽
M^2, cm^2 □			35.3▽	42.7▽	
k_∞ **		1.27	1.42	1.49	1.49
k_∞ ★		1.23	1.38	1.41	1.39
k_∞	1.22▽	1.29▽	1.48▽	1.42▽	1.40▽

* Reflected cylinder — 5 ft high
** One-Group Model
★ Gaussian Model
▽ Calculated Values
□ MUFT Code B — Self-Consistent Age Approximation — One-Group Model
△ Spectral Code, One-Group Model

1. OBJECTIVES

The objectives of TUPE experiments are to measure lattice parameters for a series of cores with metal-to-water volume ratios (M/W) in the range of 0.3 to 1.0 and for N_{02}/N_{25} = 25/1 and 15/1. Specifically, material buckling (B^2_M), critical size and mass, and nonleakage probability as a function of buckling, $P(B^2)$, are to be determined for each core.

If the above objectives are met then the infinite multiplication constant, k_∞, is

$$k_\infty = P^{-1}(B^2_m), \tag{1}$$

and k_{eff} for any core of geometric buckling B^2_g is

$$k_{eff} = P^{-1}\ (B^2_m)\ P\ (B^2_g). \tag{2}$$

Additional objectives are to determine as many detailed two-group parameters as possible, including separation of k_∞ into slow and fast components, resonance escape probability from thorium, and ratio of average thermal flux in water to average thermal flux in fuel.

2. DESCRIPTION OF CORES

Two types of fuel pins were available to the TUPE project — B&W loaded 3000 15/1 pins with sintered thorium oxide-uranium oxide pellets; ANL loaded 1500 25/1 pins to the project. Table 2 lists the properties of these two pin types.

TABLE 2
PROPERTIES OF FUEL PINS

	15/1 Pins	25/1 Pins
OD, in.	0.309	0.309
Clad Material	Al-2S	Al-2S
Clad Thickness, in.	0.014	0.034
ID, in.	0.281	0.241
Active Pin Length, in.	60	60
Pellet Diameter, in.	0.260	0.234
Effective Pellet Density, gm/cm^3	8.35	8.45
M_{25}/Pin, gm	24.04	12.04
N_{02}/N_{25}	15.00	25.34
M_{ThO_2}/Pin, gm	405.0	341.8
$M_{Pellets}$/Pin, gm	434.6	356.8

The pins were loaded in the core tank on a square pitch and held in place by two "egg-crate" grids, one placed on a 4-in.-thick aluminum plate at the bottom of the tank, the other held by an aluminum structure at about the 5-ft level in the tank. Figures 1 and 2 are photographs of two of the cores, showing both the upper and lower grid plates.

The three safety rods visible in Figures 1 and 2 were made of Type 304 stainless steel and had a 20-mil cadmium layer on one side; the

cadmium was covered with thin mylar tape. The safety rods — sized to fit in the space between fuel pins without disturbing spacing — were cocked all the way up for all measurements; therefore, the results are for a truly uniform lattice.

Each of the five cores studied is designated by a number and a letter; the number refers to the type of pin, (see Table 2) and the letter to the pin spacing. For example, consider the number 15D, where 15 designates the 15/1 pins, and D defines the spacing as given in Table 3. In core $25\sqrt{2}B$, the pins were 25/1, but the spacing used every other diagonal row of the B spacing, thus giving a square pitch equal to $\sqrt{2}$ times the B pitch. Table 3 shows volume fractions and the center-to-center spacing (p) the metal-to-water volume ratio and the water-to-fuel volume ratio (W/F) for all cores studied. Here M is the volume of the entire pin and F is the volume of fuel pellets only. The number densities of the elements in each core, including impurities, are given in Appendix 6. Figure 3 is a diagram of the just critical $25\sqrt{2}B$ core, and Figure 4 shows core diagrams used for clean core measurements on cores 25D, 15D, 15B, and 15A.

TABLE 3

CORE VOLUME RATIOS AND VOLUME FRACTIONS

	Ratios		
Core	p, in.	M/W	W/F
15A	0.3850	1.024	1.379
15B	0.4027	0.860	1.642
15C	0.4400	0.632	2.234
15D	0.4810	0.480	2.945
$25\sqrt{2}B$	0.5694	0.301	5.794
25D	0.4810	0.480	3.636

	Fractions			
Core	Water	Pellets	Aluminum	Void
15A	0.4942	0.3582	0.0875	0.0602
15B	0.5376	0.3274	0.0800	0.0550
15C	0.6127	0.2742	0.0670	0.0461
15D	0.6759	0.2295	0.0561	0.0386
$25\sqrt{2}B$	0.7687	0.1326	0.0906	0.0081
25D	0.6759	0.1859	0.1269	0.0113

FIG. 1: CORE 25-$\sqrt{2}$B

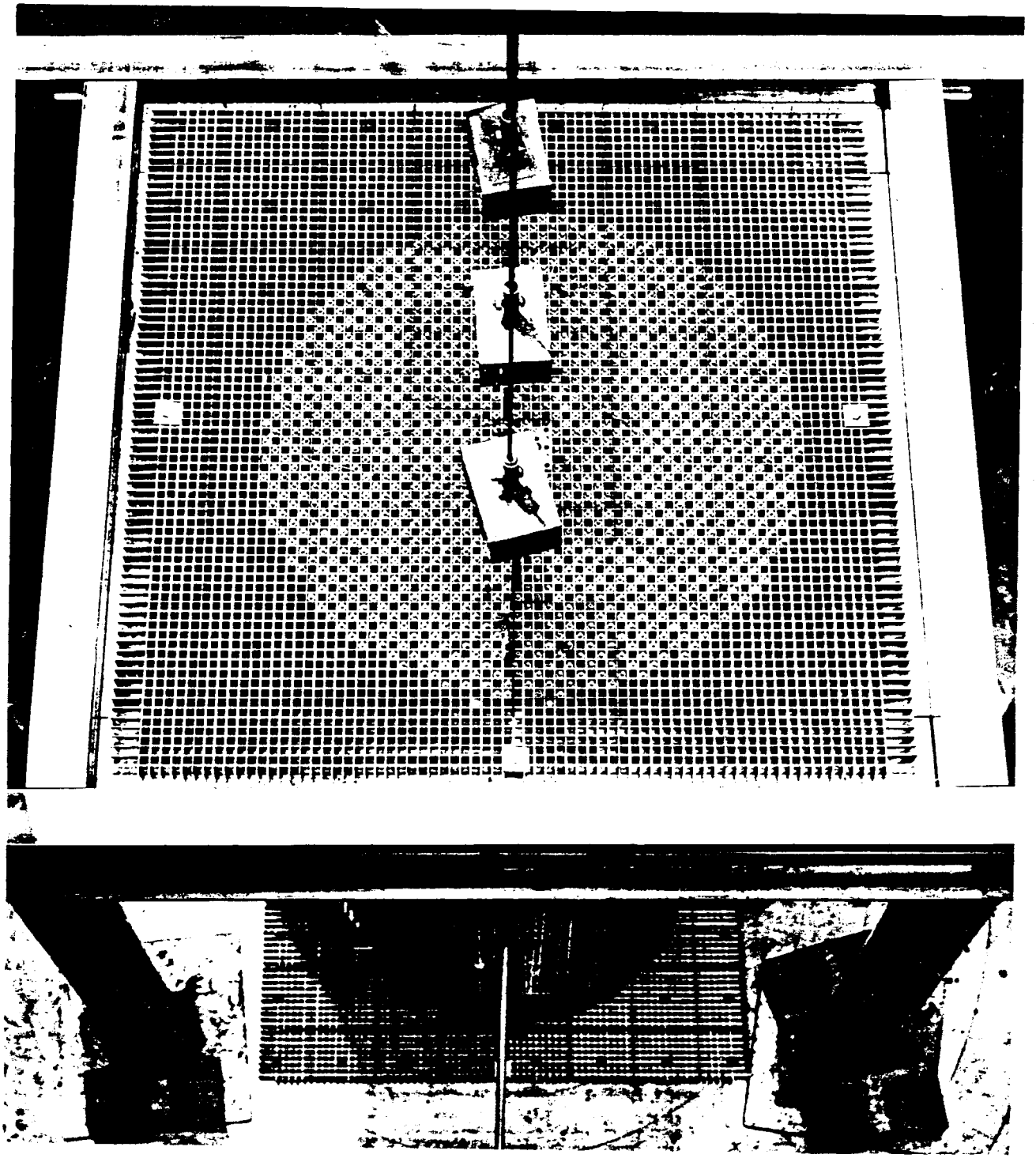

FIG. 2: CORE 25D

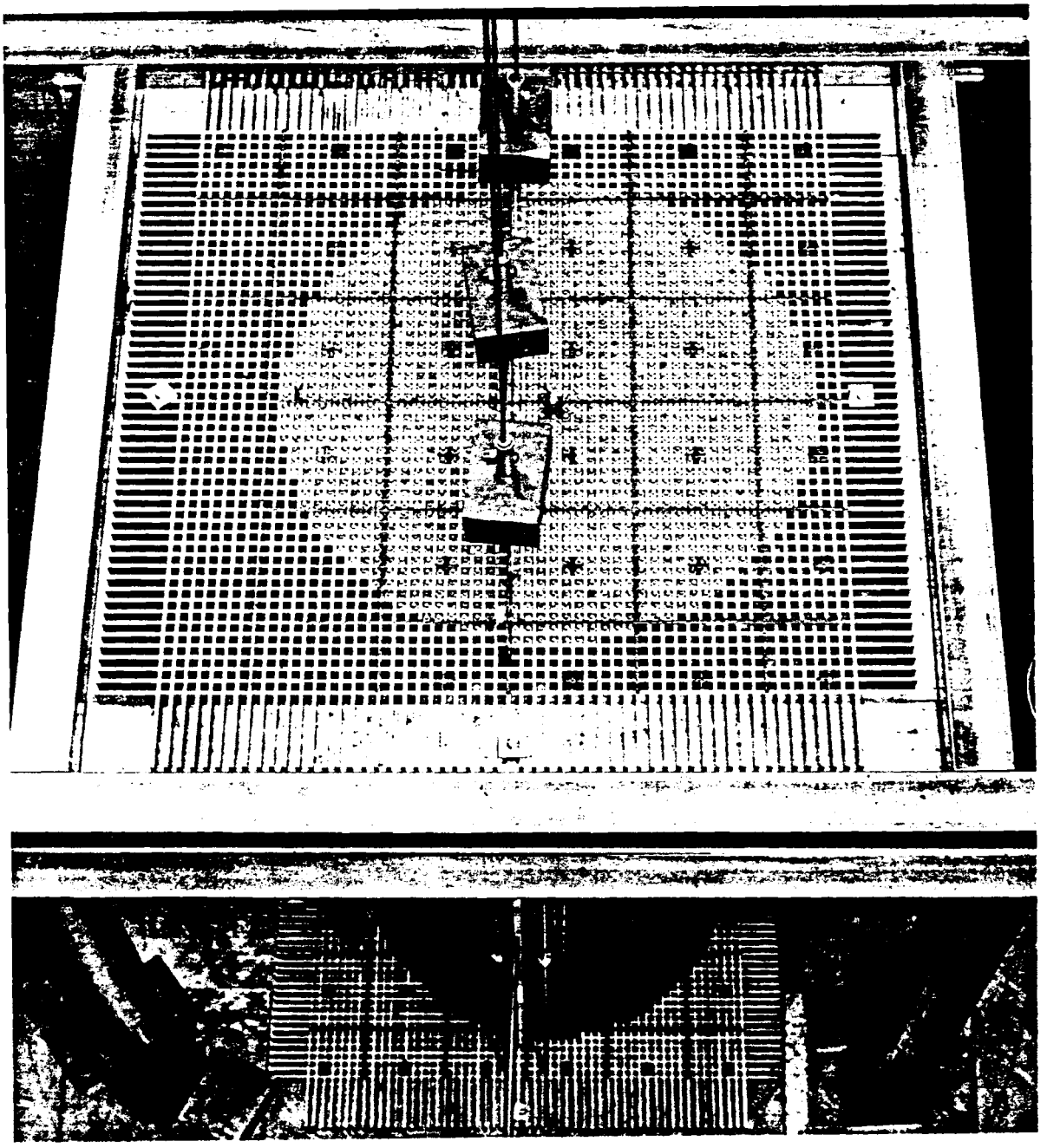

FIG. 3: DIAGRAM OF CORE $25\sqrt{2}B$

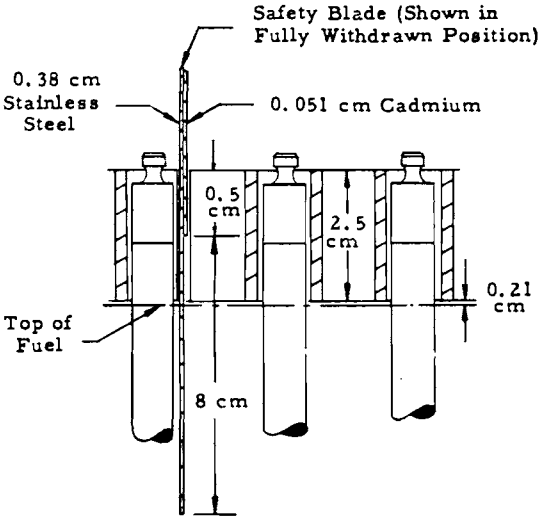

DETAIL "A"

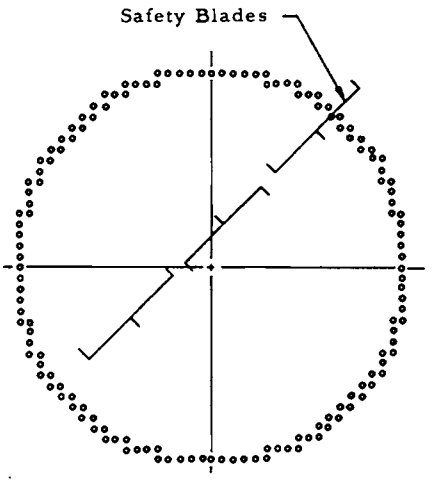

VIEW CC

K_{excess}	=	10.2 cents
Radius	=	27.3 cm
Number of Pins	=	1118
Mass U-235	=	13.46 kg
Pitch	=	1.446 cm
M/W	=	0.301

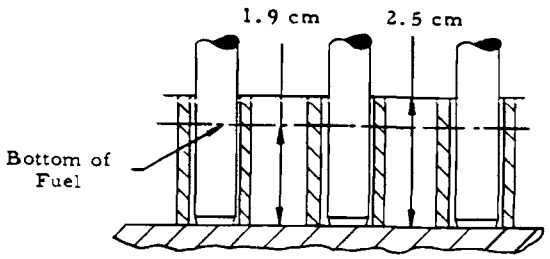

DETAIL "B"

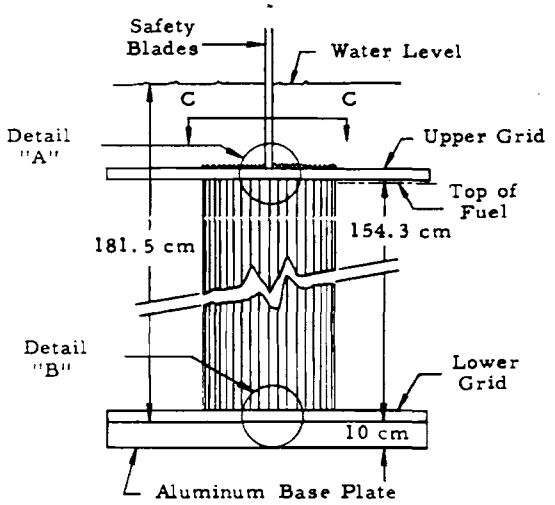

FIG. 4: CORE DIAGRAMS FOR CLEAN CORE MEASUREMENTS

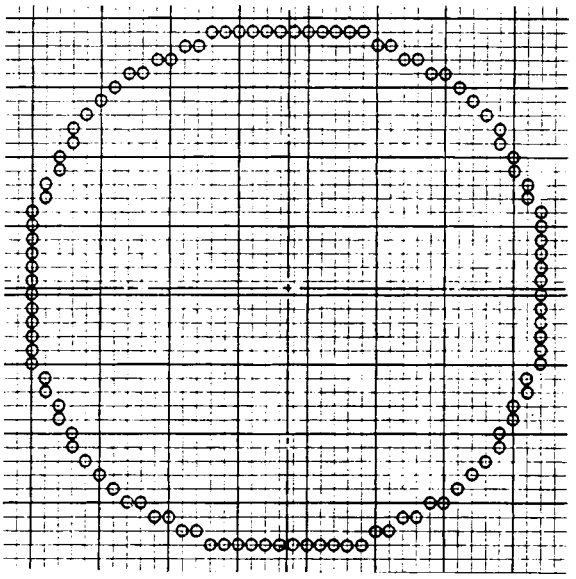

Core 25 D
Number Pins: 1176
Core Radius = 23.64 cm
Critical Water Height = 140.5 cm

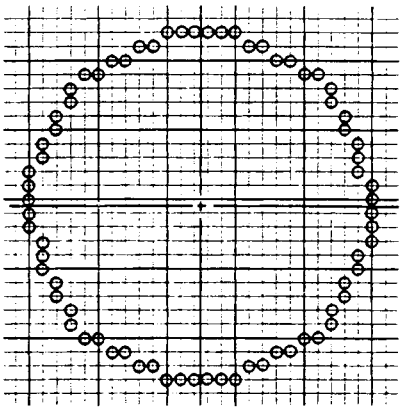

Core 15 D
Number Pins: 514
Core Radius = 15.63 cm
Critical Water Height = 135.0 cm

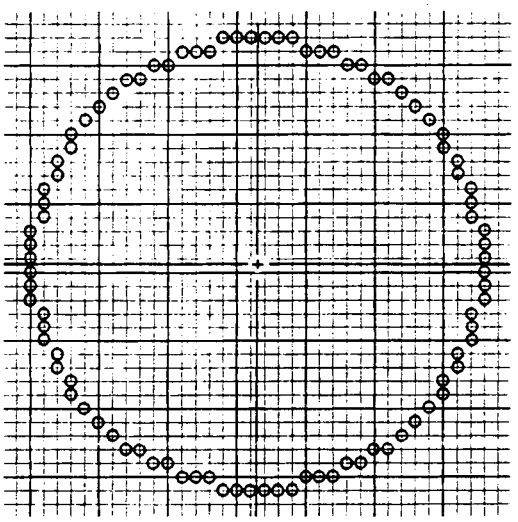

Core 15 B
Number Pins: 880
Core Radius = 17.12 cm
Critical Water Height = 133.44 cm

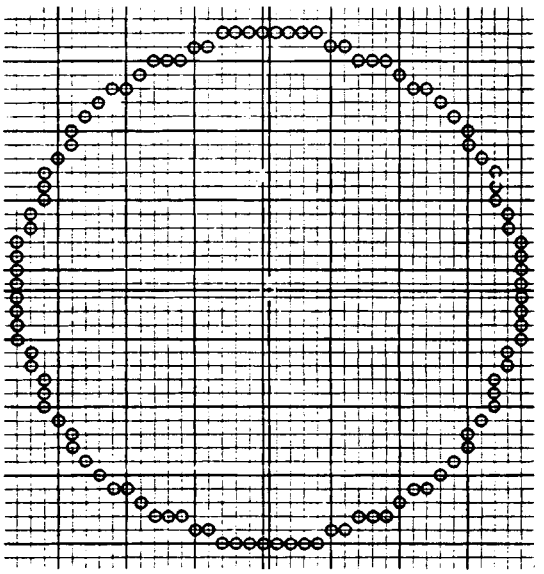

Core 15 A
Number Pins: 1108
Core Radius = 18.37 cm
Critical Water Height = 127.21 cm

NOTE:

Pins are to be assumed located at all grid line crosses inside the core.

3. CLEAN CORE MEASUREMENTS

3.1 FLUX MEASUREMENTS

3.1.1 Experimental Methods

Radial and axial flux traverses were made for five clean cores; 25$\sqrt{2}$B, 25D, 15D, 15B, and 15A. The radial flux distributions were measured with bare and cadmium covered gold foils (1/4-in. diameter) and with manganese-copper wire. The foils, encased in aluminum or cadmium boxes, were mounted in accurately spaced holes in a 60-mil lucite strip, then covered with Polyken tape and placed near the core midplane.* A 250-mil lucite grid supported the foil holder and insured uniform fuel rod spacing in the vicinity of the foils. Figure 5 shows the foil arrangement for core 25$\sqrt{2}$B. For most traverses, the spacing between foils was one lattice unit; but to determine the effect of cadmium covers on flux distribution as a function of spacing between foils, traverses were taken with foils spaced up to eight lattice units apart. The radial wire was mounted on a lucite strip and placed near the core midplane.

The axial flux distribution was measured with manganese-copper wire mounted inside concentric aluminum (outer) and lucite (inner) tubes and inserted along the core vertical centerline.

Foils were normally exposed with the reactor on a positive period, and monitor foils were included in each experimental run so that the data could be normalized. After activation, each foil was counted six times — up and down in three different end-window gas-flow proportional counters. The saturated activity was computed for each count rate and an average value obtained.

The wires were counted with a scintillation counter (beta sensitive crystal) at preset distance intervals on a master-slave

* Polyken is a trade name for a product of the Kendall Company.

automatic wire scanner. The counting time on the data wire (slave) equals the time for a fixed number of counts on a control wire (master) that was activated with the data wire. This method compensates for decay during the counting period. Each wire was counted at least three times, and an average relative activity was calculated for each count position.

3.1.2 Results

3.1.2.1 Flux Distribution

The relative activity as a function of position gives the flux distribution; radial and axial flux traverse results are shown in Appendix 5. Figure 6 is a representative plot of the radial flux distribution measured with cadmium covered gold foils; the distribution plotted in Figure 7 was measured with manganese-copper wire.

Cadmium ratios measured with the gold foils at close and at wide spacings were in good agreement. It was concluded that even with spacings as close as one lattice unit the cadmium boxes do not alter the flux distribution appreciably.

3.1.2.2 Buckling and Reflector Savings

B_r, the positive square root of the radial buckling, was determined by a least-squares fit of experimental data to the theoretical equation for radial flux distribution. In the asymptotic region the radial distribution is

$$\phi(r_i) = A J_0 [B_r (r_i - r_0)], \qquad (3)$$

where r_0 is the distance from the geometric center to the center of the fitted curve, and A and B_r are constants. In the asymptotic region, the gold-cadmium ratio is constant; therefore, the data were fitted to different radii in the region where the measured gold-cadmium ratio is essentially constant. The values of B_r obtained from the least-squares fit are shown in Appendix 5.

The radial wire measurements were consistent with the foil measurements, so manganese-copper wire can be used to measure the axial flux distribution. Values for B_z, the positive square root of axial buckling, were obtained by a least-squares fit of the

experimental data over different portions of the axial flux distribution to

$$\phi(z_i) = A\cos[B_z(z_i - z_0)], \tag{4}$$

where z_0 is the elevation of the center of the fitted curve, and A and B_z are constant. Results are shown in Appendix 5.

Each value obtained from a curve fitting was weighted according to the inverse square of its standard deviation,

$$W_i = 1/\sigma_i^2, \tag{5}$$

and weighted mean values, $\bar{B}_r$ and $\bar{B}_z$, were calculated by

$$\bar{B} = \frac{\sum_{i=1}^{n} W_i B_i}{\sum_{i=1}^{n} W_i}. \tag{6}$$

The standard deviations on the weighted mean values, based on internal and external consistency, were calculated from

$$\sigma_{int} = \frac{1}{\left[\sum_{i=1}^{n} W_i\right]^{1/2}} \tag{7}$$

and

$$\sigma_{ext} = \left[\frac{\sum_{i=1}^{n} W_i (B_i - \bar{B})^2}{(n-1)\sum_{i=1}^{n} W_i}\right]^{1/2}. \tag{8}$$

In each case, the larger and more conservative error is reported.

The reflector savings were calculated from the weighted mean values of B_r and B_z, using

$$B_r = \frac{2.4048}{R + \delta} \quad \text{and} \tag{9}$$

$$B_z = \frac{\pi}{H + \lambda}. \tag{10}$$

The radius, R, in Equation (9) is the effective radius of the experimental core, given by

$$\pi R^2 = \text{(Number of unit cells) (Area per unit cell)}. \quad (11)$$

The core height, H, in Equation (10) is the height of the water above the bottom of the fuel when the axial traverse was made.

The material buckling is equal to geometric buckling for a critical core, but the core was slightly supercritical for the flux measurements. B_z for the critical core was calculated by solving Equation (10) with H set equal to the reported critical water height, and λ set equal to the measured reflector savings. The buckling of the critical core is then calculated by

$$B_g^2 = B_r^2 + B_z^2 = B_m^2. \quad (12)$$

Clean core buckling versus M/W is shown in Figure 8, and Figure 9 shows clean core reflector savings versus M/W; both are summarized in Table 4.

3.1.2.3 Critical Mass

Critical mass is defined as the minimum mass of fuel, arranged in a particular pattern, that will support a chain reaction. The critical radius, R_c, for a cylinder having full water height (infinite top reflector) was determined by a slight extrapolation for most cores from

$$\left[\frac{2.4048}{R_c + \delta}\right]^2 + \left[\frac{\pi}{H_c + \lambda}\right]^2 = B_m^2, \quad (13)$$

where H_c is the active fuel length (152.4 cm) and B_m^2, δ, and λ are the measured buckling and reflector savings at a water height slightly below H_c. The number of fuel pins for the critical core with full water height is calculated by solving Equation (11) with R equal to the critical radius. The critical mass is then calculated by multiplying the number of fuel pins by the mass of U-235 per fuel pin. The critical mass for each clean core is shown in Table 4.

3.1.3 Discussion of Results

Since the experimental cores were not perfect cylinders, there was some question as to whether buckling is the same along

different radii. This effect could not be measured (the radial traverse could not cross the plane of the control rods) so the PDQ program was used to calculate the flux distributions along different radii for cores $25\sqrt{2}B$, 25D, and 15D, as shown in Appendix 5. The calculated flux distributions were then analyzed in the same manner as measured distributions; the results (Appendix 5) show that the weighted mean value of B_r for all radii falls within the standard deviation for radius C, where the radial traverse was measured.

The asymptotic region determined from PDQ results agrees satisfactorily with the asymptotic region determined from the gold-cadmium ratio measurements. Axial flux calculations at different radii and radial flux calculations at different elevations verify the separability of the radial and axial fluxes.

Core water heights for the flux traverses were below the top of the active fuel; therefore the region above the core was active fuel and the region below the core was mostly aluminum (grid and base plates) with 1.9 cm of water in the grid. Thermal neutrons leaking from the core will cause fissions in the fuel region above the core and provide a fast neutron source. In a sense, this fast neutron source acts as a top reflector, and since the reflector savings at the top and the bottom of the core are not equal, the axial flux distribution is not symmetric. Axial flux traverses indicated a slight tilt in the distribution, so axial flux data were fitted to

$$\phi(z_i) = A\cos[B_z(z_i - z_0)] + D\sin[2B_z(z_i - z_0)]. \qquad (14)$$

There are four unknowns — A, B_z, D, z_0 — in Equation (14), and a fit of experimental data over different portions of the flux distribution showed considerable variation in these parameters even though the fit was excellent. The weighted mean values of B_z calculated with Equation (14) were in fair agreement with values calculated with Equation (4) but results for fits to different heights were inconsistent.

TABLE 4

SUMMARY OF RESULTS
CLEAN CORE FLUX TRAVERSES

Parameter	Core				
	25√2B	25D	15D	15B	15A
Pitch, in.	0.5694	0.4810	0.4810	0.4027	0.3850
M/W	0.301	0.480	0.480	0.860	1.024
W/F	5.794	3.630	2.945	1.642	1.379
No. Fuel Pins	1146	1176	514	880	1108
Effective Radius, cm	27.62	23.64	15.63	17.12	18.37
Core Height, cm	137.79	143.06	139.52	135.14	128.91
Critical Height, cm	135.27	140.50	135.05	133.44	127.21
$\overline{B}_r \pm \sigma$, $cm^{-1} \times 10^{-4}$	701.25±0.73	773.50±2.96	1048.01±3.21	945.61±1.52	896.00±1.46
$\overline{B}_z \pm \sigma$, $cm^{-1} \times 10^{-4}$	205.74±0.92	200.78±0.54	202.93±2.09	217.30±0.78	221.59±0.48
$\overline{B}_{z\,crit} \pm \sigma$, $cm^{-1} \times 10^{-4}$	209.17±0.92	204.40±0.54	208.97±2.09	219.88±0.78	224.29±0.48
$\delta \pm \sigma$, cm	6.67±0.04	7.45±0.12	7.32±0.07	8.31±0.04	8.47±0.04
$\lambda \pm \sigma$, cm	14.92±0.68	13.41±0.42	15.29±1.61	9.44±0.51	12.86±0.31
$B^2 \pm \sigma$, $cm^{-2} \times 10^{-4}$	53.55±0.11	64.01±0.46	114.20±0.70	94.25±0.29	85.31±0.26
Critical Radius, cm (Full Water Height)	27.3	23.5	15.5	16.97	18.13
No. Fuel Rods (Full Water Height)	1118	1162	506	865	1080
Critical Mass, kg	13.46	13.99	9.73	20.79	25.96

4. LEAKAGE EXPERIMENTS

4.1 DERIVATION OF BASIC EQUATIONS

The purpose of leakage experiments is to determine the infinite multiplication constant, k_∞, and the migration area, M^2. In the one-group diffusion analysis of nuclear reactors, these parameters are related by

$$k_\infty = k_{eff}(1 + M^2 B^2), \tag{20}$$

where

$$B^2 = [2.405/(R + \delta)]^2 + [\pi/(H + \lambda)]^2 \tag{21}$$

H = Critical core height,

R = Critical core radius,

λ = Axial reflector savings, and

δ = Radial reflector savings.

From reactor kinetics,

$$\rho = (k_{eff} - 1)/k_{eff}, \text{ and,} \tag{22}$$

if $k_{eff} \approx 1.0$, then

$$d\rho = dk_{eff}. \tag{23}$$

The differentiation of Equation (20) with respect to h yields

$$\frac{dk_{eff}}{dh} = \frac{d\rho}{dh} = \frac{-k_{eff} M^2}{1 + M^2 B^2}\left[\frac{dB^2}{dh}\right]. \tag{24}$$

Again applying the condition $k_{eff} \approx 1$ and making the substitution

$$C = \frac{M^2}{1 + M^2 B^2}, \tag{25}$$

Equation (24) reduces to

$$\frac{d\rho}{dh} = -C\frac{dB^2}{dh}. \tag{26}$$

If the age critical equation

$$k_\infty = k_{eff} \exp(M^2 B^2) \tag{27}$$

is used instead of the one-group critical equation, Equation (24) becomes

$$\frac{dk_{eff}}{dh} = \frac{d\rho}{dh} = -k_{eff} M^2 \frac{dB^2}{dh} . \tag{28}$$

Applying the condition $k_{eff} \approx 1$ and defining

$$C = M^2 \tag{29}$$

Equation (28) also reduces to

$$\frac{d\rho}{dh} = -C \frac{dB^2}{dh} . \tag{26}$$

Thus Equation (26) is applicable to both models with the constant C defined either by Equation (25) for the one-group model or by Equation (29) for the age model. Note for the one-group model, C is dependent on B^2, but for the age model C is independent of B^2.

The value of $\frac{dB^2}{dh}$ can be obtained directly from Equation (21) by differentiation. Experimental measurements indicate $\frac{d\delta}{dh}$ is approximately zero, therefore,

$$\frac{dB^2}{dh} = \frac{-2\pi^2}{(H + \lambda)^3} \left[1 + \frac{d\lambda}{dh}\right], \tag{30}$$

and Equation (26) reduces to

$$\frac{d\rho}{dh} = \frac{2\pi^2 C}{(H + \lambda)^3} \left[1 + \frac{d\lambda}{dh}\right]. \tag{31}$$

Generally the value of $\frac{d\lambda}{dh}$ is assumed to be zero and Equation (31) reduces to a linear function of $\left[\frac{d\rho}{dh}\right]^{-1/3}$ versus h with an h- intercept of $-\lambda$ and a slope of $(2\pi^2 C)^{1/3}$. However, experimental determinations of λ at various water heights consistently show a variation with h. Therefore, this assumption cannot be applied for these cores.

There is not enough data collected to establish the functional relationship between h and λ, but if a linear relationship is assumed of the form

$$\lambda = Ah + D, \tag{32}$$

Equation (31) becomes

$$H = \frac{[2\pi^2 C(1 + A)]^{1/3}}{1 + A} \left[\frac{d\rho}{dh}\right]^{1/3} \frac{D}{1 + A} . \tag{33}$$

The quantities B^2 and M^2 must be determined to calculate k_∞. To determine B^2, the quantities H, R, δ, and λ are measured; to determine M^2, the value of C is calculated from measured values of H and $d\rho/dh$ and used in Equation (25) or (28). In reactors with nearly all thermal neutron absorptions occurring in the fuel, a change in the thermal absorption cross section of the moderator will produce almost no change in M^2 but an appreciable change in B^2. This change in thermal absorption cross section can be accomplished by the addition of boric acid to the moderator. Therefore, C and B^2 determinations at several boric acid concentrations will improve the determination of M^2.

4.2 EXPERIMENTAL METHODS

4.2.1 Determination of $d\rho/dh$ and H

The quantities $d\rho/dh$ and H are determined by measuring the reactivity, ρ, at corresponding water heights, h. The slope of the curve of ρ versus h is $d\rho/dh$; the zero reactivity intercept is H. Thus two measurements are required, ρ and h.

Reactivity is measured from the reactor period using the inhour equation. To measure period, a special B&W designed electronic scaler counts the pulses from two neutron detectors for 12 sec, prints the totals on IBM cards, and resets, all on a 15-sec cycle. The average ratio of adjacent counts is related to period by

$$T = \frac{15}{\ln(\overline{C_2/C_1})} \tag{34}$$

where T = reactor period in sec, and

$(\overline{C_2/C_1})$ = average ratio of adjacent counts.

An electronic computer determines the period from each detector, the standard deviation of each period, the weighted average period, and the weighted deviation. If the periods from the two detectors differ by more than 10% the average is not computed and the point is discarded. The conversion to reactivity is made using the delayed neutron fractions reported by Keepin and the total delay fraction calculated in Appendix 4.

The water height is measured by two devices; one measuring the absolute height, H_m, to ± 0.1 cm, the other measuring relative water height, h_r, to ± 0.005 cm. The true absolute water height, h,

corresponding to each reactivity measurement is

$$h = \frac{(H_m - h_r)}{n} + h_r \qquad (35)$$

where n is the total number of steps.

The electronic computer calculates $d\rho/dh$ and H by least squares using a weight on ρ of

$$W = \left[\frac{T}{\rho\sigma}\right]^2, \qquad (36)$$

where T = the weighted average period, and

σ = the weighted deviation of the period.

(The calculation of this weighting factor requires the assumption that the reactivity is proportional to the reciprocal of the period.)

4.2.2 Determination of λ, δ and R

The radial and axial reflector savings are determined from flux distributions for most cores. Two flux distributions were made for each boron concentration; one in which the core was critical at a low ($\sim$40 cm) water height and one at a high ($\sim$130 cm) water height.

The critical radius of a core is the square root of the number of pins divided by π and multiplied by the pin pitch.

4.2.3 Determination of Boron Concentration

The moderator boron content was quantitatively analyzed by titrating a sample with a standardized KOH solution after the boric acid is completely ionized by complexing with mannitol. The point of inflection in the curve of pH versus volume of KOH is the point of neutralization.

Samples were drawn every operating day and at least two analyses were run on each sample. A very slight increase in the acid concentration with time was assumed to be due to evaporation. The analyses are accurate to $\pm$ 1%, but standardization of the KOH introduces a possible additional $\pm$ 1% error.

4.3 EXPERIMENTAL RESULTS

One series of measurements was done on core 25D and one on core 15A; the moderator contained no boron here. Four series of

measurements were done on core 15D and four on core 15B at four boron concentrations (including zero).

Table 8 lists the experimental measurements used in determination of λ and B^2 for all the cores; Tables 9 through 12 list the experimental measurements used in determination of C.

4.4 METHOD OF ANALYSIS

The experimental values of λ were used to calculate the constants A and D of Equation (32) and their standard deviations, using Equations (37) through (40) (these equations apply for cases where two determinations of λ were made).

$$A = \lambda_1 - \lambda_2 / (H_1 - H_2) \tag{37}$$

$$\sigma_A = (\sigma_1^2 + \sigma_2^2)^{1/2} / (H_2 - H_2) \tag{38}$$

$$D = 1/2 [\lambda_1 + \lambda_2 - A (H_1 + H_2)] \tag{39}$$

$$\sigma_D = 1/2 \left\{ \sigma_1^2 + \sigma_2^2 + [(H_1 + H_2)\, \sigma_A]^2 \right\}^{1/2} \tag{40}$$

For cores 15A and 25D λ was determined only once; the value of A was assumed to be zero for these cores. To reduce the data in a consistent manner, a second measurement was defined at a 100 cm height of the same value and standard deviation as the measured value. Likewise, on core 15D only one measurement of λ was performed. However, this value was completely out of line with the values from other measurements and was discarded. A least squares extrapolation of λ from Series 2, 3 and 4 yielded a value of 8.53 ± 0.9. This value was then treated in the same manner as outlined above for cores 15A and 25D.

The experimental values of H and $\left[\frac{d\rho}{dh}\right]^{-1/3}$ are least-squares fit with equal weighting through the intercept D (1 + A) by Equation (33). The slope and the slope standard deviation for the resultant line are

$$\text{Slope} = \frac{\Sigma H_i X_i - (D/1 + A) \Sigma X_i}{\Sigma X_i^2}, \text{ and} \tag{41}$$

$$\sigma_s = \left[\frac{\Sigma v_i^2}{N-2}\right]^{1/2} \left[\frac{N}{N \Sigma X_i^2 - (\Sigma X_i)^2}\right]^{1/2}, \tag{42}$$

where $X = \left[\frac{d\rho}{dh}\right]^{-2/3}$,

N = Number of data points, including the intercept, and

v = Data variance from computed curve (variance on intercept was σ_D divided by the slope.

By Equation (33),

$$C = \frac{(\text{Slope})^3 (1 + A)^2}{2\pi^2}, \tag{43}$$

and $$\sigma_c = C\left[\left(\frac{2\sigma_a}{1 + A}\right)^2 + \left(\frac{3\sigma_s}{(\text{Slope})}\right)^2\right]^{1/2}. \tag{44}$$

Table 13 gives the values of C obtained for each core, and the values obtained for A, and D.

4.5 ANISOTROPY IN MIGRATION AREA

If the migration area is considered to be different in the radial and axial directions then the multiplication constant for a one-diffusion-group model is given by

$$k_{eff} = \frac{k_\infty}{1 + M_r^2 B_r^2 + M_Z^2 B_Z^2}, \tag{45}$$

and for a Gaussian slowing down model by

$$k_{eff} = k_\infty e^{-[M_r^2 B_r^2 + M_Z^2 B_Z^2]}. \tag{46}$$

For both models then

$$M_r^2 B_r^2 + M_Z^2 B_Z^2 = \text{constant, therefore} \tag{47}$$

$$\frac{1}{(H + \lambda)^2} = -\frac{(2.405)^2}{\pi^2}\frac{M_r^2}{M_Z^2}\frac{1}{(R + \delta)^2} + \text{constant}. \tag{48}$$

A plot of $\frac{1}{(H + \lambda)^2}$ versus $\frac{1}{(R + \delta)^2}$ gives a straight line with a slope of $-0.586\frac{M_r^2}{M_Z^2}$.

Since the radial reflector savings, δ, is an appreciable fraction of $R + \delta$ for the TUPE cores, the anisotropy obtained by this method is dependent on δ. The radial reflector savings were measured at two radii for most cores. To provide values at other radii, calculated curves of δ as a function of R were fitted to the measured values. Then, using a one-group model and matching the neutron current and flux at the core reflector interface, for a cylinder

$$B_c D_c \frac{J_1 (B_c R)}{J_0 (B_c R)} = \frac{D_r}{L_r} \frac{K_1 (R/L_r)}{K_0 (R/L_r)}, \tag{49}$$

where B_c is the square root of the radial buckling, D_c and D_r are the diffusion constants in core and reflector, L_r is the diffusion length in the reflector and R is the radius to the core-reflector interface. Letting $R = a\delta$ and substituting $\frac{2.405}{R + \delta}$ for B_c gives

$$\delta = \frac{2.405}{a + 1} \frac{J_1\left(\frac{2.405\,a}{a + 1}\right)}{J_0\left(\frac{2.405\,a}{a + 1}\right)} \frac{K_0\left(\frac{a}{L_r}\delta\right)}{K_1\left(\frac{a}{L_r}\delta\right)} \delta_0, \tag{50}$$

where δ_0 is $\frac{D_c}{D_r} L_r$, the reflector savings for large values of R. Then, δ was found for various values of a and δ_0 by iteration. The δ in the argument of K_0 and K_1 was first assumed to be δ_0 and Equation (50) was solved for δ. This value was then used and another δ determined. At the lowest values of R approximately four iterations were required. Figure 12 shows the calculated curves of δ (R) and its measured values. Plots of $\frac{1}{(H + \lambda)^2}$ as a function of $\frac{1}{(R + \delta)^2}$ were then made for each clean core and M_Z^2/M_r^2 was determined from the slope. These results are given in Figures 13 through 15.

When anistropy is introduced, Equation (25) (one-group model) becomes

$$C = \frac{M_Z^2}{1 + M_r^2 B_r^2 + M_Z^2 B_Z^2}. \tag{51}$$

Therefore

$$M_Z^2 = \frac{C}{1 - C\left[\frac{M_r^2}{M_Z^2} B_r^2 + B_Z^2\right]} \tag{52}$$

Using measured values of C from Table 13 and values of M_r^2/M_Z^2 obtained above, M_Z^2 and M_r^2 were then determined. An effective value of migration area for the core was then defined as

$$M_{eff}^2 = \frac{B_r^2 M_r^2 + B_Z^2 M_Z^2}{B_r^2 + B_Z^2}, \text{ therefore} \tag{53}$$

$$k_\infty = 1 + M_{eff}^2 [B_r^2 + B_Z^2]. \tag{54}$$

The values obtained for each core are shown in Table 14.

Using a Gaussian model and introducing anisotropy changes Equation (29) to

$$C = M_Z^2 \tag{55}$$

M_r^2 and M_Z^2 were obtained from the values of C in Table 13 and the ratio M_Z^2/M_r^2 determined above. Again

$$M_{eff}^2 = \frac{B_r^2 M_r^2 + B_Z^2 M_Z^2}{B_r^2 + B_Z^2}, \text{ and} \tag{53}$$

$$k_\infty = e\, M_{eff}^2 [B_r^2 + B_Z^2]. \tag{56}$$

The results for this model are also shown in Table 14.

4.6 RESULTS OF ANALYSIS

The value of C for a particular core varies inversely with B^2 when the one-group model is used, but C is independent of B^2 when the Gaussian model is used. Thus the more exact model for these cores can be determined by examining the variation of C with respect to B^2 in cores 15B and 15D. The values of C for core 15B are nearly constant, except that one series yields a lower value of C than the others — one-group theory would predict this series to have the highest value of C. Thus, on the basis of leakage experiments, core 15B appears to be more accurately described by the Gaussian model than by one-group.

Similarly, core 15D has three values of C nearly constant with one lower value. However, the low value is in the first series, as the one-group model would predict. For the Gaussian model to be true, this

value must be discarded and an average obtained from the other series; however, this low value of C gives a very low M^2 value even in the one-group model indicating that it may be in error. Thus, with the exception of this one value, core 15D also appears to be more accurately described by the Gaussian model.

Since the Gaussian model is not believed to hold true for water-moderated cores it is possible that an error exists in some other factor used in data analysis, giving rise to the apparent independence of C on B^2.

TABLE 8

EXPERIMENTAL DATA FOR DETERMINATION OF B^2 AND GAMMA VALUES USED IN LEAKAGE EXPERIMENTS

Core and Series	H, cm	R, cm	λ, cm	δ, cm	B^2, $cm^{-2} \times 10^4$
25D	140.5	23.64	13.41±0.42	7.45±0.12	64.01±0.46
15A	127.21	18.36	12.86±0.31	8.47±0.04	85.31±0.26
15B-1	46.99	22.68	11.94±0.18	8.02±0.05	89.79±0.12
	121.21	18.06	10.16±0.29	7.84±0.06	91.85±0.18
15B-2	52.14	23.77	12.83±0.28	7.42±0.03	82.86±0.11
	129.29	19.65	11.75±0.60	7.39±0.03	84.02±0.08
15B-3	47.45	27.09	13.38±0.22	7.13±0.04	76.06±0.11
	124.60	21.31	12.57±0.47	7.32±0.24	75.08±0.06
15B-4	43.87	30.99	12.84±0.25	6.92±0.03	70.92±0.13
	127.07	22.73	12.29±0.40	7.20±0.06	69.61±0.11
15D-1	135.05	15.63	15.29±1.61	7.32±0.07	114.2 ±0.7
15D-2	42.69	23.03	10.46±0.35	6.85±0.03	99.79±0.48
	94.69	18.44	9.77±0.20	6.79±0.13	99.72±0.96
	132.41	17.87	9.44±0.33	6.57±0.06	100.45±0.46
15D-3	38.25	27.85	11.51±0.97	6.73±0.06	88.2 ±1.3
	124.21	19.74	11.01±0.35	6.49±0.03	89.46±0.10
15D-4	35.72	32.30	13.62±0.69	6.57±0.04	78.81±0.56
	134.58	21.53	11.51±0.20	6.60±0.03	77.69±0.08

TABLE 9

LEAKAGE EXPERIMENT DATA FOR DETERMINATION OF C ON CORE 25D

$N_B = 0$

$\beta = 0.0076$

Step	No. Pins	Radius, cm	Critical Height, cm	$(d\rho/dh)^{-1/3}$, $cm^{1/3}$
1	1500	26.70	69.85	9.80
2	1436	26.12	75.26	10.16
3	1372	25.54	82.45	11.16
4	1304	24.89	93.59	12.45
5	1240	24.27	110.72	14.12
6	1216	24.04	121.08	15.15
7	1192	23.80	132.83	16.63

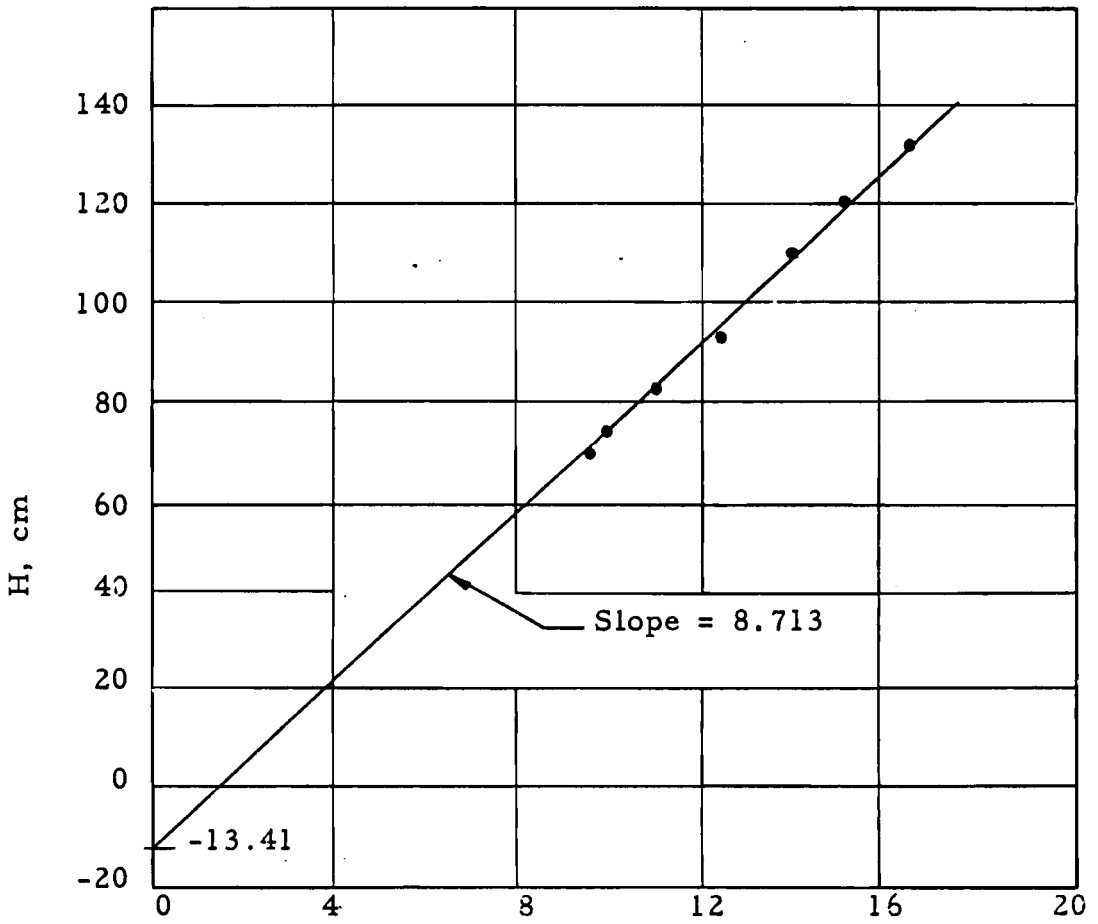

TABLE 10

LEAKAGE EXPERIMENT DATA FOR DETERMINATION OF C ON CORE 15-A

N_B = 0 gm B / liter

β = 0.00816

Step	No. Pins	Radius, cm	Critical Height, cm	$(d\rho / dh)^{-1/3}$, $cm^{1/3}$
1	1968	24.475	44.08	6.369
2	1576	21.902	54.59	7.476
3	1452	21.022	61.24	8.092
4	1340	20.196	69.84	8.706
5	1224	19.302	83.03	10.005
6	1176	18.919	92.17	10.823
7	1140	18.628	101.72	11.803
8	1108	18.364	116.19	13.375

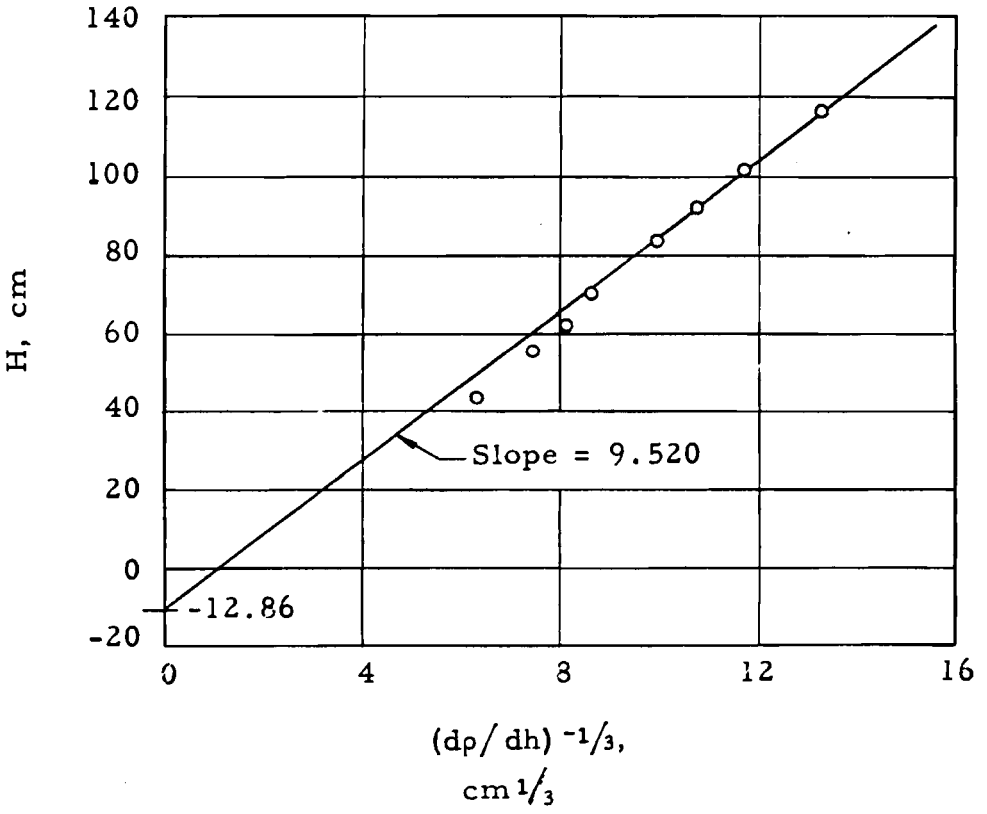

TABLE 11

LEAKAGE EXPERIMENT DATA FOR DETERMINATION OF C ON CORE 15B

N_B = 0.070 gm B/liter

β = 0.00830

Step	No. Pins	Radius, cm	Critical Height, cm	$(d\rho/dh)^{-1/3}$, $cm^{1/3}$
1	1576	22.91	46.34	6.74
2	1544	22.67	46.99	6.51
3	1484	22.23	48.86	7.02
4	1288	20.71	58.98	7.78
5	1176	19.79	68.95	8.72
6	1124	19.35	76.19	9.50
7	1044	18.65	92.66	11.02
8	1004	18.29	107.44	12.53
9	968	17.95	127.63	14.93

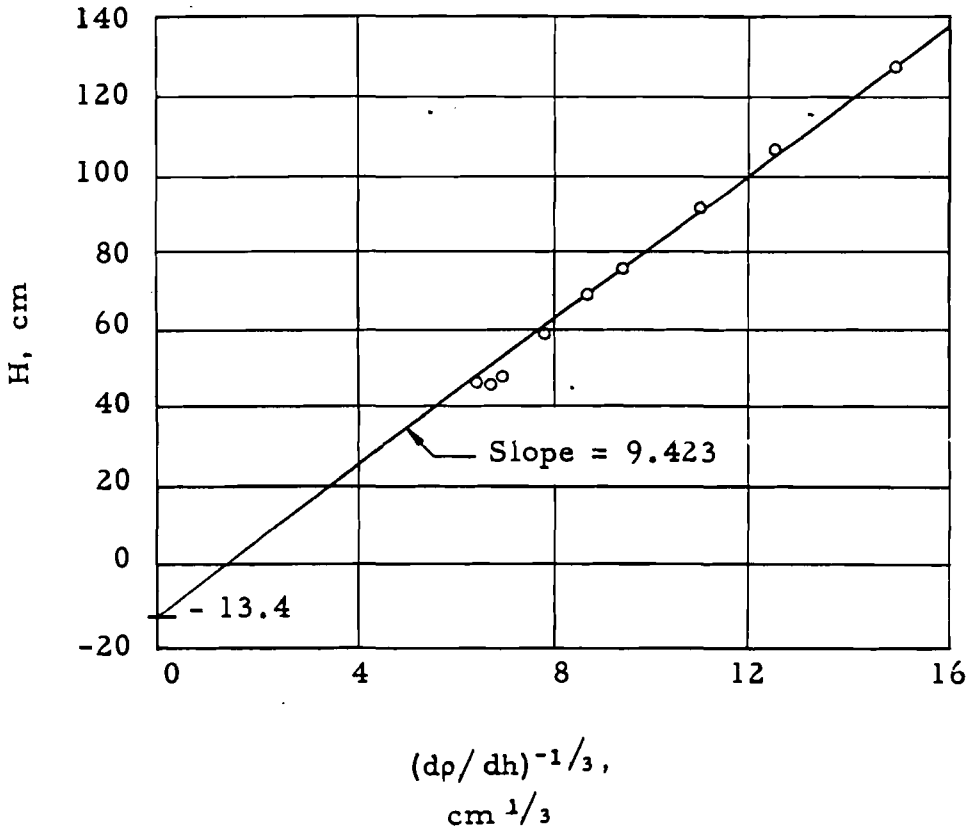

TABLE 11, CONT'D.

LEAKAGE EXPERIMENT DATA FOR DETERMINATION OF C ON CORE 15B

N_B = 0.322 gm B/liter

β = 0.00819

Step	No. Pins	Radius, cm	Critical Height, cm	$(d\rho/dh)^{-1/3}$, $cm^{1/3}$
1	2000	25.81	43.80	5.97
2	1976	25.65	44.22	6.66
3	1696	23.76	52.14	7.38
4	1576	22.91	57.23	7.70
5	1436	21.87	67.09	8.72
6	1340	21.13	77.71	10.14
7	1272	20.58	89.30	11.22
8	1208	20.06	106.60	12.92
9	1160	19.66	129.29	15.33

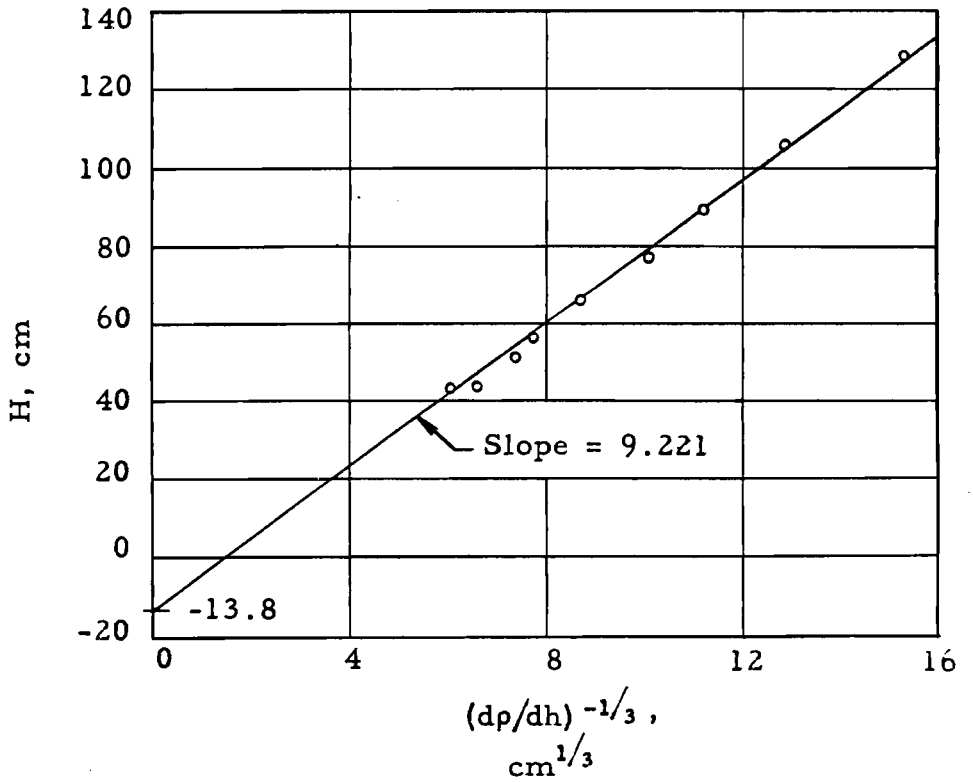

TABLE 11, CONT'D.

LEAKAGE EXPERIMENT DATA FOR DETERMINATION OF C ON CORE 15B

N_B = 0.823 gm B/liter

β = 0.00795

Step	No. Pins	Radius, cm	Critical Height, cm	$(d\rho/dh)^{-1/3}$, $cm^{1/3}$
1	2884	30.99	43.87	6.40
2	2796	30.52	44.73	6.05
3	2684	29.90	46.31	6.31
4	2348	27.97	52.33	7.14
5	2128	26.62	58.86	7.58
6	1976	25.65	65.41	8.76
7	1788	24.37	78.85	10.33
8	1672	23.60	94.08	12.15
9	1592	23.03	112.15	14.00
10	1552	22.74	127.07	15.77

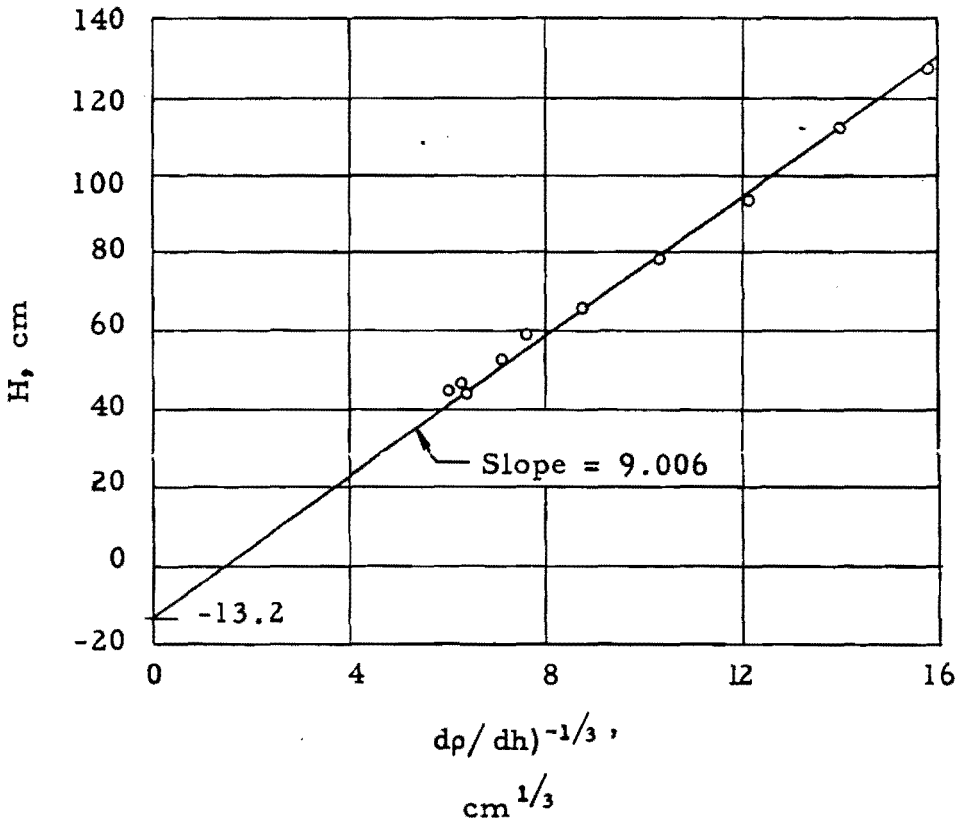

TABLE 11, CONT'D.

LEAKAGE EXPERIMENT DATA FOR DETERMINATION OF C ON CORE 15B

N_B = 0.586 gm B/ liter

β = 0.00806

Step	No. Pins	Radius, cm	Critical Height, cm	$(d\rho/dh)^{-1/3}$, $cm^{1/3}$
1	2496	28.83	42.64	5.88
2	2400	28.27	44.04	6.11
3	2300	27.68	45.68	6.29
4	2204	27.07	47.45	6.41
5	2104	26.47	49.67	6.74
6	2000	25.81	52.86	6.94
7	1788	24.40	61.47	7.90
8	1696	23.76	66.55	8.58
9	1560	22.80	78.82	9.95
10	1468	22.11	92.73	11.47
11	1396	21.56	112.22	13.75
12	1364	21.31	124.60	15.53

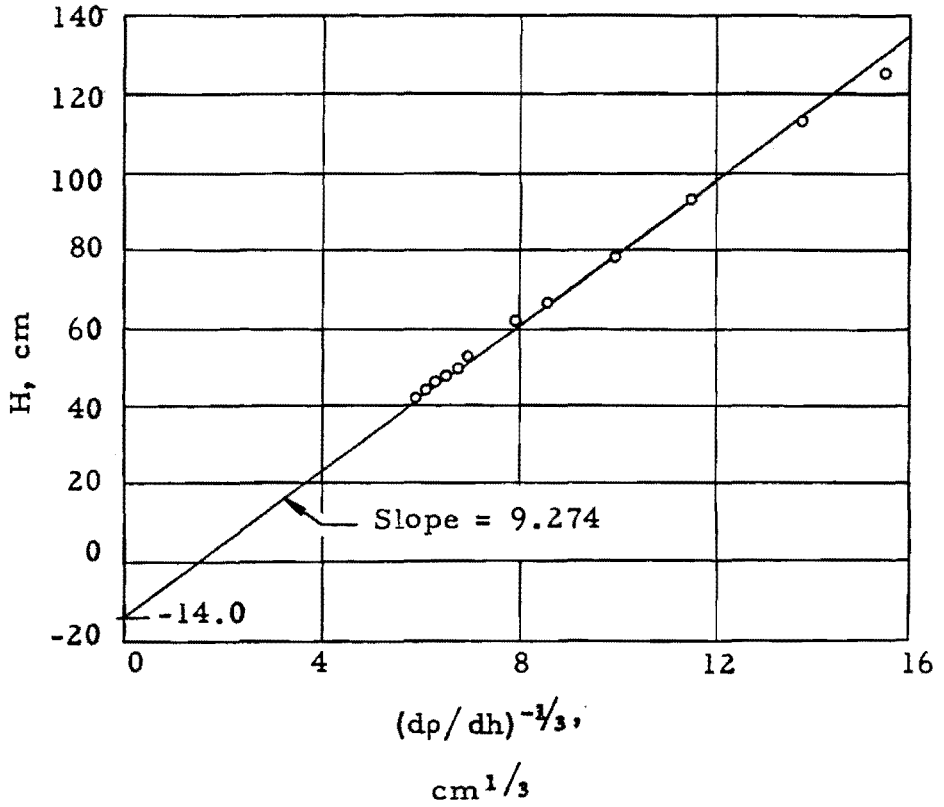

TABLE 12

LEAKAGE EXPERIMENT DATA FOR DETERMINATION OF C ON CORE 15D

N_B = 0 gm B/liter

β = 0.00846

Step	No. Pins	Radius, cm	Critical Height, cm	$(d\rho/dh)^{-1/3}$, $cm^{1/3}$
1	820	19.74	43.56	7.00
2	804	19.55	44.42	7.13
3	772	19.15	48.96	6.84
4	732	18.65	49.41	7.61
5	688	18.08	53.94	8.37
6	648	17.55	59.79	8.32
7	592	16.84	72.34	9.65
8	556	16.25	90.34	12.96
9	548	16.14	95.73	13.96
10	540	16.02	102.41	13.99

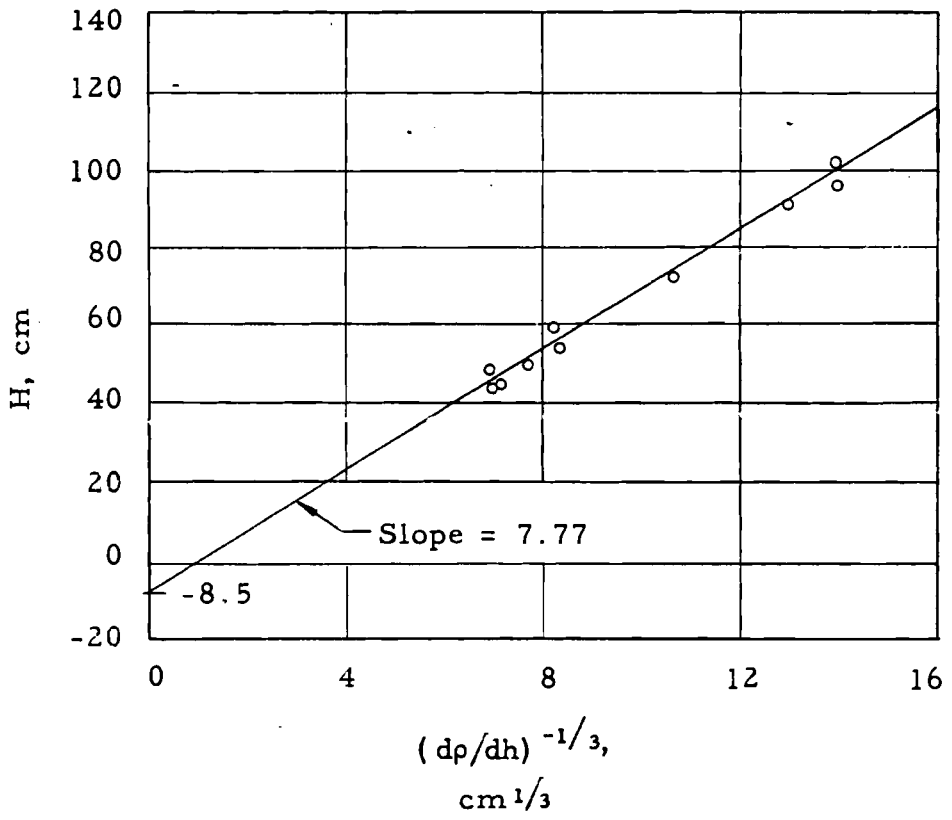

TABLE 12, CONT'D.

LEAKAGE EXPERIMENT DATA FOR DETERMINATION OF C ON CORE 15D

N_B = 0.235 gm B/liter

β = 0.00817

Step	No. Pins	Radius, cm	Critical Height, cm	$(d\rho/dh)_c^{-1/3}$ cm $^{1/3}$
1	1116	23.03	42.69	6.67
2	1100	22.86	43.34	6.58
3	1020	22.01	46.83	7.22
4	960	21.36	50.42	7.54
5	888	20.54	56.14	8.00
6	788	19.35	70.61	9.77
7	716	18.44	94.69	12.18
8	700	18.24	104.60	13.54
9	672	17.87	132.41	16.91

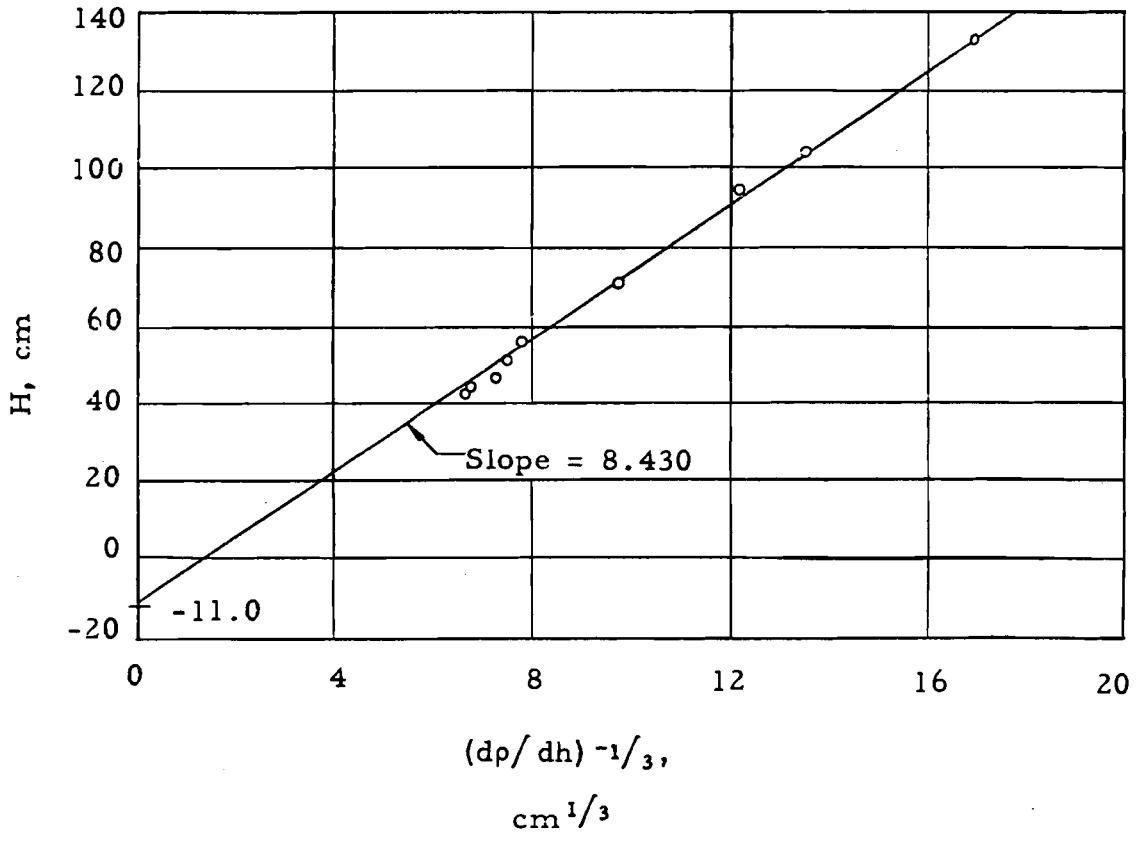

TABLE 12, CONT'D.

LEAKAGE EXPERIMENT DATA FOR DETERMINATION OF C ON CORE 15D

N_B = 0.432 gm B / liter

β = 0.00799

Step	No. Pins	Radius, cm	Critical Height, cm	$(d\rho/dh)_c^{-1/3}$ cm $^{1/3}$
1	1632	27.85	38.25	5.96
2	1568	27.30	39.33	6.25
3	1508	26.77	40.48	6.22
4	1288	24.74	46.33	7.17
5	1184	23.72	50.68	7.27
6	1004	21.84	64.14	9.44
7	936	21.09	74.59	10.31
8	888	20.54	87.21	12.35
9	864	20.26	96.81	13.38
10	840	19.98	109.40	14.72

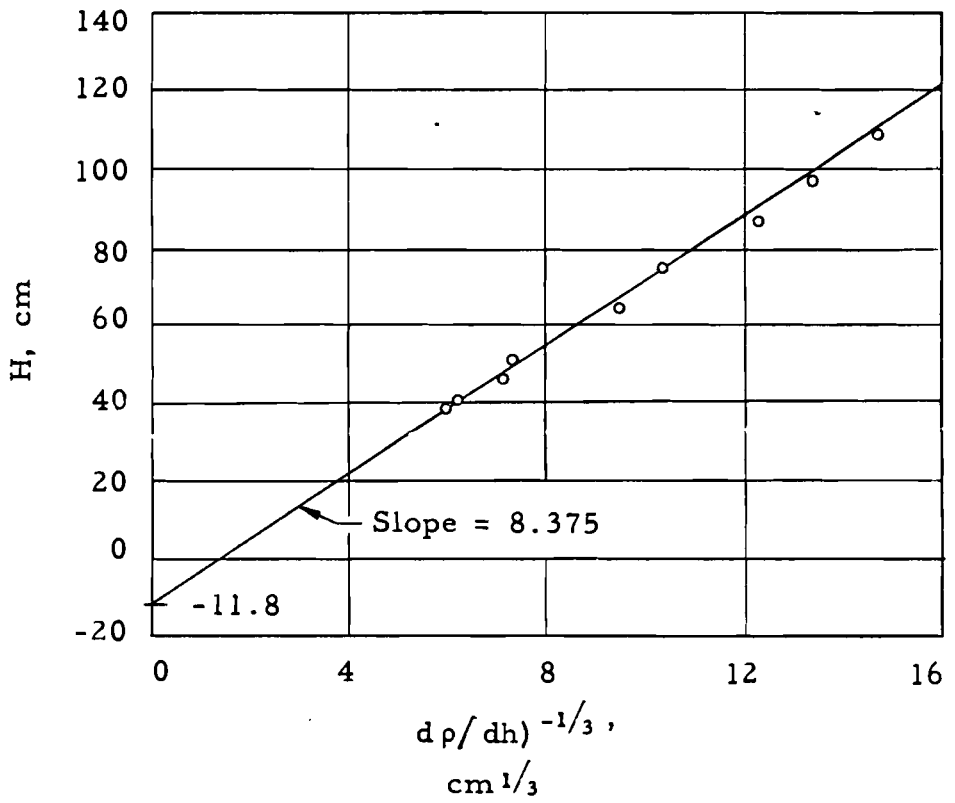

TABLE 12, CONT'D.

LEAKAGE EXPERIMENT DATA FOR DETERMINATION OF C ON CORE 15D

N_B = 0.635 gm B/liter

β = 0.00783

Step	No. Pins	Radius, cm	Critical Height, cm	$(d\rho/dh)^{-1/3}$ $cm^{1/3}$
1	2196	32.30	35.72	5.92
2	2144	31.92	36.26	6.14
3	2064	31.36	37.11	6.66
4	1852	29.66	41.03	6.28
5	1648	27.98	44.27	6.70
6	1436	26.12	51.04	7.50
7	1232	24.19	63.20	8.67
8	1116	23.03	77.51	11.01
9	1020	22.01	104.91	14.32
10	1004	21.84	112.71	15.50
11	988	21.67	124.11	16.73
12	976	21.53	134.58	17.56

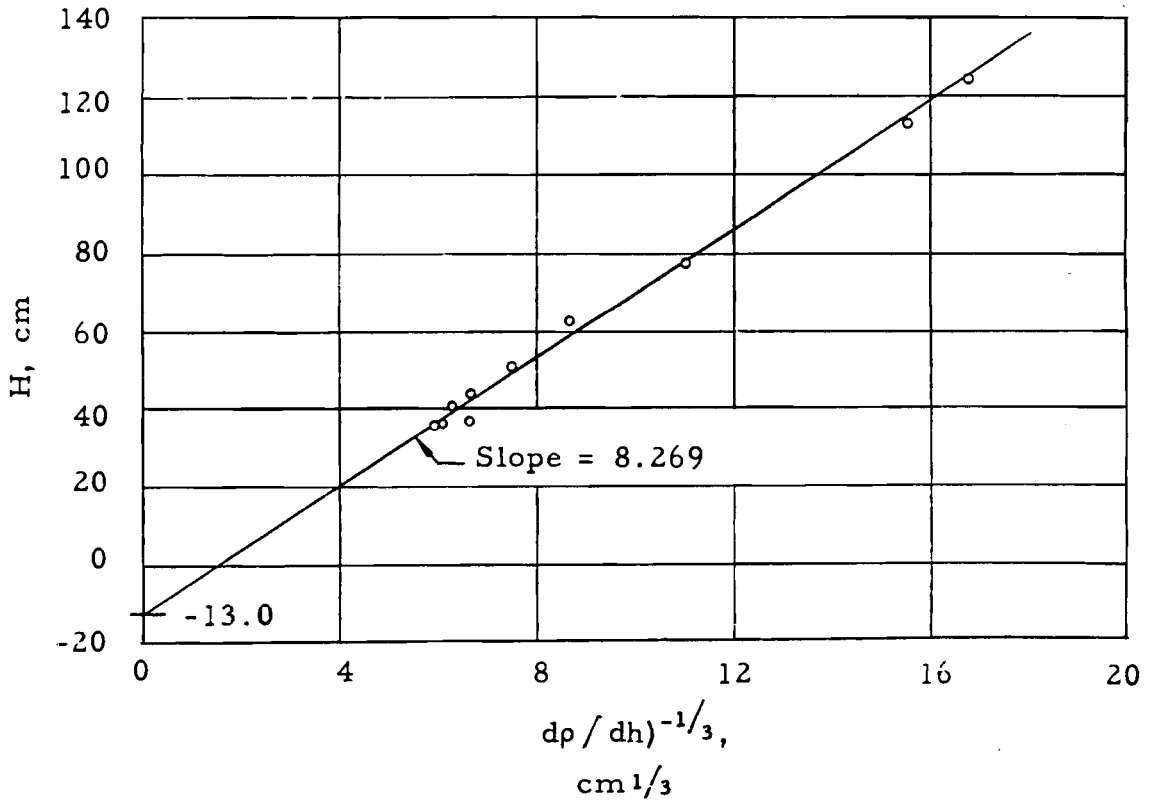

TABLE 13

RESULTS OF LEAKAGE EXPERIMENTS

Core and Series	N_B gm B/ liter	A	σ_A	$D \pm \sigma_D$, cm	$C \pm \sigma_C$, cm^2
25D	0	0	0.0085	13.41±0.94	33.5±0.6
15A	0	0	0.009	12.86±0.31	43.7±1.0
15B-1	0.070	-0.0244	0.005	13.1 ±0.6	40.3±0.6
-2	0.322	-0.0140	0.009	13.6 ±0.7	39.8±0.8
-3	0.586	-0.0105	0.007	14.0 ±0.6	40.5±0.6
-4	0.823	-0.0066	0.006	13.1 ±0.6	37.1±0.7
15D-1	0	0	0.013	8.53±0.9	23.8±0.7
-2	0.235	-0.0111	0.009	10.89±0.5	30.4±0.6
-3	0.432	-0.0058	0.012	11.73±1.1	28.0±0.7
-4	0.635	-0.0213	0.007	12.95±0.7	28.7±0.45

TABLE 14

M^2 AND k_∞ OBTAINED FROM LEAKAGE EXPERIMENTS

Core &Series	N_B	One-Group Model										Gaussian Model					
		C	B_r^2	B_z^2	$B_r^2+B_z^2$	M_z^2/M_r^2	M_z^2	M_r^2	M_{eff}^2	M_{eff}^2	k_∞	M_z^2	M_r^2	M_{eff}^2	M_{eff}^2	k_∞
25D	0	33.5±0.6	58.30	5.46	63.76	1.02	42.4±0.8	41.6±0.8	41.7±0.8		1.266±0.005	33.5±0.6	32.8±0.6	32.9±0.6		1.234±0.005
15A	0	43.7±1.0	80.34	5.93	86.27	1.15	65.3±1.6	56.8±1.6	57.4±1.6		1.49 ±0.01	43.7±1.0	38.0±1.0	38.4±1.0		1.39 ±0.01
15B-1	0.070	40.3±0.6	84.56	7.03	91.59	1.05	62.3±1.0	59.3±1.0	59.5±1.0			40.3±0.6	38.4±0.6	38.5±0.6		
-2	0.322	39.8±0.8	77.04	6.99	84.03	1.05	58.5±1.3	55.7±1.3	55.9±1.3	54.4	1.49 ±0.03	39.8±0.8	37.9±0.8	38.0±0.8	37.7	1.41 ±0.01
-3	0.586	40.5±0.6	69.99	6.30	76.29	1.05	57.5±0.9	54.8±0.9	55.0±0.9	±2.8		40.5±0.6	38.5±0.6	38.7±0.6	±0.8	
-4	0.823	37.1±0.7	63.86	6.34	70.20	1.05	49.4±1.0	47.0±1.0	47.2±1.0			37.1±0.7	35.3±0.7	35.5±0.7		
15D-1	0	23.8±0.7	103.8	10.0	113.8	1.02	32.4±1.0	31.8±1.0	31.9±1.0			23.8±0.7	23.3±0.7	23.3±0.7		
-2	0.235	30.4±0.6	91.5	9.02	100.5	1.02	43.4±0.9	42.5±0.9	42.6±0.9	36.6	1.42 ±0.03	30.4±0.6	29.8±0.6	29.9±0.6	28.5	1.38 ±0.01
-3	0.432	28.0±0.7	80.3	8.45	88.8	1.02	37.0±0.9	36.3±0.9	36.3±0.9	±2.3		28.0±0.7	27.4±0.7	27.4±0.7	±0.7	
-4	0.635	28.7±0.5	72.6	5.28	77.9	1.02	36.3±0.6	35.6±0.6	35.6±0.6			28.7±0.5	28.1±0.5	28.1±0.5		

FIG. 12: RADIAL REFLECTOR SAVINGS VERSUS RADIUS

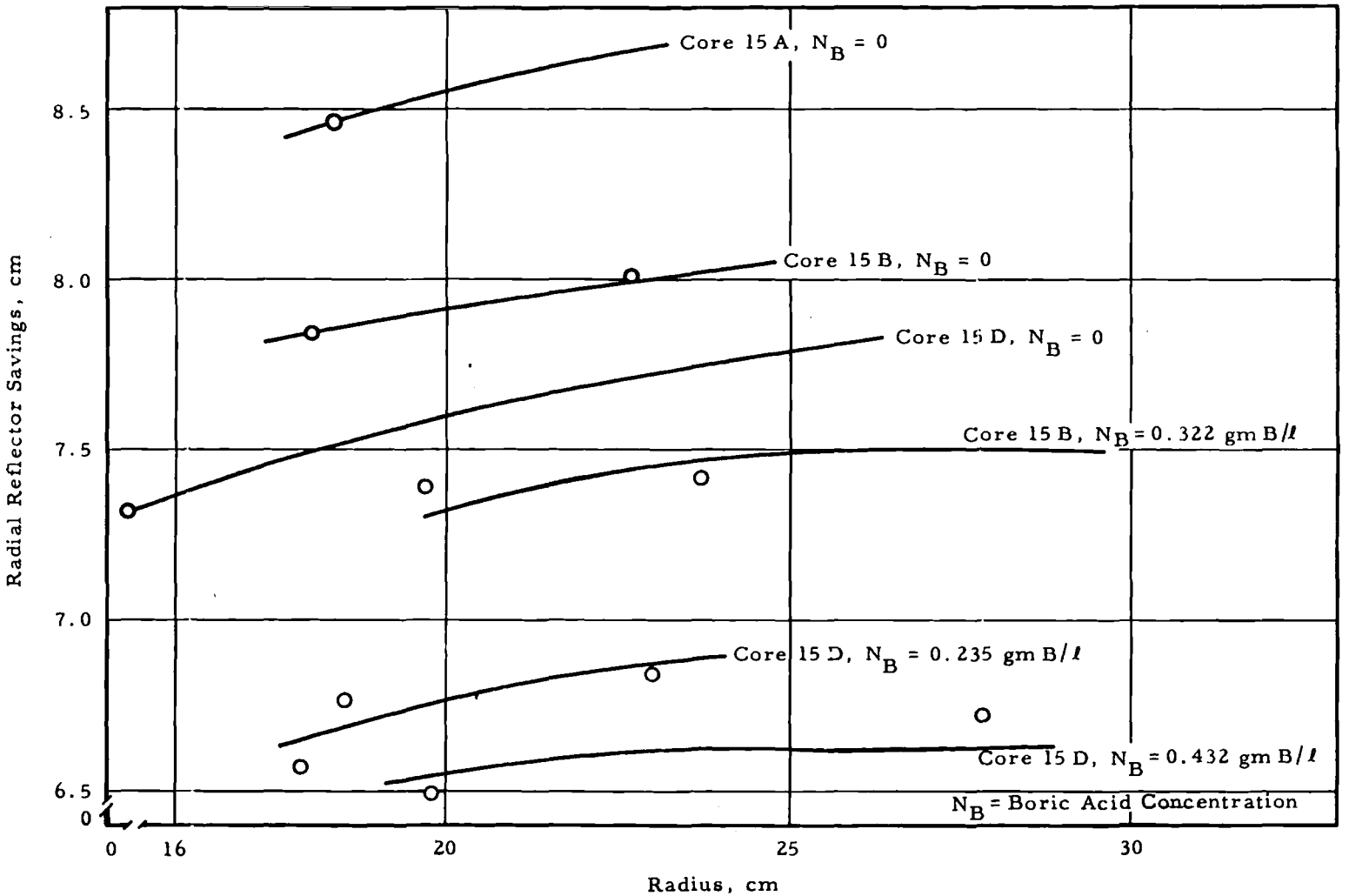

FIG. 13: DETERMINATION OF M_z^2/M_r^2 – CORES 15A AND 15B

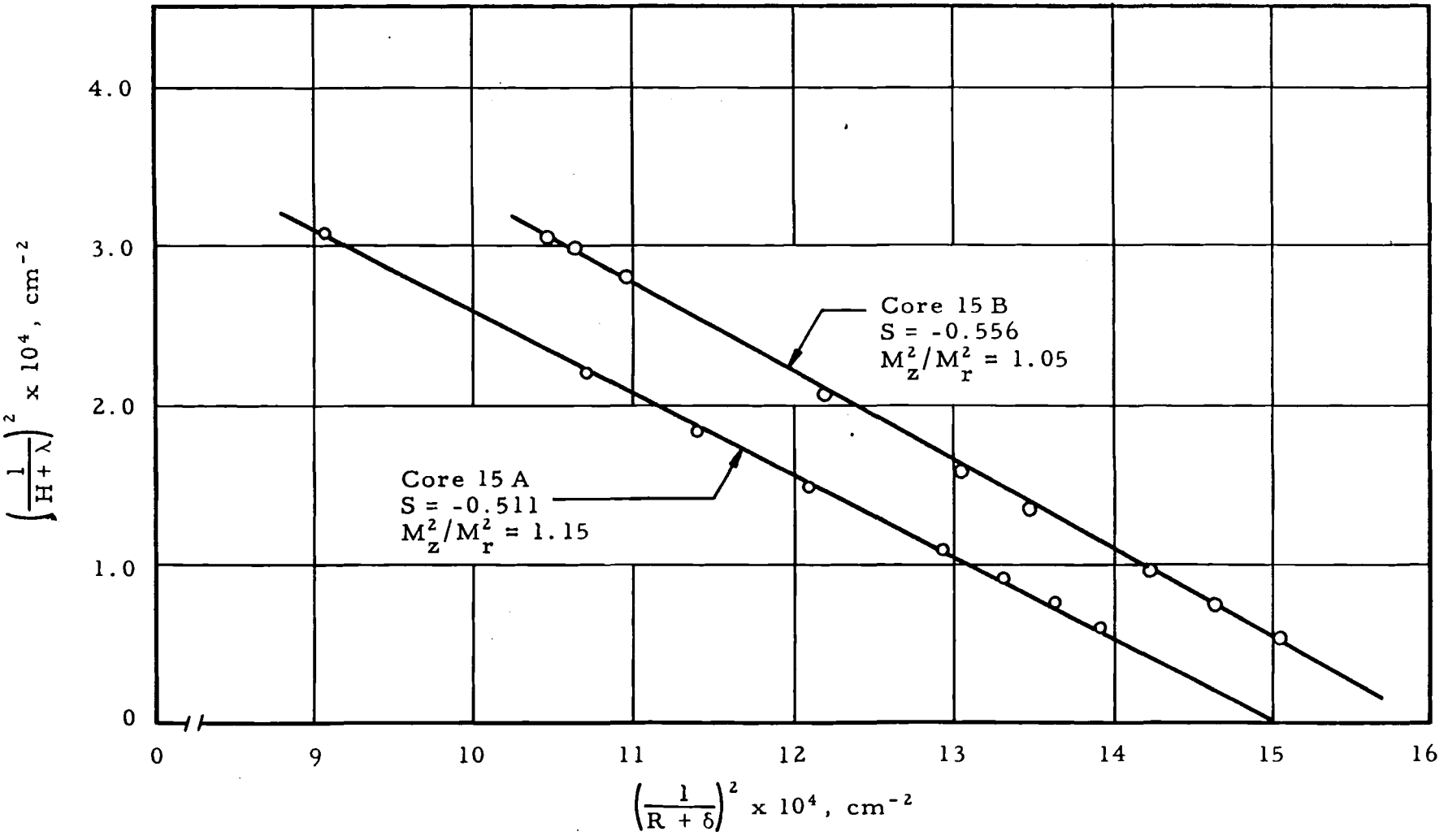

FIG. 14: DETERMINATION OF M_z^2/M_r^2 – CORE 15D

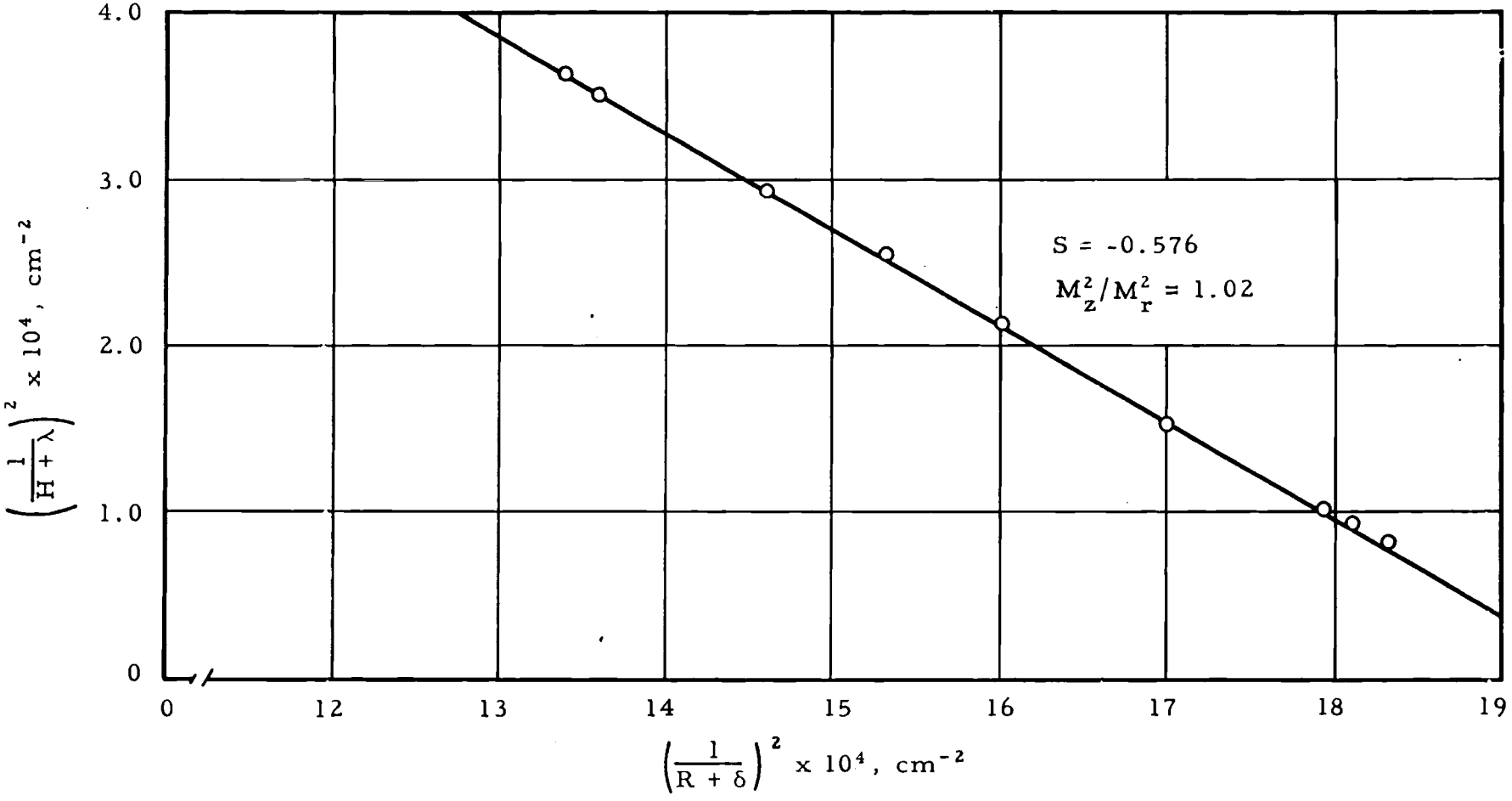

FIG. 15: DETERMINATION OF M_z^2/M_r^2 – CORE 25D

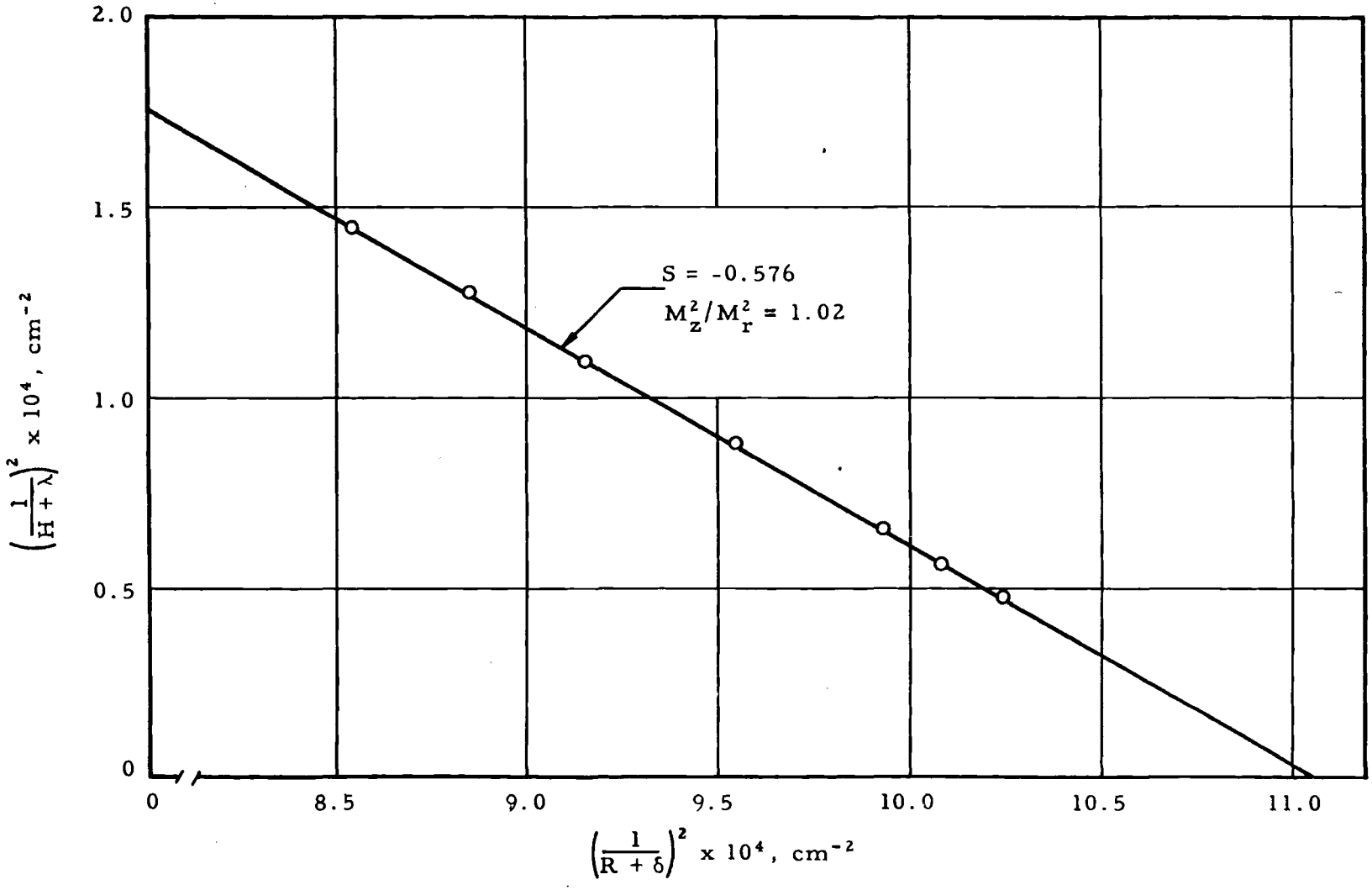

APPENDIX 6
CALCULATION OF NUMBER DENSITIES

6.1 15/1 PINS

The best reliable value for total uranium weight in a pin, 20.64 gm, was assumed, and the thorium weight was computed from this value, assuming that the following are true.

1. $N_{02}/N_{25} = 15.00$
2. 38% of the uranium is in the form of U_3O_8
3. 62% of the uranium is in the form of UO_2

This method has the advantage of giving the best value for the number density of uranium. Thorium is also well determined with the uncertainties falling into O_2.

The enrichment of the pellet and the amount of impurities were taken from a memo, "Volume Fractions and Number Densities for CETR Pin Critical Assembly Cores".[15]

The number density of the aluminum in the cladding was taken to be 0.0603 atoms/b-cm.

6.2 25/1 PINS

Three values of pin weight given in an ANL memo differ by less than 0.3%.[16] One of the values (the accountability weight) is divided into thorium, total uranium, U-235 weight, and therefore this value was used. Assuming that the length of the pin is 60 in., and that the diameter of the pellets 0.234 in., the density of the pellet is 8.42 gm/cm^3.

The number densities were computed as for the 15/1 pins. The ratio N_{Th}/N_{25} is then 25.34.

The number density obtained for O_2 is low, indicating that some of the thorium or uranium was in the metallic form. A 2.4% error would allow all the thorium to be in the form of ThO_2 and all the uranium in the form of UO_2.

6.3 WATER

The number densities in the water were taken as

N_O = 0.0334 atoms/barn-cm, and

N_H = 0.0668 atoms/barn, cm.

6.4 IMPURITIES

No data is available on impurities in the 25/1 Pins; the impurities in the 15/1 pins are shown in Table 53. All impurities are in the pellets, except as indicated by an asterisk, these impurities are in the cladding.

6.5 NUMBER DENSITIES IN THE TUPE ASSEMBLIES

The average number densities (atoms/b-cm of core) the TUPE cores are shown in Table 54.

TABLE 52

NUMBER DENSITIES IN PINS
(atoms/barn-cm of pin)

Material	25/1	15/1
0	0.02157	0.02729
Al	0.02371	0.01036
02	0.01059	0.01255
25	0.0004181	0.0008368
28	0.0000313	0.0000489
	93% enriched	~94½% enriched

TABLE 53

IMPURITIES IN 15/1 PINS, x 10^6 atoms/barn-cm OF PIN

Material	N	Material	N	Material	N
B	0.275	Mn	0.211	Zn*	3.16
C	50	Mn*	1.88	Cd	0.0028
N	41.6	Fe	2.6	Sm	0.0044
Mg	0.354	Fe*	18.5	Eu	0.0021
Al	1.73	Ni	0.197	Gd	0.0655
Si	0.413	Cu	0.458	Dy	0.045
Si*	36.8	Cu*	6.56	U-234	8.5
Ca	7.27	Zn	4.45	U-236	4.2
Cr	0.56				

TABLE 54

NUMBER DENSITIES IN TUPE CORE

Material	$25\sqrt{2}$B	25D	15D	15B	15A
H	0.0512	0.0448	0.0450	0.0357	0.0328
0	0.0305	0.0296	0.0314	0.0306	0.0303
Al	0.0056	0.0078	0.0034	0.0047	0.0052
02	0.00247	0.00346	0.00403	0.00578	0.00633
25	0.00097	0.000136	0.000273	0.000385	0.000423
28	0.0000073	0.0000102	0.0000157	0.0000225	0.0000246

Small ^{233}U Fueled Seed & Blanket Criticals (Reference 18)

Eight lattice arrangements were studied in this series of experiments. Two of them were brought critical at elevated temperatures (480° F, 650 psi) as well as at room temperature. All lattices were zoned radially into a seed region containing 26 wt% UO_2 - ZrO_2 (fully enriched with either ^{233}U or ^{235}U), plus a blanket region containing mostly thorium (either ThO_2 or 1 wt% $^{233}UO_2$ - ThO_2). Criticality was achieved by adjusting the size of the seed region, yielding clean geometry.

Reference 18 contains detailed core diagrams for the eight room temperature critical lattices, but not for the two hot critical lattices. However, schematic core layouts are included for all lattices for the purpose of indicating where flux measurement traverses were made. These schematics are included in the descriptive material reproduced below.

I. INTRODUCTION

As part of the overall effort to develop the physics technology required to design a light water-moderated seed-and-blanket reactor utilizing the uranium-233-thorium fuel cycle, an experimental program was initiated to provide confidence in the fundamental data available for uranium-233 and to verify the ability to calculate the physics characteristics of these systems. A series of eight small seed-and-blanket critical assemblies were studied at the Bettis Atomic Power Laboratory. Rod-type seed fuel elements which contained either uranium-233 or uranium-235 were utilized so that a direct comparison could be made between the lattice characteristics of the two fuels. Also, blanket regions which contained rod-type elements with either natural ThO_2 or 1 w/o $U^{233}O_2$-ThO_2 were compared. The eight assemblies were of two principal types. The first type was a rectangular array having a central seed region surrounded by a wet blanket with a metal-to-water ratio of about one, and the second was a hexagonal array having a central seed region surrounded by a tightly packed dry blanket with a metal-to-water ratio of about 9.2. All experiments on these eight assemblies were conducted at a temperature of 20° C. In addition, two of the wet blanket assemblies were studied in the Bettis High-Temperature Test Facility at 480° F and 650 psi.

The assemblies were constructed to be nearly clean critical and were used to measure a wide range of reactor physics parameters for comparison with calculation. Measurements included critical axial bucklings, thermal disadvantage factors, fast advantage factors, seed power shapes, seed-and-blanket activation shapes, ratios of epithermal-to-thermal thorium captures in blanket regions, and ratios of epithermal-to-thermal uranium-233 or uranium-235 fissions through seed-and-blanket regions. Calculations for comparison with experimentation were performed with diffusion theory and with more sophisticated Monte Carlo and neutron transport techniques.

This report summarizes the measurements and analysis performed during the experimental program and describes the LWBR facility and the critical assemblies. Inadequacies in the calculational method are evaluated and possible solutions suggested. Table 1 summarizes the measured and calculated parameters on the 8 cold and 2 hot critical assemblies.

TABLE 1. SUMMARY OF MEASURED AND CALCULATED PARAMETERS ON EIGHT COLD AND TWO HOT CRITICAL ASSEMBLIES

Parameter	Core									
	SB-1	SB-2	SB-2 1/2	SB-3	SB-4	SB-5	SB-6	SB-7	Hot SB-3	Hot SB-4
Seed-and-Blanket Activation Shapes										
U^{235} foils	X	X	--	--	X	X	X	--	--	X
U^{233} foils	--	--	--	X	--	--	X	X	X	--
Th foils	X	--	--	--	--	X	X	X	X	X
Dy-Al foils	--	--	--	--	--	X	X	X	--	--
Th Fission Shape in Blanket	--	X	--	--	--	--	--	--	--	--
ρ^{02*} in Blanket	X	--	--	--	X	X	--	X	X	--
$\delta^{25\dagger}$ in Seed	--	--	--	--	--	X	--	--	--	X
δ^{25} in Blanket	--	--	--	--	--	X	--	--	--	X
$\delta^{23\ddagger}$ in Seed	--	X	--	X	--	--	--	X	X	--
δ^{23} in Blanket	--	--	--	X	--	--	--	X	X	--
Thermal Disadvantage Factor										
Seed	X	X	--	X	X	X	X	--	X	--
Blanket	X	--	--	X	X	X	--	X	--	--
Fast Advantage Factor										
Seed	--	--	--	--	--	X	X	--	--	--
Blanket	X	--	--	--	X	--	--	--	--	--

*ρ^{02} is defined as the ratio of epithermal-to-thermal thorium captures.
†δ^{25} is defined as the ratio of epithermal-to-thermal uranium-235 fissions.
‡δ^{23} is defined as the ratio of epithermal-to-thermal uranium-233 fissions.

II. DESCRIPTION OF LWBR CRITICAL FACILITY, FUEL, AND CORES

B. LWBR Facility

The LWBR critical facility was modified for the performance of experiments with uranium-233 fuel. The developmental nature and lack of experience with uranium-233 dictated a conservative approach in modifying the facility and procedures to study the uranium-233 fuel.

Experiments were conducted in a small 6-foot diameter tank installed in a 17-foot diameter vessel. This larger vessel was also designed to contain critical assemblies, but was used in this instance (with a lid over the top) to prevent the spread of contamination if a fuel rod should leak during the uranium-233 experiments. An isometric view of the reactor tank and containment vessel is shown in Figure 2.

C. Description of Fuel

Four types of fuel elements were obtained for this program, and are given in Table 2.

The two seed types and the two blanket types had the same physical characteristics and are shown in Figure 6. These seed fuel elements were 0.255-inch OD x 20.8 inches long, while the blanket elements were 0.570-inch OD x 20.8 inches long. The seamless tubing for these rods was Zircaloy-2, and had a specified clad thickness of 0.016 inch for the seed and 0.038 inch for the blanket. All tubing was free-standing for the intended application at 480° F and 650 psi.

All elements contained 15.00 ± 0.06 inch of pressed and sintered fuel pellets with a 2.0-inch Zircaloy-2 insert in each end. Zircaloy end-caps were welded on each end of the rods. As shown in Figure 6, these end-caps had threaded holes which were used during core assembly. Also shown in Figure 6 is a typical test rod with removable end-caps. These caps contained double O-ring seals which could be tightened to make a gas-tight seal.

The uranium-233 containing pellets were manufactured from approximately 13 kg of uranium-233, which contained 38 ppm of uranium-232. Uranium-233 in the form of uranyl nitrate was solvent extracted by Oak Ridge National Laboratory (ORNL) in two batches. The first batch of 6.950 kg was used for the blanket pellets, while the second

batch of 6.039 kg was used for the seed pellets. An analysis of these batches is given in Appendix A. Appendix B gives the uranium analysis of the finished uranium-233 containing pellets. Similar analysis for the uranium-235 seed pellets is given in Appendix C.

The seed pellets were fabricated by cold pressing and sintering to a size of 0.210 ± 0.003-inch diameter by approximately 0.250 inch in length. The pellets were 100% dimensionally inspected, and oversize pellets were ground to the specified size. Similarly, the blanket pellets were fabricated to a size of 0.489 ± 0.005-inch diameter by approximately 0.6 inch in length. Pellet length measurements were not required since only the full stack length of pellets was important. The pellet nonperpendicularity and flatness of the end-faces were measured to be less than 0.004 inch and 0.003 inch, respectively, at an assurance level of 95 x 95%. All pellets were of high density. The measured densities are summarized in Appendix D.

Chemical analyses were conducted for impurity levels. These were expressed in terms of boron equivalents where the conversion factors were determined for the expected neutron spectrum. For the uranium-233 solution, the total boron equivalence was less than 80 ppm. (For most elements, the value used in the total was the lowest level of detectability of the analysis.) The only significant impurity was found in the blanket elements. It was found that the thorium starting material was contaminated with from 1 to 5 ppm of gadolinium, where the value depended on the sampling plan used in the drum of starting material. Except for this gadolinium, all impurities were well within the limits established by the specifications.

The fuel rod dimensions and material number densities are summarized in Appendix E. A detailed description of the fabrication of this fuel is given in Reference 2.

D. Description of Cores

The assemblies studied were of the seed-and-blanket type composed of a central seed region surrounded by either a wet or dry outer blanket. Overall core height was 20.83 inches, with an active fuel length of 15 inches. All cores were approximately clean critical, with an excess reactivity of only a few tenths of one percent. The eight assemblies constructed are shown schematically in Figure 7 and are shown in greater detail in Figures 16 through 23. Table 3 gives a detailed description of the lattice.

Four B-10 stainless steel blade-type control rods were located in the seeds for shutdown and control. When inserted, these blades fitted between the seed fuel rods and were guided only by the upper core structure grid. During operations the blades were almost fully withdrawn and caused no perturbation in the lattice.

The top row of assemblies in Figure 7 (SB-1, SB-2, SB-2.5, SB-3, and SB-4) are rectangular and except for SB-2.5, which is a bare seed, have a wet blanket. The mechanical arrangement for these cores is shown in Figure 8. The core rested on a 3/4-inch stainless steel base plate, which in turn rested on a 1-inch stainless steel core support structure. The lattice spacing and seed-and-blanket geometry were maintained by the upper and lower fuel rod spacer plates of 1/4 inch stainless steel. An intermediate support plate, made by welding 0.02 x 0.100 x 11-inch zirconium rectangular wire into a 11 x 11-inch grid, was used to reduce any fuel rod bowing. The design of the upper spacer plate is presented in Figure 9. Fuel rods were placed on a square array, and this design permitted the interchange of four seed rods with one blanket rod. The seed sizes were adjusted to obtain the required clean critical configuration.

The bottom row of assemblies (SB-5, SB-6, and SB-7) are hexagonal in shape with a dry outer blanket and fuel rods in a triangular array. The blanket fuel rods were spaced with a 0.001-inch nominal clearance between rods. A view of this arrangement is given in Figures 10 and 11. The design provided for the interchange of one seed fuel rod with one blanket rod. This was done by placing plastic rings which had an outer diameter equal to the blanket rod diameter at the top, bottom, and center of each seed rod. With this arrangement, the seed sizes were adjusted such that the cores were clean critical.

VII. HIGH-TEMPERATURE TEST FACILITY EXPERIMENTS

A. Introduction

Critical experiments were performed at 480° F and 650 psi on two wet blanket assemblies in the Bettis High-Temperature Test Facility. The first assembly was a hot version of the SB-3 core, and the second similar to the SB-4 core. Fuel loadings of both cores were increased in the hot versions to account for the negative temperature coefficient and allow the cores to be critical at 480° F.

Measurements similar to those made on the cold cores were performed hot and compared with analytical model calculations. The information obtained serves as a check of the ability of the model to calculate the physics characteristics of these systems in the operating temperature range.

TABLE 2. DESCRIPTION OF FUEL ELEMENT TYPES

Type	Nominal Composition	Number of Rods	Fissile Fuel (kg)
Seed	26 w/o $U^{233}O_2$-ZrO_2	396	5.3
Seed	26 w/o $U^{235}O_2$-ZrO_2	625	8.8
Blanket	ThO_2	1386	- -
Blanket	1 w/o $U^{233}O_2$-ThO_2	1331	5.4

TABLE 3. DESCRIPTION OF LATTICE CONSTRUCTION

Core	Seed Composition	Blanket Composition	Blanket Type	H/U* in Seed	W/U† in Seed	H/Th* in Blanket	W/Th† in Blanket	Core Geometry	Lattice Type
SB-1	26 w/o $U^{235}O_2$-ZrO_2	ThO_2	Wet	37	26	4.4	1.97	Rectangular	Square
SB-2	26 w/o $U^{235}O_2$-ZrO_2	ThO_2	Wet	38	27	4.4	1.97	Rectangular	Square
SB-2.5	26 w/o $U^{235}O_2$-ZrO_2	- -	- -	38	27	- -	- -	Rectangular	Square
SB-3	26 w/o $U^{235}O_2$-ZrO_2	1 w/o $U^{233}O_2$-ThO_2	Wet	38	27	4.4	1.97	Rectangular	Square
SB-4	26 w/o $U^{235}O_2$-ZrO_2	1 w/o $U^{233}O_2$-ThO_2	Wet	37	26	4.4	1.97	Rectangular	Square
SB-5	26 w/o $U^{235}O_2$-ZrO_2	ThO_2	Dry	107	76	0.46	0.21	Hexagonal	Triangular
SB-6	26 w/o $U^{235}O_2$-ZrO_2	ThO_2	Dry	110	78	0.46	0.21	Hexagonal	Triangular
SB-7	26 w/o $U^{235}O_2$-ZrO_2	1 w/o $U^{233}O_2$-ThO_2	Dry	110	78	0.46	0.21	Hexagonal	Triangular

*Atom ratio.
†Ratio of volume of water to the volume of uranium (or thorium) at 20° C.

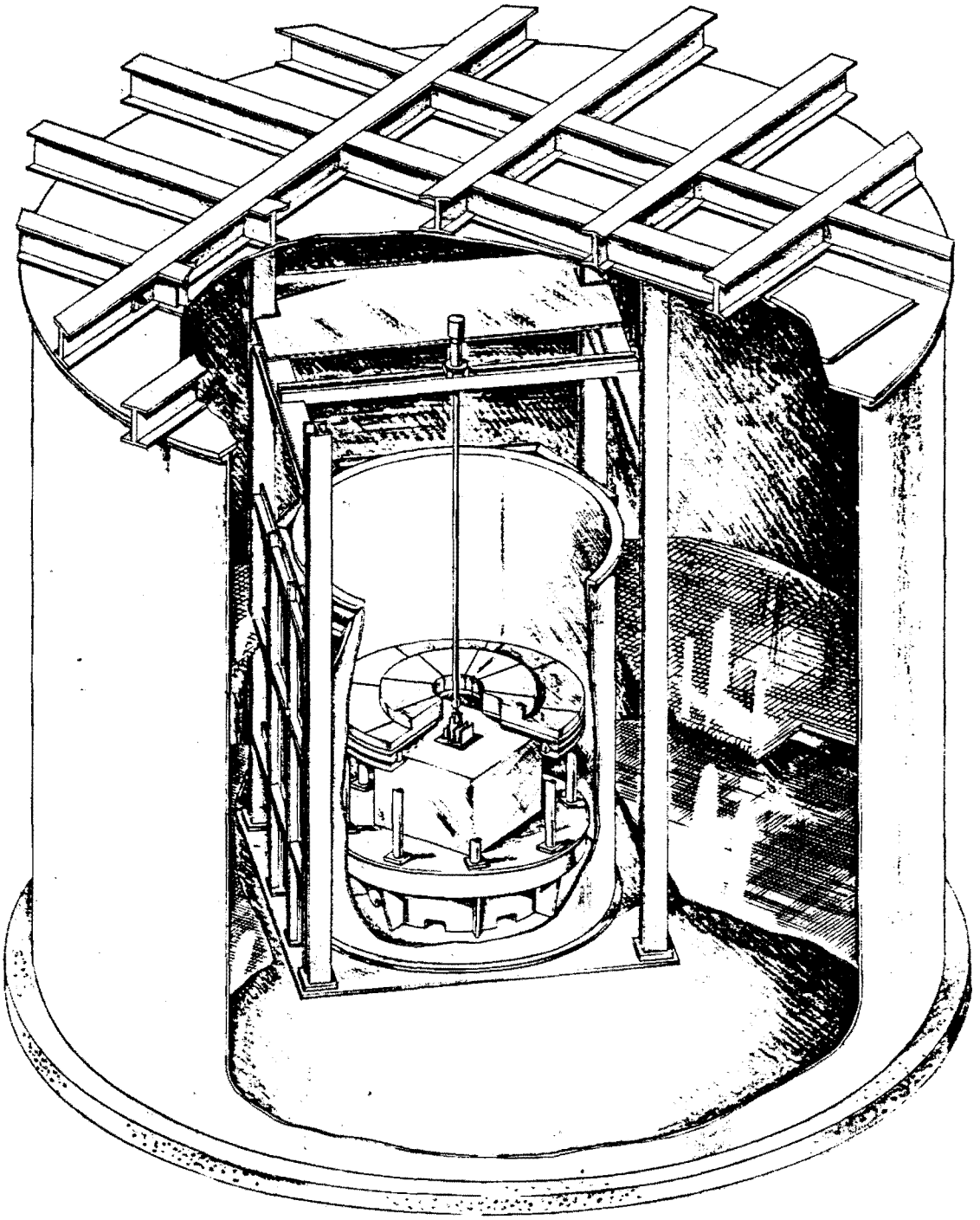

Figure 2. LWBR Uranium-233 Experiments Reactor Tank and Containment Vessel.

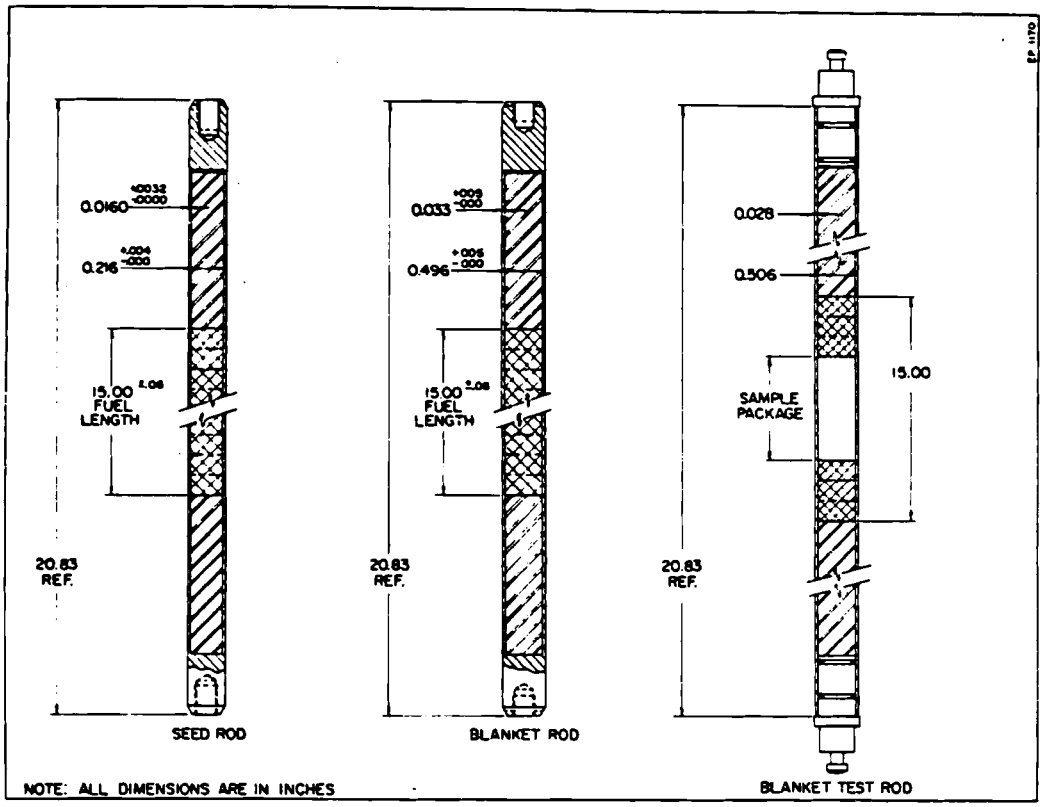

Figure 6. Diagram of Fuel and Test Rods for Uranium-233 Experiments.

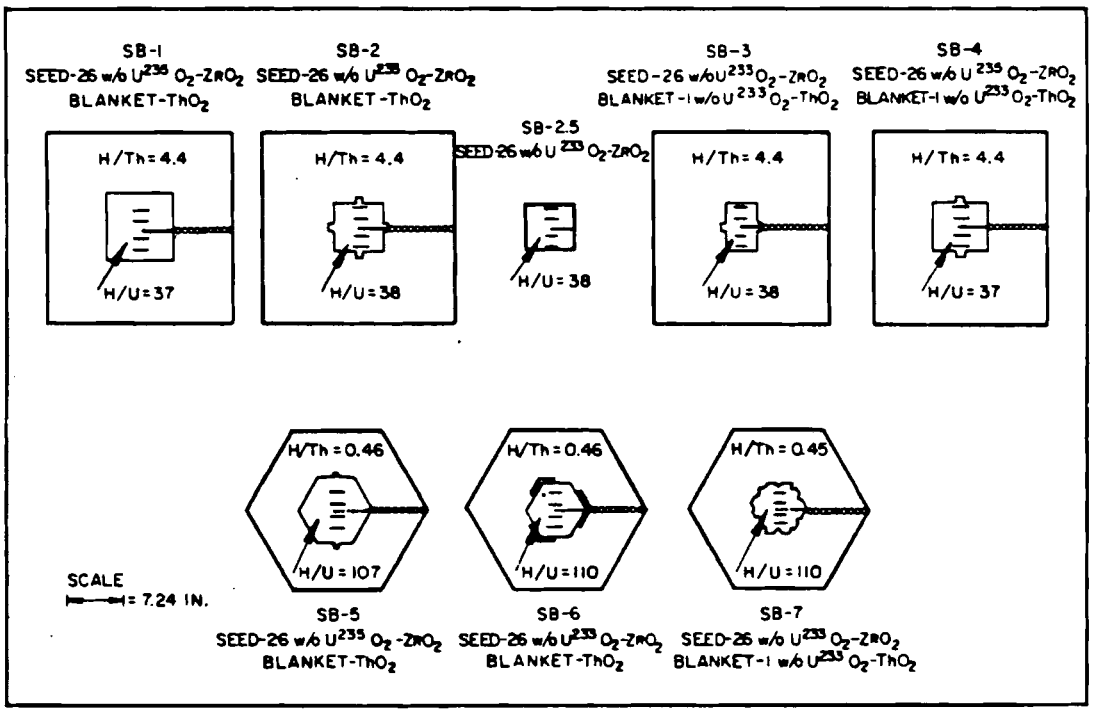

Figure 7. Schematic View (Top) of Eight Seed-and-Blanket Core Assemblies.

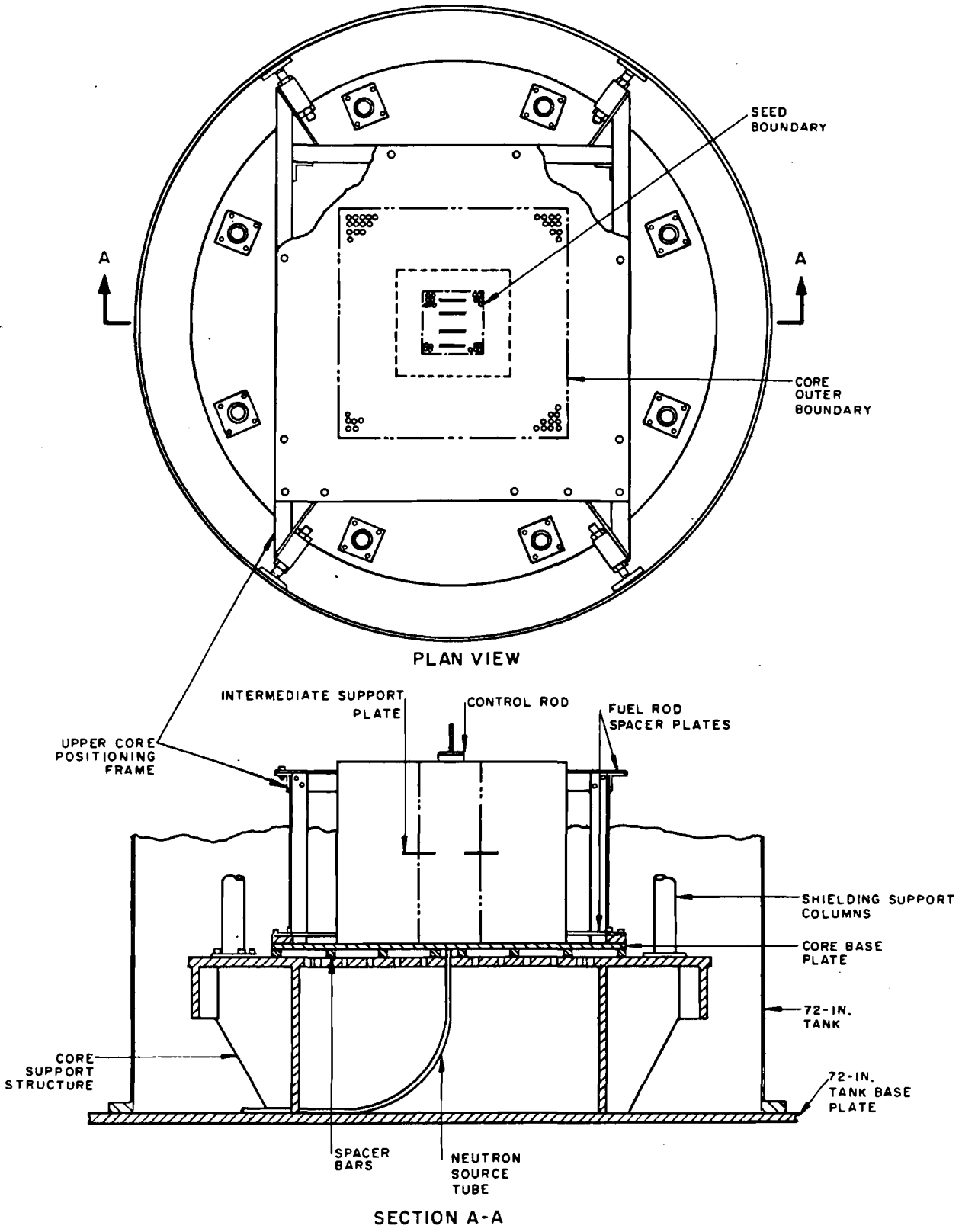

Figure 8. Core Support Structure for Wet Blanket Core Assemblies.

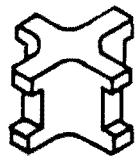

INSERT CONFIGURATION

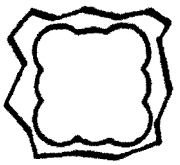

TYPICAL SEED HOLE CONFIGURATION

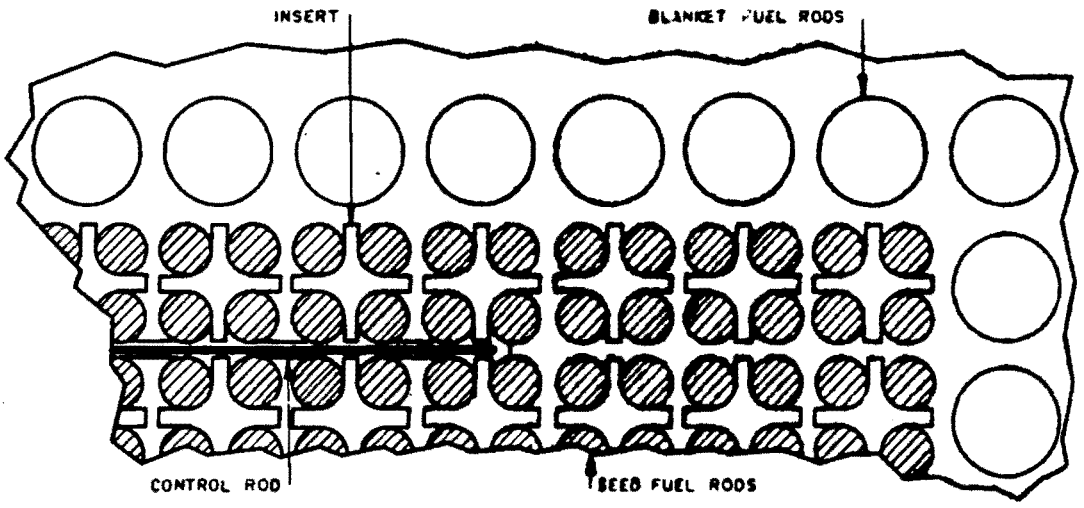

Figure 9. Diagram of Upper Spacer Plate Design.

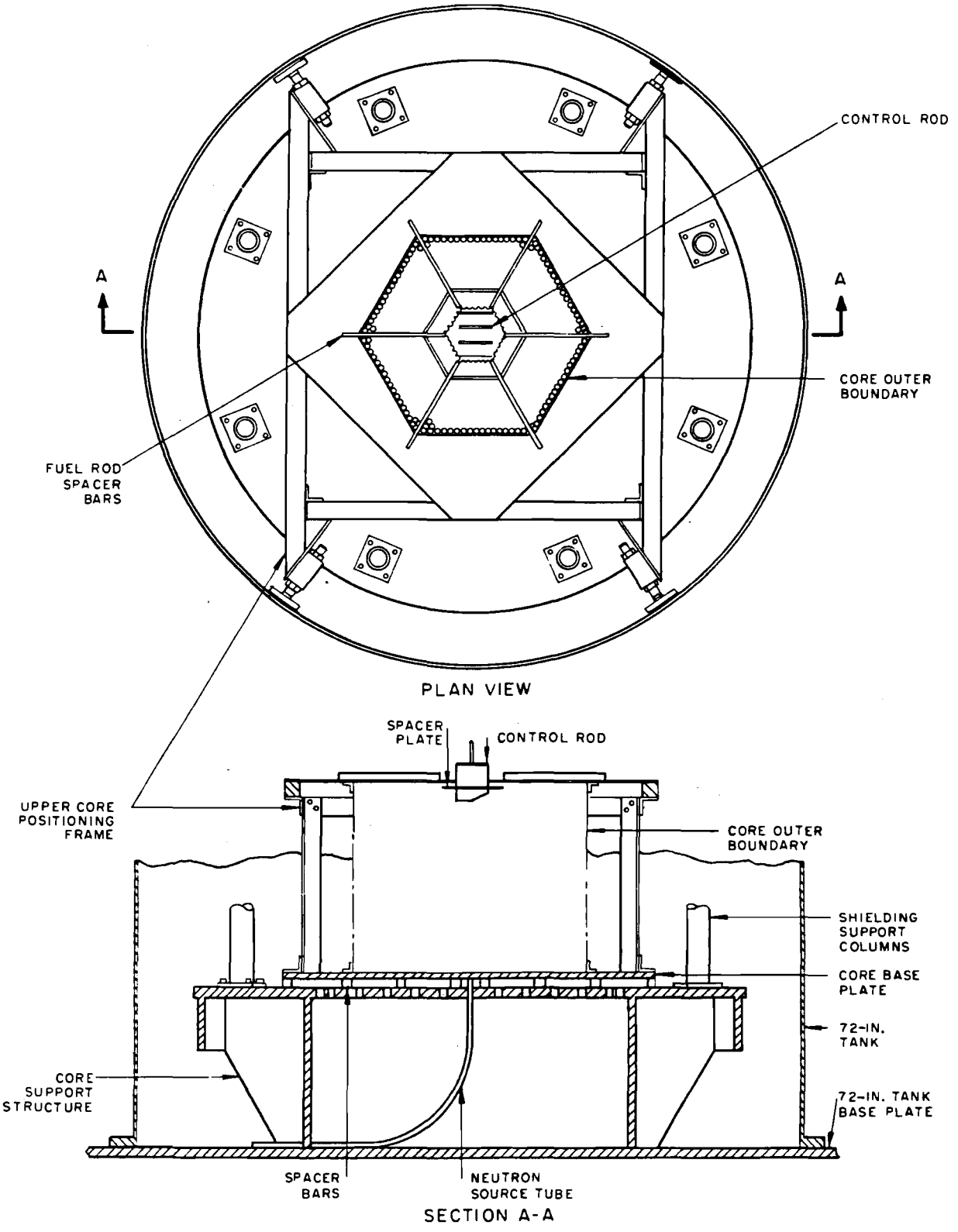

Figure 10. Core Support Structure for Dry Blanket Core Assemblies.

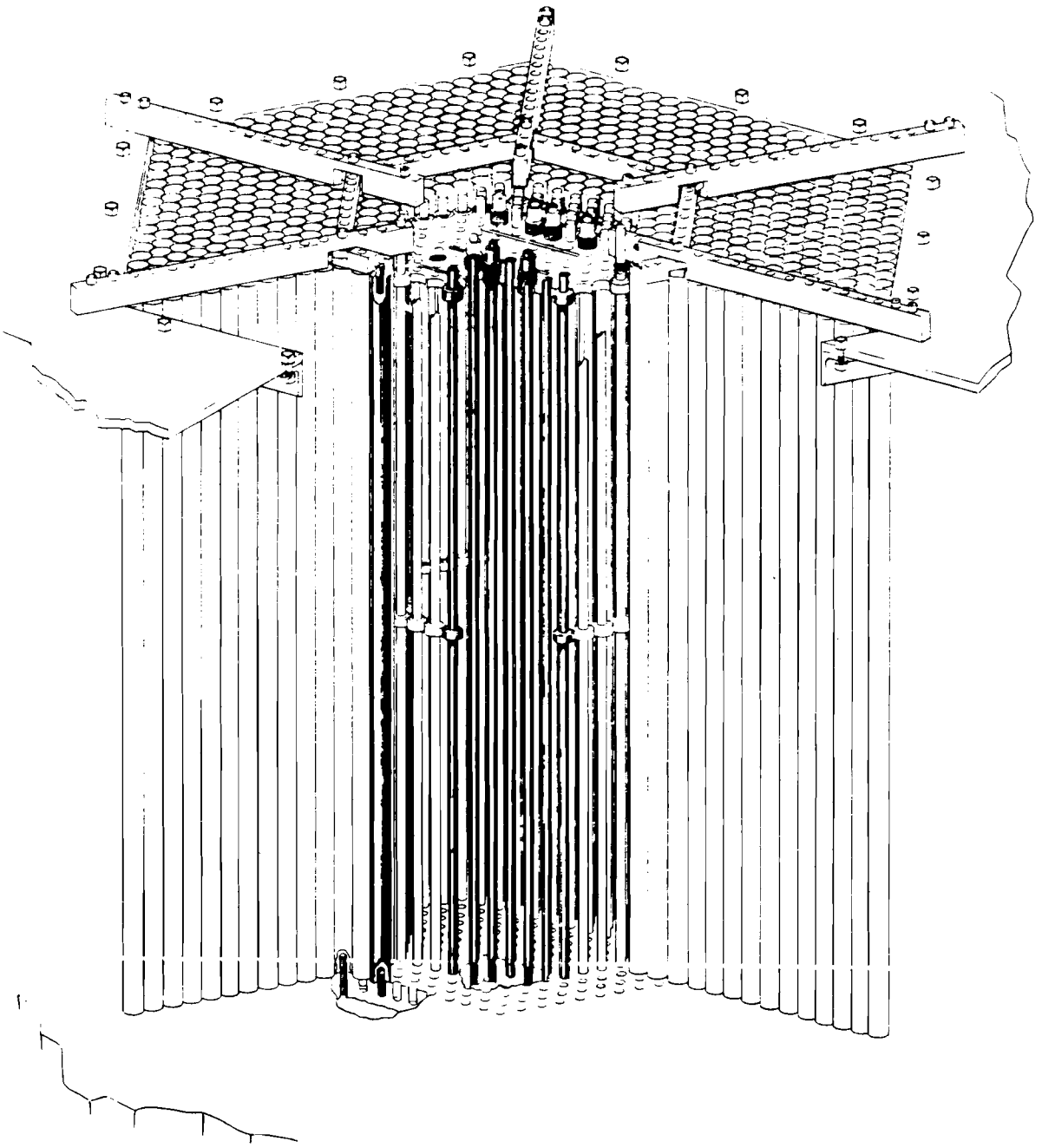

Figure 11. Grid Structure for Dry Blanket Core Assemblies.

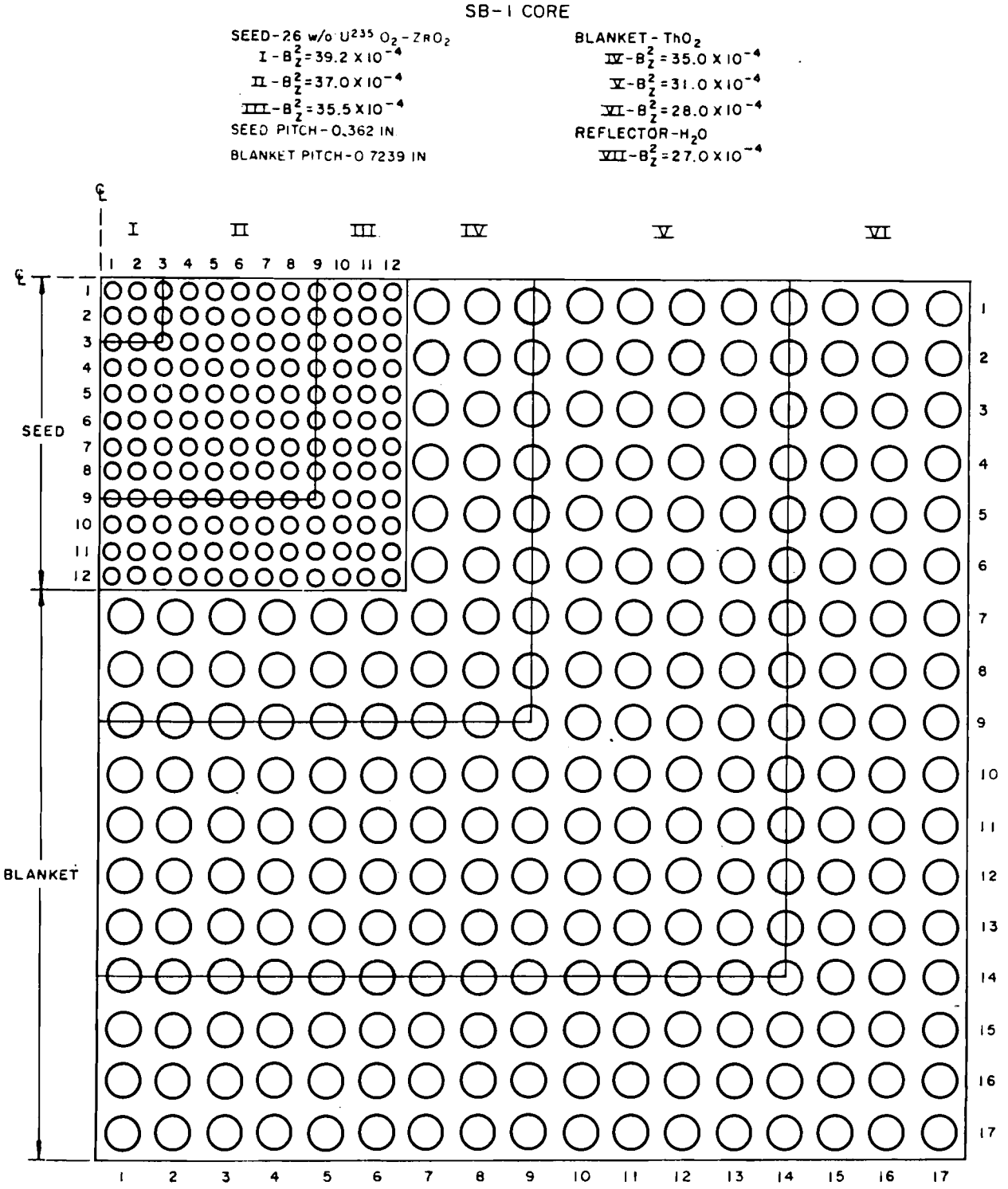

Figure 20. Diagram of LWBR SB-1 Core.

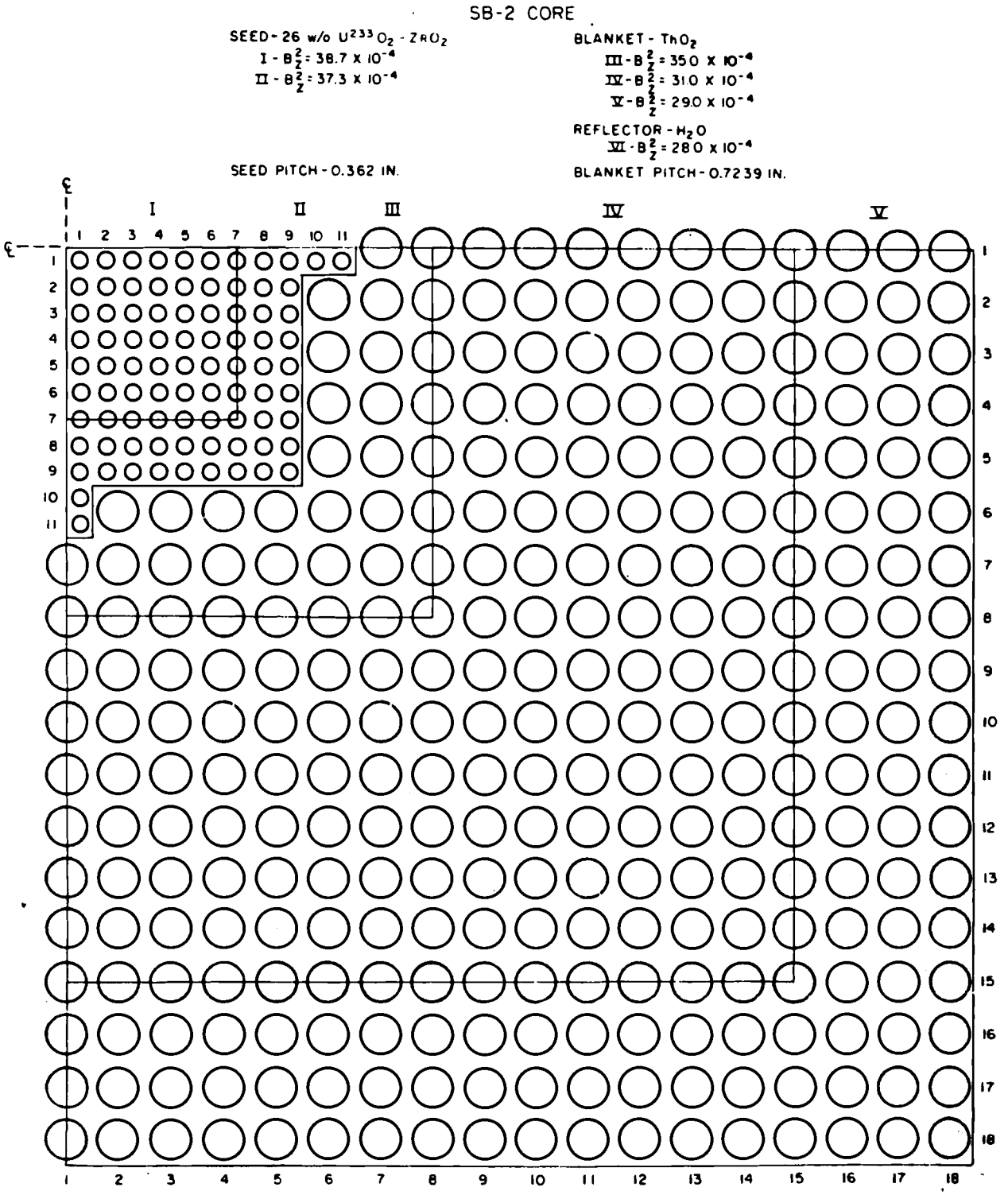

Figure 21. Diagram of LWBR SB-2 Core.

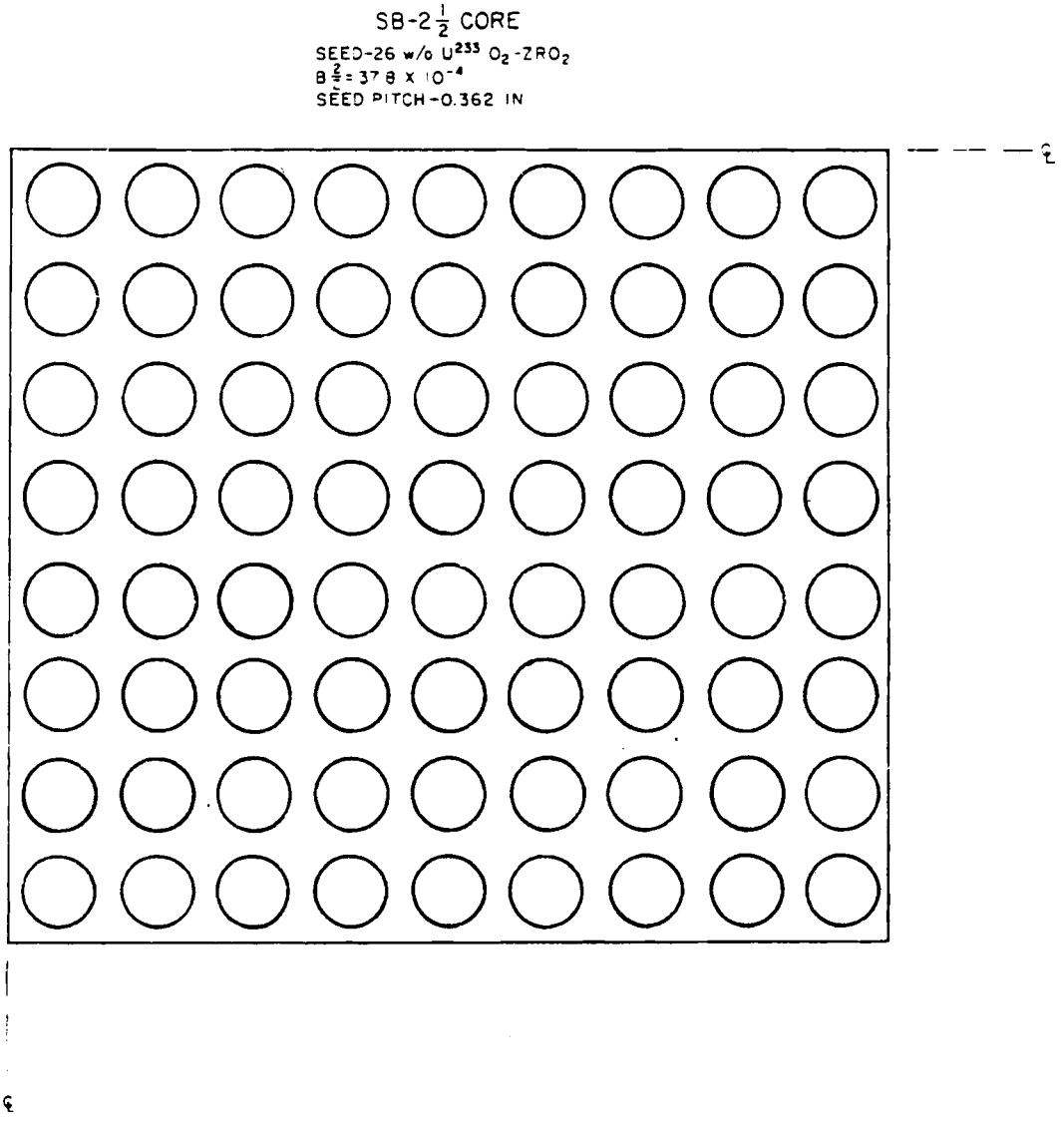

Figure 22. Diagram of LWBR SB-2 1/2 Core.

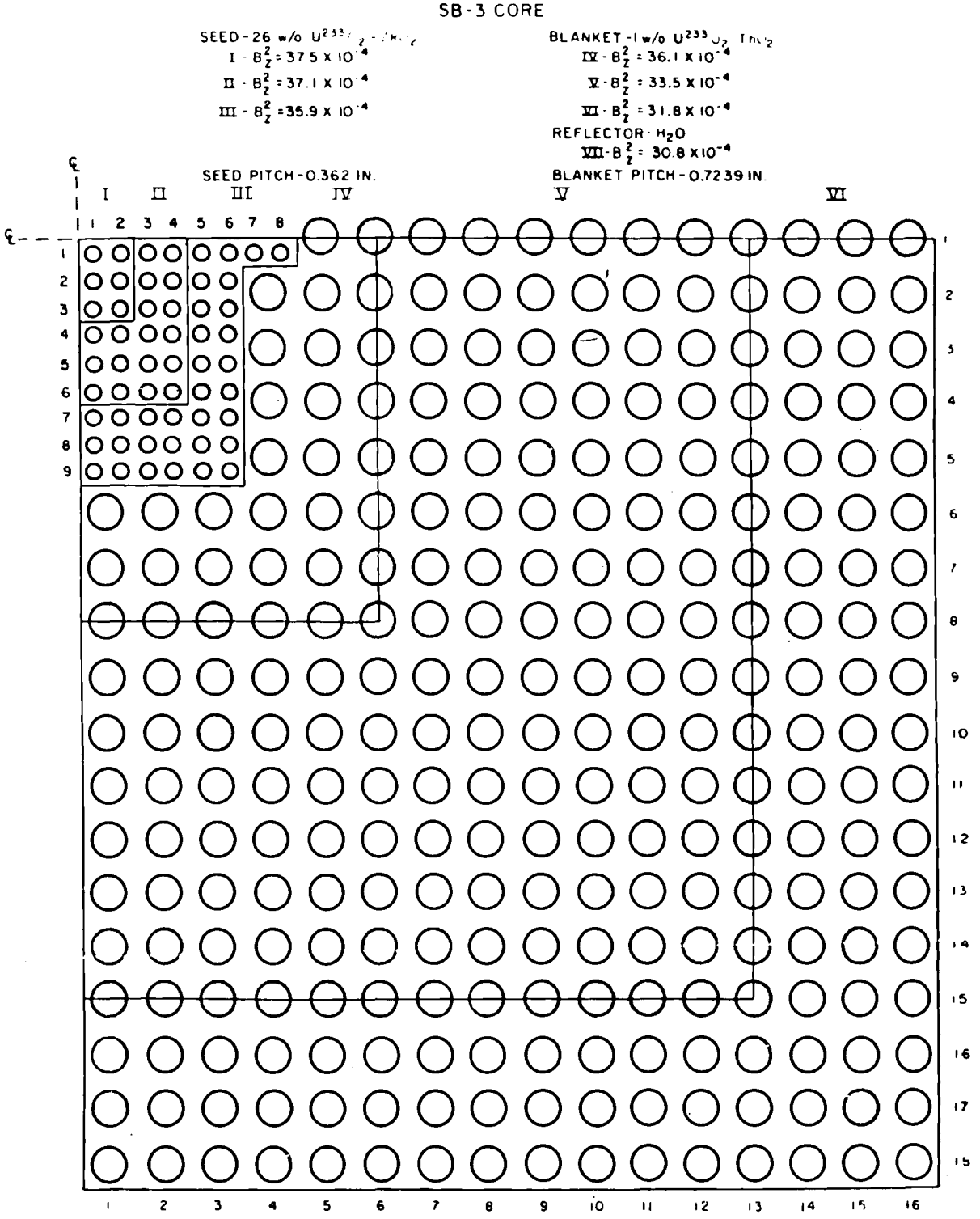

Figure 23. Diagram of LWBR SB-3 Core.

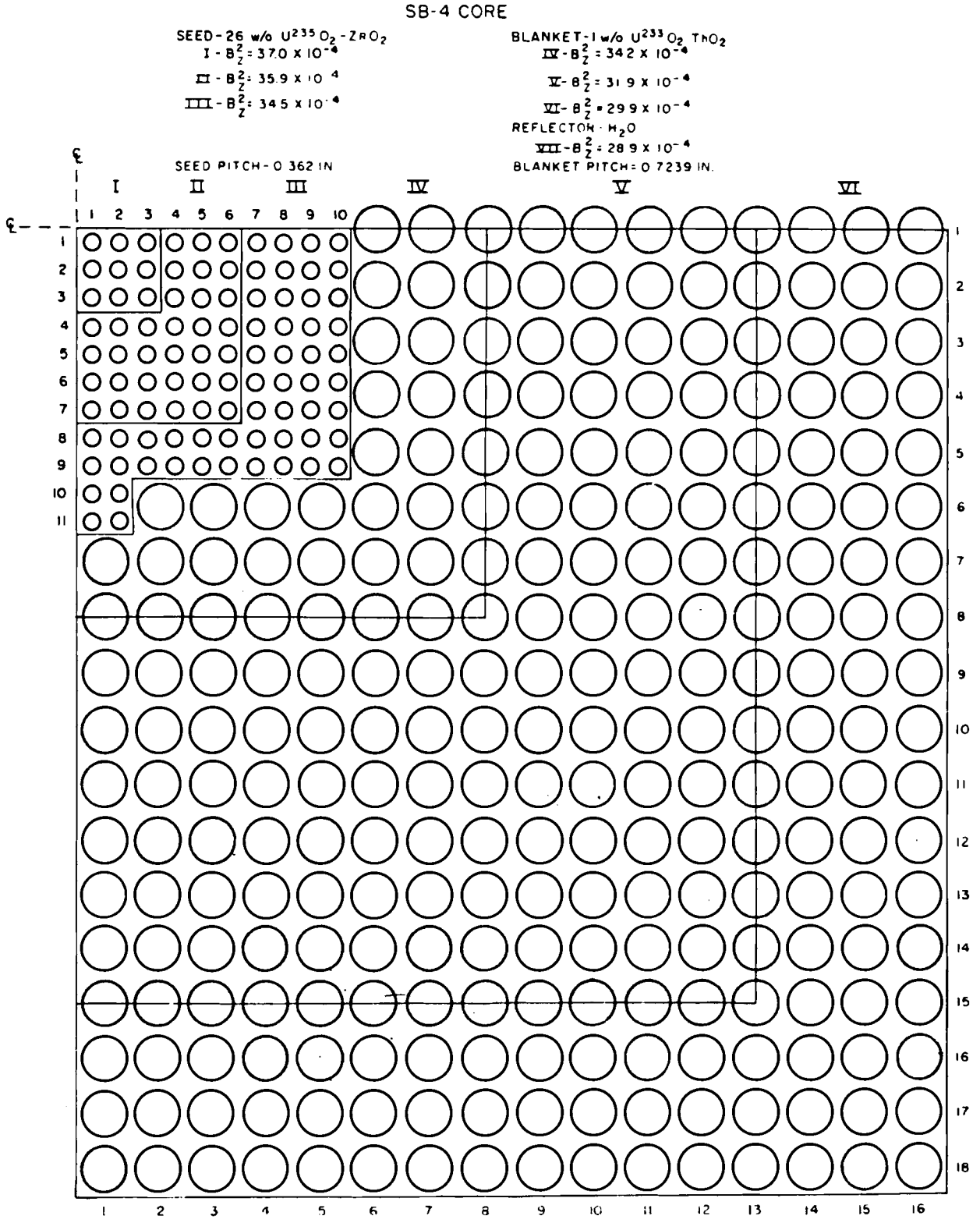

Figure 24. Diagram of LWBR SB-4 Core.

SB-5 CORE

SEED - 26 w/o $U^{235}O_2 - ZrO_2$

I - $B_z^2 = 39.4 \times 10^{-4}$

II - $B_z^2 = 37.9 \times 10^{-4}$

III - $B_z^2 = 36.9 \times 10^{-4}$

SEED PITCH - 0.5701 IN.

BLANKET PITCH - 0.5714 IN.

BLANKET - ThO_2

IV - $B_z^2 = 35.1 \times 10^{-4}$

V - $B_z^2 = 26.2 \times 10^{-4}$

VI - $B_z^2 = 26.3 \times 10^{-4}$

REFLECTOR - H_2O

VII - $B_z^2 = 25.0 \times 10^{-4}$

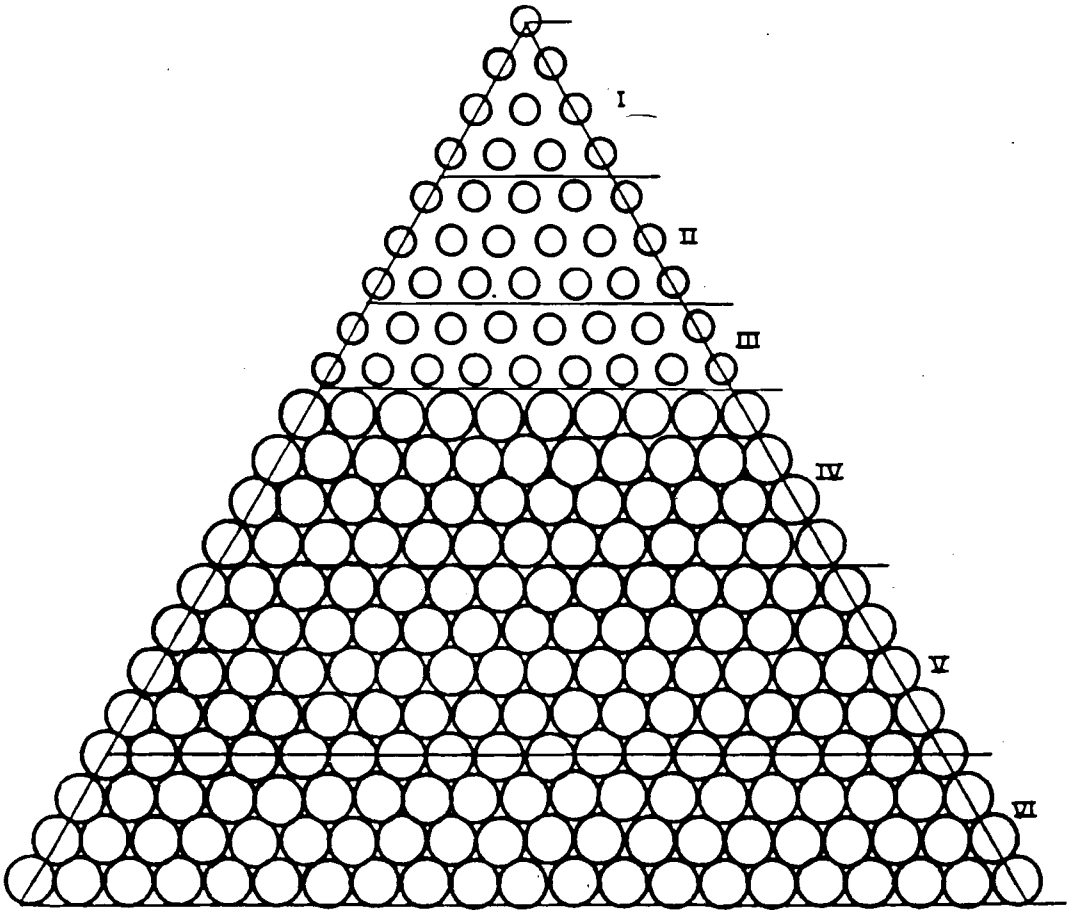

Figure 25. Diagram of LWBR SB-5 Core.

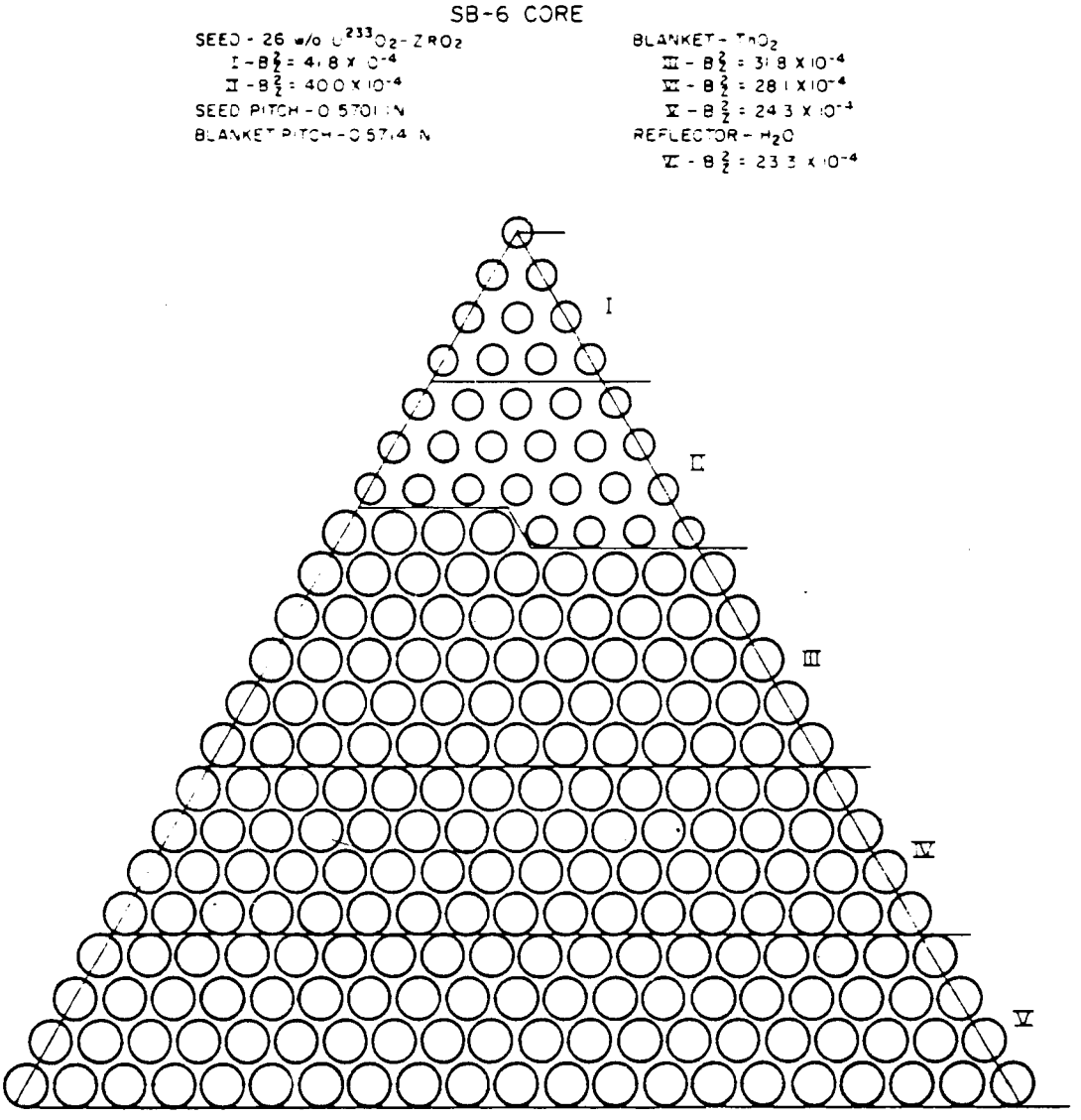

Figure 26. Diagram of LWBR SB-6 Core.

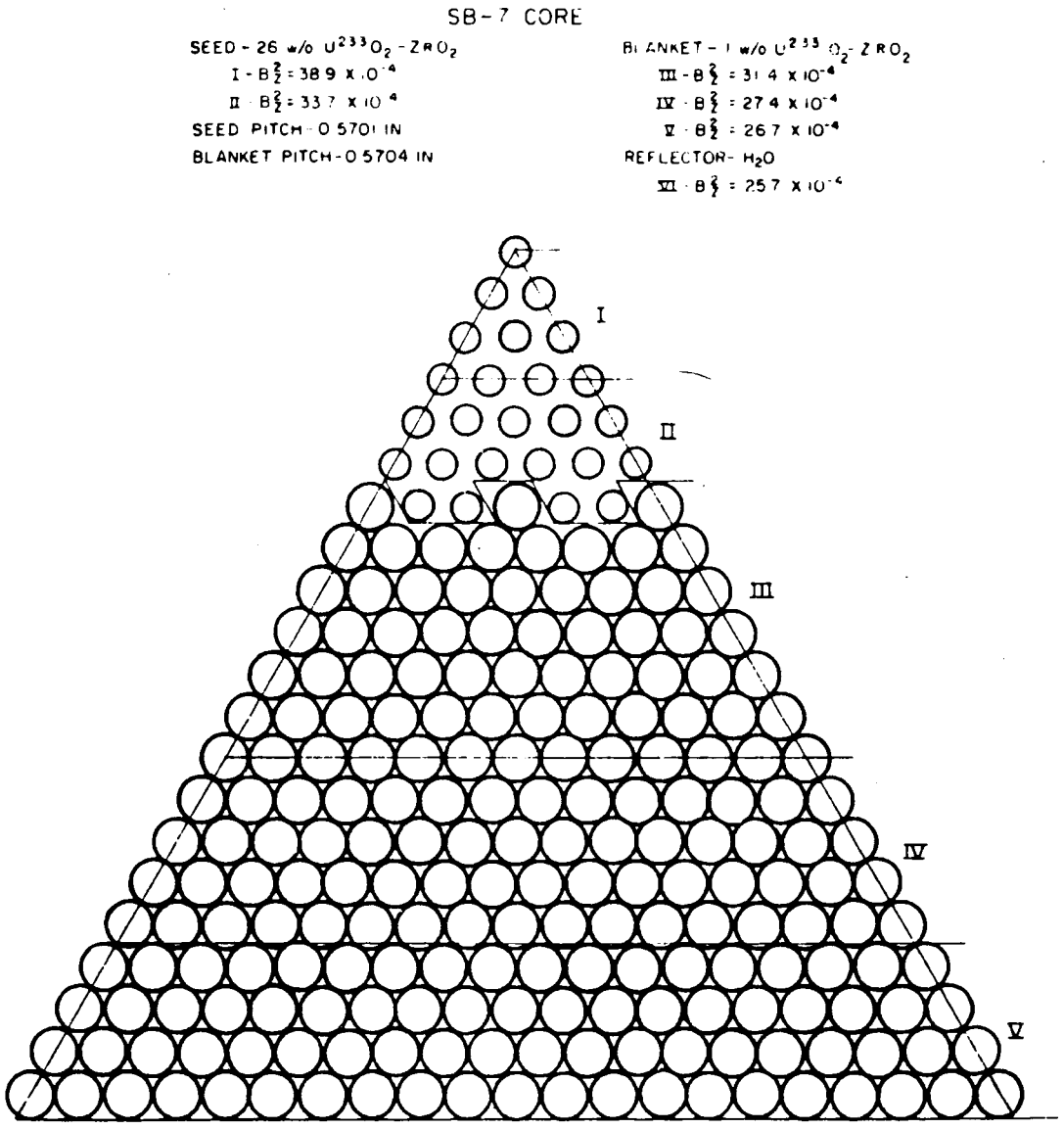

Figure 27. Diagram of LWBR SB-7 Core.

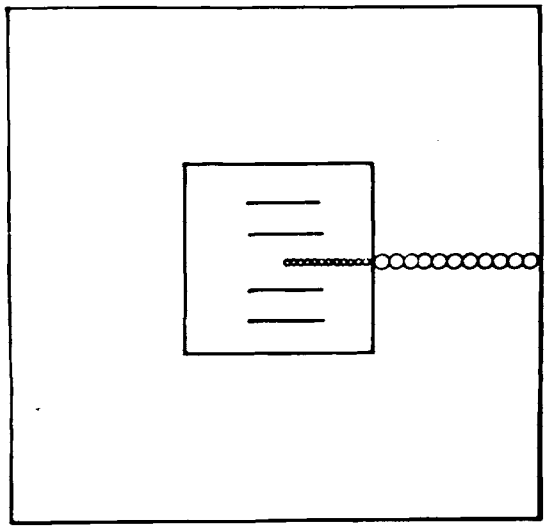

SB-1 CORE
SEED-26 w/o $U^{235}O_2$-ZrO_2
BLANKET- ThO_2

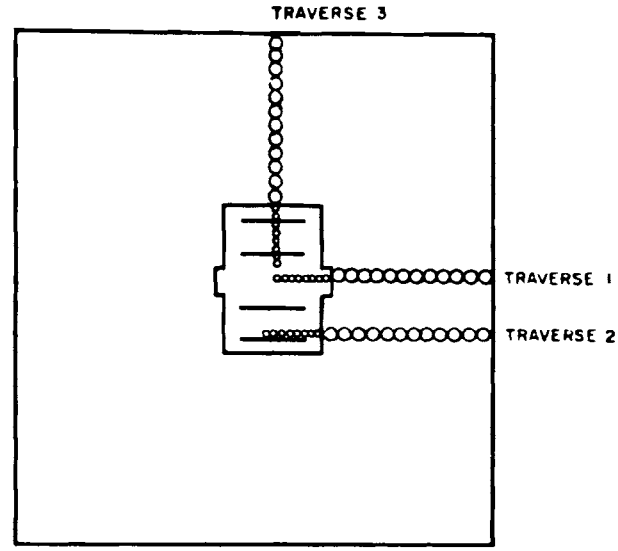

SB-3 CORE
SEED-26 w/o U^{233} O_2-ZrO_2
BLANKET-1 w/o U^{233} O_2-ThO_2

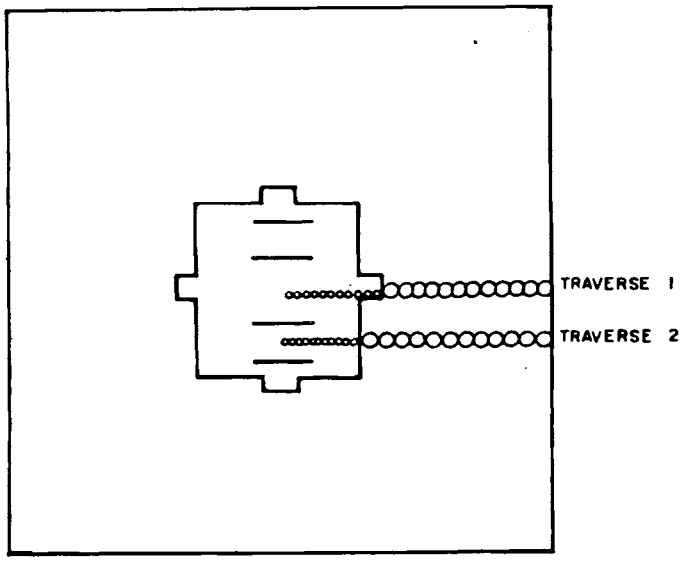

SB-2 CORE
SEED-26 w/o U^{233} O_2-ZrO_2
BLANKET- ThO_2

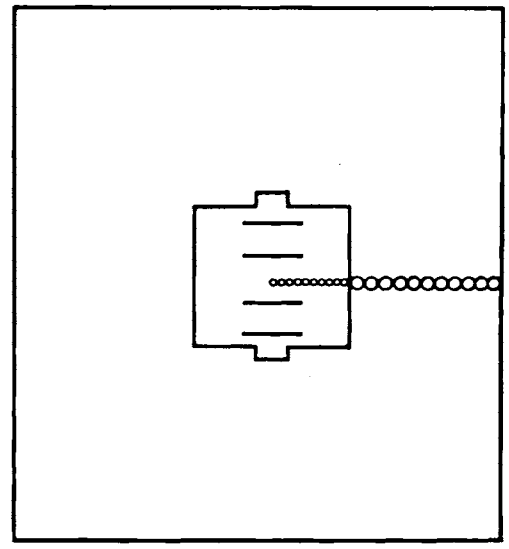

SB-4 CORE
SEED-26 w/o U^{235} O_2-ZrO_2
BLANKET-1 w/o U^{233} O_2-ThO_2

Figure 29. Schematic View (Top) of SB-1 and SB-2 Cores Showing Location of Traverses.

Figure 30. Schematic View (Top) of SB-3 and SB-4 Cores Showing Location of Traverses.

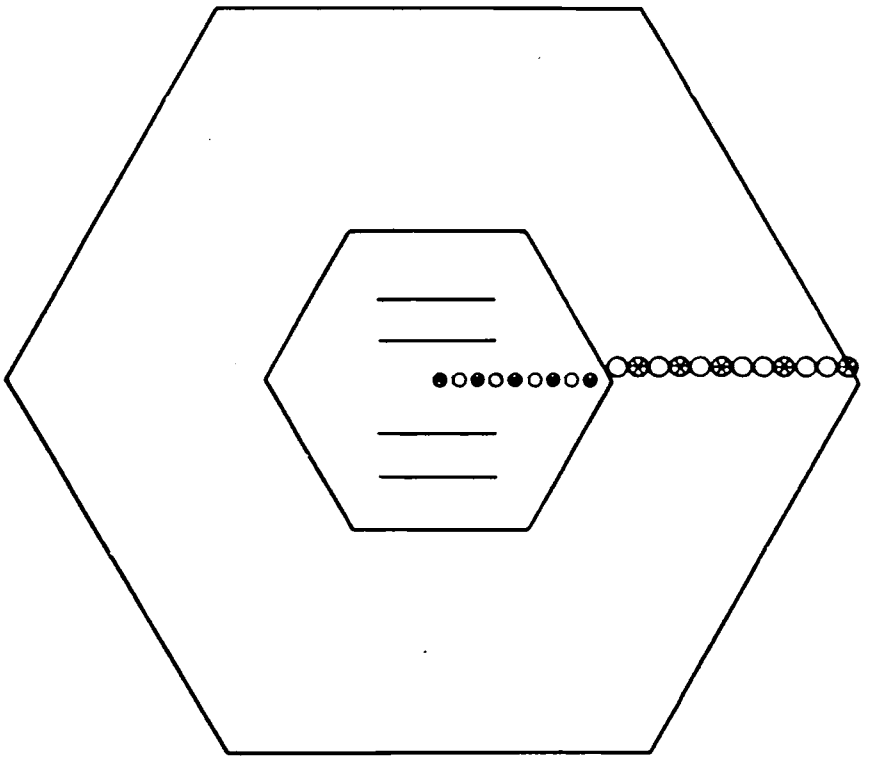

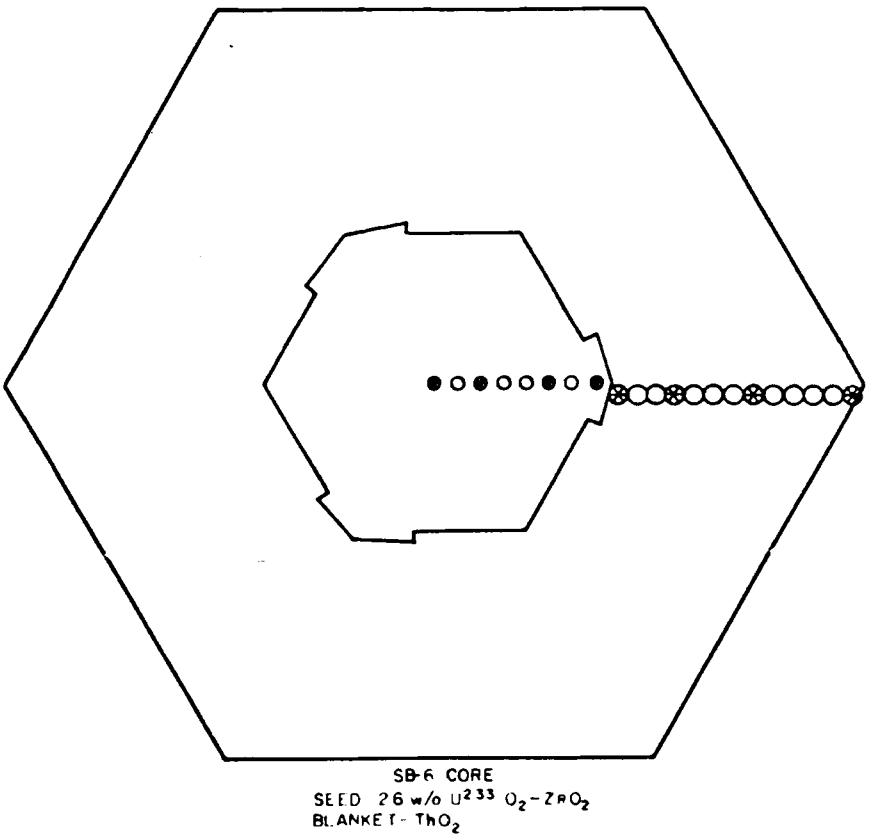

Figure 31. Schematic View (Top) of SB-5 and SB-6 Cores Showing Location of Traverses.

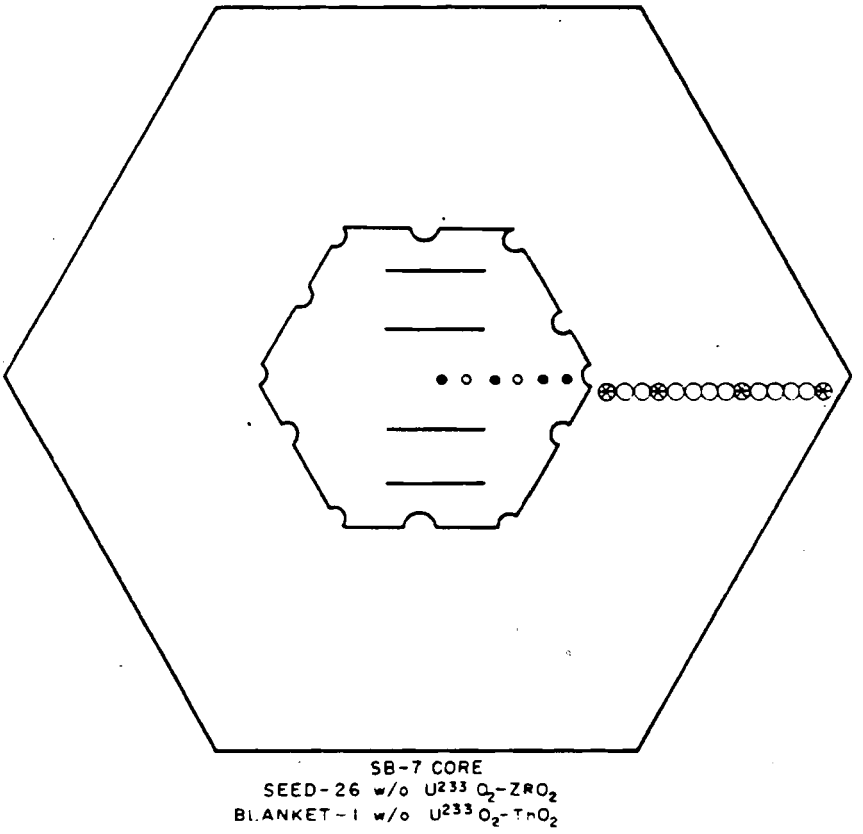

Figure 32. Schematic View (Top) of SB-7 Core Showing Location of Traverse.

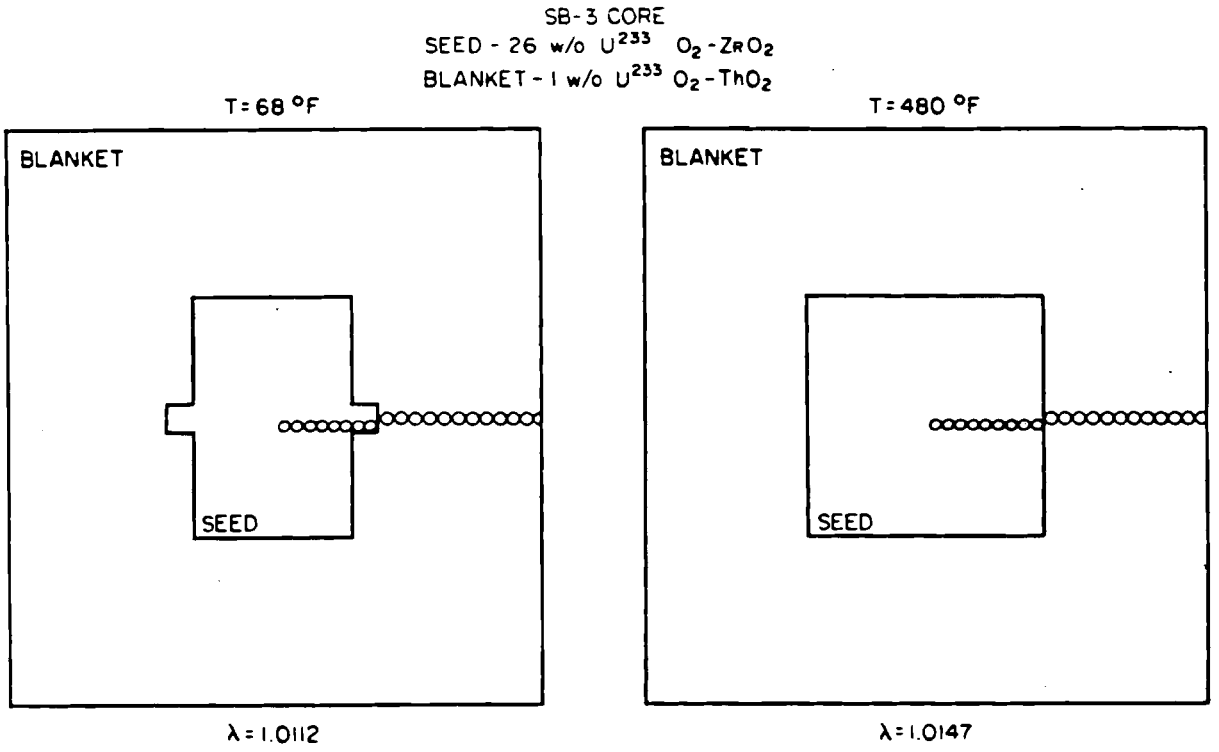

Figure 90. Schematic Views (Top) of SB-3 Core Cold and SB-3 Core Hot, Respectively.

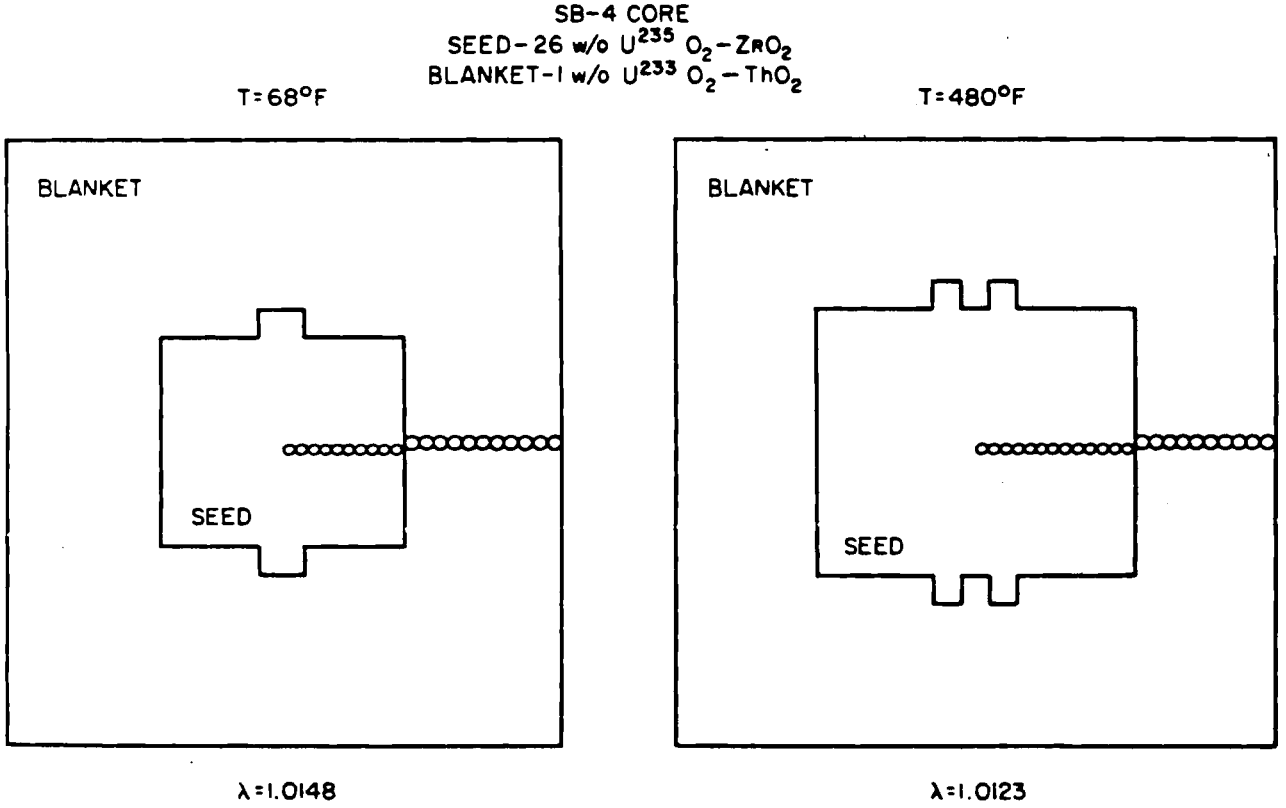

Figure 91. Schematic Views (Top) of SB-4 Core Cold and SB-4 Core Hot, Respectively.

APPENDIX B
URANIUM ANALYSIS, URANIUM-233 PROGRAM (ORNL)

TABLE B-1. URANIUM ANALYSIS OF FINISHED URANIUM-233 CONTAINING PELLETS

U^{233} (Production)	Average w/o U	No. of Analyses
1 w/o UO_2 - ORNL	0.939* (w/o U^{233} - 0.913)	52
26.8 w/o UO_2 - ZrO_2 - ORNL	24.47* (w/o U^{233} - 23.81)	46

Isotopic Analysis (ORNL)	UO_2 - ThO_2 (26 Analyses)	UO_2 - ZrO_2 (23 Analyses)
Uranium-232	<0.05	<0.05
Uranium-233	97.19	97.29
Uranium-234	1.55	1.56
Uranium-235	<0.05	<0.05
Uranium-236	<0.05	<0.05
Uranium-238	1.23	1.14

*Corrected to uranium-233 - $\frac{(233)}{(238)}$.

APPENDIX C
URANIUM-235 O_2-ZrO_2 SEED URANIUM ANALYSIS

TABLE C-1. URANIUM ANALYSIS OF FINISHED URANIUM-235 CONTAINING PELLETS

Incoming UF_6	%
Uranium-235	93.14
Uranium-234	0.892
Uranium-236	0.263
Uranium-238	5.706
Pellet	
Total U	24.70 ± 0.07 w/o
U^{235}	22.90 ± 0.07 w/o
Enrichment	92.73*

*This lower enrichment resulted from natural uranium contamination in the production line.

APPENDIX D
PELLET DENSITIES

TABLE D-1. PELLET DENSITIES

Fuel Type	% Theoretical Density (TD) Average	Minimum*	Maximum*	TD, g/cc
$U^{233}O_2$-ZrO_2	93.42	88.47	95.82	6.94
$U^{235}O_2$-ZrO_2	95.11	92.81	98.60	6.95
$U^{233}O_2$-ThO_2	94.07	90.53	96.81	10.04
ThO_2	94.6	93.0	95.5	10.03

*These values are the minimum and maximum measured values for 500 pellet samples.

APPENDIX E
FUEL ROD DATA

TABLE E-1. FUEL ROD DIMENSIONS AND PELLET NUMBER DENSITIES

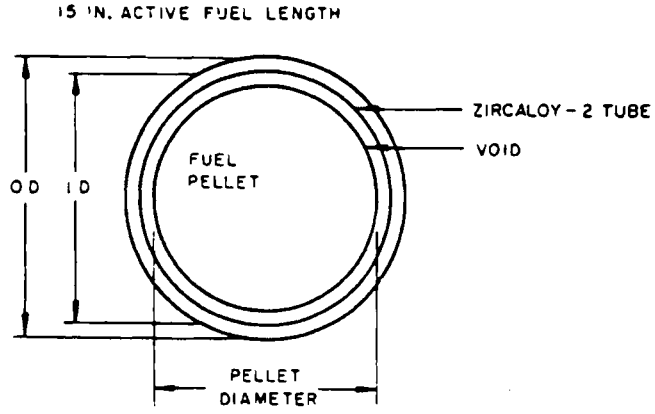

	Fuel Rod Dimensions			
	Seed Fuel		Blanket Fuel	
	U^{235}	U^{233}	ThO_2	1 w/o $U^{233}O_2$-ThO_2
Tube OD, in.	0.2545	0.2545	0.5698	0.5694
Tube ID, in.	0.2195	0.2195	0.4988	0.4984
Pellet Diameter, in.	0.2108	0.2113	0.4885	0.4903

	Fuel Pellet Number Densities			
	Pellet Number Density, 10^{24} atoms/cc			
	Seed Fuel		Blanket Fuel	
Isotope	U^{235}	U^{233}	ThO_2	1 w/o $U^{233}O_2$-ThO_2
U^{233}	--	0.0039899	--	0.00022289
U^{234}	0.0000375851	0.000063967	--	0.000003549
U^{235}	0.00387879	--	--	--
U^{236}	0.0000108258	--	--	--
U^{238}	0.000251232	0.000046986	--	0.0000028447
U^{232}	--	0.000036321	0.021594	0.021296
O	0.054868	0.053856	0.043990	0.043333
Zr	0.0232558	0.022792	--	--
Gd	--	--	0.00000011265	0.00000011214

Zircaloy-2 tube $N^{Zircaloy-2} = 0.0433788$

BMU Series of ^{233}U Fueled Criticals (Reference 19)

As has been noted, the cores of this series of experiments were quite complex. Consequently, for the sake of accuracy and completeness, the descriptions given in the source document are simply repoduced here.

I. INTRODUCTION

Eight ^{233}U fueled critical assemblies designated as the BMU series cores were studied at the Bettis Atomic Power Laboratory as part of the Light Water Breeder Reactor (LWBR) Development Program. The cores of this series followed a series of small ^{233}U fueled seed-blanket cores (Reference 1), and were the forerunners of a series of single module detailed cell experiments (Reference 2).

The various cores, assembled to investigate specific effects that are important in breeder reactor development, were either small or large, simple or had complex fuel zoning, single or multiple module. Experiments were performed both at ambient temperature and at 410°F.

Comparisons were made with calculations. These comparisons provided the basis for developing improved design analysis methods. Comparisons with models close to the model used for LWBR design analysis indicate that the effects of coupling are well predicted at both ambient and high temperature. The model was improved based on the results of the experiments, and selected calculations were redone and show good agreement with experimental results.

This report emphasizes documentation of the experimental program and includes the results of only a few typical calculations.

II. FUEL DESCRIPTION

Nine different fuel rod types were used in combinations for the BMU series cores to achieve radial and axial zoning. The rod types used and their dimensions are given in Appendix A. Four of these types were seed rods (0.25-inch diameter) and five were blanket rods (0.63-inch diameter). All rods were clad with Zircaloy-4 and had welded end caps at both ends. They were loaded with binary fuel pellets (i.e., a mixture of UO_2 and ThO_2), ThO_2 pellets, or both of these in separate sections of the rod. The composition of the fuel of each rod type is given in Appendix B.

Three of the seed-rod types were 28.16 inches overall length, and four of the blanket-rod types were 42.46 inches long. In addition, seed and blanket rods approximately 14 inches long were available for axial end reflector regions.

One seed-rod type and one blanket-rod type were uniformly loaded with ^{233}U. These seed rods contained 12 w/o $^{233}UO_2$ in ThO_2, and the blanket rods contained 2 w/o $^{233}UO_2$ in ThO_2. Also, one full length blanket-rod type and the two rod types for end reflectors were uniformly loaded with ThO_2.

The other two types of seed rods contained two different loadings in each part of the rod. One rod type was 5 w/o $^{233}UO_2$ in ThO_2 and 9 w/o $^{233}UO_2$ in ThO_2, and the other rod type was 2 w/o $^{233}UO_2$ in ThO_2 and 5 w/o $^{233}UO_2$ in ThO_2. Varying the loadings in the blanket rods divided the length into zones that were one-third and two-thirds of the total. One zoned blanket-rod type had 14 inches of 2 w/o $^{233}UO_2$ in ThO_2 and 28 inches of ThO_2. The other had 28 inches of 2 w/o $^{233}UO_2$ in ThO_2 and 14 inches of ThO_2.

III. CORE DESCRIPTIONS

A. BMU-1A

Figures 1 and 2 show a schematic diagram of the side view of the BMU-1 core and a top view of one-sixth of the BMU-1A core, respectively. A photograph of this core is shown in Figure 3.

The seed of the BMU-1A formed a symmetric hexagon containing 810 of the 12 w/o uniform seed rods resting on an equal number of short seed rods (ThO_2). The rods were spaced on a 0.3229-inch triangular pitch. What would have been the central seven rods of this hexagon was replaced by a metal and water region consisting of a Zircaloy-4 pipe (0.75-inch outside diameter and 0.037-inch wall thickness) running the entire height of the seed (42 inches). The reflector water was excluded from the bottom 14 inches of the pipe by a 5/8-inch diameter, 0.035-inch wall thickness, stainless steel tube through which the reactor source could be moved (see Figure 28). The top 28 inches of pipe contained a 0.65-inch diameter solid Zircaloy-4 plug. A channel formed by two Zircaloy-4 hexagonal cans surrounded the

seed region. Each can was 0.125 inch thick and there was a 0.125-inch water gap between them. A control rod guide was formed by the cans themselves and solid Zircaloy-4 pieces that fitted in the corners of the hexagon, leaving an opening 0.125 by 4.60 inches on each flat. The distance across the flats to the inside wall of the inner can was 9.212 inches.

The blanket surrounding the control guide also formed a symmetric hexagon. There were 13 rows of long ThO_2 blanket rods spaced on a 0.6961-inch triangular pitch. The region contained 1170 rods.

The rod pitches were maintained by five stainless steel tube sheets in the seed and two in the blanket. These tube sheets were made from flat plates and had holes slightly larger than the rod diameter drilled on the appropriate pitches. The top and bottom sheets were 0.125 inch thick; the three center sheets in the seed were 0.0625 inch thick. The distances to the bottom of each tube sheet in the seed with respect to the bottom of the ThO_2 seed reflector rod were 1.06, 13.06, 15.12, 28.28, and 41.25 inches. The corresponding blanket tube sheet distances were 6.68 and 33.06 inches.

Reactivity control was maintained by six hafnium control rods; each rod was 4.25 inches wide by 0.062 inch thick by 38 inches long. The critical bank height was 23.67 inches above the seed binary fuel zero at 28.1°C.

The fuel rods rested on a perforated stainless steel plate. The plate was 0.038 inch thick and was perforated by evenly spaced holes of 0.187-inch diameter. There were 18 2/3 holes per square inch of plate and therefore 0.4837 square inch of metal per square inch of plate.

The perforated plate rested on a stainless steel base plate which was 38 inches square and 0.75 inch thick. There was some material removed from this plate under the region of the seed: a square array (34 × 34) of 0.261-inch diameter blind holes on a 0.362-inch pitch was drilled through 0.5 inch of the thickness of the plate.

Stainless steel support bars were used below the base plate. The bars were 0.5 inch thick by 1.0 inch wide and had an accumulated length under the core region of 183.5 inches. This implies a metal volume fraction of 0.1354 for this region.

The assembly was supported by a core support plate 16 inches above the bottom of a tank 6 feet high by 6 feet in diameter. The support plate was 78 inches in diameter and 1 inch thick with three 0.75-inch thick concentric cylindrical supports 15 inches high. A roughly circular array of 0.5-inch diameter holes on a 1.77-inch square pitch was drilled through the plate for almost all of its surface. In addition, five 4.5-inch diameter holes allowed for the passage of instrument thimbles. To allow for water circulation below the core, cylindrical supports which were located 9, 22, and 36 inches from the plate center, had 8, 12, and 12 holes, respectively, each 9 inches in diameter.

All the tube sheets extended well beyond the fueled region of the core so that the structure that restrained lateral movement of the top of the core was more than 8 inches from the fueled region.

Figure 2, the top view of one-sixth of the BMU-1A, gives distances to various important locations.

B. BMU-1B

The BMU-1B core, shown in Figure 4, was the second step in the investigation of zoning. This was achieved by replacing the 810 seed rods loaded with 12 w/o $^{233}UO_2$ with the same number of 5/9 seed rods loaded with the 9 w/o end on the bottom and by replacing 360 of the ThO_2 blanket rods with uniform 2 w/o blanket rods. The new configuration of the blanket starting from the seed interface was (1) two complete rows of ThO_2 and four complete rows of 2 w/o blanket, (2) one row containing ten enriched blanket rods located in the center of the flat and five ThO_2 rods at each corner, and (3) six complete rows of ThO_2. The seed reflector of short ThO_2 seed rods was the same as in the BMU-1A core.

The six hafnium control rods were located 24.53 inches above the seed binary fuel zero when the core was critical at 27.34°C.

All of the structural regions were identical to the BMU-1A.

C. BMU-1C

The BMU-1C, shown in Figure 5, was the high-temperature version of the BMU-1 and the last in the BMU-1 series. The experiments were performed in the Bettis High Temperature Test Facility. The 810 seed rods used in the BMU-1B were also used in the BMU-1C but were turned upside down (i.e., with the 5 w/o end on the bottom). In order to compensate for the temperature defect, the loading in the blanket had to be increased; the new blanket contained seven complete rows of 2 w/o surrounded by six complete rows of ThO_2.

At criticality, the six hafnium control rods were located 26.75 inches above the seed binary fuel zero at the operating temperature and pressure of 410.1°F and 312 psi. This critical bank height was calculated from a selsyn reading (26.55 inches) calibrated at room temperature and expansion coefficients of stainless steel, Zircaloy-4, and hafnium of 9.6×10^{-6}, 2.7×10^{-6}, and 3.3×10^{-6} inch/inch/°F, respectively.

The support bars and core support plate of BMU-1A and BMU-1B were replaced by an egg crate structure below the core base plate. This structure was made of stainless steel ligaments 3/4 inch thick and 6 inches high, making a square array with a 7.5-inch pitch.

D. BMU-2-1

The second series of cores was designed to investigate the effects of coupling in multiple module cores and the effects of rod support grids with relatively large metal volumes. The first of this series was the BMU-2-1, a single module version to be used as a reference core, shown in Figures 6 and 7.

The seed was a symmetric hexagon composed of 907 rods on a 0.302-inch triangular pitch in the upper 28 inches. The first 15 rows (631 rods) were 12 w/o seed; next were two rows (186 rods) of 2/3 seed with the 3 w/o end on the bottom, and finally one row (90 locations) of ThO_2 seed. The ThO_2 seed rods were only half the length of the other rods; therefore, two rods were loaded one above the other in each location with a metal and water region in the middle where the ends butted together. Two rod locations on each flat in this outer row were displaced by a Zircaloy-4 support bar. These bars ran the entire length of the seed and were 0.567 inch along the direction of the flat and extended 0.310 inch into the seed from the inner can wall. Spacing was maintained in the upper section of the seed by 1/16-inch stainless steel tube sheets in three axial locations. The lowest axial height had a single tube sheet 14.95 inches above the seed support plate. The other two heights had grid assemblies made of three tube sheets equally spaced over 1.5 inches. These grid assemblies were held together at the six corners and the center by stainless steel spacers, and in addition had 49 places where ligaments between holes were cut out to allow for flux plotting; the average weight of one assembly was 488.86 grams. The bottoms of the assemblies were located 13.327 and 25.992 inches from the bottom of the binary seed pellets.

To complete the 42-inch height of the seed, a ThO_2 reflector was located below the section of the seed just described. This reflector was made up of 127 short-blanket rods spaced on a 0.770-inch triangular pitch and held laterally by two egg crate grids made of stainless steel. These grids were made from 1/16-inch strips 0.76 inch high. The total volume of steel in a grid was 10.066 cubic inches, and the grid was 9.26 inches across the flats. Resting on top of this reflector was a plate made from the same material as the perforated plate described in Section III.A. This plate served as the base for the upper seed region.

The entire seed rested on a seed support plate that was fastened to the support bars and allowed the seed to be lifted from the blanket. This support plate was 0.5-inch stainless steel with 834 holes, 0.234-inch diameter, drilled through it on a 0.302-inch pitch.

Surrounding the seed was a control rod channel formed (as in the case of the BMU-1) by two Zircaloy-4 hexagonal cans and Zircaloy-4 corner spacers. The distance across the inside flats of the inner can was 9.289 inches; the walls of the inner can were 0.100 inch thick. The outer can was 0.150 inch thick. The corner pieces were not solid but were formed from two rectangles 0.124 inch thick by 0.38 inch wide fastened to the inner wall of the outer can such that their inner corners touched. This formed a control rod channel 0.124 inch wide by 4.71 inches long.

Reactivity control was maintained by three hafnium control rods (located on every other flat). Each rod was 4.157 inches wide by 0.063 inch thick by 38 inches long. The critical position was 27.63 inches above the seed-binary fuel zero at 27.9°C.

The inner blanket region was a hollow hexagon composed of six rows of rods. The first two rows were zoned rods; the inner row had rods containing 14 inches of binary pellets (54 rods), and the next row contained rods with 28 inches of binary pellets (60 rods); in both cases the binary pellets were at the top of the core. The next four rows had uniformly loaded 2 w/o blanket rods (294 rods). One rod in each corner of the last row was displaced by a Zircaloy-4 rod of the same diameter.

The outer blanket consisted of six rows of ThO_2 blanket rods. This blanket region was formed from six rhombic grid plates, each with space for 103 fuel rods. At each inner corner of each plate, a rod location was occupied by a Zircaloy-4 rod like the one in the inner blanket. At each corner of the hexagon three Zircaloy-4 rods were fastened together (one from the inner blanket and one from each of two of the outer blanket plates) to form a 0.920-inch triangular pitch and hence define a water channel between the inner and outer blankets and between sections of the outer blanket.

Four stainless steel grid assemblies maintained the 0.694-inch triangular pitch in the inner blanket. Each grid assembly was composed of three tube sheets 1/16 inch thick and spaced to cover 1.5 inches in height. The average weight of a grid assembly was 1284.4 grams. The bottoms of the grids were located 0.762, 13.280, 27.712, and 40.377 inches from the bottom of the fuel pellets in the blanket. The triangular pitch in the outer blanket was 0.694 inch and was maintained by two 1/8-inch thick tube sheets located 1.75 inches from the bottom and 1.00 inch from the top of the ThO_2 blanket rods. These tube sheets extended well away from the core edge so that the vertical support members were far from the active region of the core.

The core assembly described above rested on a stainless steel core base plate which was 48.5 inches square and 0.76 inch thick. There was a square pattern of 169 holes, 0.75 inch in diameter, spaced over the central 2-foot section of the plate; and 117 holes, 0.5 inch in diameter, concentrated in three regions roughly where the seeds of the three-module core were located. This plate rested on seven support bars, 1.5 inches wide by 0.5 inch thick by 50 inches long equally spaced under the base plate. These rested on the same core support structure described in the BMU-1A.

E. BMU-2-3

BMU-2-3 was a core composed of three modules in a triangular array. A one-sixth top view is shown in Figure 8, and a photograph of the entire core is shown in Figure 9. The three seeds and three inner blankets were structurally identical to the corresponding regions in the BMU-2-1 core. Surrounding the array was an outer blanket (i.e., there was no outer blanket between the modules).

The upper section of the three seeds each contained 15 rows (631 rods) of the 5/9 seed with the 9 w/o end on the bottom, then two rows (186 rods) of the 2/5 seed with the 5 w/o end on the bottom, and finally one row (90 locations) of the ThO_2 seed rods stacked two high. The same lower seed section was used for each seed as in BMU-2-1.

The first row of each inner blanket contained 23 ThO_2 blanket rods, 28 zoned blanket rods with 14 inches of binary fuel at the top, and three 2 w/o blanket rods. The second row contained 19 of the same zoned blanket rods and 41 blanket rods containing 2 w/o of $^{233}UO_2$. The rest of the region consisted of four rows (294 rods) of 2 w/o blanket. At the core center where the three inner blankets met, three Zircaloy-4 rods were fastened in the same manner as between inner and outer blankets, defining a water channel between inner blankets. The location of the rods in the first two blanket rows is indicated in Figure 8.

Reactivity was controlled by nine hafnium control rods, three in each module. The critical height at 26.2°C was 25.78 inches above the seed binary fuel zero.

F. BMU-2-4U

The BMU-2 four-module cores were designed to test coupling in an array of many modules. Therefore, the four modules were arranged in a straight line as shown in Figure 10. A photograph of this core is shown in Figure 11.

All four seeds of the BMU-2-4U were loaded with 15 rows of 5/9 seed rods with the 9 w/o end on the bottom (631 rods) and three rows of 2/5 seed rods with the 5 w/o end on the bottom (276 rods). The same grids were used as described in the BMU-2-1 section (0.302-inch triangular pitch), as well as the same lower reflector of short ThO_2 blanket rods and seed support plate.

Reactivity control was maintained by 12 hafnium control rods, three in each module. The critical height was 24.97 inches from the seed binary fuel zero at 26.9°C. The control rod channel was formed by the same Zircaloy-4 cans and spacers as in the BMU-2-1.

The four inner blankets of this core were identically loaded, accounting for the designation, "uniform." The first row of blanket contained 54 ThO_2 rods. The second row contained 12 zoned blanket rods with 14 inches of binary fuel at the top and the rest uniformly loaded 2 w/o rods. The next three rows contained 2 w/o rods. The last row contained 16 zoned blanket rods with 28 inches of binary fuel at the top and the rest uniformly loaded 2 w/o rods. The outer blanket, which surrounded the entire assembly, contained six rows of ThO_2 rods. The location of these rods is indicated in Figure 10, which also indicates the locations of the control rods. The same Zircaloy-4 rods and fasteners as in the BMU-2-1 were used at the corner locations to hold the inner and outer blankets together.

The entire assembly rested on a perforated plate made from the same material described in Section III A.

The stainless steel core support table held the assembly 48 inches above the bottom of a tank 15 feet high by 17 feet in diameter. The top of this table was 0.75 inch thick, and had an array of 0.75-inch diameter holes on a 2.0-inch triangular pitch under each seed. The area under the inner blanket region was solid. The structure that reinforced the table top under the assembly had rib-type supporting members 1 inch wide by 9 inches thick. These members formed rectangular supports about 1 foot square. There were square pads (3 inches on a side and 0.5 inch thick) in the corners of the rib supports to hold the table top.

G. BMU-2-4PF

The second core of the four-in-line series was designed to investigate power flattening by preferential fuel loading of the outermost modules.

All four seeds in this core were loaded the same as the BMU-2-4U. However, the two inner module blankets (referred to as modules 2 and 3 in Figure 12) were loaded less heavily than in the uniform core, while module 1 and 4 blankets (the outer modules) were more heavily loaded.

In the blanket of the inner modules, the first row contained 54 rods of ThO_2, the second row contained 38 rods of ThO_2, and the remainder were uniformly loaded 2 w/o blanket rods. The next four rows were the same as in the BMU-2-4U; that is, three rows of uniform binary fuel and one row which had 16 zoned fuel rods with 28 inches of binary fuel.

The blankets of the outer modules contained uniform 2 w/o blanket rods except for 16 ThO_2 rods in the first row outside the seed and 24 zoned blanket rods with 28 inches of binary fuel in the last row.

The critical height of the 12 hafnium control rods at 24.4°C was 22.90 inches above the seed binary fuel zero.

The outer blanket of ThO_2 and all the structural materials were identical to those in the BMU-2-4U.

H. BMU-2-4T

The last of the BMU series cores was a "tilted" loading shown in Figure 13. Three modules were

loaded identically and one module had a different loading to introduce a cross gradient across the core.

The seeds of all four modules were again identical to BMU-2-4U. In addition, the modules indicated as 2, 3, and 4 in Figure 13 were loaded the same as the inner modules of BMU-2-4PF; that is, the first two rows of inner blanket contained a total of 92 ThO_2 rods and the last row contained 16 zoned blanket rods with 28 inches of binary fuel. The fourth module, the outer module designated as module 1 in Figure 13, was more heavily loaded than previous cores; there were only 10 rods containing ThO_2 in the first row. The outer row again contained 24 zoned blanket rods with 28 inches of binary fuel.

The outer blanket of ThO_2 and all the structural regions were identical to those in BMU-2-4U.

The critical height of the 12 hafnium control rods at 23.5°C was 23.92 inches above the seed binary fuel zero.

VI. SUMMARY

The objectives of the BMU series program were met. The effects of zoning, coupling, and grids of relatively large volumes were investigated.

During the course of the program, deficiencies in the nuclear analysis model were uncovered, changes were made in cross sections, and transport corrections were incorporated into the constants for diffusion theory calculations. Selected calculations that were redone show improved agreement. By comparing pairs of eigenvalues from calculations performed with a refined nuclear analysis model, it can be seen that the effects of coupling are well predicted and that no new problems occur at high temperatures.

The initial experiments leading to the determination of three-dimensional core power by counting rods were done in this series of cores and an experimental procedure, as well as data reduction techniques, was developed to be used in subsequent assemblies.

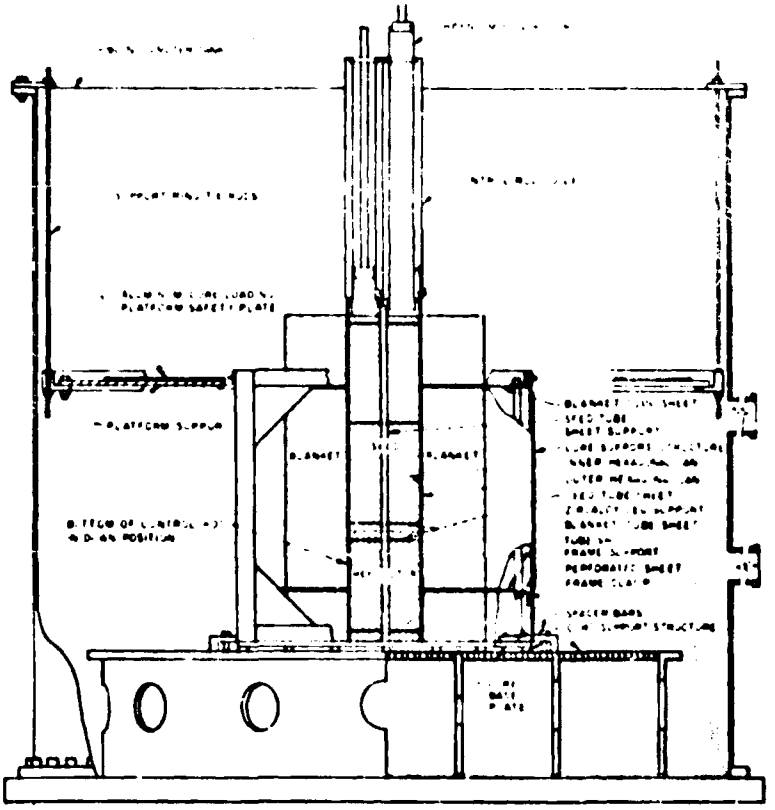

Figure 1. BMU-1 Side View

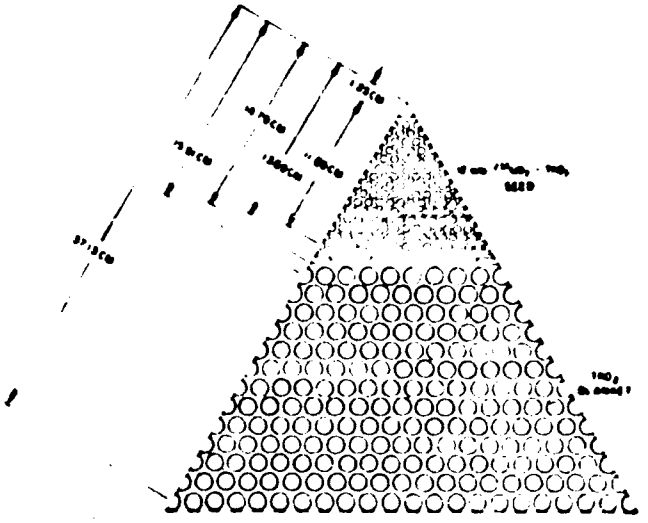

Figure 2. BMU-1A One-Sixth Core Top View

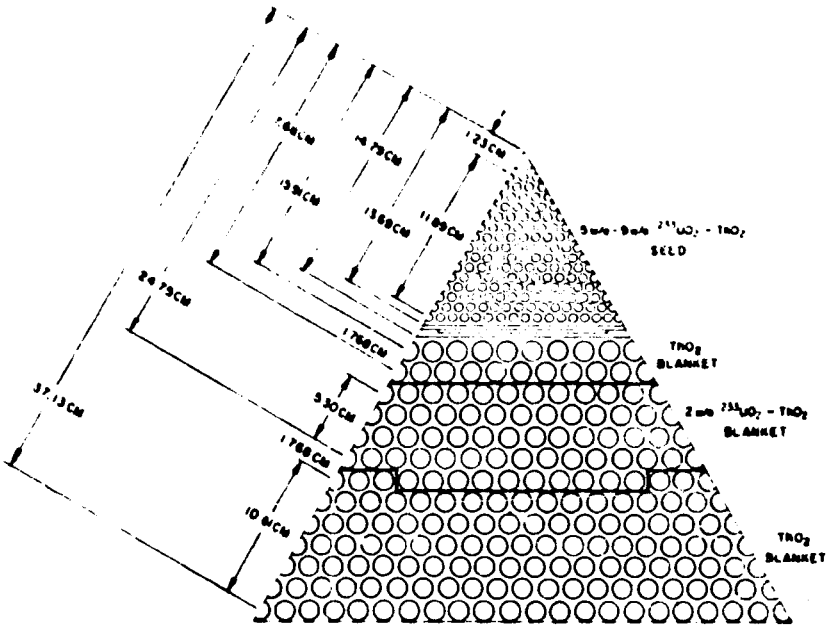

Figure 4. BMU-1B One-Sixth Core Top View

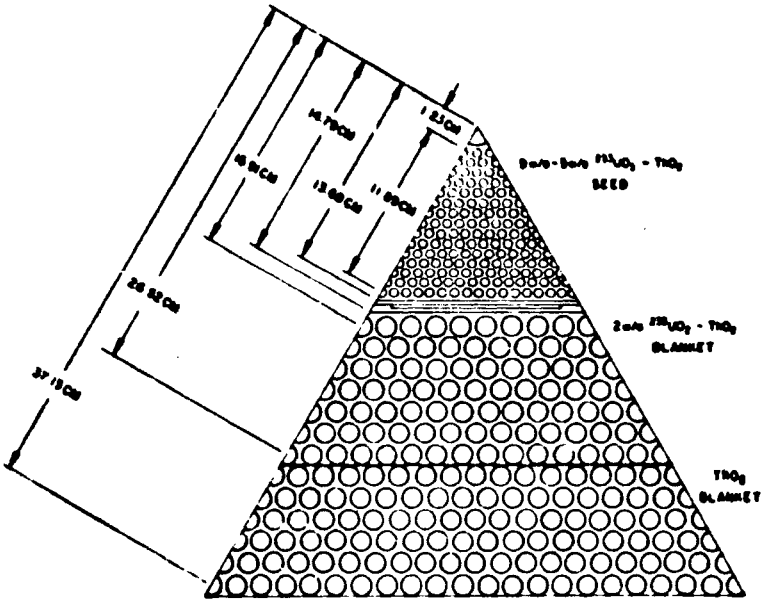

Figure 5. BMU-1C One-Sixth Core Top View

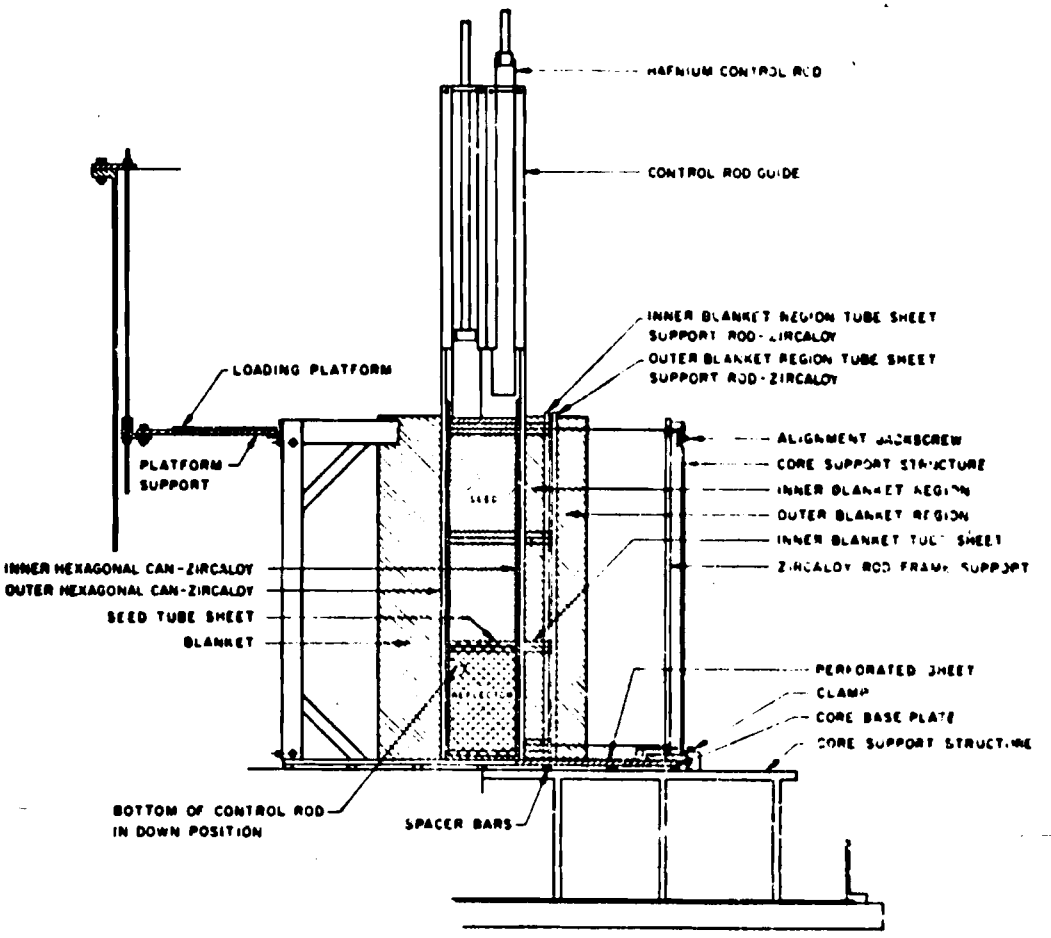

Figure 6. BMU-2 Side View

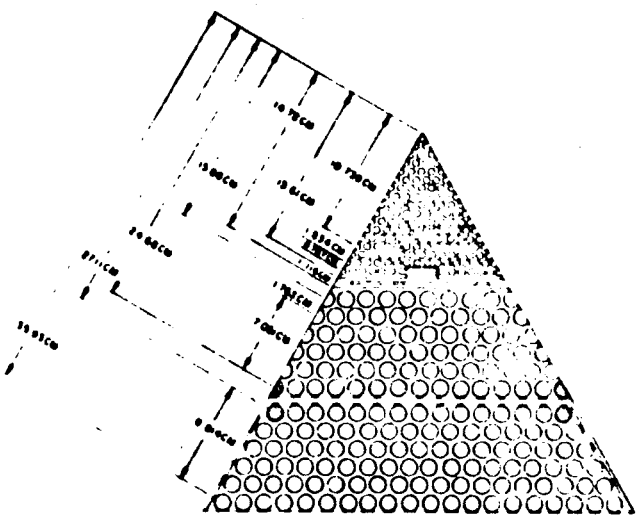

Figure 7. BMU-2 One-Sixth Core Top View

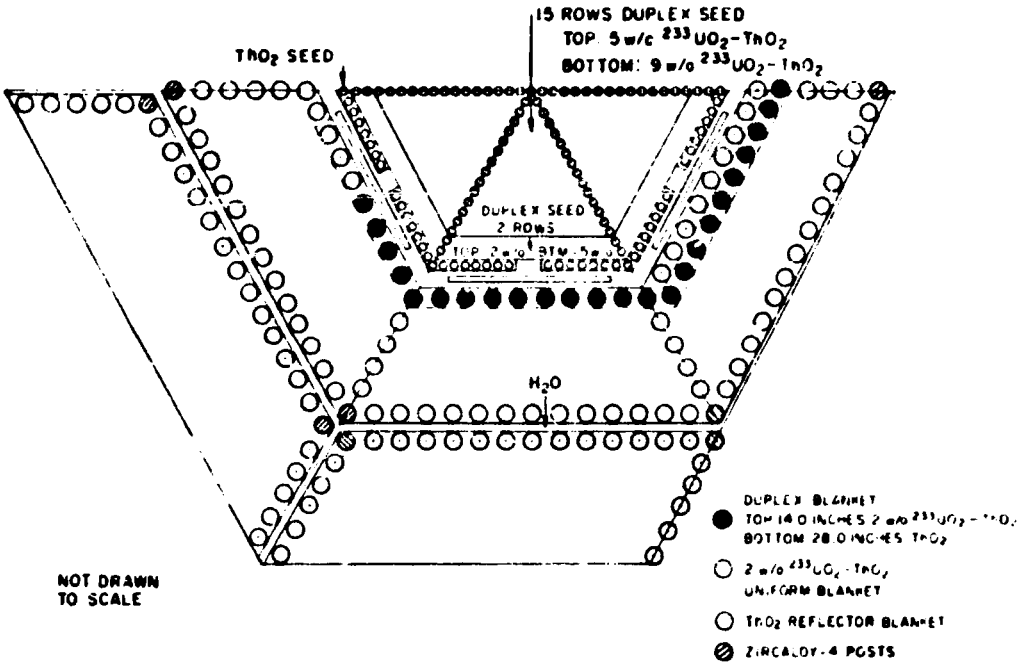

Figure 8. BMU-2 Three-Module, One-Sixth Core

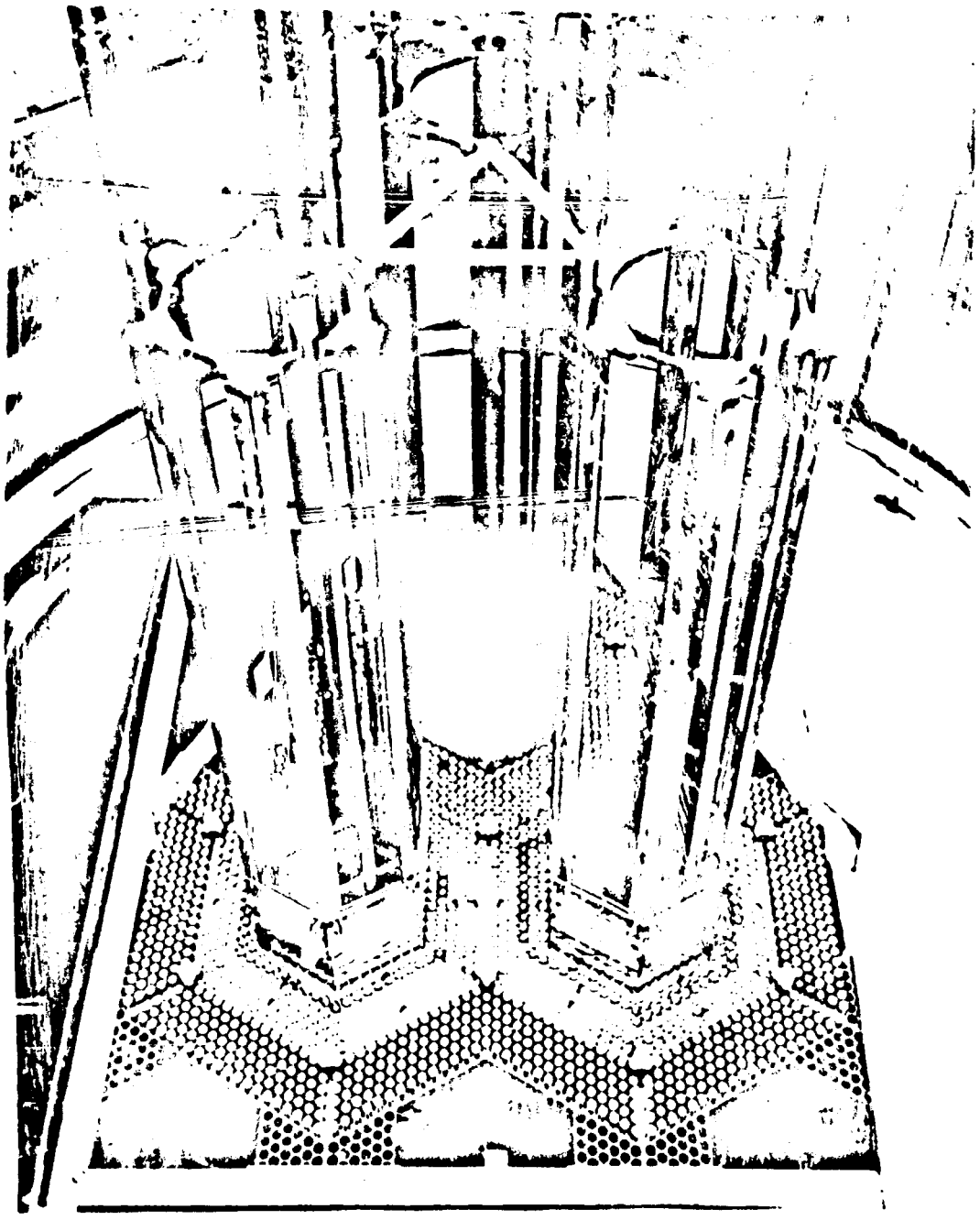

Figure 9. Photograph of BMU-2 Three-Module Core

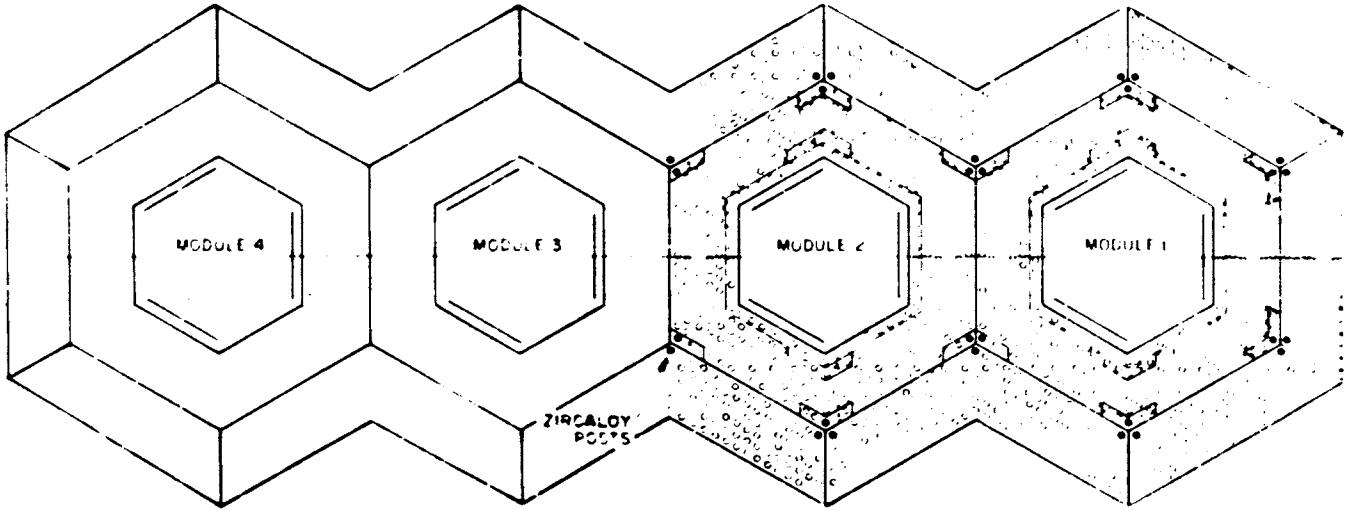

UNIFORM LOADING

ZONE	[illegible]	CENTER SECTION	[illegible]
1	[illegible]	[illegible]	[illegible]
2	ThO_2	ThO_2	ThO_2
3	[illegible]	[illegible]	[illegible]
4	[illegible]	ThO_2	ThO_2

EACH SECTION IS APPROXIMATELY 14 INCHES LONG
ALL BOARY FUEL IS [illegible] - ThO_2

Figure 10. BMU-2 Four-Module Core, Uniform Loading

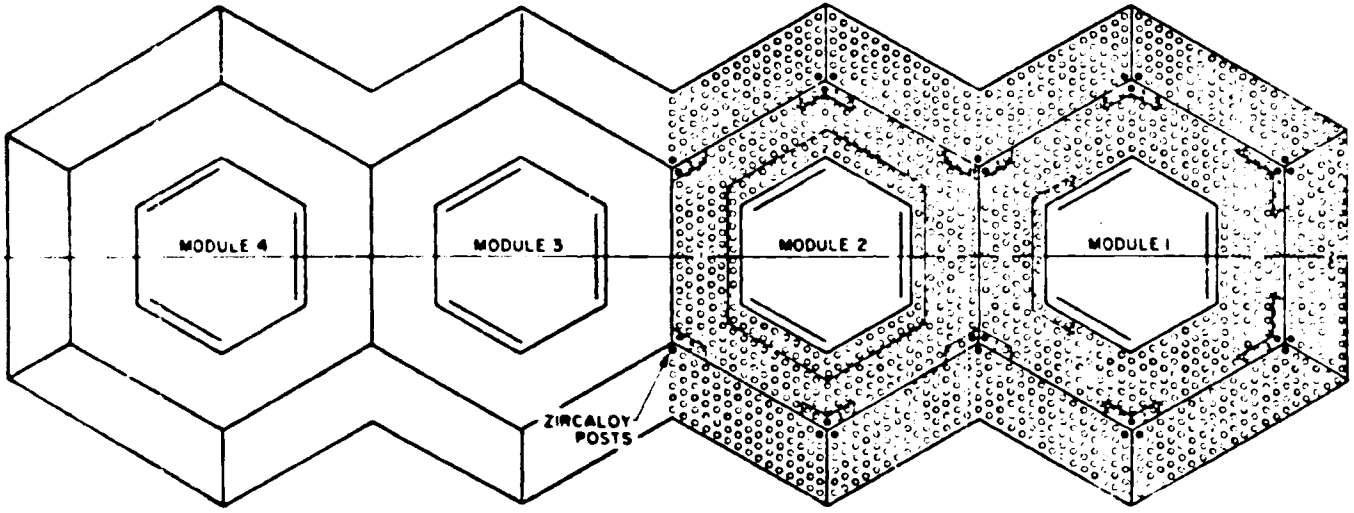

POWER FLATTENED LOADING

ZONE	TOP SECTION	CENTER SECTION	BOTTOM SECTION
1	2 w/o	2 w/o	2 w/o
2	ThO_2	ThO_2	ThO_2
3	2 w/o	2 w/o	ThO_2

EACH SECTION IS APPROXIMATELY 14 INCHES LONG
ALL BINARY FUEL IS $^{233}UO_2 - ThO_2$

Figure 12. BMU-2 Four-Module Core, Power Flattened Loading

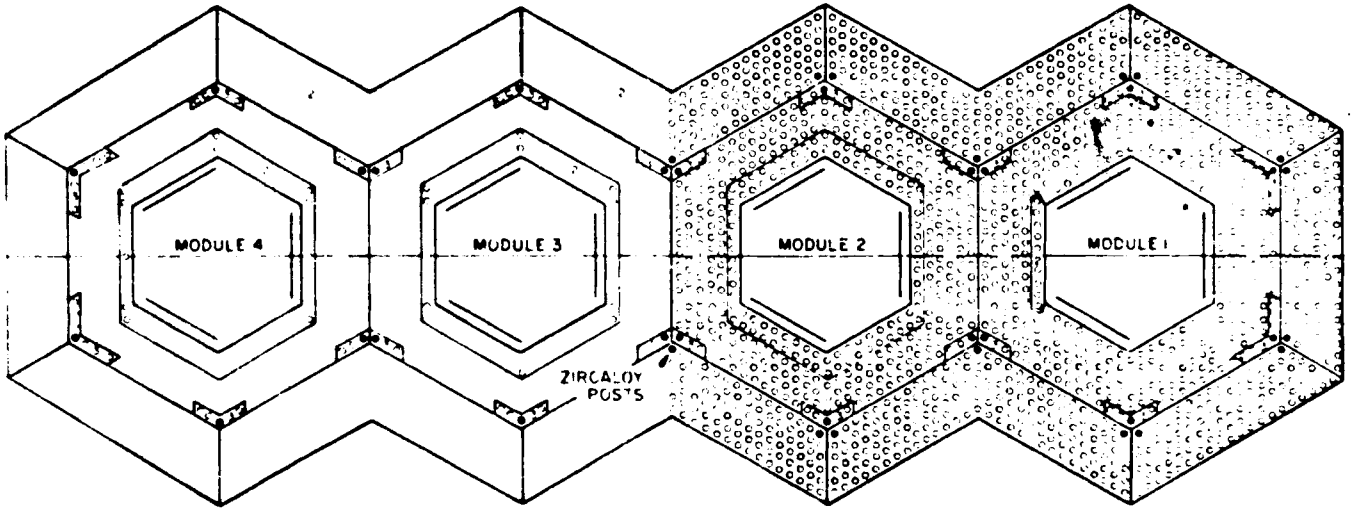

FLUX TILTED LOADING

ZONE	TOP SECTION	CENTER SECTION	BOTTOM SECTION
1	2 w/o	2 w/o	2 w/o
2	ThO_2	ThO_2	ThO_2
3	2 w/o	2 w/o	ThO_2

EACH SECTION IS APPROXIMATELY 14 INCHES LONG
ALL BINARY FUEL IS $^{233}UO_2 - ThO_2$

Figure 13. BMU-2 Four-Module Core, Flux Tilted Loading

APPENDIX A

BMU FUEL AND ROD DIMENSIONS

Fuel	Pellet Stack Length, Inches	Rod Length, Inches	Rod Ends, Inches	Void Length, Inches	Measured Rod OD, Inches	Rod ID, Inches	Measured Pellet Diameter, Inches
12 w/o Seed	27 80 ± 0 07	28 16	0 17	0 04	0 2506	0 2130	0 2064
(5/9) w/o Seed	---	28 16	0 17	0 04	0 2502	0 2126	
5 w/o	13 89 ± 0 01						0 2068
9 w/o	13 90 ± 0 07						0 2069
(2/5) w/o Seed	---	28 16	0 17	0 04	0 2492	0 2126	
2 w/o	13 900 ± 0 001						0 2067
5 w/o	13 900 ± 0 001						0 2068
ThO_2 Small Diameter Seed	13 72*	14 08	0 17	0 02	0 2506	0 2130	0 2062
ThO_2 Short Blanket	13 23*	13 92	0 38 (Top) 0 25 (Bottom)	0 06	0 6257	0 5527	0 5432*
2 w/o Blanket	42 013 ± 0 0007	42 46	0 20	0 06	0 6240	0 5510	0 5432
(2/0) w/o Blanket	---	42 46	0 20	0 06	0 6240	0 5510	
2 w/o	14 008 ± 0 001						0 5432
0 w/o	28 00*						0 5432*
(2/0) w/o Blanket	---	42 46	0 20	0 06	0 6240	0 5510	
2 w/o	28 004 ± 0 001						0 5432
0 w/o	14 00*						0 5432*
ThO_2 Full Length Blanket	42 0*	42 46	0 20	0 06	0 6261	0 5531	0 5470

*Value not measured
†Rod ID calculated from measured OD and nominal wall thickness

APPENDIX B

COMPOSITION OF BMU FUEL

Fuel	Fuel Density, g/cm³	Measured w/o^{T} U**	Measured w/o^{T} UO_2**
12 w/o Seed	8.387	10.37	11.79
9 w/o Seed	8.453	7.825	8.900
5 w/o Seed	8.478	4.351	4.948
2 w/o Seed	8.494	1.719	1.955
2 w/o Blanket	9.493	1.724	1.961
ThO_2 Full Length Blanket	9.376	--	--
ThO_2 Small Diameter Seed	9.376	--	--
ThO_2 Short Blanket	9.532	--	--
ThO_2 Zoned Blanket	9.532	--	--

ISOTOPIC COMPOSITION OF BMU FUEL

Fuel	^{233}U	^{234}U	^{235}U	^{238}U
12 w/o Seed				
w/o Uranium	98.094	0.863	0.027	1.015
Atom Percent*	98.1198	0.8595	0.0268	0.9939
9 w/o Seed				
w/o Uranium	98.16	0.914	0.017	0.934
Atom Percent*	98.1589	0.910044	0.0168562	0.915404
5 w/o Seed				
w/o Uranium	97.909	0.877	0.024	1.190
Atom Percent*	97.9482	0.87363	0.0238051	1.16554
2 w/o Seed				
w/o Uranium	98.082	0.867	0.026	1.025
Atom Percent*	98.107	0.8634	0.0259	1.0037
2 w/o Blanket				
w/o Uranium	97.966	0.859	0.026	1.159
Atom Percent*	97.9953	0.850583	0.0208275	1.13007

$$*\text{Atom Percent} = \frac{\dfrac{\text{w/o Uranium}_i}{\text{Atomic Weight}_i}}{\sum_i \dfrac{\text{w/o Uranium}_i}{\text{Atomic Weight}_i}}$$

**T = Total

APPENDIX E

COMPOSITIONS OF TEST MATERIALS

PERCENT COMPOSITION

Element	Zircaloy-4	AM-350	A-286	304 SS	Hastelloy-N	Iron	Nickel	Cr-Ni
Fe	0 18-0 24	72 0	55 00	71 00	5 0	100	100	
Cr	0 07-0 13	16 50	14 75	18 0-20 0	6 0-8 0			20 0
Ni	0 007 Max	4 25	25 20	8 0-12 0	70 00			80 0
C		0 1	0 05	0 08 Max	0 04-0 08			
Si		0 30	0 6	1 00 Max	1 0 Max			
Co					0 20 Max			
Mn		0 75	1 45	2 00 Max	1 00 Max			
W					0 50 Max			
V			0 28		0 50 Max			
Mo		2 75	1 30		15 0 8 0			
Al			0 22					
Sn	1 2-1 7							
Cu					[illegible] x			
B			0 004		[illegible] Max			
Ti			2 15					
N		0 09						
P					0 015 Max			
Zr	97 7							

^{233}U Oxide-Thorium Oxide Detailed Cell Criticals (Reference 20)

As has been noted, the cores of this series of experiments were quite complex. Consequently, for the sake of accuracy and completeness, the descriptions given in the source document are simply reproduced here.

I. INTRODUCTION

As part of the Light Water Breeder Reactor (LWBR) Development Program, a detailed cell critical assembly (Figure 1) was constructed to provide basic experimental data and confirmation of the nuclear analysis methods. The detailed cell program is the most recent of a series of critical experiments (Reference 1) which have contributed much to the knowledge of ^{233}U fission operations.

The major effort in the detailed cell critical experiments was devoted to three-dimensional power distribution measurements in the seed and blanket regions of the core. Configurations which represented different movable seed positions were studied. Experiments were also performed at 476.7°F to test the analytical model under hot conditions. Surrounding the detailed cell is a driver blanket zone (Figures 2 and 3) which contains either thorium oxide rods or ^{233}U bearing rods and thorium oxide rods. This driver is necessary to attain criticality with some seed positions or temperatures which are not critical with a single module configuration. Some reactivity coefficient experiments and lattice spectrum parameter measurements were performed. Uranium fission and thorium capture gradients across fuel pellets were also measured.

In general, experimental results confirm nuclear analysis model calculations.

II. DESCRIPTION OF DETAILED CELL

A. Mechanical and Structural Layout

The detailed cell is a single seed and blanket core, approximately 105 inches high, with a movable central seed region. Side and top views of the core are shown in Figures 2 and 3. The central seed region forms a symmetric hexagon containing 15 rows of 0.303-inch diameter fuel rods on a 0.368-inch triangular pitch. A unique feature of this mock-up is the capability to move the entire seed assembly remotely. As shown in Figure 4, the seed assembly can be fastened to a stainless steel roller chain which is driven remotely by an electric motor through a gear reduction train. This drive train produces a variable seed drive speed of up to 2.8 inches per minute, which is slow enough to keep resulting reactivity insertion rates within allowable limits.

An inner blanket region surrounds the seed and is separated from it by a double-walled hexagonal Zircaloy can. The inner blanket forms a nonsymmetric hexagon with six rows of ordinary blanket fuel on four sides and 10 rows of power flattening blanket fuel on the other two sides. The ordinary blanket fuel region is composed of 0.572-inch diameter rods on a 0.631-inch triangular pitch. The power flattening fuel region is composed of 0.528-inch diameter rods on a 0.631-inch triangular pitch. An outer blanket region surrounds the nonsymmetric hexagon and has provisions for driver and reflector regions of fuel rods 0.626 inch in diameter spaced on a 0.718- or 0.728-inch triangular pitch.

The seed rods are supported at the bottom by a base plate of 3/4-inch stainless steel, drilled with 0.281-inch diameter holes on a 0.368-inch triangular pitch. These holes are smaller than the seed rods and spaced on the same pitch; however, the hole pattern is displaced so that each fuel rod is designed to land in the middle of a triangular cuspid ligament for uniform support and circulation of coolant.

The detailed cell blanket rods rest directly on the top of a 4-foot high stainless steel table. This table top is 3/4-inch stainless steel drilled with 3/4-inch holes on a 2-inch triangular pitch. A perforated stainless steel sheet covers this table top except where a hexagonal hole allows the seed assembly to move through the table top. This perforated sheet is 0.038 inch thick with 0.487 square inch of metal per square inch of sheet.

To align the bottom of the fuel bearing region in the driver blanket with the bottom of the ^{233}U bearing fuel in the detailed cell blanket, the driver blanket rods rest on a 10.00-inch high stainless steel pedestal. This pedestal is mounted on top of the 4-foot table.

The entire assembly of core and support table is contained within a framework of stainless steel angle bars bolted to the support table, which rests on the bottom of a 17-foot diameter tank.

B. Fuel Rods

A schematic drawing of a detailed cell fuel rod is shown in Figure 5. The fuel rods are seamless Zircaloy tubes with welded end caps, top and bottom, and contain pellets of both thoria and binary fuel. The binary fuel is a mixture of UO_2-ThO_2 with various fuel densities arranged in axial zones varying from 42 to 84 inches long. The top and bottom zones have a minimum of 9 inches of thoria, giving a total pellet length of 102 inches in all detailed cell fuel rods. In the seed there are four different fuel rod types containing four different lengths of binary fuel and two different fuel loadings. The ordinary blanket and power flattening blanket each have five different fuel rod types containing four different binary fuel lengths and three different fuel loadings. Since all rods of a given diameter look the same externally, identification rings were machined at the top of the seed and ordinary blanket rods and letters were stamped at the top of the power flattening blanket rods. The in-core arrangement of these various fuel rods, with their axial zoning and fuel loadings, is shown in Figure 6. In this configuration the seed and blanket regions are in the aligned position, and the seed assembly is defined to be at the zero position.

The fuel rods used in the driver blanket are 42.46 inches long and have an active fuel rod height of 42.00 inches of 2 w/o $^{233}UO_2$-ThO_2. Reflector blanket rods have the same dimensions but contain natural thoria. These rods are stacked two high and arranged so that they are aligned axially with the 84-inch binary region of the detailed cell blanket.

C. Fuel Rod Grids

The seed rods are held laterally by six stainless steel grids which are spaced over the height of the seed and held in place by six support bars, each of which displaces two fuel rods in the last seed rod row. Each grid is 1.2 inches high and the distances from the top of the seed support plate to the bottom of each grid are 1.828, 21.338, 41.336, 59.338, 76.838, and 93.838 inches, respectively. Each grid is a welded assembly of spool-shaped elements made of 347-stainless steel and having an outer diameter equal to the seed fuel rod pitch as shown in Figure 7.

The ordinary and power flattening blanket rods are held laterally by six stainless steel grids spaced over the height of the fuel rods. The grids are held in place by 10 Zircaloy posts. Each grid, which contains locations for both ordinary and power flattening blanket rods, is 1.5 inches high. Distances from the top of the blanket base plate to the bottom of each grid are 1.15, 22.0, 43.0, 63.0, 79.60, and 96.20 inches, respectively. As with the seed grid, each blanket grid assembly is made up of spool-shaped elements with an outer diameter equal to the blanket fuel rod pitch. Figure 8 shows a sketch of a single blanket grid.

The driver and reflector blanket rods are held laterally by four 1/8-inch thick stainless steel tube sheets with holes drilled on the triangular pitch for the particular region. The tube sheets are spaced over the height of the fuel rods, with the distances from the pedestal on which the fuel rods rest to the bottom of each tube sheet being 3.031, 40.031, 45.031, and 83.031 inches, respectively. The tube sheets are supported by Zircaloy posts in 12 locations adjacent to the ordinary and power flattening blanket and by the grid frame support on the periphery of the core (Figure 2). A water gap approximately 1/4 inch wide separates the inner blanket from the driver and reflector region. The gap is created by mechanically fastening the Zircaloy posts to adjacent posts in the inner blanket.

D. Seed Assembly

The seed fuel, together with six grids, six support bars, and a 3/4-inch thick perforated support plate, forms a unit assembly free to slide up and down inside a hexagonal Zircaloy can. Each support bar is 0.643 by 0.317 inch and is notched in eight places to accept the six grids and the key of the bottom support plate. With the eighth notch at the top, the seed assembly is connected to an adapter assembly for raising and lowering the seed. Each of the 619 seed rods weighs 1072 grams (2.36 pounds) for a total weight of seed fuel of 663.6 kilograms (1463 pounds).

Seed position is adjusted by a mechanism attached to the tops of the six Zircaloy support bars by an adapter assembly (see Figure 4). This is made to be readily removable and consists of a 9/16-inch thick circular stainless plate having six milled lugs at its periphery. These lugs engage in slots or keyways near the top of the support bars and are then held in place by a keeper plate which is dropped down over the support bars. The support plate is threaded and welded at its center to a 3/4-inch diameter stainless vertical shaft about 40

inches long. The retainer plate is captive and operated by a 3/4-inch pipe sleeve concentric with the vertical shaft, and is held in proper position with a Ball-lok pin. Atop the center shaft is a clevis or yoke carrying a shaft and chain sprocket which serves as the lower block of a two-part chain fall. A 3/4-inch pitch A6060 stainless steel roller chain is used and is driven remotely by a 1/10-hp gearhead motor.

E. Zircaloy Can

Surrounding the hexagonal seed assembly and separating it from the inner blanket region is a double-walled Zircaloy can 9 feet high. The wall is made double with a 1/8- by 1/2-inch Zircaloy spacer attached at the corners between the inner and outer positions, forming a 1/8-inch channel for the control rods. The inside can wall is 0.003 inch thick while the outside can wall is 0.192 inch thick, and the inside dimension across the flats is 9.403 inches.

The inside can has fourteen 1-inch diameter holes drilled through each of the six pieces. These holes are arranged in two staggered rows 2.76 inches between centers, with seven holes in each row drilled on 13.80-inch centers.

F. Control Rods

The detailed cell has provisions for six hafnium control rod blades for reactivity control during operations. To provide access for experimental measurements in the seed region, one control rod was eliminated between the seed and power flattening blanket region for all but the high temperature configuration. Each blade is 4.353 by 0.035 by 102.0 inches.

The experimental program was performed with the seed position and the driver blanket loading adjusted to produce a critical control rod height near the top of the core in a region of small worth.

A complete set of physical dimensions and fuel atom densities is given in Appendix A, Tables A-1 through A-12.

G. Configurations Used in the Experimental Program

To study a wide range of seed positions and reactivity swing, the detailed cell was operated with four configurations defined by differences in driver blanket loading or power flattening blanket configuration as shown in Figures 9 through 12.

To operate the detailed cell at an elevated temperature (477°F) additional welding of the seed and inner blanket grids was needed. After this was done, accurate measurements of the weight and fuel rod pitch of each grid were again made. The triangular seed pitch had changed from 0.368 inch to 0.3662 inch. The triangular pitch in the blankets changed from 0.631 inch to 0.6282 inch in the ordinary blanket and from 0.631 inch to 0.6264 inch in the power flattening blanket. Also, the distance from the center of the seed to the interface of the first row of inner blanket fuel rods is based on the 0.6282-inch pitch. These small changes in pitch apply to Configuration IIIb with the seed at +3.5 inches, Configuration IVb with the seed at −14.0 inches, Configuration IIb with the seed at −2.0 inches, and Configuration Ib with the seed at +17.8 inches and explain, in part, the change in the critical seed height in Configurations I and II.

Table 1 gives the seed position, control rod height, and temperature for the four critical configurations shown in Figures 9 through 12. The seed position is measured from the aligned position and the control rod height is measured from the bottom of the binary fuel in the Group 4 blanket rods (see Figure 6).

V. SUMMARY

From the calculational and experimental data given in this report, it is concluded that the construction and operation of the detailed cell critical facility successfully completed its objective. This objective as stated in the Introduction, was to provide basic experimental data and experimental confirmation of the nuclear analysis model calculations.

In the primary area of power distribution information, a new fuel rod counting system was developed. This system demonstrated its designed ability to produce such large amounts of reliable data easily and quickly that it is now possible to produce complete three-dimensional power maps of the detailed cell for a number of seed positions, at ambient as well as elevated temperatures.

A comparison of these data with the nuclear analysis model calculations shows that nearly always the calculations accurately predict the gross power sharing between the seed and blanket regions. In addition, the nuclear analysis model adequately describes the power in small regions of the core.

Three spectrum parameters were also measured and calculated. Two, δ^{23} and δ^{02}, are well predicted by calculation, but the third, ρ^{28}, shows disagreement outside of experimental uncertainty.

The gradients across fuel pellets are predicted conservatively in high power locations. The depression of ^{233}U power by the grids is predicted very well by the nuclear analysis model.

Also, two experiments were performed to obtain basic information that was judged difficult to calculate.

Appropriate adjustment factors may be included in the nuclear analysis model to compensate for the few instances where agreement between experiment and analytical results is outside of experimental error.

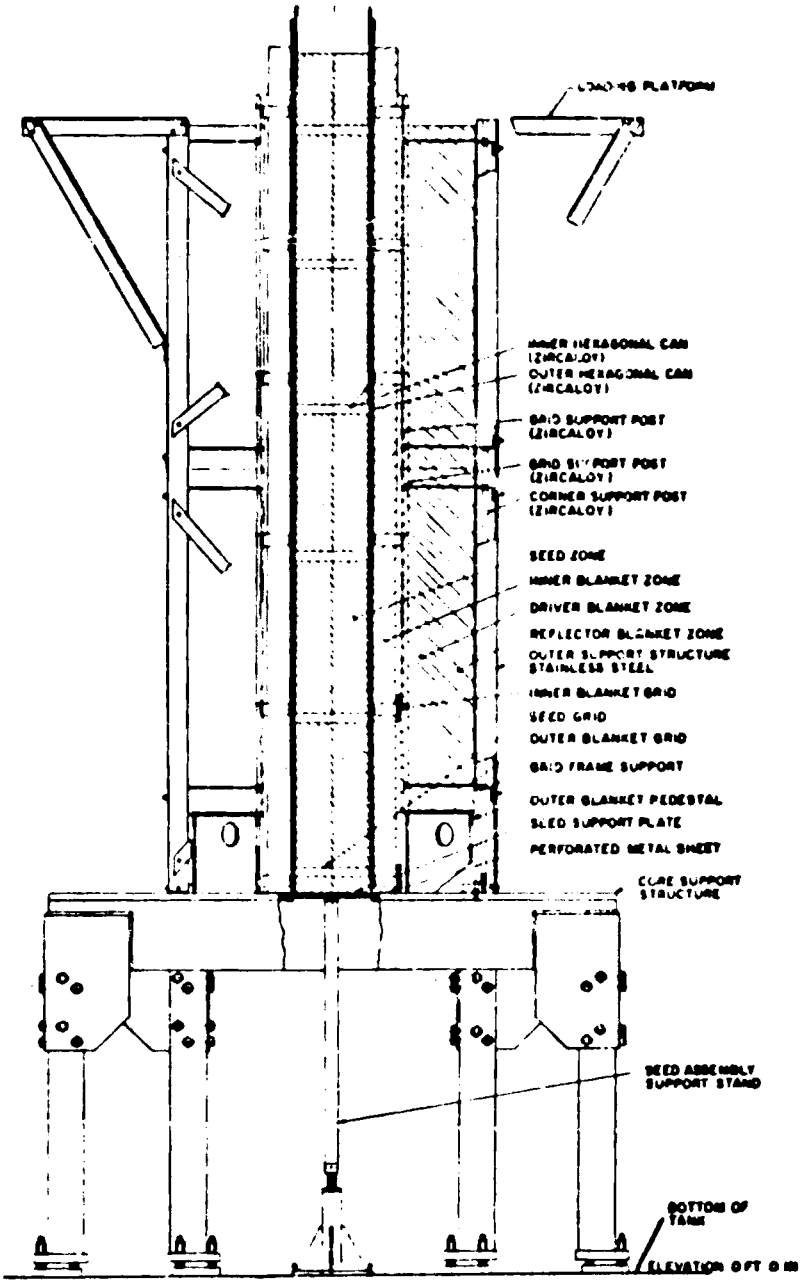

Figure 2. Detailed Coil Core—Side View

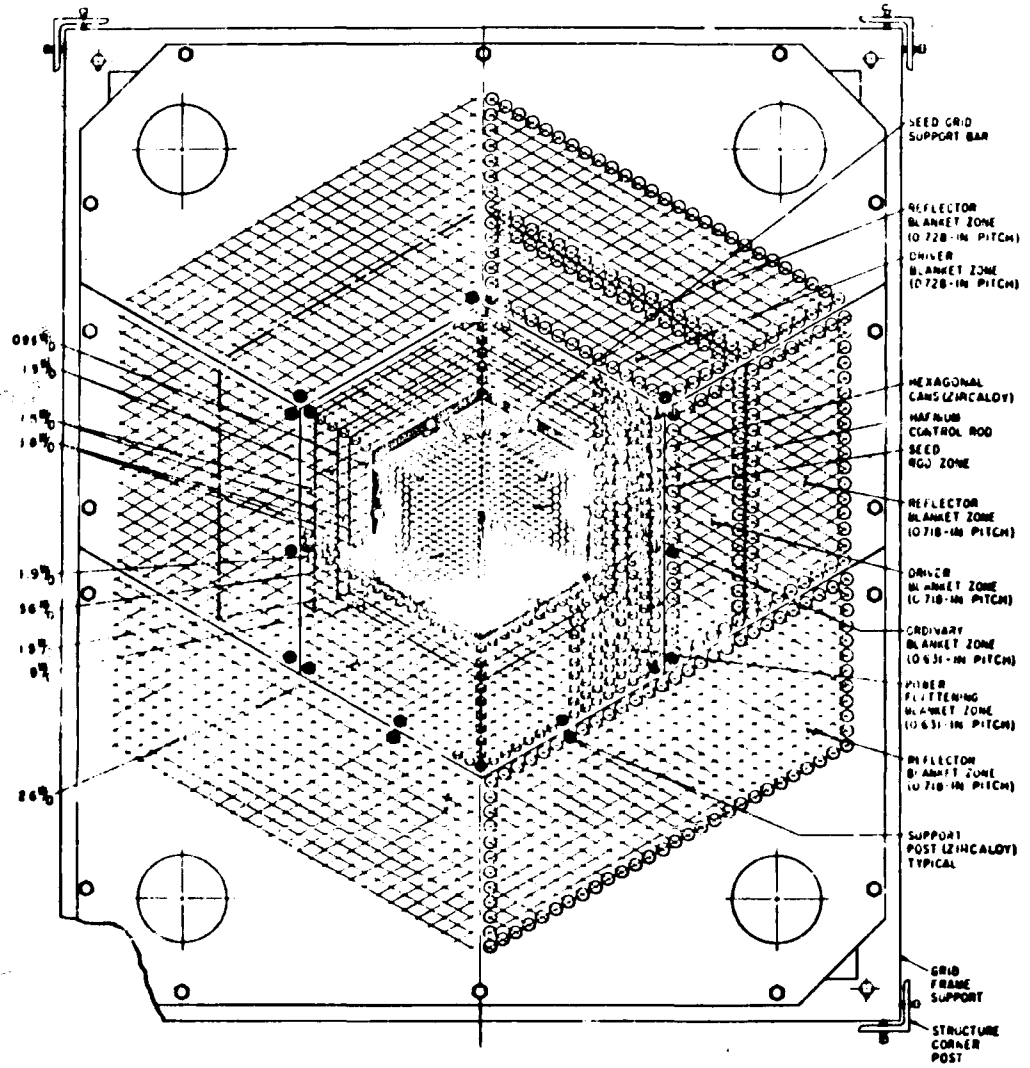

Figure 3. Detailed Cell Core—Top View

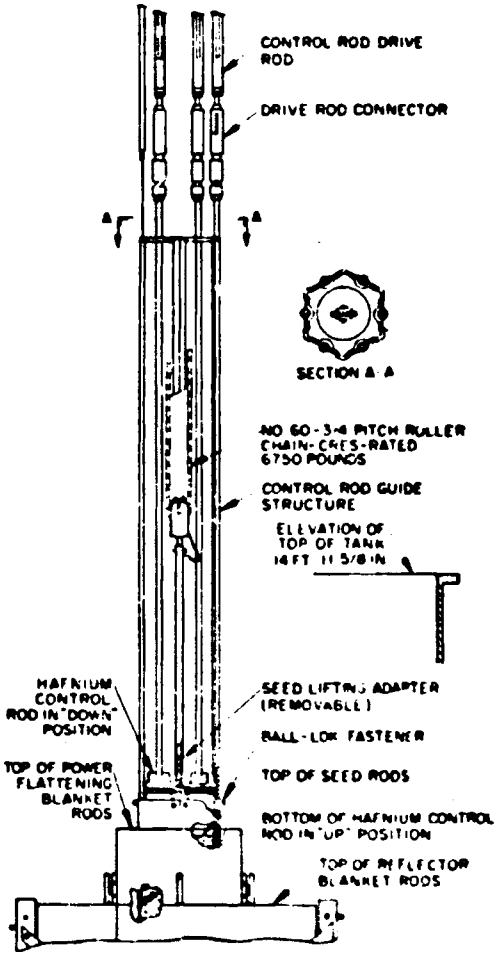

Figure 4. Elevation at Control Rod Guides

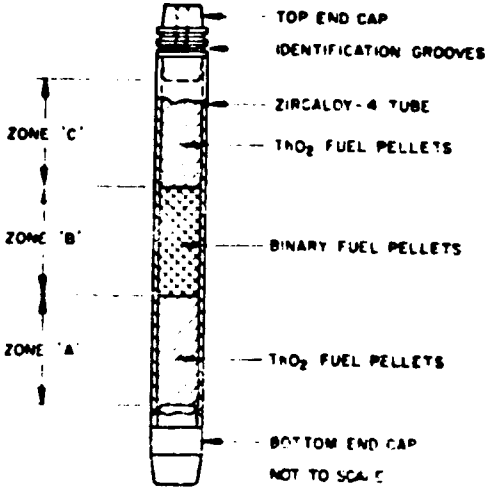

Figure 5. Detailed Cell Fuel Rod

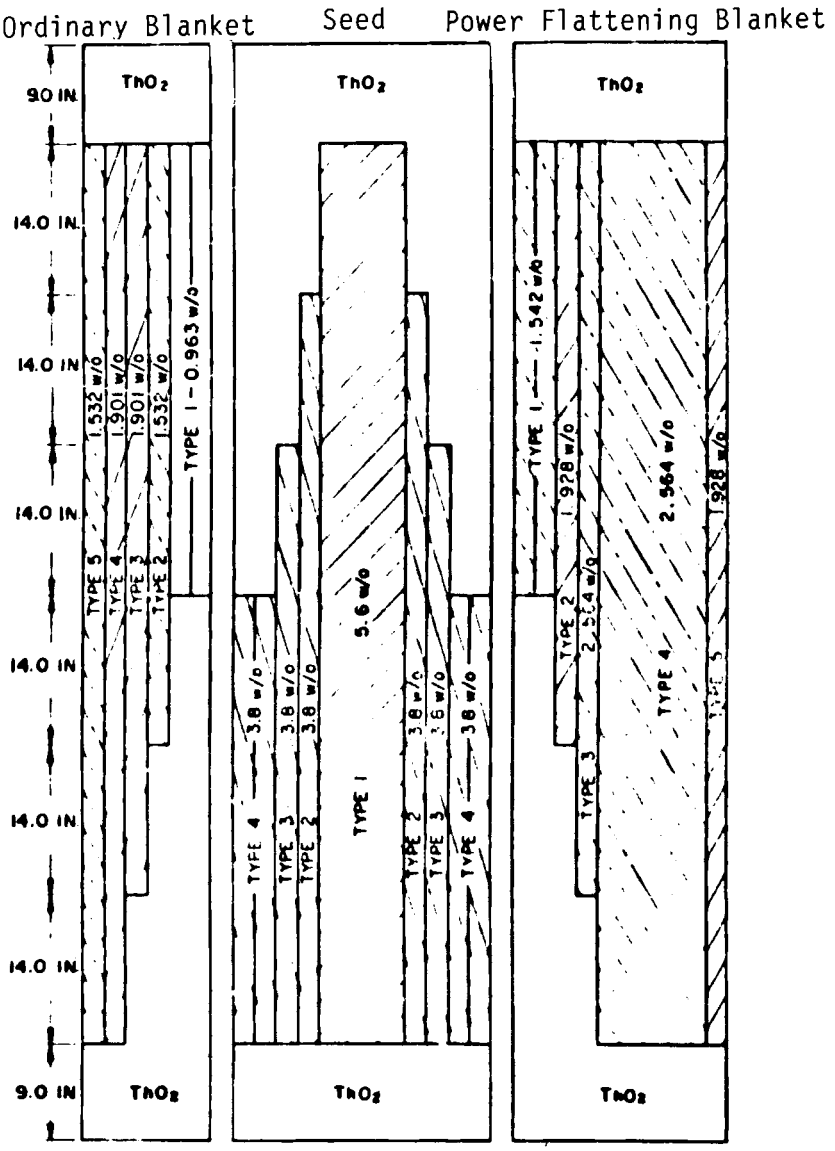

Figure 6. Detailed Cell Fuel Zoning

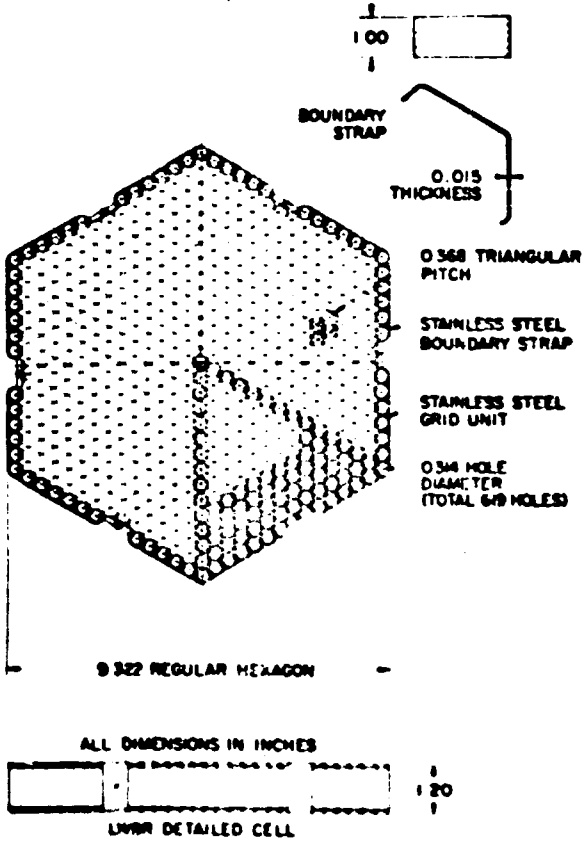

Figure 7. Seed Rod Grid

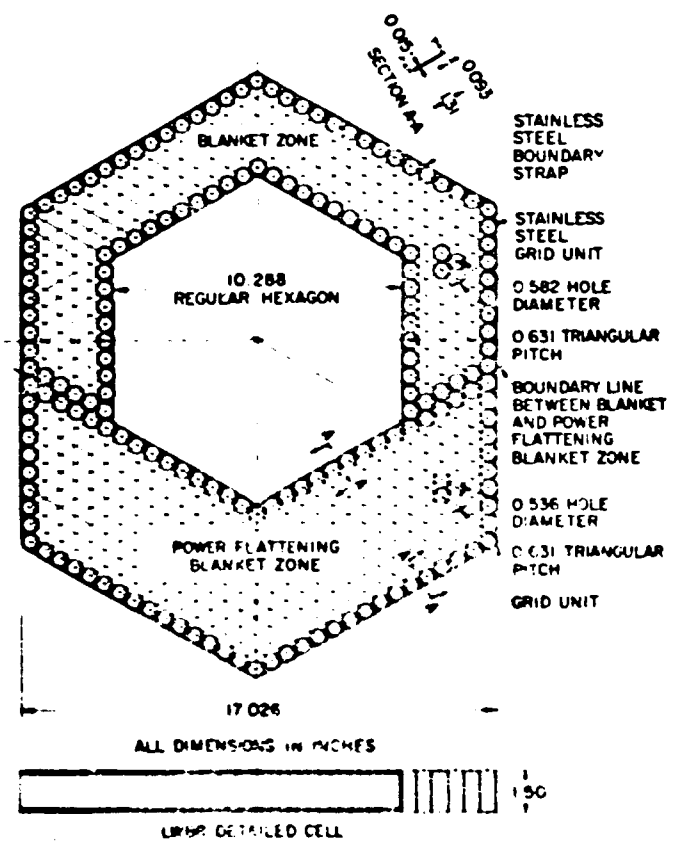

Figure 8. Inner Blanket Grid

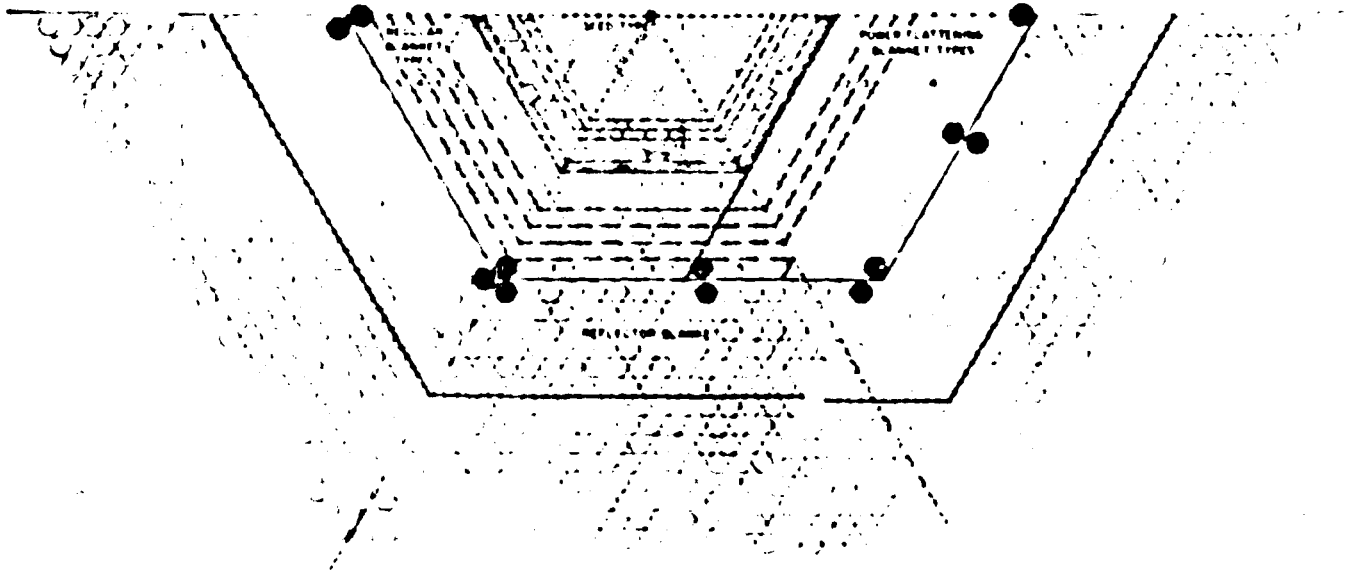

Figure 9. Detailed Cell Configuration I (+ 16 inches

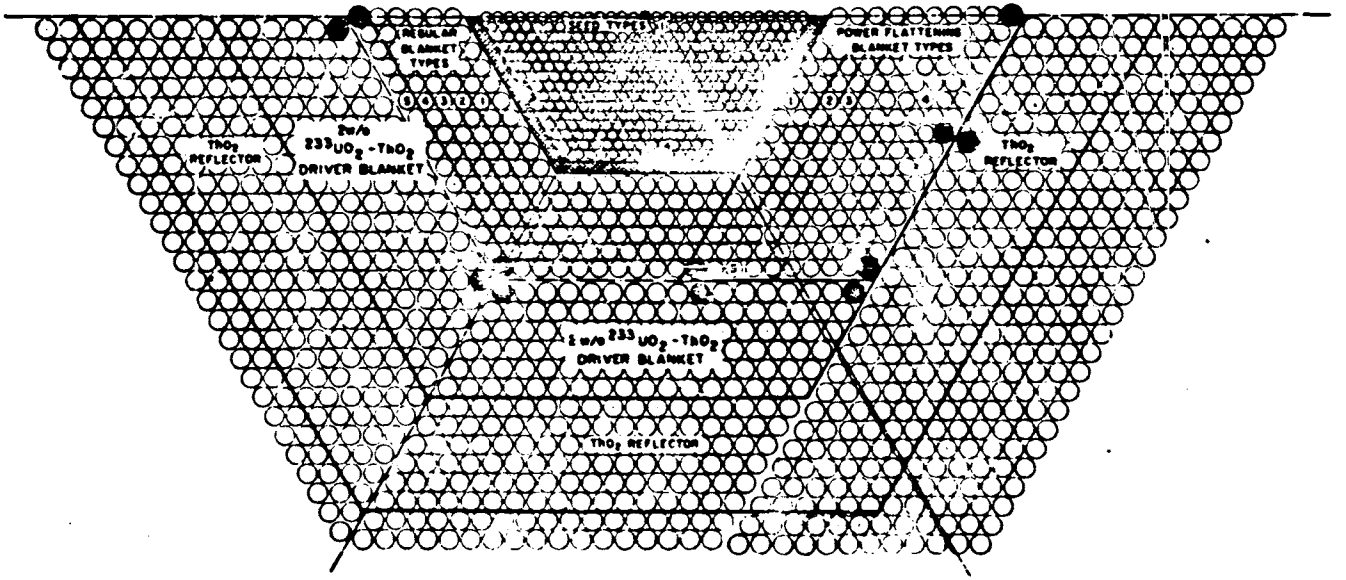

Figure 10. Detailed Cell, Configuration II (−3.5 inches)

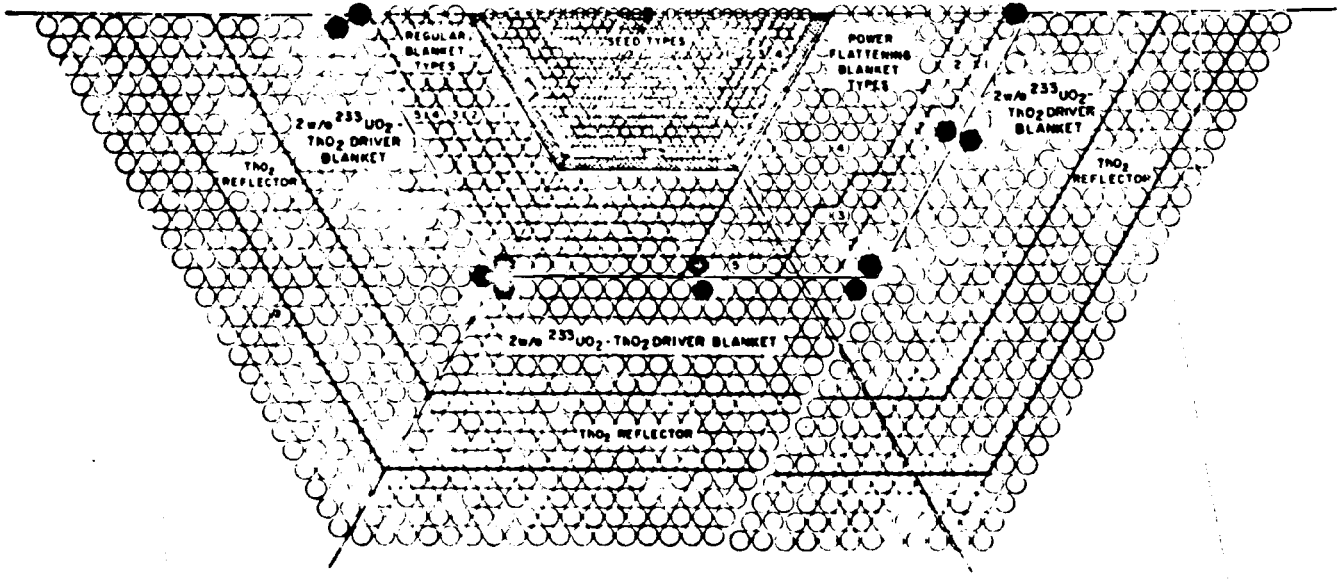

Figure 11. Detailed Cell Configuration III (+3.5 inches) Hot

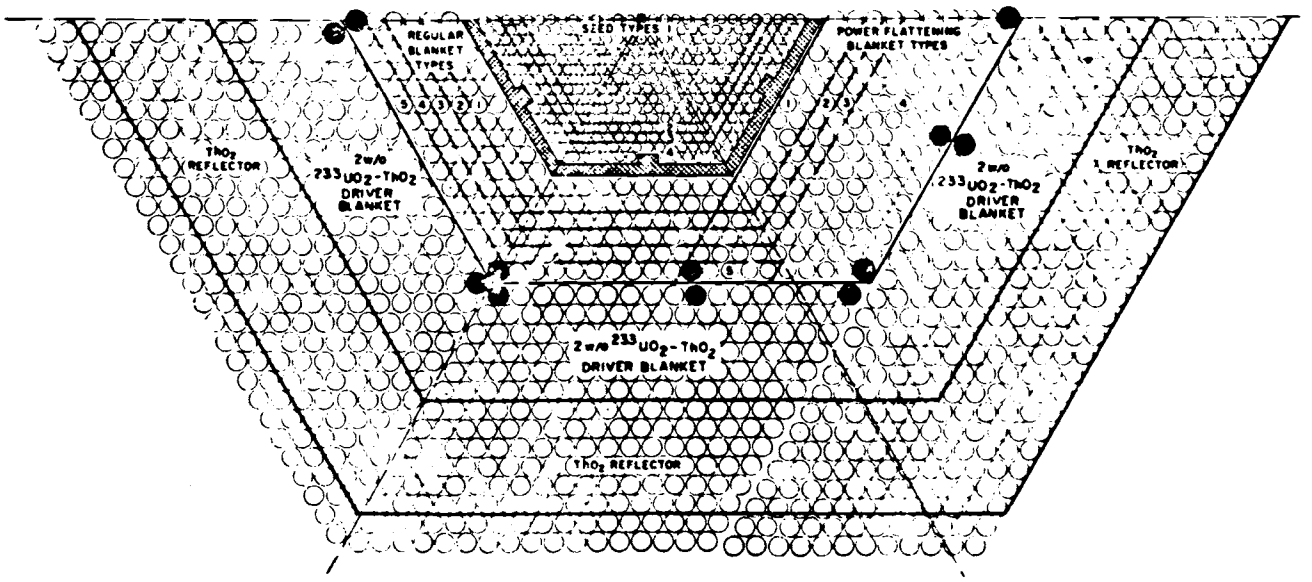

Figure 12. Detailed Cell, Configuration IV (– 14 inches)

TABLE 1. DETAILED CELL CONFIGURATIONS

Configuration	Seed Position (in.)	Control Rod Bank Height (in.)	Temperature at Critical
Ia	+14.0	72.25†	21.7°C
Ib	+17.8	70.35*	20.1°C
IIa	−3.5	65.04†	23.6°C
IIb	−2.0	66.84*	22.0°C
IIIa	−26.35	53.60††	25.6°C
IIIb	+3.5	57.60††	476.7°F
IVb	−14.0	63.50*	26.0°C

a—Configurations which contain original grids.
b—Configurations which contain reworked grids.
*One rod at 81.0 inches—4-rod bank.
†5-rod bank.
††6-rod bank.

TABLE 2. CALCULATED EIGENVALUES

Seed Position (in.)	λ PDQ	k_{eff} RECAP
+17.8	1.0024	1.003 ±0.001
+14.0	1.0046	0.998 ±0.001
+3.5	0.9947	0.995 ±0.001
−2.0	1.0014	1.000 ±0.001
−3.5	1.0032	0.996 ±0.001
−14.0	1.0020	0.996 ±0.001
−26.35	1.0024	0.997 ±0.002

APPENDIX A

PHYSICAL DIMENSIONS OF FUEL COMPOSITIONS AND FUEL ATOM DENSITIES

TABLE A-1. DETAILED CELL AT 27°C, CELL DIMENSIONS IN INCHES

5.6 w/o Seed (Type 1)	
Pellet Diameter	0.2501
Pellet Length	0.711
1/2 (Pellet OD – Pellet Dish Diameter)	0.025
End Dish Depth	0.008
Rod OD	0.3051 ±0.0007
Rod ID	0.257
Pitch	0.3685 ±0.0002
3.8 w/o Seed (Types 2 to 4)	
Pellet Diameter	0.2503
Pellet Length	0.591
1/2 (Pellet OD – Pellet Dish Diameter)	0.025
End Dish Depth	0.008
Rod OD	0.3054 ±0.0005
Rod ID	0.257
Pitch	0.3685 ±0.0002
ThO_2 Seed (Type 1)	
Pellet Diameter	0.2525
Pellet Length	0.471
1/2 (Pellet OD – Pellet Dish Diameter)	0.025
End Dish Depth	0.008
Rod OD	0.3051 ±0.0007
Rod ID	0.257
Pitch	0.3685 ±0.0002
ThO_2 Seed (Types 2 to 4)	
Pellet Diameter	0.2525
Pellet Length	0.471
1/2 (Pellet OD – Pellet Dish Diameter)	0.025
End Dish Depth	0.008
Rod OD	0.3054 ±0.0005
Rod ID	0.257
Pitch	0.3685 ±0.0002

0.963 w/o Regular Blanket (Type 1)	
Pellet Diameter	0.5056
Pellet Length	0.740
1/2 (Pellet OD – Pellet Dish Diameter)	0.050
End Dish Depth	0.015
Rod OD	0.5725 ±0.0004
Rod ID	0.511
Pitch	0.6308 ±0.0002
1.532 w/o Regular Blanket (Types 2 and 5)	
Pellet Diameter	0.5053
Pellet Length	0.860
1/2 (Pellet OD – Pellet Dish Diameter)	0.050
End Dish Depth	0.015
Rod OD	0.5723 ±0.0008
Rod ID	0.511
Pitch	0.6308 ±0.0002
1.901 w/o Regular Blanket (Types 3 and 4)	
Pellet Diameter	0.5053
Pellet Length	0.980
1/2 (Pellet OD – Pellet Dish Diameter)	0.050
End Dish Depth	0.015
Rod OD	0.5725 ±0.0005
Rod ID	0.511
Pitch	0.6308 ±0.0002
ThO_2 Regular Blanket (Types 1, 3, and 4)	
Pellet Diameter	0.5055
Pellet Length	0.590
1/2 (Pellet OD – Pellet Dish Diameter)	0.051
End Dish Depth	0.015
Rod OD	0.5725 ±0.0005
Rod ID	0.511
Pitch	0.6308 ±0.0002

Table A-1 (Cont)

ThO_2 Regular Blanket (Types 2 and 5)

Pellet Diameter	0.5055
Pellet Length	0.590
1/2 (Pellet OD – Pellet Dish Diameter)	0.051
End Dish Depth	0.015
Rod OD	0.5723 ±0.0008
Rod ID	0.511
Pitch	0.6308 ±0.0002

1.542 w/o Power Flattening Blanket (Type 1)

Pellet Diameter	0.4646
Pellet Length	0.653
1/2 (Pellet OD – Pellet Dish Diameter)	0.050
End Dish Depth	0.015
Rod OD	0.5278 ±0.0005
Rod ID	0.470
Pitch	0.6308 ±0.0002

1.928 w/o Power Flattening Blanket (Types 2 and 5)

Pellet Diameter	0.4648
Pellet Length	0.778
1/2 (Pellet OD – Pellet Dish Diameter)	0.050
End Dish Depth	0.015
Rod OD	0.5277 ±0.0005
Rod ID	0.470
Pitch	0.6308 ±0.0002

2.564 w/o Power Flattening Blanket (Types 3 and 4)

Pellet Diameter	0.4647
Pellet Length	0.898
1/2 (Pellet OD – Pellet Dish Diameter)	0.050
End Dish Depth	0.015
Rod OD	0.5280 ±0.0005
Rod ID	0.470
Pitch	0.6308 ±0.0002

ThO_2 Power Flattening Blanket (Type 1)

Pellet Diameter	0.4645
Pellet Length	0.508
1/2 (Pellet OD – Pellet Dish Diameter)	0.047
End Dish Depth	0.015
Rod OD	0.5278 ±0.0005
Rod ID	0.470
Pitch	0.6308 ±0.0002

ThO_2 Power Flattening Blanket (Types 2 and 5)

Pellet Diameter	0.4645
Pellet Length	0.508
1/2 (Pellet OD – Pellet Dish Diameter)	0.047
End Dish Depth	0.015
Rod OD	0.5277 ±0.0005
Rod ID	0.470
Pitch	0.6308 ±0.0002

ThO_2 Power Flattening Blanket (Types 3 and 4)

Pellet Diameter	0.4645
Pellet Length	0.508
1/2 (Pellet OD – Pellet Dish Diameter)	0.047
End Dish Depth	0.015
Rod OD	0.5280 ±0.0005
Rod ID	0.470
Pitch	0.6308 ±0.0002

ThO_2 Reflector Blanket

Pellet Diameter	0.5470
Rod OD	0.6261
Rod ID	0.5531
Pitch	0.728

ThO_2 Reflector Blanket

Pellet Diameter	0.5470
Rod OD	0.6261
Rod ID	0.5531
Pitch	0.718

2 w/o Driver Blanket

Pellet Diameter	0.5432
Rod OD	0.6240
Rod ID	0.5510
Pitch	0.728

2 w/o Driver Blanket

Pellet Diameter	0.5432
Rod OD	0.6240
Rod ID	0.5510
Pitch	0.718

TABLE A-2. DETAILED CELL AT 27°C, ISOTOPIC WEIGHT PERCENT MEASURED

5.6 w/o Seed (Type 1)

Isotope	w/o Uranium
^{233}U	98.112
^{234}U	1.448
^{235}U	0.1039
^{236}U	0.0067
^{238}U	0.3295

3.8 w/o Seed (Types 2 to 4)

Isotope	w/o Uranium
^{233}U	98.201
^{234}U	1.472
^{235}U	0.0745
^{236}U	0.0066
^{238}U	0.2461

0.963 w/o Regular Blanket (Type 1)

Isotope	w/o Uranium
^{233}U	96.637
^{234}U	1.058
^{235}U	0.5883
^{236}U	0.0089
^{238}U	1.7053

1.532 w/o Regular Blanket (Types 2 and 5)

Isotope	w/o Uranium
^{233}U	98.108
^{234}U	1.447
^{235}U	0.1051
^{236}U	0.0067
^{238}U	0.3331

1.901 w/o Regular Blanket (Types 3 and 4)

Isotope	w/o Uranium
^{233}U	96 994
^{234}U	1 1522
^{235}U	0.4710
^{236}U	0.0084
^{238}U	1.3721

All Power Flattening Blanket Binary Regions

Isotope	w/o Uranium
^{233}U	98.201
^{234}U	1.472
^{235}U	0.0745
^{236}U	0.0066
^{238}U	0.2461

2 w/o Driver Blanket

Isotope	w/o Uranium
^{233}U	97.966
^{234}U	0.059
^{235}U	0.026
^{238}U	1.159

TABLE A-3. DETAILED CELL AT 27°C, w/o UO_2, w/o U-TOTAL, AND PELLET FRACTION OF THEORETICAL DENSITY

Composition	w/o UO_2	Measured w/o U-Total	Pellet Fraction of Theoretical Density
5.6 w/o Seed (Type 1)	6.362	5.594	0.9547
3.8 w/o Seed (Types 2 to 4)	4.321	3.799	0.9698
ThO_2 Seed (Types 1 to 4)	0.0	0.0	0.9545
0.963 w/o Regular Blanket (Type 1)	1.096	0.9633	0.9646
1.532 w/o Regular Blanket (Types 2 and 5)	1.742	1.532	0.9608
1.901 w/o Regular Blanket (Types 3 and 4)	2.162	1.901	0.9598
ThO_2 Regular Blanket (Types 1 to 5)	0.0	0.0	0.9525
1.542 w/o Power Flattening Blanket (Type 1)	1.754	1.542	0.9711
1.928 w/o Power Flattening Blanket (Types 2 and 5)	2.192	1.928	0.9718
2.564 w/o Power Flattening Blanket (Types 3 and 4)	2.916	2.564	0.9598
ThO_2 Power Flattening Blanket (Types 1 to 5)	0.0	0.0	0.9548
2 w/o Driver Blanket	1.961	1.724	0.9469
ThO_2 Reflector Blanket	0.0	0.0	0.9377

TABLE [illegible] DETAILED CELL AT 27°C.
SOLID ATOMIC DENSITY, N_i (Atoms/Barn-Cm)

Isotope	5.6 w/o Seed (Type 1) N_i	3.8 w/o Seed (Types 2 to 4) N_i	ThO_2 Seed (Types 1 to 4) N_i	0.963 w/o Regular Blanket (Type 1) N_i
^{233}U	0.136330 – 2	0.939180 – 3	0.0 + 0	0.232338 – 3
^{234}U	0.200389 – 4	0.140178 – 4	0.0 + 0	0.253172 – 5
^{235}U	0.143090 – 5	0.706431 – 6	0.0 + 0	0.140245 – 5
^{236}U	0.923588 – 7	0.623176 – 7	0.0 + 0	0.211678 – 7
^{238}U	0.448194 – 5	0.230412 – 5	0.0 + 0	0.401361 – 5
^{232}Th	0.205272 – 1	0.212593 – 1	0.217698 – 1	0.217852 – 1
O	0.438331 – 1	0.444312 – 1	0.435395 – 1	0.440510 – 1

Isotope	1.832 w/o Regular Blanket (Types 2 and 5) N_i	1.901 w/o Regular Blanket (Types 3 and 4) N_i	ThO_2 Regular Blanket (Types 1 to 5) N_i	1.542 w/o Power Flattening Blanket (Type 1) N_i
^{233}U	0.373875 – 3	0.458454 – 3	0.0 + 0	0.380677 – 3
^{234}U	0.549178 – 1	0.542266 – 5	0.0 + 0	0.566181 – 5
^{235}U	0.397276 – 6	0.220730 – 5	0.0 + 0	0.286337 – 6
^{236}U	0.253515 – 7	0.391450 – 7	0.0 + 0	0.252591 – 7
^{238}U	0.124277 – 5	0.634887 – 5	0.0 + 0	0.933926 – 6
^{232}Th	0.215715 – 1	0.214664 – 1	0.217241 – 1	0.217991 – 1
O	0.439051 – 1	0.438777 – 1	0.434483 – 1	0.443734 – 1

Isotope	1.928 w/o Power Flattening Blanket (Types 2 and 5) N_i	2.564 w/o Power Flattening Blanket (Types 3 and 4) N_i	ThO_2 Power Flattening Blanket (Types 1 to 5) N_i	ThO_2 Reflector Blanket N_i
^{233}U	0.476471 – 3	0.626444 – 3	—	—
^{234}U	0.711158 – 5	0.935000 – 5	—	—
^{235}U	0.358391 – 6	0.471197 – 6	—	—
^{236}U	0.316154 – 7	0.415665 – 7	—	—
^{238}U	0.116894 – 5	0.153687 – 5	—	—
^{232}Th	0.217280 – 1	0.213177 – 1	0.217766 – 1	0.213868 – 1
O	0.444263 – 1	0.439111 – 1	0.435532 – 1	0.427736 – 1
Gd	—	—	—	0.803775 – 7

TABLE A-4. (Cont)

Isotope	2 w/o Driver Blanket N_i	Zircaloy-4 N_i	347 Stainless Steel N_i	304 Stainless Steel N_i
^{233}U	0.414089 – 3	—	—	—
^{234}U	0.361534 – 5	—	—	—
^{235}U	0.108961 – 6	—	—	—
^{236}U	—	—	—	—
^{238}U	0.479581 – 5	—	—	—
^{232}Th	0.212168 – 1	—	—	—
Zircaloy-4	—	0.432478 – 1	—	—
347 SS	—	—	0.89846 – 1*	—
304 SS	—	—	—	0.88518 – 1
O	0.432789 – 1	—	—	—

Isotope	H_2O N_i
O	0.333126 – 1
H	0.666252 – 1

*Modified Ni for AM-350 Deck

TABLE A-5. DETAILED CELL AT 27°C, CELL SMEARED
ATOMIC DENSITY, N_i (Atoms/Barn-Cm)

Isotope	5.6 w/o Seed (Type 1) N_i	3.8 w/o Seed (Types 2 to 4) N_i	ThO_2 Seed (Type 1) N_i	ThO_2 Seed (Types 2 to 4) N_i
^{233}U	0.565383−3	0.389409−3	0+0	0+0
^{234}U	0.831046−5	0.581214−5	0+0	0+0
^{235}U	0.593422−6	0.292905−6	0+0	0+0
^{236}U	0.383028−7	0.258385−7	0+0	0+0
^{238}U	0.185874−5	0.955349−6	0+0	0+0
^{232}Th	0.851298−2	0.881468−2	0.916812−2	0.916812−2
Zircaloy-4	0.780921−1	0.785770−2	0.780921−2	0.785770−2
347 SS	0.101129−2	0.101129−2	0.101129−2	0.101129−2
O	0.304061−1	0.306128−1	0.305640−1	0.305266−1
H	0.244555−1	0.243808−1	0.244555−1	0.243808−1

Isotope	0.963 w/o Regular Blanket (Type 1) N_i	1.832 w/o Regular Blanket (Types 2 and 5) N_i	1.901 w/o Regular Blanket (Types 3 and 4) N_i	ThO_2 Regular Blanket (Types 1, 3, and 4) N_i
^{233}U	0.133608−3	0.215149−3	0.264208−3	0+0
^{234}U	0.145589−5	0.316029−5	0.312510−5	0+0
^{235}U	0.806491−6	0.228616−6	0.127207−5	0+0
^{236}U	0.121727−7	0.145887−7	0.225594−7	0+0
^{238}U	0.230806−5	0.715164−6	0.365887−5	0+0
^{232}Th	0.125278−1	0.124135−1	0.123711−1	0.124467−1
Zircaloy-4	0.656816−2	0.653993−2	0.656816−2	0.656816−2
347 SS	0.759915−3	0.759915−3	0.759915−3	0.759915−3
O	0.334779−1	0.334335−1	0.334331−1	0.330394−1
H	0.162919−1	0.163357−1	0.162919−1	0.162919−1

TABLE A-8. (Cont)

Isotope	ThO_2 Regular Blanket (Types 2 and 8) N_i	1.542 w/o Power Flattening Blanket (Type 1) N_i	1.928 w/o Power Flattening Blanket (Types 2 and 8) N_i	2.564 w/o Power Flattening Blanket (Types 3 and 4) N_i
^{233}U	0+0	0.184645−3	0.231816−3	0.305082−3
^{234}U	0+0	0.275592−5	0.345998−5	0.455350−5
^{235}U	0+0	0.138886−6	0.174367−6	0.229476−6
^{236}U	0+0	0.122518−7	0.153818−7	0.202431−7
^{238}U	0+0	0.452994−6	0.568722−6	0.748465−6
^{232}Th	0.124467−1	0.105739−1	0.105713−1	0.103818−1
Zircaloy-4	0.653993−2	0.568479−2	0.567434−2	0.570867−2
347 SS	0.759915−3	0.759915−3	0.759915−3	0.759915−3
O	0.330611−1	0.334033−1	0.335028−1	0.332468−1
H	0.163357−1	0.237604−1	0.237764−1	0.237237−1

Isotope	ThO_2 Power Flattening Blanket (Type 1) N_i	ThO_2 Power Flattening Blanket (Types 2 and 8) N_i	ThO_2 Power Flattening Blanket (Types 3 and 4) N_i	ThO_2 Reflector Blanket Pitch = 0.728 in. N_i
^{232}Th	0.105071−1	0.105071−1	0.105071−1	0.109501−1
Gd	—	—	—	0.411896−7
Zircaloy-4	0.568475−2	0.567434−2	0.570867−2	0.637046−2
347 SS	0.759915−3	0.759915−3	0.759915−3	—
O	0.328944−1	0.329024−1	0.328760−1	0.328671−1
H	0.237604−1	0.237764−1	0.237237−1	0.219339−1

TABLE A-8 (Cont)

Isotope	ThO_2 Reflector Blanket Pitch = 0.718 in. N_i
^{232}Th	0.112572−1
Gd	0.422447−7
Zircaloy-4	0.654915−1
O	0.328546−1
H	0.206804−1

Isotope	2 w/o Driver Blanket Pitch = 0.728 in. N_i	2 w/o Driver Blanket Pitch = 0.718 in. N_i
^{233}U	0.209079−3	0.214943−3
^{234}U	0.182543−5	0.187663−5
^{235}U	0.550159−7	0.565591−7
^{236}U	0+0	0+0
^{238}U	0.242146−5	0.248938−5
^{232}Th	0.107126−1	0.110131−1
Zircaloy-4	0.634766−2	0.652571−2
O	0.329694−1	0.329597−1
H	0.222347−1	0.209893−1

TABLE A-6. BINARY PELLET STACK LENGTH

Binary Type	Measured Stack Length
5.6 w/o Seed (Type 1)	84 013
3.8 w/o Seed (Type 2)	7[illegible]2
3.8 w/o Seed (Type 3)	5[illegible]9
3.8 w/o Seed (Type 4)	4[illegible]
0.963 w/o Regular Blanket (Type 1)	41[illegible]
1.532 w/o Regular Blanket (Type 2)	55[illegible]9
1.901 w/o Regular Blanket (Type 3)	70 947
1.901 w/o Regular Blanket (Type 4)	84 167
1.532 w/o Regular Blanket (Type 5)	84 536
1.542 w/o Power Flattening Blanket (Type 1)	42 058
1.928 w/o Power Flattening Blanket (Type 2)	56 177
2.564 w/o Power Flattening Blanket (Type 3)	70 149
2.564 w/o Power Flattening Blanket (Type 4)	83 697
1.928 w/o Power Flattening Blanket (Type 5)	83 863

TABLE A-7. COLD DETAILED CELL, SEED AT -14.00 INCHES

Region	Cell Pitch (After Welding Grids) Triangular Pitch (in.)
Seed	0.3662
Regular Blanket	0.6282
Power Flattening Blanket	0.6264
Driver Blanket	0.728
Driver Blanket	0.718
Reflector Blanket	0.728
Reflector Blanket	0.718

TABLE A-8. COLD DETAILED CELL, SEED AT −14.00 INCHES, CELL SMEARED ATOMIC DENSITY, N_i (Atoms/Barn-Cm)

Isotope	5.6 w/o Seed (Type 1) N_i	3.8 w/o Seed (Types 2 to 4) N_i	ThO_2 Seed (Type 1) N_i	ThO_2 Seed (Types 2 to 4) N_i
^{233}U	0.572508−3	0.394316−3	0+0	0+0
^{234}U	0.841518−5	0.588538−5	0+0	0+0
^{235}U	0.600900−6	0.296596−6	0+0	0+0
^{236}U	0.387854−7	0.261641−7	0+0	0+0
^{238}U	0.188216−5	0.967387−6	0+0	0+0
^{232}Th	0.862025−2	0.892576−2	0.928364−2	0.928364−2
Zircaloy-4	0.790761−2	0.795671−2	0.790761−2	0.795671−2
347 SS	0.101258−2	0.101258−2	0.101258−2	0.101258−2
O	0.303737−1	0.305830−1	0.305336−1	0.304958−1
H	0.239327−1	0.238570−1	0.239327−1	0.238570−1

Isotope	0.963 w/o Regular Blanket (Type 1) N_i	1.532 w/o Regular Blanket (Types 2 and 5) N_i	1.901 w/o Regular Blanket (Types 3 and 4) N_i	ThO_2 Regular Blanket (Types 1, 3, and 4) N_i
^{233}U	0.134716−3	0.216934−3	0.266400−3	0+0
^{234}U	0.146797−5	0.318651−5	0.315102−5	0+0
^{235}U	0.813181−6	0.230512−6	0.128263−5	0+0
^{236}U	0.122737−7	0.147097−7	0.227465−7	0+0
^{238}U	0.232721−5	0.721096−6	0.368922−5	0+0
^{232}Th	0.126317−1	0.125165−1	0.124738−1	0.125500−1
Zircaloy-4	0.662264−2	0.659418−2	0.662264−2	0.662264−2
347 SS	0.736673−3	0.736673−3	0.736673−3	0.736673−3
O	0.334903−1	0.334454−1	0.334450−1	0.330481−1
H	0.159963−1	0.159405−1	0.158963−1	0.158963−1

TABLE A-8 (Cont)

Isotope	ThO_2 Regular Blanket (Type 1) N_i	1.542 w/o Power Flattening Blanket (Type 1) N_i	1.928 w/o Power Flattening Blanket (Types 2 and 5) N_i	2.564 w/o Power Flattening Blanket (Types 3 and 4) N_i
^{233}U	0+0	0.187248−3	0.235085−3	0 309383−3
^{234}U	0+0	0 279477−5	0.350876−5	0 461770−5
^{235}U	0+0	0.140844−6	0.176826−6	0 232711−6
^{236}U	0+0	0.124245−7	0.155986−7	0 205285−7
^{238}U	0+0	0.459380−6	0 576739−6	0 759017−6
^{232}Th	0.125500−1	0 107226−1	0 107203−1	0 105282−1
Zircaloy-4	0.659418−2	0.576489−2	0.575434−2	0 578915−2
347 SS	0.736673−3	0.740912−3	0 740912−3	0 740912−3
O	0.330700−1	0 334155−1	0 335165−1	0 332569−1
H	0.159405−1	0 231782−1	0.231944−1	0 231409−1

Isotope	ThO_2 Power Flattening Blanket (Type 1) N_i	ThO_2 Power Flattening Blanket (Types 2 and 5) N_i	ThO_2 Power Flattening Blanket (Types 3 and 4) N_i	2 w/o Driver Blanket Pitch = 0.728 in. N_i
^{233}U	0+0	0+0	0+0	0 209079−3
^{234}U	0+0	0+0	0+0	0 182943−5
^{235}U	0+0	0+0	0+0	0 555159−7
^{236}U	0+0	0+0	0+0	0+0
^{238}U	0+0	0+0	0+0	0 242146−5
^{232}Th	0 106552−1	0 106552−1	0 106552−1	0 107126−1
Zircaloy-4	0 576489−2	0 575434−2	0 578915−2	0 634766−2
347 SS	0 740912−3	0 740912−3	0 740912−3	0+0
O	0 328995−1	0 329077−1	0 328808−1	0 329694−1
H	0 231782−1	0 231944−1	0 231409−1	0 232347−1

TABLE A-8. (Cont)

Isotope	2 w/o Driver Blanket Pitch = 0.718 in. N_i	ThO_2 Reflector Blanket Pitch = 0.728 in. N_i	ThO_2 Reflector Blanket Pitch = 0.718 in. N_i
^{235}U	0.214943−3	0+0	0+0
^{234}U	0.167663−5	0+0	0+0
^{236}U	0.565591−7	0+0	0+0
^{238}U	0.248938−5	0+0	0+0
^{232}Th	0.110131−1	0.109501−1	0.112572−1
Zircaloy-4	0.652571−2	0.637046−2	0.654915−2
O	0.329597−1	0.328671−1	0.328546−1
H	0.209895−1	0.219339−1	0.206804−1
Gd	—	0.41896−7	0.423447−7

TABLE A-9. DETAILED CELL AT 476.72°F, CELL DIMENSIONS IN INCHES

5.6 w/o Seed (Type 1)	
Pellet Diameter	0.2506
Pellet Length	0.7124
1/2 (Pellet OD – Pellet Dish Diameter)	0.02505
End Dish Depth	0.008016
Pellet-to-Clad Radial Gap Thickness	0.003337
Clad Thickness	0.02407
Rod OD	0.3054
Rod ID	0.2573
Pitch	0.3676

3.8 w/o Seed (Types 2 to 4)	
Pellet Diameter	0.2508
Pellet Length	0.5922
1/2 (Pellet OD – Pellet Dish Diameter)	0.02505
End Dish Depth	0.008016
Pellet-to-Clad Radial Gap Thickness	0.003258
Clad Thickness	0.02422
Rod OD	0.3057
Rod ID	0.2573
Pitch	0.3676

ThO_2 Seed (Type 1)	
Pellet Diameter	0.2530
Pellet Length	0.4719
1/2 (Pellet OD – Pellet Dish Diameter)	0.02505
End Dish Depth	0.008016
Pellet-to-Clad Radial Gap Thickness	0.002133
Clad Thickness	0.02407
Rod OD	0.3054
Rod ID	0.2573
Pitch	0.3676

ThO_2 Seed (Types 2 to 4)	
Pellet Diameter	0.2530
Pellet Length	0.4719
1/2 (Pellet OD – Pellet Dish Diameter)	0.02505
End Dish Depth	0.008016
Pellet-to-Clad Radial Gap Thickness	0.002133
Clad Thickness	0.02422
Rod OD	0.3057
Rod ID	0.2573
Pitch	0.3676

0.983 w/o Regular Blanket (Type 1)	
Pellet Diameter	0.5066
Pellet Length	0.7415
1/2 (Pellet OD – Pellet Dish Diameter)	0.0501
End Dish Depth	0.01503
Pellet-to-Clad Radial Gap Thickness	0.002599
Clad Thickness	0.03079
Rod OD	0.5731
Rod ID	0.5115
Pitch	0.6306

1.532 w/o Regular Blanket (Types 2 and 5)	
Pellet Diameter	0.5063
Pellet Length	0.8617
1/2 (Pellet OD – Pellet Dish Diameter)	0.0501
End Dish Depth	0.01503
Pellet-to-Clad Radial Gap Thickness	0.002599
Clad Thickness	0.03066
Rod OD	0.5729
Rod ID	0.5115
Pitch	0.6306

1.901 w/o Regular Blanket (Types 3 and 4)	
Pellet Diameter	0.5064
Pellet Length	0.9820
1/2 (Pellet OD – Pellet Dish Diameter)	0.0501
End Dish Depth	0.01503
Pellet-to-Clad Radial Gap Thickness	0.002589
Clad Thickness	0.03079
Rod OD	0.5731
Rod ID	0.5115
Pitch	0.6306

ThO_2 Regular Blanket (Types 1, 3, and 4)	
Pellet Diameter	0.5065
Pellet Length	0.5912
1/2 (Pellet OD – Pellet Dish Diameter)	0.05110
End Dish Depth	0.01503
Pellet-to-Clad Radial Gap Thickness	0.002515
Clad Thickness	0.03079
Rod OD	0.5731
Rod ID	0.5115
Pitch	0.6306

TABLE A-9. (Cont)

ThO_2 Regular Blanket (Types 2 and 5)

Pellet Diameter	0.5065
Pellet Length	0.5912
1/2 (Pellet OD – Pellet Dish Diameter)	0.05110
End Dish Depth	0.01503
Pellet-to-Clad Radial Gap Thickness	0.002515
Clad Thickness	0.03066
Rod OD	0.5729
Rod ID	0.5115
Pitch	0.6306

1.542 w/o Power Flattening Blanket (Type 1)

Pellet Diameter	0.4655
Pellet Length	0.6593
1/2 (Pellet OD – Pellet Dish Diameter)	0.0501
End Dish Depth	0.01503
Pellet-to-Clad Radial Gap Thickness	0.002486
Clad Thickness	0.02893
Rod OD	0.5284
Rod ID	0.4705
Pitch	0.6288

1.928 w/o Power Flattening Blanket (Types 2 and 5)

Pellet Diameter	0.4657
Pellet Length	0.7796
1/2 (Pellet OD – Pellet Dish Diameter)	0.0501
End Dish Depth	0.01503
Pellet-to-Clad Radial Gap Thickness	0.002386
Clad Thickness	0.02888
Rod OD	0.5283
Rod ID	0.4705
Pitch	0.6288

2.364 w/o Power Flattening Blanket (Types 3 and 4)

Pellet Diameter	0.4656
Pellet Length	0.8998
1/2 (Pellet OD – Pellet Dish Diameter)	0.0501
End Dish Depth	0.01503
Pellet-to-Clad Radial Gap Thickness	0.002458
Clad Thickness	0.02905
Rod OD	0.5286
Rod ID	0.4705
Pitch	0.6288

ThO_2 Power Flattening Blanket (Type 1)

Pellet Diameter	0.4654
Pellet Length	0.5060
1/2 (Pellet OD – Pellet Dish Diameter)	0.04709
End Dish Depth	0.01503
Pellet-to-Clad Radial Gap Thickness	0.002536
Clad Thickness	0.02893
Rod OD	0.5284
Rod ID	0.4705
Pitch	0.6288

ThO_2 Power Flattening Blanket (Types 2 and 5)

Pellet Diameter	0.4654
Pellet Length	0.5090
1/2 (Pellet OD – Pellet Dish Diameter)	0.04709
End Dish Depth	0.01503
Pellet-to-Clad Radial Gap Thickness	0.002536
Clad Thickness	0.02888
Rod OD	0.5283
Rod ID	0.4705
Pitch	0.6288

ThO_2 Power Flattening Blanket (Types 3 and 4)

Pellet Diameter	0.4654
Pellet Length	0.5090
1/2 (Pellet OD – Pellet Dish Diameter)	0.04709
End Dish Depth	0.01503
Pellet-to-Clad Radial Gap Thickness	0.002536
Clad Thickness	0.02905
Rod OD	0.5286
Rod ID	0.4705
Pitch	0.6288

2 w/o Driver Blanket

Pellet Diameter	0.5443
Pellet-to-Clad Radial Gap Thickness	0.003647
Clad Thickness	0.03654
Rod OD	0.6247
Rod ID	0.5516
Pitch	0.7308

TABLE A-9. (Cont)

2 w/o Driver Blanket	
Pellet Diameter	0.5443
Pellet-to-Clad	
Radial Gap Thickness	0.003647
Clad Thickness	0.03654
Rod OD	0.6247
Rod ID	0.5516
Pitch	0.7207

ThO_2 Reflector Blanket	
Pellet Diameter	0.5481
Pellet-to-Clad	
Radial Gap Thickness	0.002798
Clad Thickness	0.03654
Rod OD	0.6268
Rod ID	0.5537
Pitch	0.7207

ThO_2 Reflector Blanket	
Pellet Diameter	0.5481
Pellet-to-Clad	
Radial Gap Thickness	0.002798
Clad Thickness	0.03654
Rod OD	0.6268
Rod ID	0.5537
Pitch	0.7308

TABLE A-10. DETAILED CELL AT 476.72°F. PELLET FRACTION OF THEORETICAL DENSITY

Fuel Type	Pellet Fraction of Theoretical Density
3.6 w/o Seed (Type 1)	0.9509
3.8 w/o Seed (Types 2 to 4)	0.9659
ThO_2 Seed (Types 1 to 4)	0.9507
0.963 w/o Regular Blanket (Type 1)	0.9608
1.532 w/o Regular Blanket (Types 2 and 5)	0.9569
1.901 w/o Regular Blanket (Types 3 and 4)	0.9560
ThO_2 Regular Blanket (Types 1 to 5)	0.9487
1.542 w/o Power Flattening Blanket (Type 1)	0.9672
1.928 w/o Power Flattening Blanket (Types 2 and 5)	0.9679
2.564 w/o Power Flattening Blanket (Types 3 and 4)	0.9560
ThO_2 Power Flattening Blanket (Types 1 to 5)	0.9510
2 w/o Driver Blanket	0.9412
ThO_2 Reflector Blanket	0.9321

TABLE A-11. DETAILED CELL AT 478.72°F, SOLID ATOMIC DENSITY, N_i (Atoms/Barn-Cm)

Isotope	8.6 w/o Seed (Type 1) N_i	3.8 w/o Seed (Types 2 to 4) N_i	ThO_2 Seed (Types 1 to 4) N_i	0.963 w/o Regular Blanket (Type 1) N_i
^{235}U	0.135786−2	0.935438−3	0+0	0.231421−3
^{234}U	0.199590−4	0.139619−4	0+0	0.252173−5
^{233}U	0.142521−5	0.703616−6	0+0	0.139691−5
^{236}U	0.919906−7	0.620693−7	0+0	0.210842−7
^{238}U	0.446408−5	0.229494−5	0+0	0.399777−5
^{232}Th	0.204454−1	0.211746−1	0.216830−1	0.216992−1
O	0.436584−1	0.442541−1	0.433659−1	0.438772−1

Isotope	1.532 w/o Regular Blanket (Types 2 to 5) N_i	1.901 w/o Regular Blanket (Types 3 and 4) N_i	ThO_2 Regular Blanket (Types 1 to 5) N_i	1.542 w/o Power Flattening Blanket (Type 1) N_i
^{235}U	0.372349−3	0.456625−3	0+0	0.379159−3
^{234}U	0.546937−5	0.540103−5	0+0	0.565915−5
^{233}U	0.395655−6	0.219842−5	0+0	0.285196−6
^{236}U	0.252480−7	0.389889−7	0+0	0.251584−7
^{238}U	0.123770−5	0.532354−4	0+0	0.930202−6
^{232}Th	0.214835−1	0.213807−1	0.216375−1	0.217122−1
O	0.437260−1	0.437027−1	0.216375−1	0.217122−1

Isotope	1.928 w/o Power Flattening Blanket (Types 2 and 5) N_i	2.564 w/o Power Flattening Blanket (Types 3 and 4) N_i	ThO_2 Power Flattening Blanket (Types 1 to 5) N_i	2 w/o Driver Blanket N_i
^{235}U	0.474572−3	0.623936−3	0+0	0.411647−3
^{234}U	0.700323−5	0.931257−5	0+0	0.359402−5
^{233}U	0.356963−6	0.469311−6	0+0	0.108319−6
^{236}U	0.314893−7	0.414001−7	0+0	0+0
^{238}U	0.116428−5	0.153072−5	0+0	0.476752−5
^{232}Th	0.216414−1	0.212324−1	0.216898−1	0.210891−1
O	0.442492−1	0.437353−1	0.433797−1	0.430183−1

TABLE A-11. (Cont)

Isotope	ThO_2 Reflector Blanket N_i
^{233}U	0+0
^{234}U	0+0
^{235}U	0+0
^{236}U	0+0
^{238}U	0+0
^{232}Th	0.212591−1
O	0.425182−1
Gd	0.798977−7

Isotope	304 Stainless Steel N_i	347 Stainless Steel N_i	H_2O N_i	Zircaloy-4 N_i
347 SS	—	0.891670−1*	—	—
304 SS	0.885180−1	—	—	—
O	—	—	0.268924−1	—
H	—	—	0.537648−1	—
Zircaloy-4	—	—	—	0.430693−1

*Modified Water Mix for AM-350 Deck

TABLE A-12. DETAILED CELL AT 476.72°F. CELL SMEARED ATOMIC DENSITY, N_i (Atoms/Barn-Cm)

Isotope	5.6 w/o Seed (Type 1) N_i	3.8 w/o Seed (Types 2 to 4) N_i	ThO_2 Seed (Type 1) N_i	ThO_2 Seed (Types 2 to 4) N_i
^{233}U	0.568186-3	0.391340-3	0+0	0+0
^{234}U	0.835165-5	0.584095-5	0+0	0+0
^{235}U	0.596364-6	0.294357-6	0+0	0+0
^{236}U	0.384926-7	0.259666-7	0+0	0+0
^{238}U	0.186795-5	0.960084-6	0+0	0+0
^{232}Th	0.855518-2	0.885838-2	0.921357-2	0.921357-2
Zircaloy-4	0.782833-2	0.788168-2	0.782833-2	0.788168-2
347 SS	0.997339-3	0.997339-3	0.997339-3	0.997339-3
O	0.280219-1	0.282339-1	0.281806-1	0.281473-1
H	0.195070-1	0.194404-1	0.195070-1	0.194404-1

Isotope	0.963 w/o Regular Blanket (Type 1) N_i	1.532 w/o Regular Blanket (Types 2 and 5) N_i	1.901 w/o Regular Blanket (Types 3 and 4) N_i	ThO_2 Regular Blanket (Types 1, 3, and 4) N_i
^{233}U	0.133703-3	0.215273-3	0.264384-3	0+0
^{234}U	0.145692-5	0.316211-5	0.312718-5	0+0
^{235}U	0.807061-6	0.228747-6	0.127292-5	0+0
^{236}U	0.212813-7	0.145971-7	0.225744-7	0+0
^{238}U	0.230970-5	0.715575-6	0.366131-5	0+0
^{232}Th	0.125366-1	0.124207-1	0.123794-1	0.124550-1
Zircaloy-4	0.655982-2	0.653188-2	0.655982-2	0.655982-2
347 SS	0.725574-3	0.725574-3	0.725574-3	0.725574-3
O	0.318759-1	0.318230-1	0.318759-1	0.318460-1
H	0.130520-1	0.130871-1	0.130520-1	0.130520-1

TABLE A-12. (Cont)

Isotope	ThO_2 Regular Blanket (Types 2 and 5) N_i	1.542 w/o Power Flattening Blanket (Type 1) N_i	1.928 w/o Power Flattening Blanket (Types 2 and 5) N_i	2.564 w/o Power Flattening Blanket (Types 3 and 4) N_i
^{233}U	0+0	0.185833-3	0.233308-3	0.307040-3
^{234}U	0+0	0.277366-5	0.348224-5	0.458273-5
^{235}U	0+0	0.139780-6	0.175489-6	0.230949-6
^{236}U	0+0	0.123306-7	0.154807-7	0.203731-7
^{238}U	0+0	0.455909-6	0.572381-6	0.753270-6
^{232}Th	0.124550-1	0.106415-1	0.106393-1	0.104485-1
Zircaloy-4	0.653188-2	0.571011-2	0.569967-2	0.573422-2
347 SS	0.729574-3	0.729757-3	0.729757-3	0.729757-3
O	0.314534-1	0.311093-1	0.312080-1	0.309550-1
H	0.130871-1	0.188956-1	0.189086-1	0.188656-1

Isotope	ThO_2 Power Flattening Blanket (Type 1) N_i	ThO_2 Power Flattening Blanket (Types 2 and 5) N_i	ThO_2 Power Flattening Blanket (Types 3 and 4) N_i	2 w/o Driver Blanket Pitch = 0.73077 in. N_i
^{233}U	0+0	0+0	0+0	0.207096-3
^{234}U	0+0	0+0	0+0	0.180814-5
^{235}U	0+0	0+0	0+0	0.544948-7
^{236}U	0+0	0+0	0+0	0+0
^{238}U	0+0	0+0	0+0	0.229853-5
^{232}Th	0.105747-1	0.105747-1	0.105747-1	0.107999-1
Zircaloy-4	0.571011-2	0.569967-2	0.573422-2	0.628705-2
347 SS	0.729757-3	0.729757-3	0.729757-3	0.365509-3
O	0.309972-1	0.306038-1	0.305822-1	0.306607-1
H	0.188956-1	0.189086-1	0.188656-1	0.189765-1

TABLE A-12. (Cont)

Isotope	2 w/o Driver Blanket Pitch = 0.72073 in. N_i	ThO_2 Reflector Blanket Pitch = 0.73077 in. N_i	ThO_2 Reflector Blanket Pitch = 0.72073 in. N_i
^{233}U	0.212908−3	0+0	0+0
^{234}U	0.185887−5	0+0	0+0
^{235}U	0.650237−7	0+0	0+0
^{236}U	0.246582−5	0+0	0+0
^{232}Th	0.109075−1	0.108456−1	0.111498−1
Zircaloy-4	0.646343−2	0.630971−2	0.648672−2
304 SS	0.170152−3	0.151245−3	0.155489−3
O	0.307667−1	0.305931−1	0.306972−1
H	0.170342−1	0.178039−1	0.167950−1
Gd	—	0.407965−7	0.419407−7

BNL Exponential Experiments (Reference 21)

Uniform subcritical lattices were constructed of 3% $^{233}UO_2$ - 97% ThO_2 fuel in light water moderator, and flux measurements were used to infer the material buckling Bm^2 of the lattices. Measurements were made for hexagonal lattices using a single rod type, at eight different lattice pitches. Additional measurements were made for these lattices poisoned with H_3BO_3, yielding a total of 21 values of Bm^2. Fuel rod sizes and compositions are given in "Table I." Buckling and reflector savings values are listed with lattice parameters and H_3BO_3 concentrations in "Table II."

TABLE I (Ref. 21)

$^{233}UO_2$-ThO_2 Fuel Pin Composition

Average Density = 8.9618 g/cm^3 [a];
diameter = 0.430 in. = 1.09220 cm
Active length = 42.5 in. = 107.98 cm
($^{233}U/^{233}U$ + Th) weight ratio = 0.03000

Isotope	Weight Fraction	Atoms/cm^3
^{16}O	0.121197	0.408832×10^{23}
^{232}Th	0.851764	0.198115
^{233}U	0.026343	0.0061021
^{234}U	0.000394	0.0000909
^{235}U	0.000012	0.0000027
^{238}U	0.000289	0.0000655
B	0.0000044	0.0000220
Clad Composition: Zircaloy-2 density = 6.8365 g/cm^3 o.d. = 1.26746 cm = 0.499 in. i.d. = 1.09220 cm = 0.430 in.		
Isotope	Weight Fraction	Atoms/cm^3
Zr	0.9827	0.44355×10^{23}
Sn	0.0145	0.005030
Cr	0.0010	0.000792
Fe	0.0013	0.000958
Ni	0.0005	0.000351
Co	5×10^{-6}	0.0000035
B	1.4×10^{-6}	0.0000053
Cd	0.5×10^{-6}	0.0000002
Hf	3×10^{-6}	0.0000007

[a]The fuel was prepared by the sol gel process and consists of compacted particles of a solid solution of UO_2 in ThO_2. The compacted particles are of three size grades, 60 wt% 6/16 mesh, 15 wt% 50/140 mesh, and 25 wt% -200 mesh.[1]

TABLE II (Ref. 21)

$^{233}UO_2$-ThO_2-H_2O Lattices

Buckling and Reflector Savings

Lattice Pitch (in)	Moderator Fuel Volume Ratio	H_3BO_3[a] Conc. (mg/cm^3)	"Best" Values[b] of Measured B_m^2 (m^{-2})	"Best" Values of Measured λ (cm)
0.627	0.997	0.0	75.88 ± 2.0	7.60 ± 0.3
		13.3	42.1 ± 0.5	5.30 ± 0.10
		25.0	18.8 ± 0.5	5.10 ± 0.10
0.677	1.384	0.0	86.06 ± 1.3	7.24 ± 0.17
		7.82	50.6 ± 0.5	5.60 ± 0.10
		22.9	3.65 ± 0.5	5.10 ± 0.10
0.716	1.7134	0.0	89.34 ± 2.0	7.05 ± 0.3
		4.74	60.4 ± 0.5	5.70 ± 0.10
		18.88	-1.8 ± 0.2	5.25 ± 0.15
0.771	2.1943	0.0	90.35 ± 1.6	6.80 ± 0.2
		4.71	50.5 ± 0.2	5.75 ± 0.05
		13.3	-2.1 ± 1.0	5.50 ± 0.10
0.854	3.0043	0.0	85.54 ± 0.8	6.57 ± 0.1
		4.99	26.5 ± 0.3	5.85 ± 0.20
		7.82	1.99 ± 0.2	5.60 ± 0.15
0.971	4.2722	0.0	69.8 ± 1.0	6.44 ± 0.15
		2.68	22.6 ± 0.4	6.0 ± 0.15
		4.96	-7.67 ± 0.2	6.0 ± 0.05
1.172	6.8449	0.0	32.2 ± 0.2	6.25 ± 0.05
		1.7	-10.8 ± 1.0	6.40 ± 0.20
1.335	9.2747	0.0	-1.22 ± 0.3	6.65 ± 0.05

[a] Solutions at normal room temperatures (~20°C). (For densities see: The International Critical Tables.)

[b] As measured values are compiled by Price.[11]

CRITICAL ARRAYS, AND RASCHIG RING POISONED SOLUTIONS OF ^{233}U

The unlikely grouping of array experiments and raschig ring poisoned solution experiments in this section is due to the small amount of data available, plus the fact that one paper treats both.

Only two papers treat arrays. In both cases the arrays are composed of bottles of well moderated uranyl nitrate solution, both reflected and unreflected. The paper with the most cases (22) studied[22] includes the effects of moderation internal to the arrays in some cases. However, most of the arrays are planar, and only one case has two layers. The other paper with array data, a brief article in an annual report,[4] presents criticality data on the disparate topics of arrays, raschig ring poisoned solutions, and solutions in simple geometries. It reports a total of eight experiments using cubical arrays of ^{233}U solution containers. Number of units per array side, solution concentration, and reflection are varied.

A total of three individual experiments, all subcritical, are reported in the two papers which treat ^{233}U solutions poisoned with borosilicate raschig rings. Two of these experiments were reported in ORNL-4280, where it is noted that the solutions were subcritical, and were driven as an exponential experiment by a critical slab of unpoisoned solution above the rings. Flux traverses through the solution are mentioned, but no results are given. Additional information on these experiments, including reciprocal relaxation lengths plus data from an additional unreported experiment, is presented in the background document[23] for ANSI standard N16.4-1971, which governs the use of raschig rings in fissile solutions.

Lloyd, Clayton & Chalmers: Arrays (Reference 22)

Twenty two experiments are reported, of which twenty one are for planar arrays, and one for a two-layer array. Descriptions of the experiments, their results, and discussion of experimental errors are reproduced below.

MEASUREMENTS

The ^{233}U was in the form of uranyl nitrate hexahydrate, $UO_2(NO_3)_2 + 6H_2O$, at a concentration of ≈ 330 g ^{233}U/liter; the uranium solution, ≈ 0.53 *M* in excess nitrate acid concentration, was contained in three-liter polyethylene bottles. The isotopic content of the solution is given in Table I. The bottles were 17.75-in. high and 4.7-in. o.d., with a wall thickness of 0.100 in. The average solution height was ≈ 11.5 in., corresponding to 960 g uranium per bottle. Table II shows that the bottles varied in content and given averages of solution contents for each experiment. This variation amounted to less than ± 20 g ^{233}U/liter except for Experiment 21 where it was ± 40 g

TABLE I (Ref. 22).

Isotopic Content of the Uranium Solution

^{232}U	≈ 4 ppm
^{233}U	98.2%
^{234}U	0.8%
^{238}U	1.0%

TABLE II (Ref. 22)

Averages for Actual Bottles Used in Experiments

Experiment Number	Solution Height in.	U g	Volume liter	^{233}U Concentration g/liter	Specific Gravity
1	11.78	946	2.98	318.3	1.437
2	11.67	951	2.94	323.1	1.444
3	11.59	947	2.93	323.0	1.444
4	11.40	961	2.89	332.5	1.455
5	11.77	947	2.95	321.1	1.445
6	11.72	962	2.95	326.2	1.450
7,8,9,10,11	11.71	934	2.94	318.1	1.438
12	11.64	947	2.93	323.2	1.444
13A	11.67	951	2.94	323.1	1.444
13B,14,15,16,17	11.59	947	2.94	323.0	1.444
18,19,20	11.40	961	2.89	332.5	1.455
21	11.25	895	2.87	312.6	1.429

U/liter. Use of the average concentration should introduce minimum error since criticality is quite insensitive to concentration over this range.

The bottles were placed in subcritical arrays on a remotely operated split-table device. Because the reactivity of an array can change rapidly with spacing, separate neutron multiplication measurements were made to determine that the number of bottles for each spacing could be safely loaded. The neutron multiplication for the fixed number of bottles at each spacing was then, in turn, used to predict the critical spacing for the array. Thus, the experiments required a series of multiplication measurements—one for each spacing.

The remote split-table machine (RSTM), used in these experiments, has a table top of 0.03-in.-thick steel plate supported by an aluminum honeycomb material that provides good support strength but low neutron reflection. A low-density aluminum honeycomb material was also used to provide accurate spacing between bottles and to ensure that the bottles remained upright.

Criticality of the bottles of solution was determined for both bare and Lucite-reflected systems. In the unreflected assemblies, stability of the outer bottles was maintained by aluminum frames attached to small magnets fixed to the thin-steel base plate. Unreflected assemblies of 9 and 16 bottles and a double-tier array of 18 bottles were measured.

In the reflected arrays, the Lucite was placed touching the outside surface of the bottles, i.e., boxing in the array. The thickness of the top and bottom Lucite reflector was 4.5 in. and the side reflectors were 6 in. Experiments were performed with Lucite moderator positioned between the bottles of an array in both unreflected and reflected assemblies. Figure 1 shows a 16-bottle unreflected assembly, with this internal moderator at the same height as the solution.

RESULTS

Results obtained from plotting the reciprocal count rate (inverse neutron multiplication curves) as the arrays were built up, and extrapolating these curves to predict criticality, are presented in Table III. During the experiments it was noted that an improvement in linearity of the neutron multiplication curves could be obtained by plotting

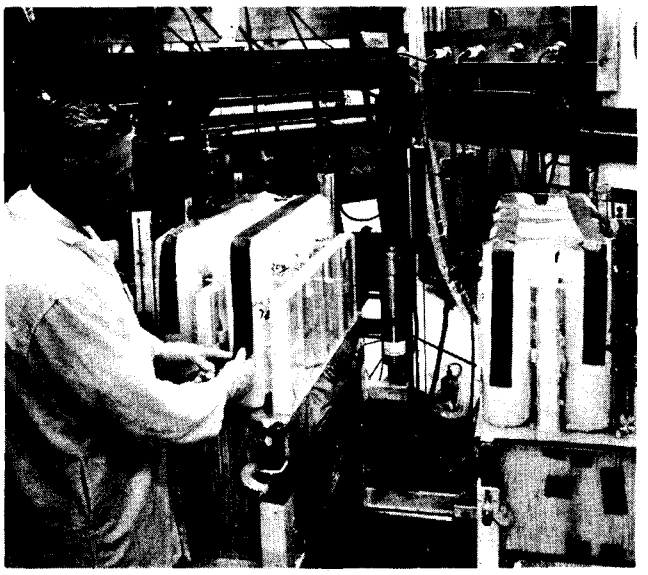

Fig. 1. 16-Bottle moderated unreflected array of ^{233}U solution. (Ref. 22)

the spacing count-rate ratio vs spacing, rather than reciprocal count rate vs spacing. This permitted an earlier, better estimate of criticality; however, either method of plotting the data provides the same estimate in the limit as criticality is approached. The usefulness of the first type plot is that a better estimate of criticality is obtained during the initial portion of the experiment, although we have not found a theoretical explanation for this empirical observation. A single row of nine bottles unreflected was observed to be subcritical, and extrapolation of the inverse neutron multiplication curves indicated an infinitely long, single line would probably be subcritical as well. The data for the reflected row of bottles indicated that criticality would be achieved with more than two but less than three bottles. Three bottles in line with surface-to-surface (S-S) spacing[a] of 0.6 in. would be critical when reflected. S-S spacings for criticality were determined for unreflected arrays of 2×3, 3×3, and 4×4 bottles in single-tier geometry and for reflected arrays of 2×2 and 3×3 bottles.

A S-S critical spacing of 0.75 in. was also measured for a double-tier 3×3 bottle unreflected array, which compares with a 0.60-in. spacing for the 3×3 bottle single-tier array. The double-tier array had a spacing of 7.0 in. between the fuel of the upper and lower tiers.

Figure 2 shows the number of bottles required for criticality plotted vs S-S separation. The critical number of bottles is much more sensitive to

[a]S-S spacing refers to the outer bottle surface-to-outer bottle surface spacing.

TABLE III (Ref. 22)

Interaction Data for Bottles of ^{233}U Solution

Experiment Number	Reflector Condition	Configuration	Number of Bottles for Criticality[a]	Estimated Critical Surface-to-Surface Spacing (in.)	Remarks
U-1	Unreflected	1×9	> 9	0	Single Row
U-2	Unreflected	2×3	6.1	0	Double Row
U-3	Unreflected	3×3	9	0.60	
U-4	Unreflected	4×4	16	1.16	
U-5	Reflected	1×2	> 2	0	$\approx$ 2.8 Bottles, Single Row
		1×3	< 3	0	Table stopped at 0.9 in.
U-6	Reflected	1×3	3	0.6	Single Row
U-7	Reflected	2×2	4	2.18	
U-8	Reflected	2×2	4	2.48	$\frac{1}{2}$-in. Lucite Moderator Between Bottles
U-9	Reflected	2×2	4	2.58	$\frac{3}{4}$-in. Lucite Moderator Between Bottles
U-10	Reflected	2×2	4	2.66	1-in. Lucite Moderator Between Bottles
U-11	Reflected	2×2	4	2.50	$1\frac{1}{2}$-in. Lucite Moderator Between Bottles
U-12	Reflected	3×3	9	3.98	
U-13A	Unreflected	2×3	6.3	1.00	1-in. Lucite Moderator Between Bottles
U-13B	Unreflected	3×3	9	1.60	1-in. Lucite Moderator Between Bottles
U-14	Unreflected	3×3	9	1.17	$\frac{1}{2}$-in. Lucite Moderators Between Bottles
U-15	Unreflected	3×3	9	1.78	$1\frac{1}{2}$-in. Lucite Moderator Between Bottles
U-16	Unreflected	3×3	9	1.87	$1\frac{3}{4}$-in. Lucite Moderator Between Bottles
U-17	Unreflected	3×3	9	1.90	2-in. Lucite Moderator Between Bottles
U-18	Unreflected	4×4	16	2.50	2-in. Lucite Moderator Between Bottles
U-19	Unreflected	4×4	16	2.47	$2\frac{1}{2}$-in. Lucite Moderator Between Bottles
U-20	Unreflected	4×4	16	2.42	$1\frac{1}{2}$-in. Lucite Moderator Between Bottles
U-21	Unreflected	$3 \times 3 \times 2$	18	0.75	Double Tier

[a]Fractional number of bottles indicates extrapolation to the critical number with the spacing fixed.

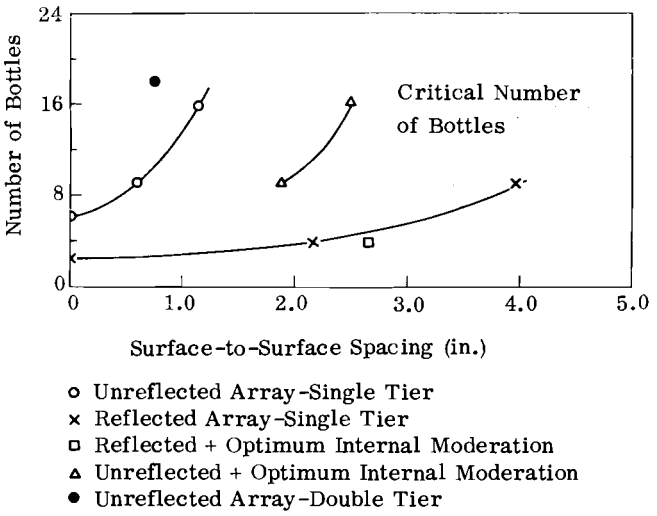

Fig. 2. Criticality of ^{233}U solution in polyethylene bottles. (Ref. 22)

spacing for the unreflected array than for the reflected array. Points of optimum internal moderation for maximum critical spacing of the array are also shown for comparison as determined from plotting spacing vs moderator thickness (Figs. 3 through 5). Figure 3 gives data on critical S-S spacing vs thickness of added Lucite moderator for a four-bottle reflected array. The most effective thickness, as here defined, is that thickness of moderator that results in the smallest critical number of bottles, or conversely, the largest critical spacing for a given number of bottles. The most effective thickness of added moderator was about 1 in. in the reflected array. Figures 4 and 5 give results of critical S-S spacing vs added Lucite moderator thickness for unreflected arrays comprising 9 and 16 bottles. These results indicate the most reactive unreflected loading to be obtained with a moderator thickness of about two inches between the bottles.

EXPERIMENTAL ERRORS

The error in critical spacing is due primarily to the uncertainty in extrapolation of the inverse neutron multiplication curves and the uncertainty in positioning the bottles within the array. Three counters were used simultaneously for the neutron multiplication measurements in which the inverse multiplication curves were plotted vs spacing. The arrays were subcritical in each case, but the uncertainty in critical spacing, as a result of extrapolation, is estimated to be about 0.03 in. This uncertainty comes from the difference in values for criticality predicted by the separate curves, while another uncertainty of about 0.02 in. can

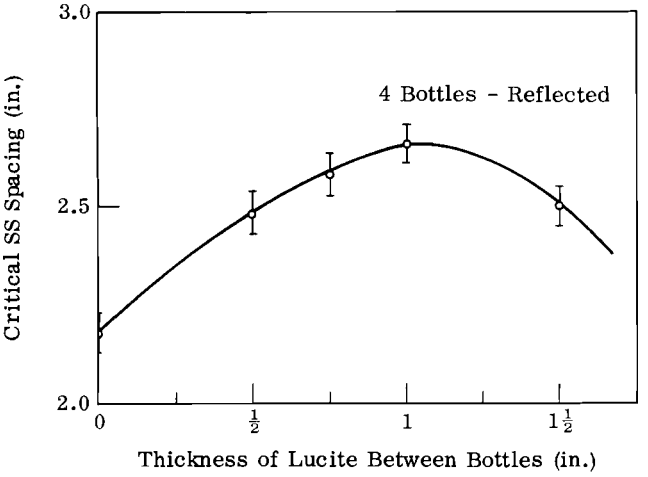

Fig. 3. Effectiveness of moderation between bottles of ^{233}U. (Ref. 22)

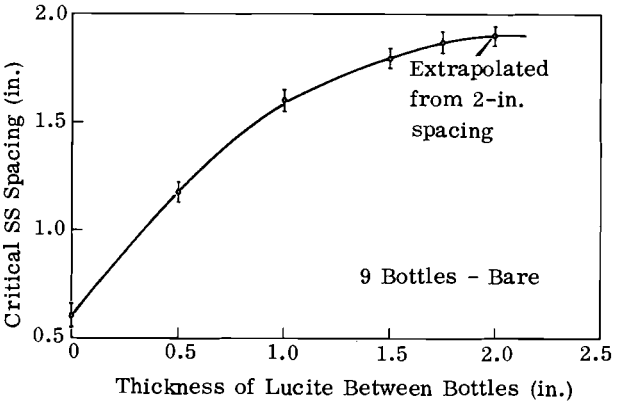

Fig. 4. Effectiveness of moderation between bottles of ^{233}U solution (9-bottle unreflected array). (Ref. 22)

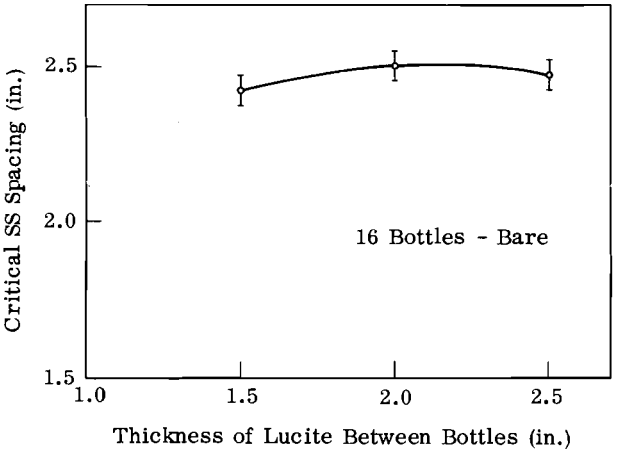

Fig. 5. Effectiveness of moderation between bottles of ^{233}U solution (16-bottle unreflected array). (Ref. 22)

result from positioning error in loading the arrays. Therefore, the uncertainty in the quoted critical spacings is ≈ 0.05 in.

This error does not apply to Experiments 1 and 5 which involved unreflected single rows of bottles. Due to the nature of the arrays and the observed neutron multiplication in these two cases, it was only possible to define upper or lower limits, i.e., critical number of bottles >9 in one case and between 2 and 3 in the other.

In the unreflected unmoderated array, an experimental uncertainty of 0.05 in. would correspond to a variation in k_{eff} of about ±0.006. This is concluded from examination of the values of k_{eff} calculated over a range of spacings from 0 to 0.6 in. (Fig. 6).

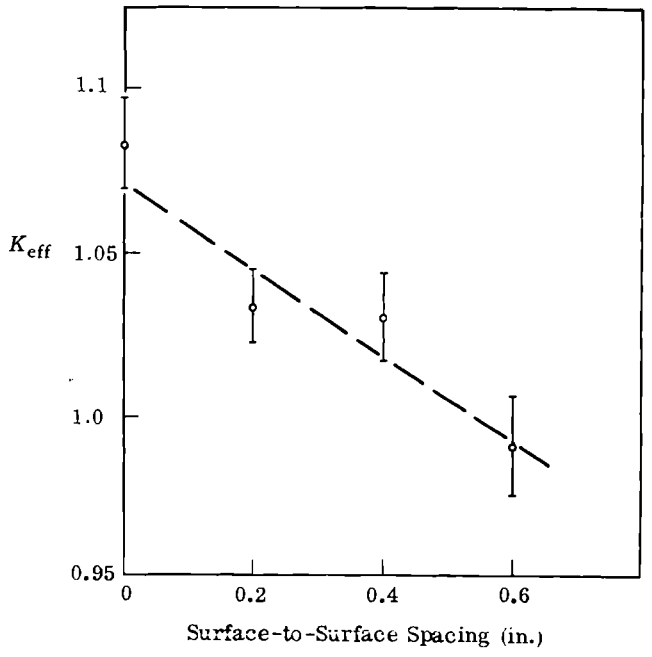

Fig. 6. Sensitivity of k_{eff} on S-S spacing. (Ref. 22)

ORNL-4280: Arrays & Raschig Rings (Reference 4)

In just two pages this paper presents data from experiments with arrays, raschig ring poisoned solutions, and solutions in simple geometries. Due to its brevity it is reproduced in full despite the fact that its solution data are also included in the section on geometrically simple systems.

The criticality of ^{233}U under conditions of interest to nuclear criticality safety as well as in basic geometries suitable for theoretical analysis has been studied in a series of experiments conducted over the past 18 months. In one series aqueous uranyl nitrate solutions of ^{233}U were examined in a large capacity vessel containing borosilicate glass in order to define systems having k_∞ of unity or less. In a second series as many as 27 nearly identical subcritical cylindrical volumes of the solution were assembled in air-spaced arrays both unreflected and reflected by polyethylene to establish parameters useful in storage and transport specifications. A final series of experiments determined the criticality of water-reflected and unreflected spherical and cylindrical volumes.

The ^{233}U isotopic content of the uranium of the uranyl nitrate solution was 97.59%. There were no impurities present in significant quantities.

Borosilicate Glass Experiments

Exponential experiments with uranyl nitrate solution having uranium concentrations of 333 and 204 g/liter were performed in an unreflected aluminum cylinder 50.8 cm in diameter and 18.3 cm high having a lateral wall thickness of 1.5 mm and a 1.27-cm-thick bottom. Flux traverses were made with a 6.4-mm-diam BF_3 counter along the axis of the cylinder through a mixture of solution and randomly oriented glass raschig rings. A neutron source was provided by adding sufficient solution above the glass rings to produce a critical slab.

A description of the raschig rings is given in Table 2.16.1. The conditions described in this table define mixtures having a negative material buckling and hence values of k_∞ less than unity. Thus, ^{233}U as an aqueous uranyl nitrate solution at a uranium concentration of 333 g/liter may be stored in any quantity, either mass or volume, provided that the borosilicate glass uniformly occupies 38% of the volume of the container.

Table 2.16.1. Conditions for Mixtures of Uranyl Nitrate Solutions of ^{233}U and Glass Raschig Rings Whereby $k_\infty < 1$ (Ref. 4)

Uranium concentration (g/liter)	333	204
Natural-boron content of glass (wt %)	3.9	3.9
Glass content of mixture (vol %)	38	33
Dimensions (cm) of borosilicate glass raschig rings		
Length	4.45	1.59
Outside diameter	3.81	1.59
Wall thickness	0.56	0.43
Isotopic content of uranium (%)		
^{232}U (ppm)	6.47	
^{233}U	97.54	
^{234}U	1.05	
^{235}U	0.03	
^{236}U	<0.01	
^{238}U	1.39	
Isotopic content of boron (%)		
^{10}B	19.74	
^{11}B	80.26	

Spaced Subcritical Components

Cylindrical containers, of 4.63 liters capacity and fabricated of 0.25-mm-thick stainless steel, had an outside diameter and a height of 18.28 and 17.67 cm, respectively. They were identically filled to within ±0.5 g of solution. Critical assemblies of reflected and unreflected arrays at uranium concentrations of 333 and 204 g/liter were constructed. The reflector material was 15.2-cm-thick polyethylene (ρ = 0.93 g/cm^3) located from the peripheral cylinders of the array by a distance equal to one-half the surface separation between cylinders. The critical conditions for the arrays of cylinders at the two uranium concentrations are summarized in Table 2.16.2.

Table 2.16.2. Critical Parameters for Unreflected and Reflected Arrays of Units of Uranyl Nitrate Solution of Uronium Containing 97.5% ^{233}U (Ref. 4)

No. of Units in Array[a]	Polyethylene Reflector Thickness[b] (cm)	Center-to-Center Separation of Units (cm)		Average Uranium[c] Density (g/cm^3)
		Horizontal	Vertical	
333 g of U per liter; H:^{233}U = 73; specific gravity, 1.468; 1.432 kg of U per container				
8 (2 × 2 × 2)	0	20.44	19.13	0.179
27 (3 × 3 × 3)	0	25.72	24.57	0.088
8 (2 × 2 × 2)	15.2	31.95	30.36	0.046
27 (3 × 3 × 3)	15.2	41.03	38.57	0.022
204 g of U per liter; H:^{233}U = 119; specific gravity, 1.280; 0.885 kg of U per container				
8 (2 × 2 × 2)	0	20.16	18.81	0.116
27 (3 × 3 × 3)	0	25.01	23.89	0.059
8 (2 × 2 × 2)	15.2	30.23	25.51	0.034
27 (3 × 3 × 3)	15.2	38.05	36.74	0.017

[a]The solution was contained in cylinders of 0.25-mm-thick stainless steel with an outside diameter of 18.28 cm and height of 17.67 cm. The number of units along the edges of the array is given in parentheses.

[b]The polyethylene reflector was located at the cell boundaries.

[c]See Table 2.16.1 for isotopic content.

Simple Geometries

Presented in Table 2.16.3 are the critical conditions for water-reflected and unreflected spherical and cylindrical volumes of the solution which had a value of k_{eff} of 1.0000 ± 0.0005. A concentration at which a sphere was critical was first established, and then several critical cylindrical volumes were measured. The results for unreflected cylinders have been corrected for the 1.27-cm-thick aluminum base of the container, so the results describe cylindrical volumes having aluminum on the lateral surface only.

Table 2.16.3. Critical Conditions of $^{233}UO_2(NO_3)_2$ Aqueous Solution in Water-Reflected and Unreflected Simple Geometries (Ref. 4)

$UO_2(NO_3)_2$ Solution[a]			Critical Dimensions									
			Spheres		Cylinders[b]							
					50.8-cm diam		38.1-cm diam		25.3-cm diam		20.3-cm diam	
Uranium Concentration (g/liter)	Specific Gravity	H:^{233}U	Radius (cm)	Mass (kg of U)	Height (cm)	Mass (kg of U)	Height (cm)	Mass (kg of U)	Height (cm)	Mass (kg of U)	Height (cm)	Mass (kg of U)
Unreflected Assemblies												
333	1.468	73			13.36	9.02						
204	1.280	122			13.51	5.59	15.14	3.52	24.69	2.53		
131	1.183	195	14.579	1.70	14.07	3.74	16.35	2.44	28.52	1.88		
102	1.144	253	15.078	1.46			17.60	2.05	33.40	1.71		
74.6	1.106	349	15.821	1.24			19.35	1.65	43.69	1.64		
44.6	1.050	581	18.378	1.16			26.37	1.34				
Water-Reflected Assemblies[c]												
132	1.186	194	11.170	0.769			13.42	1.77	17.22	1.14	22.86	0.976
95.0	1.135	273	11.847	0.662			[d]	[d]	19.67	0.939	20.02	0.824
47.9	1.068	548	14.579	0.621			19.6	1.07	31.53	0.757	[d]	[d]

[a] See Table 2.16.1 for isotopic content of the uranium.

[b] Aluminum cylinders had a 1.5-mm-thick wall and 1.27-cm-thick bottom. Spheres were of aluminum with 1.22-mm-thick wall.

[c] There was no reflector on the top of any cylinder. The surface of the reflector water was 24.3 cm above the solution, a distance equal to the bottom reflector thickness.

[d] There was insufficient solution inventory to achieve criticality; the maximum solution height was 12.5 cm in the 38.1-cm-diam cylinder and 68.2 cm in the 20.3-cm-diam cylinder.

Y-CDC-8: Raschig Rings (Reference 23)

Although this document references ORNL-4280[4] as the source of the data which it contains, it actually presents additional data in the form of reciprocal flux relaxation lengths for the two subcritical experiments reported therein. Also, data from an additional experiment not reported in ORNL-4280 are also reported in this document. The section reproduced below contains, in addition to the data, a discussion of how the data have been used to infer values of k_∞ for comparison with calculated values.

This document is the basis for ANSI standard N16.4-1971 governing the use of raschig rings in fissile solutions, and presents data and analyses used to support the adequacy of the standard within its limits of applicability.

5.3 Raschig Ring Exponential Experiments

A calculational scheme was used to evaluate some of the parameters in a simple model for raschig ring exponential experiments in cylindrical geometry so that an experimental value for $k_\infty(\text{exp})$ is obtained from measured reciprocal relaxation lengths for comparison to k_∞ calculated from the Cylindrical Tube Model. The equation for obtaining k_∞ from the experimental data is

$$k_\infty(\text{exp}) = 1 + M^2B_r^2 - M^2\gamma^2$$

where

M^2 = $L^2 + \tau$ = the migration area

τ = the neutron age to thermal energy

B_r^2 = the radial buckling

γ = the reciprocal relaxation length

L = the thermal diffusion length.

The reciprocal relaxation length is determined from the exponential dependence of the neutron flux in the z direction of the cylinder filled with raschig ring-solution mixture in the exponential experiment. $M^2 (= \tau + L^2)$ and $M^2 B_r^2$ are calculated parameters. The neutron age, τ, which is equal to one-sixth the second moment of the slowing down distribution from a point fission source, was calculated using the ANISN-S_{32} method of Raffety and Mihalczo.[43] The thermal diffusion length, L, is inversely proportional to $\sqrt{\Sigma_{at}}$. The radial nonleakage probability, $1/(1 + M^2 B_r^2)$, was calculated from the equation

$$k_{eff} = \frac{k_\infty}{1 + M^2 B_r^2}$$

where k_∞ was calculated for the fissile solution-raschig ring mixture using the Cylindrical Tube Model. Cell-averaged, homogenized cross sections, generated from the k_∞ calculation, were used in a subsequent ANISN-reactor calculation of k_{eff} for an infinitely long cylinder of the fissile solution-raschig ring mixture. Thus, $M^2 B_r^2$ was derived from the two calculations. The calculated values of M^2, $M^2 B_r^2$ and the experimental value of γ were then used to obtain $k_\infty(exp)$ for comparison to the calculated value of k_∞.

Table 6 summarizes these calculations for the ^{235}U and ^{233}U exponential experiments[39,44] where there were available measurements of the raschig ring inside and outside diameters. k_∞ was also calculated for the raschig rings and the plutonium solution concentration which was determined experimentally[45] to have $k_\infty(exp) = 1$ and is included in the table. The raschig rings used in the experiments are described in Table 7.

The differences between the experimental values and the calculated values of k_∞ for these raschig ring-fissile solution systems are used to determine the value of the calculated k_∞ for which subcriticality is assured, see Section 5.6.

Table 6. Comparison of Calculated k_∞ with Experimentally Determined k_∞ Values. (Ref. 23)

U or Pu Concentration (g/liter)	Raschig Ring Type[a]	Cylinder Diameter (in.)	Reflector	Reciprocal (Relaxation Length) γ^2 (cm^{-2})	ANISN Calculations k_∞	ANISN Calculations k_{eff}	ANISN Calculations τ (cm^2)	L^2 (cm^2)	M^2 (cm^2)	$M^2B_r^2 = \frac{k_\infty}{k_{eff}} - 1$	k_∞(exp)
Uranyl Nitrate Solution Containing 92.6 wt % ^{235}U[b]											
415	EN-1	48	Air	0.00554	0.8180	0.7765	39.03	0.19	39.22	0.0534	0.836 ± 0.048
415	EN-1	48	H_2O	0.00497	0.8180	0.7816	39.03	0.19	39.22	0.0466	0.852 ± 0.054
415	Pyrex	30	H_2O	0.00131	1.0674	0.9766	38.25	0.20	38.45	0.0930	1.043 ± 0.015
415	Pyrex	30	Air	0.00216	1.0674	0.9520	38.25	0.20	38.45	0.1212	1.038 ± 0.020
415	EN-1	20	H_2O	0.01024	0.8180	0.6957	39.03	0.19	39.22	0.1758	0.774 ± 0.051
415	Pyrex	20	H_2O	0.00326	1.0674	0.9047	38.25	0.20	38.45	0.1798	1.062 ± 0.011
415	Pyrex	20	Air	0.00453	1.0674	0.8522	38.25	0.20	38.45	0.2525	1.078 ± 0.021
415	Pyrex	20	H_2O	0.00313	1.0674	0.9047	38.25	0.20	38.45	0.1798	1.060 ± 0.027
415	KG-33	20	H_2O	0.01461	0.7115	0.5968	42.91	0.15	43.06	0.1922	0.563 ± 0.053
415	KG-33	20	Air	0.01607	0.7115	0.5596	42.91	0.15	43.06	0.2714	0.579 ± 0.051
415	R6	20	Air	c	1.5467	c	41.11	0.28	41.39		
415	R6	20	H_2O	d	1.5467	d	41.11	0.28	41.39		
141	R6	20	Air	0.00194	1.1990	0.9417	39.81	0.65	40.46	0.2732	1.195 ± 0.009
141	R6	20	H_2O	0.00085	1.1990	0.9919	39.81	0.65	40.46	0.2088	1.174 ± 0.011
141	R6	20 + 0.032 Cd	Air	0.00181	1.1990	0.9417	39.81	0.65	40.46	0.2732	1.200 ± 0.008
141	R6	20 + 0.032 Cd	H_2O	0.00120	1.1990	0.9613	39.81	0.65	40.46	0.2473	1.199 ± 0.005
94.4	R6	20 + 0.032 Cd	Air	0.00530	1.0178	0.7986	39.75	0.77	40.52	0.2745	1.060 ± 0.024
94.4	R6	20 + 0.032 Cd	H_2O	0.00480	1.0178	0.8135	39.75	0.77	40.52	0.2745	1.057 ± 0.023
63.3	R6	20 + 0.032 Cd	Air	0.01080	0.8278	0.6495	39.86	0.93	40.79	0.2745	0.834 ± 0.052
63.3	R6	20 + 0.032 Cd	H_2O	0.01088	0.8278	0.6614	39.86	0.93	40.79	0.2516	0.808 ± 0.045
Uranyl Nitrate Solution Containing 97.6 at. % ^{233}U[e]											
332.6	A	20	Air	0.00863	0.9362	0.7079	49.58	0.20	49.78	0.3225	0.893 ± 0.007
345.9	B	20	Air	0.00723	0.8927[f]	0.6888	47.50	0.15	47.65	0.2960	0.951 ± 0.006
204.1	B	20	Air	0.01432	0.6329	0.4921	45.27	0.18	45.45	0.2861	0.632 ± 0.014
Plutonium Nitrate Solution Containing 95.8 at. % ^{239}Pu[g]											
182	C	--	--	0.00000	1.0274	--	--	--	--	--	1.000

a. See Table 8 for raschig ring descriptions.
b. See Ref. 39 for complete description.
c. Critical height = 10.86 in. k_{eff} was calculated by KENO to be 0.956 ± 0.006 using cell-averaged cross sections from the ANISN k_∞ calculation.
d. Critical height = 8.34 in. k_{eff} was calculated by KENO to be 0.925 ± 0.006 using cell-averaged cross sections from the ANISN k_∞ calculation.
e. See Ref. 44 for complete description.
f. S_8 calculation was 0.9042 which should be compared to 0.951.
g. See Ref. 45 for complete description.

References

1. J. K. Fox, L. W. Gilley, and E. R. Roher, "Critical Mass Studies, Part VIII. Aqueous Solutions of U^{233}," Oak Ridge National Laboratory report ORNL-2143 (September 23, 1959).

2. R. Gwin and D. W. Magnuson "The Measurement of Eta and Other Nuclear Properties of ^{233}U and ^{235}U In Critical Aqueous Solutions" NSE 12, 364 (1962).

3. A. Staub, D. R. Harris and M. Goldsmith, "Analysis of A Set of Critical Homogeneous U-H_2O Spheres," NSE 34, 263 (1968).

4. J. T. Thomas, "Critical Experiments with Aqueous Solutions of $^{233}UO_2(NO_3)_2$" in Neutron Physics Division Annual Progress Report for the Period Ending May 31, 1968, ORNL-4280, Oak Ridge National Laboratory, pp 53-55, (1968).

5. J. T. Thomas, J. K. Fox, and D. Callihan, "A Direct Comparison of Some Nuclear Properties of U-233 and U-235." Nucl. Sci. Eng. 1, 20-32 (March 1956).

6. J. T. Thomas, J. K. Fox, and D. Callihan "A Direct Comparison of Some Nuclear Properties of U-233 and U-235." ORNL - 1992, Oak Ridge National Laboratory (1965).

7. W. G. Clarke, C. C. Horton, and M. F. Smith, "Critical Assemblies of Aqueous Uranyl Fluoride Solutions, Part I, Experimental Techniques," AERE R/R 2051, United Kingdom Atomic Energy Authority report, A.E.R.E. Harwell, England, September 20, 1956.

8. J. G. Bruna, J. P. Brunet, R. Caizergues, C. Clouet D'Orval et P. Verriere,"Critical Experiments Carried Out with ^{239}Pu, ^{235}U and ^{233}U," (in French) Criticality Control of Fissile Materials, Proc. Stockholm Symposium, IAEA, Vienna, pp. 235-248, 1966.

9. G. E. Hansen, and H. C. Paxton, "Reevaluated Critical Specifications of Some Los Alamos Fast-Neutron Systems," Los Alamos Scientific Laboratory report LA-4208 (September 1969).

10. H. C. Paxton, "Los Alamos Critical Mass Data," USAEC Report LAMS-3067, Los Alamos Scientific Lab (May 1964).

11. G. E. Hansen, Status of Computational and Experimental Correlations for Los Alamos Fast-Neutron Critical Assemblies, Physics of Fast and Intermediate Reactors, IAEA, Vienna, pp. 445-455, 1962.

12. E. A. Plassmann and D. P. Wood, Critical Reflector Thicknesses for Spherical U^{233} and Pu^{239} Systems, Nuclear Sci. and Eng. 8, 615-620 (1960).

13. H. C. Paxton, Experimental Criticality Specifications, an Annotated Bibliography Through 1976, LA-UR-77-684, (Undated).

14. Wallace Webster, "Calculated Neutron Multiplication Factors of Uniform Aqueous Solutions of ^{233}U and ^{235}U," ORNL-CDC-2, Oak Ridge National Laboratory (1967).

15. M. L. Batch and N. L. Snidow, Consolidated Edison Thorium Reactor Critical Experiments With Oxide Fuel, BAW-119, Rev. 1, Babcock & Wilcox Co. (July 1960).

16. N. L. Snidow, R. C. Anderson, M. L. Batch, G. A. G. de Coulon, R. H. Lewis and W. M. Vannoy, Thorium Uranium Physics Experiments Final Report, BAW-1191, Babcock & Wilcox Co. (May 1960).

17. J. R. Fisher and E. D. Kendrich, "Comparison of Measured and Predicted Characteristics of the Elk River Reactor," in Thorium Fuel Cycle, AEC Symposium Series # 12, CONF-660524, p. 685, USAEC (Feb. 1968).

18. S. Milani and S. H. Weiss, Small Uranium-233 Fueled Seed-and-Blanket Critical Experiments, WAPD-TM-614, Bettis Atomic Power Lab (Nov. 1967).

19. J. A. Mitchell, Ed, BMU Series of ^{233}U Fueled Critical Experiments, WAPD-TM-1117, BAPL (Jan. 1975).

20. G. G. Smith, J. P. Semans and J. A. Mitchell, Eds, ^{233}U Oxide-Thorium Oxide Detailed Cell Critical Experiments, WAPD-TM-1101, BAPL (Oct. 1974).

21. H. H. Windsor, W. J. Tuney and G. A. Price, "Exponential Experiments With Lattices of Uranium-233 Oxide and Thorium Oxide in Light and Heavy Water," NSE 42, 150-161 (1970).

22. R. C. Lloyd, E. D. Clayton and J. H. Chalmers, "Criticality of Arrays of ^{233}U Solution," Nuclear Applications 4, 136 (1968).

23. J. P. Nichols, C. L. Schuske and D. W. Magnuson, Use of Borosilicate Glass Raschig Rings as a Neutron Absorber in Solutions of Fissile Material, Y-CDC-8, Union Carbide Corp., pp. 33 - 36, July, 1971.

DISTRIBUTION

No. of Copies

OFFSITE

1 A. A.Churm
DOE Patent Group
9800 S. Cass Avenue
Argonne, IL 60439

1 Mr. T. B. Hindman, Jr.,
Director
Fuel Cycle Programs Office
Savannah River Operations
Office
P. O. Box A
Aiken, SC 29801

3 Dr. Joe Spencer
Savannah River Laboratory
E. I. du Pont de Nemours
and Company
Aiken, SC 29801

126 Distribution Category UC-83

ONSITE

37 Battelle-Northwest

T. W. Ambrose
S. R. Bierman
C. L. Brown
N. E. Carter
E. D. Clayton
W. E. Converse
B. M. Durst
L. C. Davenport
D. E. Friar
B. F. Gore (10)
O. F. Hill
B. W. Howes
U. P. Jenquin
B. R. Leonard
R. A. Libby
R. C. Lloyd
J. S. McPherson
D. F. Newman
D. R. Oden
D. E. Olesen
T. J. Trapp

No. of Copies

Battelle-Northwest - Cont.

Technical Information (5)
Publishing Coordination (2)

ONSITE

Richland Operations

P. A. Craig
H. E. Ransom